DESIGN, SYNTHESIS AND CHARACTERIZATION OF SMART SURFACES AND INTERFACES

ZHAI GUANGQUN

(B. ENG.; M. ENG, BUCT)

A THESIS SUBMITTED

FOR THE DOCTOR OF PHILOSOPHY DEFENSE

DEPARTMENT OF CHEMICAL AND BIOMOLECULAR

NATIONAL UNIVERSITY OF SINGAPORE

2005

Acknowledgements

My deepest gratitude is directed to the **National University of Singapore** (NUS), which provides the sufficient financial assistance for me to survive from the hard life through this 39-month Ph.D study.

I am indebted to my academic supervisors, Prof. **Kang En-Tang** and Prof. **Neoh Koon-Gee**. Their guidance during my Ph.D research work helped me to step out one stalemate after another.

The assistances from my seniors, **Zhang Yan**, **Ying Lei** and **Wang Wencai** are greatly appreciated. They helped me to have a quick participation in the research work.

Table of Contents

Summary

Molecular modification poly(vinylidene fluoride) (PVDF) and surface modification of silicon wafer had been carried out to enhance their surface properties in this work.

Ozone-pretreated PVDF was graft-copolymerized with 4-vinylpyridine (4VP) to produce the PVDF-*g*-P4VP copolymers. The microfiltration (MF) membranes were fabricated by phase inversion in aqueous media. X-ray photoelectronic spectroscopy (XPS) results indicated surface enrichment of the P4VP graft chains on the membrane surfaces. The flow rate through the PVDF-*g*-P4VP MF membranes increases with the increases in the solution pH, resulting from the weak base nature. XPS studies revealed that when the proton concentration was low, hydrogen bonding predominated. Pyridine protonation became significant only when the proton concentration was higher than 0.01M. On the other hand, the PVDF-*g*-P4VP/PNIPAm blend membranes were cast from the blend of PVDF-*g*-P4VP and poly(N-isopropylacrylamide) (PNIPAm). In presence of both P4VP side chains and the PNIPAm homopolymer, the blend membrane exhibits a both pH- and temperature-sensitive characteristics in surface morphology, pore size distribution, and flux behavior.

The electrolyte-responsive membrane was prepared *via* the copolymerization of *N*,*N*′-dimethyl(methylmethacryloyl ethyl) ammonium propane sulfonate (DMAPS) with the ozone-pretreated PVDF (PVDF-*g*-PDMAPS copolymer), followed by phase inversion. The aqueous solution of DMAPS homopolymer (PDMAPS) exhibits both temperature- and electrolyte-sensitive phase behavior. Accordingly, the surface

composition of the PVDF-*g*-PDMAPS membranes was shown to be dependant on the temperature and ionic strength of the casting bath. However, the flux behavior of aqueous media through the PVDF-*g*-PDMAPS membrane exhibited only electrolyte-responsive behavior. The permeability decreases with the increases in the ionic strength of the aqueous solution, resulting from the globular-to-coiled conformational transition (*anti-polyelectrolyte effect*) of the PDMAPS side chains on the pore walls. The low degree of polymerization of the PDMAPS side chain probably accounts for the absence of temperature-sensitive flux behavior of the PVDF-*g*-PDMAPS membrane.

Inimer 2-(2-bromoisobutyryloxy)ethyl acrylate (BIEA) was graft-copolymerized with ozone-pretreated PVDF to produce the PVDF-*g*-PBIEA copolymer. With the ATRP-initiatiing ability of BIEA side chains, sodium styrenic sulfonate (NaSS) was graft-copolymerized with the PBIEA side chains to produce the PVDF-*g*-PBIEA-*ar*-NaPSS arborescent copolymer. The PVDF-*g*-PBIEA-*ar*-NaPSS copolymer was fabricated into MF membrane by phase inversion. XPS and SEM studies revealed that both the surface composition and the morphology exhibit an electrolyte-responsive behavior as the electrostatic repulsion among the NaPSS side chains was shielded in a high ionic strength solution (*polyelectrolyte effect*). The surface-initiated ATRP of PEGMA was undertaken on the PVDF-g-PBIEA membrane to produce the PVDF-*g*-PBIEA-*ar*-PPEGMA membranes. With the presence of the biocompatible PEGMA polymer layer, the anti-fouling properties of the membranes had been greatly enhanced.

Surface-initiated free radical polymerization was extended on the silicon wafer substrate to prepare the inorganic/organic hybrid materials. The azo initiator was immobilized onto the hydroxyl-terminated silicon substrate *via* esterification reaction. The surface-initiated reversible addition-fragmentation chain transfer (RAFT) polymerization of DMAPS was carried out to produce Si-*g*-PDMAPS surface. The thickness of the PDMAPS film increases linearly with the polymerization time. The end functionality of the PDMAPS brush allowed for the synthesis of diblock copolymer brush. NaSS was block copolymerized to produce the Si-*g*-PDMAPS-*b*-NaPSS brushes. Such a combination of polybetaine and polyelectrolytes allowed further investigation on their electrolyte-responsive behavior.

Nomenclatures

4VP: 4-vinylpyridine

AAc: acrylic acid

AAm: acrylamide

AFM: atomic force microscopy

ATRP: atom transfer radical polymerization

BIEA: 2-(2-bromoisobutyryloxy)ethyl acrylate

BMA: butyl methacrylate

DMAEMA: (*N*,*N*-dimethylamino) ethyl methacrylate

DMAPS: *N*,*N*-dimethyl(methylmethacryloyl ethyl) ammonium propane sulfonate

DPE: 1,1-diphenylethylene

EVA: ethylene-vinyl acetate copolymer

FTIR: Fourier-transform infrared spectroscopy

HEMA: 2-hydroethyl methacrylate

IEP: isoelectric point

LCST: lower critical solution temperature

NaSS: sodium styrenic sulonate

NIPAm: *N*-isopropylacrylamide

NMP: n-methyl pyrrilidone

NMR: nuclear magnetic resonance spectroscopy

MAAc: methacrylic acid

MF: microfiltration

PBT: poly(butylene terephthalate)

PC: polycarbonate

PDMS: poly(dimethylsiloxane)

PE: polyethylene

PEGMA: poly(ethylene glycol) methacrylate

PEI: poly(ethyleneimine)

PEOX: poly(2-ethyl-2-oxazoline)

PET: poly(ethylene terephthalate)

PI: polyimide

PiP: polyisoprene

PP: polypropylene

PS: polystyrene

PTFE: poly(tetrafluoriethylene)

PVDF: poly(vinylidene fluoride)

RAFT: reversible addition-fragmentation chain transfer process

ROMP: ring-opening metathesis polymerization

SAM: self-assembled monolayer

SAN: styrene-acrylonitrile copolymer

SEM: scanning electron microscopy

Si-H: hydrogen-terminated silicon substrate

SIP: surface-initiated polymerization

SPP: 3-(*N*-(3-ethylacrylamidopropyl)-*N*,*N*-dimethyl)ammoniopropane sulfonate)

SRP: stimuli-responsive polymer

UCST: upper critical solution temperature

XPS: X-ray photoelectron spectroscopy

List of Figures

solution and the preparation of the PVDF-*g*-P4VPMF membranes by phase inversion.

Figure 3.2: Effect of [4VP]/[-CH_2CF_2-] molar feed ratio on the bulk [N]/[C] ratio and bulk graft concentration ([-4VP-]/[-CH_2CF_2-]$_{bulk}$ ratio) of the PVDF-*g*-P4VP copolymer.

Figure 3.3: Thermogravimetric analysis curves of (1) the pristine PVDF; the PVDF-*g*-P4VP copolymers of bulk graft concentrations ([-4VP-]/[-CH_2CF_2-]$_{bulk}$ ratios) of (2) 0.038, (3) 0.068, (4) 0.083; (5) the 4VP homopolymer.

Figure 3.4: XPS C 1s core-level spectra of the MF membranes cast by phase inversion from 12 wt% NMP solutions of (a) the pristine PVDF homopolymer, (b) the PVDF after 15 min of ozone pretreatment, and the PVDF-*g*-P4VP copolymers prepared from the [4VP]/[-CH_2CF_2-] molar feed ratios of (c) 0.61, (d) 2.44 and (e) 3.66.

Figure 3.5: Effect of [4VP]/[-CH_2CF_2-] molar feed ratio on the surface [N]/[C] ratio and the surface graft concentration ([-4VP-]/[-CH_2CF_2-]$_{surface}$ ratio) of the PVDF-*g*-P4VP MF membranes.

Figure 3.6: Comparison between the bulk graft concentration and the surface graft concentration of the PVDF-*g*-P4VP MF membrane cast by phase inversion from the 12 wt% NMP solution of the respective PVDF-*g*-P4VP copolymer.

Figure 3.7: SEM micrographs of the MF membranes cast by phase inversion from the 12 wt% NMP solution of (a) the pristine PVDF, and the PVDF-*g*-P4VP copolymers of bulk graft concentrations ([-4VP-]/[-CH_2CF_2-]$_{bulk}$ ratios) of (b) 0.038, (c) 0.068 and (d) 0.083.

Figure 3.8: Effect of pH of the casting bath on the surface graft concentration (([-4VP-]/[-CH_2CF_2-]$_{surface}$ ratio) and the mean pore radius of PVDF-*g*-P4VP (([-4VP-]/[-CH_2CF_2-]$_{bulk}$=0.056) MF membranes cast from 12 wt% NMP solution in aqueous HCl solution with specific pH value. Sodium chloride was added to fix the ionic strength of the casting bath at 0.1 mol/L.

Figure 3.9: Effect of pH of the casting bath on the C 1s core-level lineshape of the PVDF-*g*-P4VP MF membranes (([-4VP-]/[-CH_2CF_2-]$_{bulk}$=0.056); (a) cast in pH=1 and (b) cast in pH=6.

Figure 3.10: pH-dependant permeability of aqueous solution through the PVDF-*g*-PAAc, pristine PVDF and PVDF-*g*-P4VP MF membranes. Curve 1 is from the flux through the PVDF-g-PAAc MF membrane (average pore size 1.52 μm, surface graft concentration ([-AAc-]/[-CH_2CF_2-]$_{surface}$)=0.97). Curves 2 and 3 are from fluxes through the commercial PVDF membranes (standard pore diameter: *d*=0.65 and 0.45 μm, respectively, and with characteristic pore size distribution similar to those of PVDF-*g*-P4VP copolymer membranes); Curves 4 and 5 are

])=0.029) after being immersed for 10 min in aqueous solutions of different pH values.

Figure 4.1: Effect of the [DMAPS]/[-CH_2CF_2-] molar feed ratio on the $([N]/[C])_{bulk}$ ratio and the bulk graft concentration ($([\text{-DMAPS-}]/[\text{-}CH_2CF_2\text{-}])_{bulk}$ ratio) of the PVDF-*g*-PDMAPS MF membrane.

Figure 4.2: Thermogravimetric analysis curves of (a) the pristine PVDF, the PVDF-*g*-PDMAPS copolymers of bulk graft concentrations ($([\text{-DMAPS-}]/[\text{-}CH_2CF_2\text{-}])_{bulks}$ ratios) of (b) 0.05, (c) 0.12 and (d) 0.20, and (e) the PDMAPS homopolymer.

Figure 4.3: (a) UV-visible absorbance of aqueous solutions of PDMAPS of different concentrations as a function of temperature. (b) UV-visible absorbance of aqueous solutions of PDMAPS of different electrolyte concentration as a function of temperature.

Figure 4.4: XPS C 1s core-level spectra of the membranes cast by phase inversion at 25ºC and at about 100ºC from 12 wt% DMSO solutions of (a) the pristine PVDF homopolymer, the PVDF-*g*-PDMAPS copolymers prepared from the [DMAPS]/[-CH_2CF_2-] molar feed ratios of (b) 0.05, (c) 0.11 and (d) 0.23.

Figure 4.5: Effect of [DMAPS]/[-CH_2CF_2-] molar feed ratio on the $([N]/[C])_{surface}$ ratio and the surface graft concentration ($([\text{-DMAPS-}]/[\text{-}CH_2CF_2\text{-}])_{surface}$ ratio) of the PVDF-*g*-PDMAPS MF membrane cast at room temperature and at 100ºC, respectively.

Figure 4.6: XPS C 1s core-level spectra of PVDF-*g*-PDMAPS MF membrane ($([\text{-DMAPS-}]/[\text{-}CH_2CF_2\text{-}])_{bulk}$=0.20) cast from 12 wt% DMSO solution at room temperature by phase inversion in aqueous media of different electrolyte strength: (a) doubly distilled water, (b) 10^{-4}, (c) 10^{-3} and (d) 10^{-1} mol/L of the electrolyte.

Figure 4.7: SEM micrographs of the MF membranes cast by phase inversion from the 12 wt% DMSO solutions of (a) the pristine PVDF, and the PVDF-*g*-PDMAPS copolymers of different bulk graft concentrations of (b) 0.10, (c) 0.12 and (d) 0.20.

Figure 4.8: Electrolyte-dependant permeability of aqueous solution through the PVDF-*g*-PDMAPS MF membranes. Curves 1 and 2 are the permeability through the MF membranes cast from PVDF-*g*-PDMAPS copolymer ($([\text{-DMAPS-}]/[\text{-}CH_2CF_2\text{-}])_{bulk}$=0.10) in the coagulation bath with an electrolyte strength of 10^{-7} and 10^{-4} mol/L, respectively, at room temperature. Curve 3 is through the PVDF-*g*-PDMAPS ($([\text{-DMAPS-}]/[\text{-}CH_2CF_2\text{-}])_{bulk}$=0.20) cast in doubly distilled water. Curve 4 is through the membrane cast from the PVDF homopolymer. Curve 5 is through the commercial PVDF membrane with a standard pore diameter of d=0.22 μm.

Lists of Tables

Chapter 1:

Introduction

Graft polymer chains were introduced onto the surface or bulk of the parent materials to impart specific functionalities. The combination of multiple components, which may exhibit diametrically different physicochemical properties, could lead to an amphiphilic system. With the differentiated affinity to other matrices, the graft copolymers can function as an inter-phase and bridge the two completely immiscible materials.

The objective of the thesis is to study the effect of the stimuli-responsive polymer side chains on the properties, especially the surface properties, of the so-obtained polymer materials, in particular, the polymeric membrane in this thesis. Different from the conventional surface modification, a molecular-level copolymerization was employed in this work, which facilitated the control over the surface properties of the polymeric membranes. Through this study, the rules how the surface properties of multicoponent system with stimuli-responsive polymer was determined and controlled by the external conditions were hoped to be revealed.

In this thesis, graft polymer chains were introduced onto the poly(vinylidene fluoride) (PVDF) backbones and single crystal Si(100) wafer surfaces to produce the graft copolymers and inorganic/organic hybrid, respectively. The smart microporous membranes, which exhibited a stimuli-responsive flux behavior, were fabricated by phase inversion from the copolymer solution. The functional polymer brushes on the silicon surface are potentially useful to the semiconductor and microelectronics industry.

Chapter 2 presents an overview of the stimuli-responsive polymers, the methodologies for preparing the graft copolymer and the surface-modified substrates.

Chapter 3 is dedicated to fabrication of pH-sensitive microfiltration membranes. The poly(vinylidene fluoride) graft copolymer with 4-vinylpyridine side chains (the PVDF-g-P4VP copolymer)were synthesized through the ozone-pretreatment and thermally induced graft copolymerization, prior to the membrane fabrication by phase inversion. Not only the flux behavior, but also the surface morphology and the surface chemical composition of the PVDF-*g*-P4VP membranes exhibit a pH-sensitive behavior because of base nature of the P4VP side chains. The PVDF-*g*-P4VP/PNIPAm composite membranes were cast from the blend of the PVDF-*g*-P4VP copolymer and PNIPAm in solution. The composite membrane exhibited both temperature- and pH-sensitive characteristics in the surface morphology, pore size and flux behavior.

Chapter 4 reports on the design and preparation of electrolyte-responsive MF membranes. PVDF copolymer with zwitterionic polymer side chains was prepared initially, followed by the membranes fabrication by phase inversion. The permeability of the aqueous solution through the MF membrane exhibited an electrolyte-responsive behavior.

In Chapter 5, a novel graft copolymer was synthesized *via* graft copolymerization of an ATRP inimer, BIEA, with PVDF. Porous membranes could be fabricated from the copolymer solution by phase inversion. ATRP of specific functional monomers

were initiated from the BIEA side chains both at the molecular level and on the membrane surface (including pore surfaces).

Chapter 6 describes the synthesis of well-defined polybetaine brushes *via* controlled radical polymerization of DMAPS. Azo moiety was immbolized on Si-H substrate to initiate the surface-initiated reversible addition-fragmentation chain transfer (RAFT) polymerization process.

Chapter 2:

Literature Review

2.1 Stimuli-Responsive Polymers

Because of their large dimension *vis-à-vis* the atomic size and sufficient flexibility of the carbon-carbon single bond, the polymer chains tend to assume a random-walk conformation. However, driven by hydrogen bonding, ionic interaction and lyophilic/lyophobic effect, stimuli-responsive polymers, or SRPs, can switch their conformation, as shown in Figure 2.1, in response to external stimuli, such as temperature, pH value and ionic strength (Lowe, 2000). Such a conformational transition of SRP chains can lead to an abrupt shift in segregation-aggregation equilibrium, intrinsic viscosity, hydrodynamic volume, turbidity and phase behavior. SRPs can be classified into several major classes, *viz.* pH-sensitive polymers, electrolyte-sensitive polymers and thermoresponsive polymers.

2.1.1 pH-Sensitive Polymers

In general, the pH-sensitive behavior of SRPs originates from the weak acid or base groups within the polymer structures. For the acidic polymers, such as poly(acrylic acid) (PAAc), they can be depronated when dissolved in basic aqueous media, which gives rise to a distribution of the carboxylic anions alongside the polymer chains. The resulting electrostatic repulsion among the negatively charged groups drives the polymer chains to switch from a globular conformation to a coiled one. On the other hand, for basic polymers such as poly(4-vinylpyridine) (P4VP), they can become protonated when exposed to aqueous acidic media, leading to the formation of positive charges alongside the polymer chains. As a result, the polymer chains assume a rod-like structure due to electrostatic repulsion.

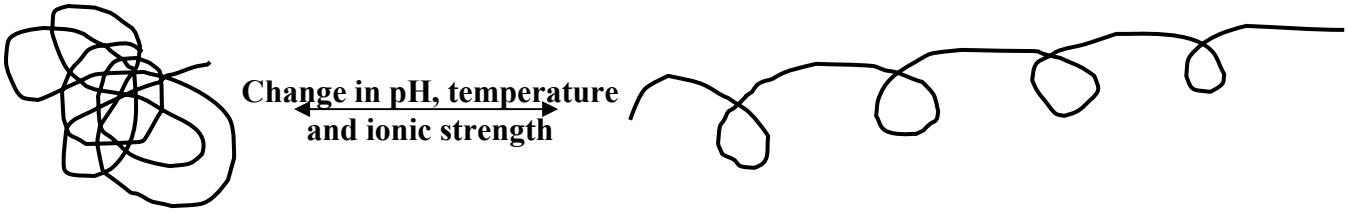

Figure 2.1: Schematical illustration of the conformational change of stimuli-responsive polymers in response to the external change in pH, temperature and ionic strength.

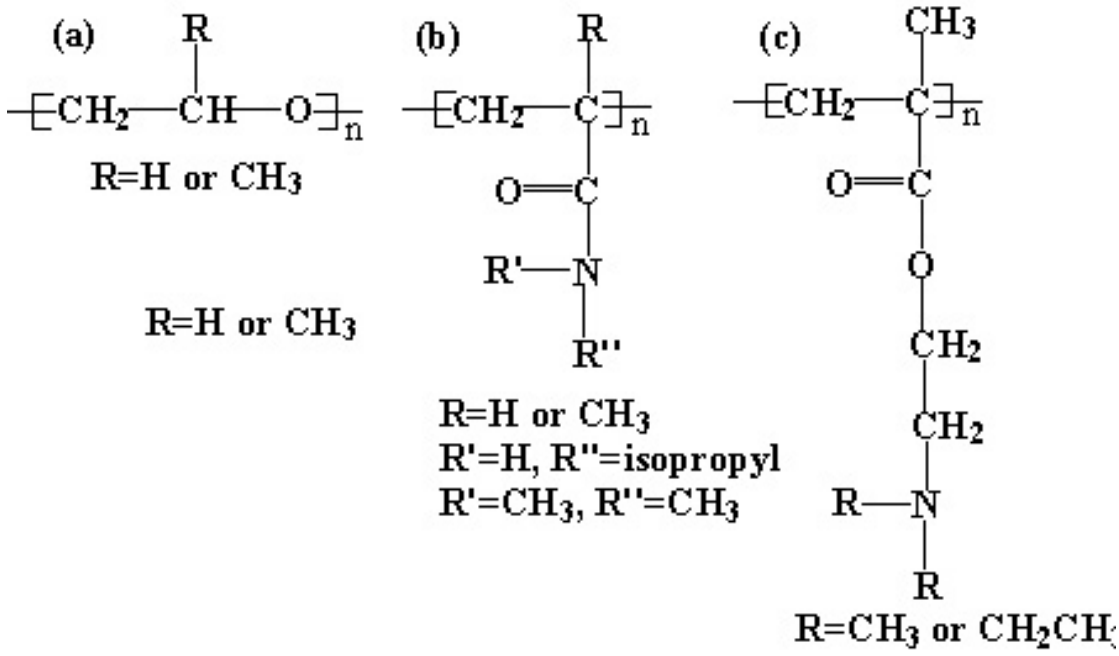

Figure 2.2: Chemical structures of three families of thermoresponsive synthetic polymers with a lower critical solution temperature (LCST).

Acrylic acid (AAc) and methacrylic acid (MAAc) are the predominant acid monomer involved in the pH-sensitive polymers. Their hydrogel microparticles exhibit a swell-deswell behavior in response to pH of the aqueous media (Jones, 2000; Uchida *et al.*., 1995). Polymer chains assume a globular conformation in acid media. When the external pH is adjusted to over 7, polymer chains expand As a result, hydrogel particles become swollen when the external pH shifts from acidic to basic. AAc and MAAc had been grafted onto the polymer membrane surface and the pore surface (Ito *et al.*., 1997; Iwata *et al.*., 1998). After graft copolymerization, when the aqueous medium shifts from acidic to basic, PAAc and PMAAc chains adopt an expanded conformation, leading to a pH-sensitive flux behavior (Ito *et al.*., 1997).

On the other hand, basic pH-sensitive polymers include poly(amines) (Kirwan *et al.*., 2004b; Bokias *et al.*.，2000), poly(amides) (Wang, 2002), poly(pyridine) (Ionov *et al.*., 2003; Minko *et al.*., 2002) and poly(imidazole) (Sui, 2003). The conformational changes in these polymers has been well visualized by AFM. AFM has revealed that the conformation of poly(vinyl amine) (PVA) single chains undergoes a coil-to-globule transition when the pH of the aqueous solution shifts from 3 to 9 (Kirwan *et al.*., 2004b).

2.1.2 Thermoresponsive Polymers

The thermoresponsive polymers herein are defined as the polymers that can undergo a sharp conformational change during a narrow temperature range (Lowe, 2000). Some non-ionic polymers transform from hydrophilic to hydrophobic character abruptly at a lower critical solution temperature (LCST), while some polyzwitterions

undergo a diametrically opposite transition at an upper critical solution temperature (UCST).

Most of the synthetic thermoresponsive polymers which show the LCST character fall into several families of polymers, namely, poly(*N*-substituted (meth)acrylamide), poly(olefin oxide), and poly(*N,N*-disubstituted aminoethyl methacrylate). Their chemical structures were schematically shown in Figure 2.2(a), (b) and (c), respectively. These polymers are water-soluble and hydrophilic at low temperature but precipitate at high temperature. Accordingly, the polymer chains adopt a coil-to-globule conformational change, triggered by the increase in the thermodynamic environment.

Poly(*N*-isopropylacrylamide) (PNIPAm) is the most extensively studied polymer with a LCST (Virtanen., 2002). PNIPAm is hydrophilic at room temperature but undergoes a phase transition at 32 ^{o}C. The volume change of the PNIPAm chains can be as high as 100 times (Wu. 1995). Copolymerization with hydrophilic comonomers, such as acrylamide (AAm), AAc and (*N,N*-dimethylamino) ethyl methacrylate (DMAEMA) resulted in a pronounced increase in LCST, while that with butyl methacrylate (BMA) accounted for an observed decrease in the LCST. Static and dynamic light scattering techniques had revealed that the PNIPAm single chain underwent a coil-to-globule transition in an extremely dilute solution (Wu. 1995).

Polyzwitterions are polymers containing both cations and anions covalently bonded on the *identical* repeat units. The polymer prepared from zwitterionic monomers, especially sulfobetaines (Kudaibergenov, 1999) and carboxybetiane

(Gnambodoe *et al.*., 1996), as shown in Figure 2.3 (a) to (d), respectively, exhibit an opposite behavior to PNIPAm. These polymers are water-soluble only at high temperature and undergo a phase separation upon cooling. The aqueous solution of the polymers undergoes a dissolution-to-micellization transition, with the polymer chains undergoing a coil-to-globule conformational transition, in response to the decrease in the solution temperature.

Poly(*N*,*N*′-dimethyl(methacryloyl ethyl) ammonium propane sulfonate) (PDMAPS) probably is the most widely investigated polyzwitterions. Aqueous solution of PDMAPS is homogenous at high temperature, but phases-separated when the aqueous media cool down to below the UCST. The PDMAPS solution undergoes a sharp decrease in transmittance over the narrow range of temperature around the UCST. (Chen *et al.*., 2000). In comparison to that of PNIPAm, the phase behavior of the aqueous solution of PDMAPS is more affected by polymer molecular weight, ionic strength, polymer concentration, electrolyte structure, non-electrolytic species *etc*.

2.1.3 Electrolyte-Responsive Polymer

Electrolyte-responsive polymers are termed as those which undergo conformational change and phase behavior in response to the change in the ionic strength of the aqueous media. Electrolyte-responsive polymers also exhibit two opposite electrolyte-responsive behaviors.

For polymers with only anions or cations distributed along chains with the counterions mobile in the surrounding media, *i.e.* polyelectrolyte, there exists a strong electrostatic repulsion among the charged sites of the polymer chains, which drives the polymer chains to adopt a coiled conformation. With low molecular electrolyte added, the electrostatic repulsion is gradually shielded by the surrounding mobile ions. As a result, the polyelectrolyte chains could assume a collapsed conformation in a high ionic strength (Vasilevskaya, 2001), leading to a reduced intrinsic viscosity of the polyelectrolyte aqueous solution, or "*the polyelectrolyte effect*" (Armentrout *et al.*., 2000a).

Polyanions, *i.e.* the polyelectrolyte with anions bonded on the polymer chains, mainly results from the alkali salt of poly(carboxylic acid) (Minakata *et al.*., 2003) and poly(sulfonic acid) (Yim *et al.*., 2002). On the other hand, polycations, *i.e.* the polyelectrolytes with cations bonded on the polymer chains, are derivatized from the *N*-alkylated poly(bases) (Biesalski *et al.*, 2004; Armentrout, 2000b).

Poly(sodium acrylate) (NaPAAc) and poly(sodium styrenesulfonate) (NaPSS) are widely studied among various polyanion. It was found that the NaPAAc can be adsorbed to the mineral particle surface to a significant amount only in a concentrated NaCl aqueous solution, because the electrostatic repulsion inhibits the aggregation of the NaPAAc chains. However, it was screened when the ionic strength is increased to 1M (Kirwan *et al.*, 2004a). The electrolyte-responsive conformational changes of the polyelectrolyte chain can be visualized from the electrolyte-induced collapse of polyelectrolyte brushes densely bonded on the silicon substrates. The thickness of poly(*N*-methyl vinylpyridinium iodine) (PMVP) brushes swollen in salt-free aqueous

media could be 30 times that swelled in 1 M NaI solution (Biesalski *et al.*, 2004). AFM images revealed that single poly(methacryloyloxyethyl dimethylbenzylammonium chloride) (PMB) chain underwent a coil-to-globule transition when the electrolyte concentration of Na_3PO_4 in aqueous solution was increased from 0 to 18 M (Kiriy *et al.*, 2002). However, with the addition of multivalent cations, such as Ca^{2+}, the polyelectrolyte chains can aggregate to undergo a phase separation from the aqueous solution (Drifford , 2001).

Different from polyelectrolyte, polyzwitterions exhibit an opposite electrolyte-responsive behavior. When dissolved in aqueous media of low ionic strength, the intra-chain and inter-chain electrostatic attractions, together with the hydrophobic interaction of the main chains, drive the polymer chains to adopt a globular conformation. However, such interactions are disrupted by the addition of a low molecular weight electrolyte or polyelectrolyte, leading to a globule-to-coil transition in the chain conformation, or "*anti-polyelectrolyte effect*" (Galin, 1996; McCormick, 1996).

Various polyzwitterions have been synthesized to study their bulk and solution properties (Galin, 1996). However, only the sulfobetaines and carboxybetaines have been well studied on their electrolyte-responsive behavior. Polybetaines are water-insoluble in pure water due to the ionic interactions, which give rise to a *de facto* networked structure. However, it is disrupted by the addition of low molecular weight electrolyte, because the electrolyte penetrates the ionic network, shielding the electrostatic attraction (Armentrout, 2000b). Such an electrolyte-induced conformational expansion corresponds to a discernible increase in the hydrodynamic

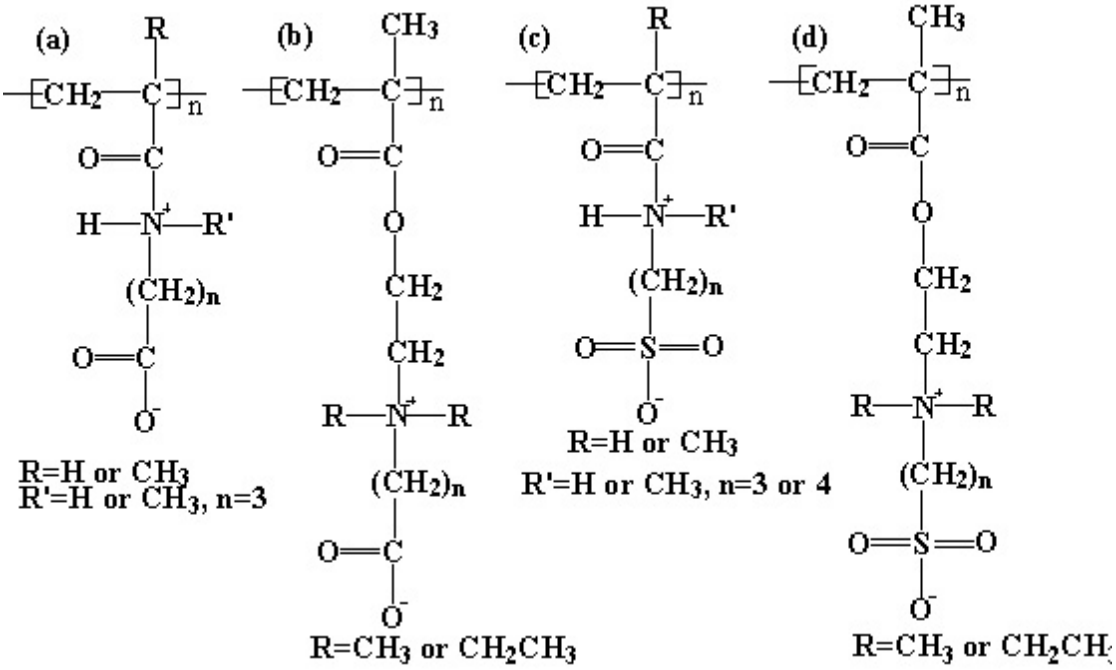

Figure 2.3 Chemical structures of polyzwitterions with a upper critical solution temperature (UCST)

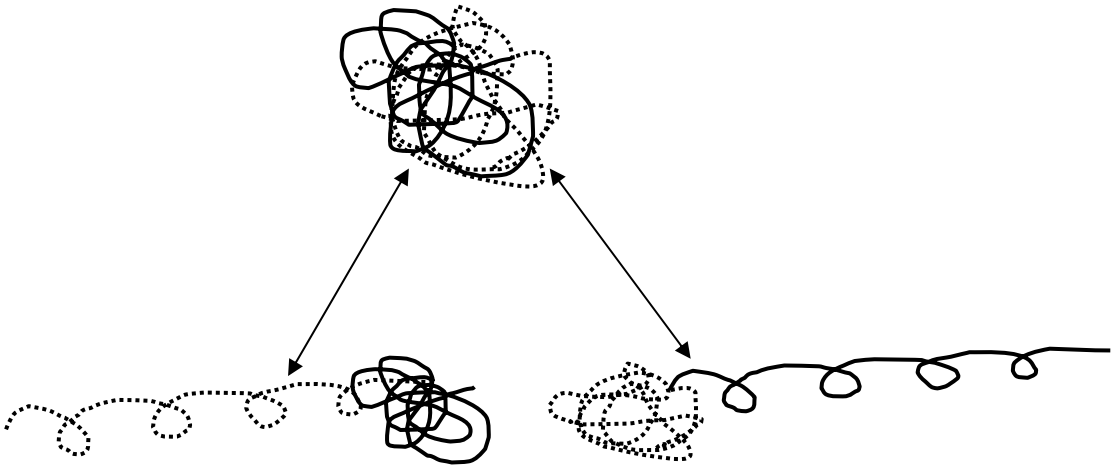

Figure 2.4 Hyperbolically stimuli-responsive conformational transitions of amphiphilic diblock copolymers in response to external change in pH, temperature or ionic strength.

volume and thus, in the reduced viscosity of the polyzwitterion aqueous solution (Armentrout *et al.*, 2000a). It was observed that the adsorption of PDMAPS on silica surface from aqueous salt solution decreases with the increase in the electrolyte concentration (Kato *et al.*, 1999).

It is noteworthy that due to weak acid nature, poly(carboxybetaines) may also be pH-sensitive and behave like polelectrolyte in some case. In contrast, poly(sulfobetaiens) revealed a consistent polyzwitterion behavior as the sulfonic acid is a strong acid (Kathmann *et al.*, 1997).

2.1.4 Hyperbolically Stimuli-Responsive Copolymers

As stated in the previous part, since both pH-sensitive, thermoresponsive and electrolyte-responsive polymers could exhibit two opposite behavior in response to changes in pH, temperature, and ionic strength, respectively, it is conceivable that coupling of polymer segments with opposite stimuli-responsive behaviors may give rise to copolymer which could exhibit a hyperbolically stimuli-responsive behavior in response to pH, temperature or ionic strength, respectively. *Hyperbolically* stimuli-responsive behavior here is directed to the universal phenomenon that some properties of such copolymers achieve maxima (minima) in middle range of the external stimuli, and reach minima (maxima) in two extremes. In other words, some properties of such *hyperbolically* SRP, especially conformation and hydrodynamic volume, exhibit a turning point in the course of changes in response to the external factors, as illustrated in Figure 2.4.

Polyampholytes, polymers containing cations and anions covalently bonded on the *different* repeat units, are a family of hyperbolically stimuli-responsive copolymers, which could be prepared from weak acid/weak base, strong acid/weak base, weak acid/strong base and strong acid/strong base (McCormick, 1996). However, most of polyampholytes were prepared from the weak acid/weak base and strong acid/weak base, so they exhibit a complicated stimuli-responsive behavior. The weak acid groups in the polyampholytes typically is limited to carboxylic acid (Kudaibergenov, 1999) and sufonic acid (McCormick, 1996), while the weak base groups include tertiary amines (Kudaibergenov, 1999), pyridine (Vedikhina *et al.*, 2000; Sfika, 2003), and imidazole (Annenkov *et al.*, 2003).

The polyampholytes in aqueous solution, in terms of pH, is a mixture of polyanions, polycations, intrapolymer complex and neutral polymers (Kudaibergenov, 2002). At a low solution pH (strongly acidic), the weak acid groups on the polyampholyte chains maintains electroneutral. However, the the weak base groups undergo the protonation or quatenization reaction and transform to polycations. At a neutral pH solution, both weak acid groups and weak base groups either exist in their neutral form or form an intrachain complex, leading to an electroneutral polymer chains. This specific pH is also defined as *isoelectric point* (IEP) where the contents of polycations and polyanions are minimal while those of neutral polymer and intrachain complex are maximal. In a high pH solution, the polyampholytes switch to polyanions because the weak acid groups undergo the deprotonation reaction (Kudaibergenov, 2002).

The hyperbolically pH-sensitive behavior of polyampholyte aqueous solution was revealed in intrinsic viscosity (Barbucci *et al.*, 1989), hydrodynamic volume (Sfika, 2003), turbidity (Sfika, 2003), equilibrium swelling ratio (Mafe *et al.*, 1997; Kudaibergenov, 1999), surface adsorption (Walter *et al.*, 1999) and aggregate size (Goloub *et al.*, 1999), with a turning point at IEP. The copolymers prepared from AAc and N-methyl-2-vinyl pyridinium chloride (the PAAc-*co*-PMVP copolymers), as shown in Figure 2.5(a), assume a typical weak acid/weak base polyampholyte behavior. Their aqueous solutions exhibited minimum reduced viscosity and electric conductance, as well as a maximum turbidity around the IEP of about 5.4 (Vedikhina *et al.*, 2000). Measurement of adsorption of PMAAc-*b*-PDMAEMA diblock polyampholytes, as shown in Figure 2.5(b) onto the silicon wafer revealed that the maximum adsorption was achieved when the aqueous pH was close to the IEP. At the minimum transmission of the solution, where the polyampholyte chains carry an equal number of positive and negative charges, strong attraction and the macroscopic precipitation occurred (Walter *et al.*, 1999).

The hyperbolically thermoresponsive copolymers are constructed from the combination of polymer segments with a LCST and a UCST, respectively. Such a copolymer has been synthesized from NIPAm and a sulfobetaine, 3-(N-(3-ethacrylamidopropyl)-N, N -dimethyl) ammoniopropane sulfonate) (SPP), to produce the PNIPAm-*b*-PSPP copolymer, as shown in Figure 2.5(c). The temperature-programmed spectrophotometric measurement showed that the optical absorbance of

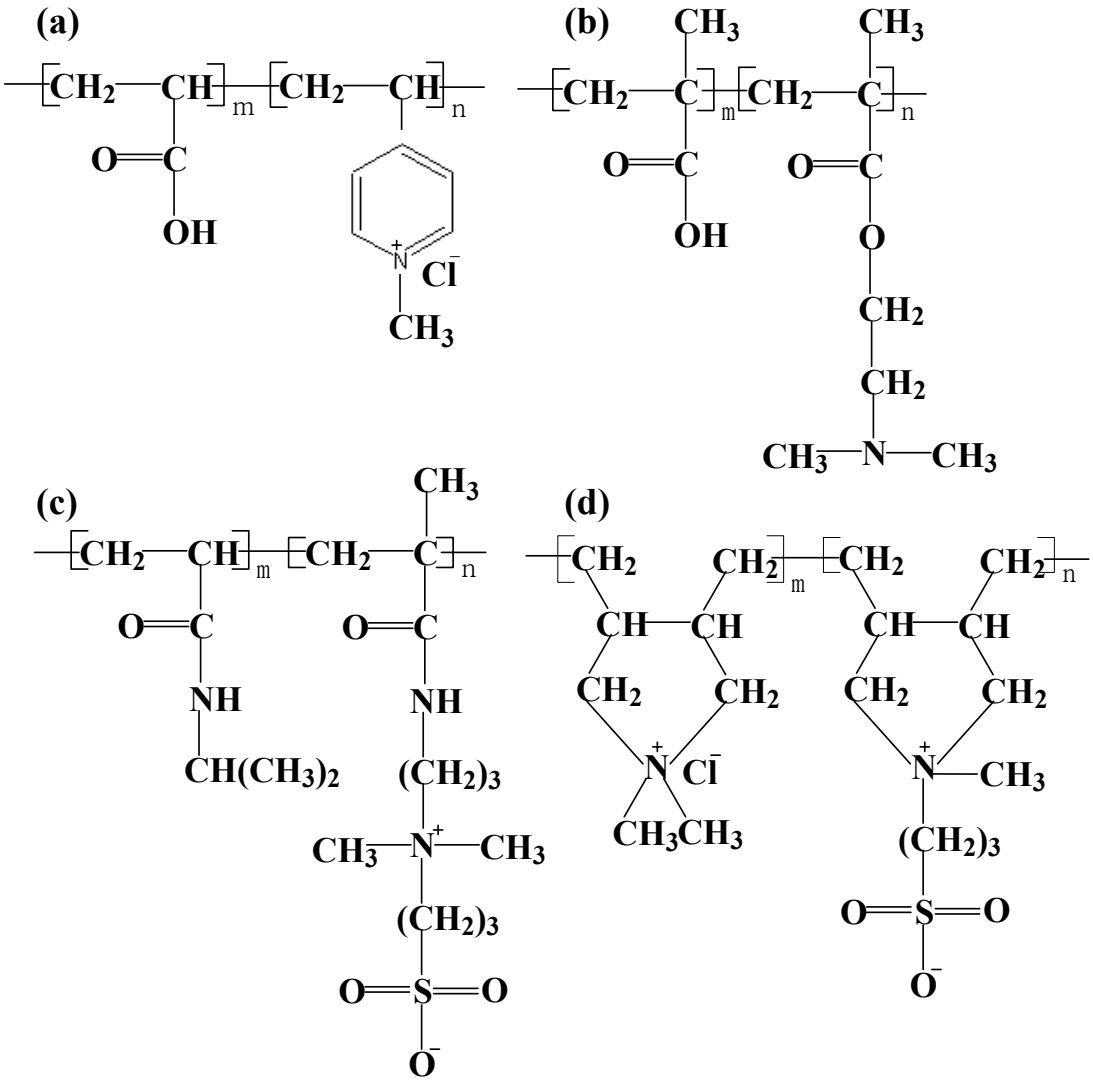

Figure 2.5 Chemical structures of PAAc-*b*-PMVP, PMAAc-*b*-PDMAEMA, PNIPAm-*b*-PSPP and PDADMAC-*co*-PDAMAPS

the aqueous solutions of PSPP and PNIPAm homopolymer decreases and increases, respectively, with the solution temperature, and their optical densities reach a plateau when the solution temperature is beyond UCST of PSPP (7^oC) or below LCST of PNIPAm (32^oC). However, optical absorbance of the aqueous solutions of the PNIPAm-b-PSPP copolymer reaches a minimum in the intermediate temperature. It was also found that the reduced viscosity, scattering intensity, polarity and hydrodynamic radii, aggregate size of the copolymer aqueous solution also exhibits a hyperbolically theremoresponsive behavior (Arotcarena *et al.*, 2002).

The hyperbolically electrolyte-responsive copolymers are prepared from the coupling of polyelectrolytes and polyzwitterions. The aqueous solutions of the random copolymer prepared from *N,N*-diallyl-*N,N'*-dimethyl ammonium chloride (DADMAC) and 3-(N,N-diallyl-N-methyl ammonio) propane sulfonate (DAMAPS), the PDADMAC-*co*-PDAMAPS copolymer as shown in Figure 2.5(d), exhibit a combination of polyelectrolyte effect and *anti-polyelectrolyte effect*, especially in the reduce viscosity. As the PDADMAC segments dominate the copolymer, the copolymer aqueous solution behaves in a polyelectrolyte pattern, and the reduced viscosity decreases with the addition of electrolyte. On the other hand, for the copolymer with a majority of DAMAPS segments, the reduced viscosity of their aqueous solution enhances with the addition of electrolyte. The hyperbolically electrolyte-responsive behavior emerges only on the copolymer with comparable DADMAC and DAMAPS segments. The reduced viscosity of their aqueous solution decreases initially with the addition of electrolyte, followed by an increase as the electrolyte concentration shifts beyond a critical concentration (Armentrout *et al.*, 2000a, Armentrout *et al.*, 2000b). The dynamic light scattering measurement also

confirmed that, as the ionic strength of the medium is increased, the hydrodynamic radii of the PDADMAC-*co*-PDAMAPS copolymers decreases initially, reaches a minimum and increases again gradually (Armentrout *et al.*, 2000b).

2.2 Preparation of Polymer with Grafted Chains

Grafted chains here mean, in general, any regular branched polymer chains. Grafted polymer chains are introduced into the polymer backbones to improve the compatibility and miscibility. The polymer chains can be incorporated into the polymer chains and give rise to a grafted structure *via* (i) reactive coupling/grafting of living polymer chains with side-functional polymer main chains (*grafting onto*), (ii) copolymerization with macromonomers (*grafting through*), and (iii) polymerization initiated from the side functional groups of the main chains(*grafting from*), as shown in Figure 2.5, respectively.

2.2.1 Reactive Coupling/Grafting of "Living" Polymer Chains (g*rafting to*)

Grafting to approach involves the reactions of functional groups alongside the polymer backbone with the end-functional or side-functional groups of another polymer chains. Such reactions include chain transfer, anionic/cationic coupling, and other organic group reactions.

Chain Transfer of propagating radicals or macroradicals to polymer chains could generate a grafted structure (Russell, 2002). Such chain transfer can be initiated from chemical initiator, irradiation, thermal induction and metal salts (Boutevin, 2000).

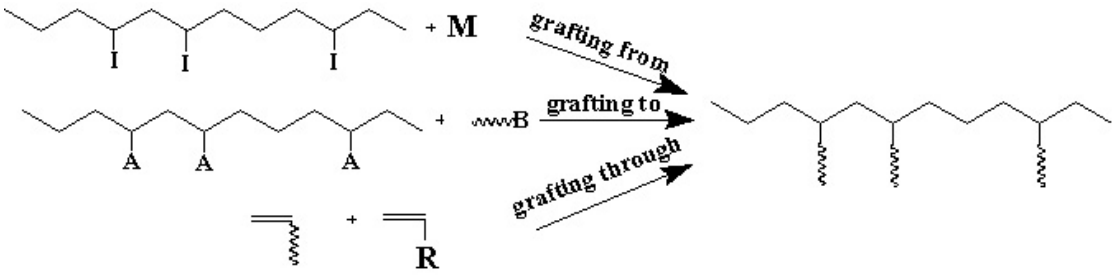

Figure 2.6 Schematic illustration of *grafting from*, *grafting to* and *grafting through* approaches to produce graft copolymer.

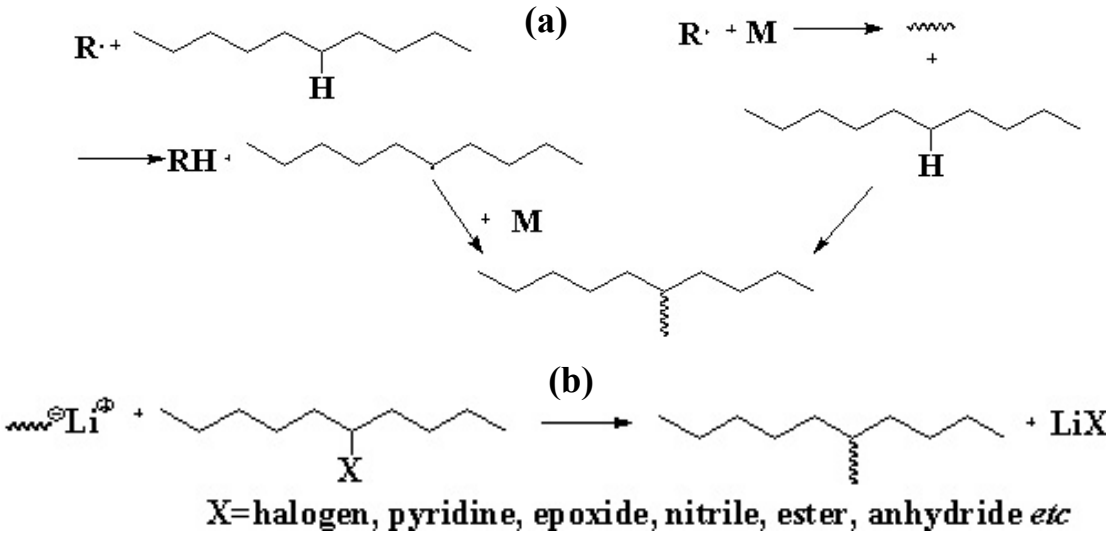

Figure 2.7: Chain transfer process and reactive coupling of anionically living polymer with side-functional polymers to produce graft copolymers.

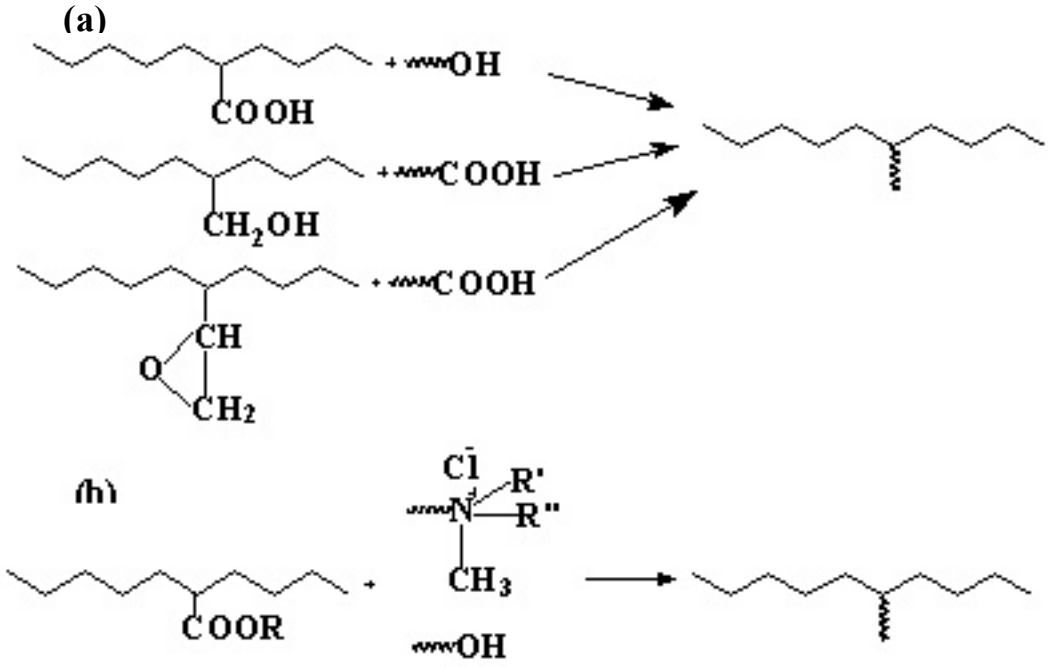

Figure 2.8: Esterification and transesterification reaction to produce graft copolymers.

Such a process is intensively used in the reactive processing of the polymer blend, as the graft copolymer formed *in situ* could promote the compatibility (Moad, 1999). For instances, the telomerization of vinylic monomers was performed on the PVDF-*co*-PTFE copolymer chains, leading to a grafted structure (Wang *et al.*, 2004). The co-extrusion of peroxide-pendant polystyrene (PS) with polyethylene (PE) at high temperature leads to the PS-*g*-PE graft copolymer as a result of the chain transfer of the PS macroradicals to the PE chains (Yamamoto *et al.*, 1991). The extrusion of PE (Yang *et al.*, 2003; Navarre, 2000), polypropylene (PP) (Liu *et al.*, 1993; Cartier, 1998), polyester (Mani *et al.*, 1999), with vinylic monomers in the presence of free radical initiators also leads to the graft copolymer. Free radicals can abstract the hydrogen from the silylmethyl groups of poly(dimethylsiloxane) (PDMS), to produce the copolymer with inorganic backbone and organic side chains (Okaniwa, 1997). Such a chain transfer process is in principle shown in Figure 2.7(a).

Anionic Coupling occurs between the living anionic polymer and other polymers with side-functional groups, including anhydride, ester, benzylic halides, nitrile, expoxide and pyridine groups (Teertstra, 2004; Bywater, 1975), as shown in Figure 2.7(b). Living anionic PS-Li had been intensively utilized to create such graft structures. For examples, the coupling between PSLi with chloromethylated or acetylated PS had given rise to the PS homopolymer with graft structures, and graft density can be controlled by the degree of chloromethylation or acetylation, respectively (Gauthier, 1991; Gauthier *et al.*, 1996; Li, 2001). This strategy had also been implemented to synthesize polystyrene-graft-poly(2-vinylpyridine) (the PS-*g*-P2VP copolymers) (Kee, 2002; Gauthier *et al.*, 2003) and polystyrene-graft-polyisoprene (the PS-g-PiP copolymers) (Kee, 1999; Li *et al.*, 2004). The P2VP-*g*-PiP

and P2VP-*g*-PS copolymers can be simply prepared by the anionic coupling of P2VP with PiP-Li and PS-Li living polymers (Watanabe *et al.*, 1994). A novel strategy to synthesize PiP homopolyme with graft structure involved the hydrosilylation of PiP with chlorodimethylsilane, followed by the anionic coupling with PiP-Li (Hempenius *et al.*, 1997). In addition, PS-Li had also been used to couple with poly(chloroethyl vinyl ether) (PCEVE) to produce the PCEVE-*g*-PS copolymers (Schappacher, 2000; Schappacher *et al.*, 2003; Deffieux, 1999; Muchtar *et al.*, 2001) while the coupling between the partially chloromethylated PS and poly(ferrocenyldimethylsilane) (PFDMS-Li) living polymer leads to the first organic-organometallic graft copolymer, PS-g-PFDMS (Power-Billard *et al.*, 2004).

Cationic Coupling occurs between the living cationic polymers and the side-functional polymer. The poly(ethyleneimine) (PEI) homopolymer was prepared by the coupling of living poly(2-ethyl-2-oxazoline) (PEOX) with deacylated PEOX, followed by the deacylation to give rise a PEI homopolymer with a graft structure (Tomalia *et al.*, 1991).

Other organic group reactions among the side-functional groups of the polymer backbone and end-functional groups of the graft polymers are most widely studied coupling approaches because of their versatility. It covers *esterification*, *transesterification*, *amidization*, *imidization etc*.

Esterification: for examples, hydroxyl-terminated polymer can be readily *grafted onto* the PAAc chains *via* esterification (Poe, 2004). The telechelic poly(methyl methacrylate) PMMA (PMMA-COOH) was grafted onto the polyethylene-co-

poly(glycidol methacrylate) (PE-*co*-PGMA copolymer) chains also through the esterification reaction of the PMMA chains and the GMA repeat units (Kwak *et al.*, 2003). Similarly, PS-COOH was also grafted onto the PMMA-*co*-PGMA chains *via* the esterification between the PS end functionality and the epoxy group (Kim *et al.*, 2003). This process was illustrated in Figure 2.8 (a).

Transesterfication: for instance, the poly(tetrahydrofuran) (PTHF) with quaternary ammonium end functionality can be grafted onto PMMA chains to produce PMMA-g-PTHF as a result of *transesterification* reaction (Tong *et al.*, 2001). It can also occur between ester and hydroxyl groups, by blending ethylene-methyl acrylate copolymer (PEMA copolymer) and hydroxylated PS at high temperatures, to obtain PEMA-*g*-PS (Hu, 1995). The transesterification reaction to produce graft copolymer is shown in Figure 2.8(b).

Amidization: for instance, the polyurethane (PU) with peptide side chains can be synthesized from the coupling reaction of carboxylated PU and peptide *via* amidization reaction (Lin *et al.*, 1992).

Imidization: the graft structure can be formed between amine-functionalized polymers and maleic anhydride-containing polymers. Such protocol had been adopted on grafting of polyamide onto PS (Dedecker, 1999), styrene-acrylonitrile copolymer (Takeda, 1992), ethylene - propylene rubber (Marechal *et al.*, 1995) and PP (Liu *et al.*, 2001), grafting of PS with ethylene-propylene rubber (Dharmarajan, 1992) and grafting poly(ethylene oxide) (PEO) onto styrene-maleic acid copolymer (Eckert, 1996).

2.2.2 Molecular Graft Copolymerization (*grafting from*)

Grafted polymer chains can also be introduced into the polymer *via* the "*grafting from"* approach. Monomers with functional terminal functionality were homopolymerized or copolymerized to produce the linear (co)polymers, followed by the graft polymerization initiated from the side-functional groups. For some initiator-monomer or inimer, they could produce the graft structure directly from their polymer. For some existing polymers, it is also possible to introduce initiator moiety by post-polymerization treatment of the polymer chains for the subsequent graft copolymerization. Various approaches had been adopted to *graft-copolymerize* polymer chains *from* the backbone chains.

Genuine and *Pseudo Inimer-involved Copolymerization*

AB* inimers refer to the monomers with initiator moieties (Mori H., 2003). The copolymers prepared from inimers have functional pendant groups which can initiate another polymerization to produce the graft structure directly, so it was termed as ***genuine*** *inimer-involved copolymerization*. On the other hand, for the polymer with functional side chains, chemical reactions were undertaken to transform them to be initiation-capable, or ***pseudo*** *inimer-involved copolymerization*. Both genuine and pseudo inimer-involved copolymerization are schematically shown in Figure 2.9.

Conventional Free Radical Polymerization is initiated by chemical initiators, such as azo, peroxide, perester etc. A typical strategy is to prepare a linear polymer from

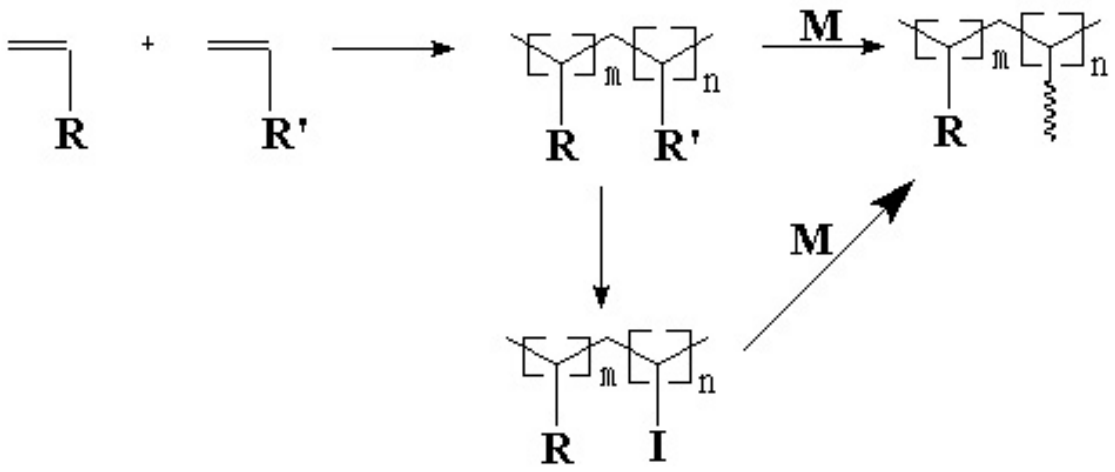

Figure 2.9: Inimer-involved copolymerization to produce graft copolymers

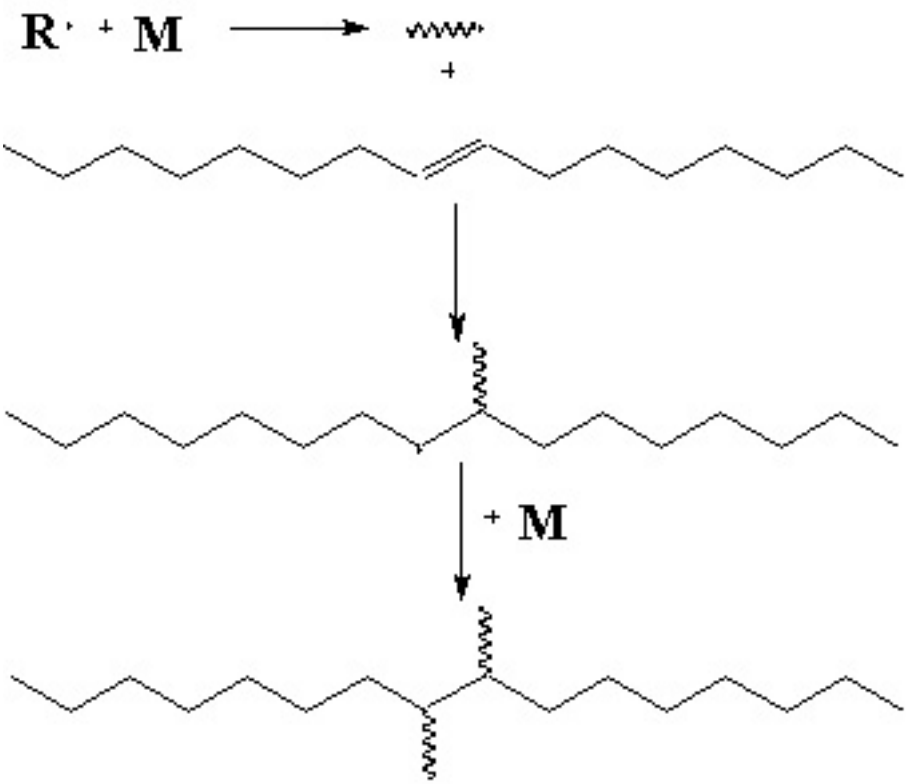

Figure 2.10: Utilizing the backbone unsaturations to produce graft copolymers.

monomers with peroxide pendant group, followed by graft copolymerization of vinyl monomers to produce graft structure (Yamamoto *et al.*, 1991).

Atom Transfer Radical Polymerization can be initiated by pendant alkyl halide moiety to produce the graft copolymer. PE polymer contains pendant bromoisobutyryl groups, which initiate the ATRP of styrene to form the PE-g-PMMA graft copolymer (Inoue *et al.*, 2004).

Cationic Polymerization can also be initiated from the alkyl halide. Specific moieties had been introduced into the polymer chains as the pendant groups to initiate the subsequent cationic ring-opening polymerization (Aoi, 1996). For example, PiB-*co*-PVBC copolymers have chloromethyl pendant groups alongside the chains, which could initiate both cationic polymerization of 2-substituted 2-oxazoline (Grasmuller *et al.*, 1998) and isobutene (Schafer *et al.*, 2002) to produce the graft copolymers.

Anionic Polymerization is suitable for the polymer with pendant aromatic groups. Initiators are formed after the lithiation of these aromatic rings, followed by the polymerization to create grafted polymer structure. Styrene or methylstyrene had been copolymerized with ethylene and propylene *via* metallocene copolymerization to produce the PE and PP copolymer with phenyl rings, followed by lithiation and anionic living polymerization of MMA, styrene, methylstyrene (Chung, 2000; Chung, 2002). *Anionic ring-opening polymerization* is proposed for the cyclomonomer such as ε-caprolactone. Samarium poly(oxamide) has in-chain *N*-anions, which could initiate the anionic ring-opening polymerization to produce poly(ε-caprolactone) (PCL) as the graft chains (Wang *et al.*, 1996).

Stable free radical polymerization, especially the *nitroxide-mediated polymerization*, is another controlled radical polymerization techniques (Hawker *et al.*, 2001). Nitroxide vinylic monomers can be copolymerized with ethylene *via* the metallocene-catalyzed polymerization to produce copolymer chains with nitroxide pendant groups, which could initiate the nitroxide-mediated polymerization to produce the graft copolymers (Bowden *et al.*, 2002).

Backbone unsaturation, the C=C double bond alongside or on the chains, could also be utilized to form the graft structures, as shown in Figure 2.10. Bifunctional monomers can be copolymerized to form the linear chains with unsaturation residues, and polymer chains can be grafted through copolymerization with these unsaturation residues. The terpolymer from ethylene, propylene and norborene-functionalized ethylene have norborene groups as the pendant groups, and the PP chains can be grafted onto termpolymer chains *via* cationic polymerization through the norborene functionalities (Lohse *et al.*, 1991). Polybutadiene (PBD) has pendant or in-chain vinyl groups, which can copolymerize with styrene, MMA to produce PBD-*g*-PS and PBD-*g*-PMMA graft copolymer (Huang, 1995). PBD, PiP, PS and poly(methylstyrene) can also be *metalation-graft*ed *via* anionic polymerization with MMA (Chung, 2000; Chung, 2002). The C=C double bond of ethylene-propylene-diene terpolymer(EPDM) copolymers can be hydroborated, followed by oxidation to introduce the peroxide functionalities, where the graft copolymerization was undertaken to produce the EPDM-*g*-PMMA graft copolymer (Chung *et al.*, 1994).

Ozone pretreatment is a general strategy for those chemically inert polymers, such as PVDF, PE, EVA and PI, because few chemical transformations could be performed on their chains to introduce initiator moiety (Robin, 2004). Thermally labile peroxides were introduced onto the polymer backbone during the ozone pretreatment of those polymers in solution. Thermally-induced graft copolymerization of specific monomers had been undertaken on the ozone-pretreated polymer chains, leading to corresponding graft copolymers.

2.2.3 Copolymerization with Macromonomers (*Grafting through*)

Macromonomers are any telechelic polymer or oligomer with a polymerizable functionality. Copolymerization of macromonomers with conventional monomers results in a grafted structure (Ito, 1999).

PEO macromonomers had been extensively utilized as they can readily form graft copolymers with hydrophilic and biocompatible properties. The copolymerization of NIPAm, *N*,*N*-diethylacrylamide (DEAm) and poly(ethylene glycol) methacrylate (PEGMA) was performed to produce PNIPAm-*g*-PEO and PDEAm-*g*-PEO graft copolymers, respectively (Schmaljohann *et al.*, 2003). PEGMA has also been copolymerized to obtain PMAAc-*g*-PEO (Kim, 2003), PMMA-*g*-PEO (Capek, 1999), PS-*g*-PEO (Capek, 1999), PBMA-*g*-PEO (Kawaguchi *et al.*, 1995) and PAAm-*g*-PEO (Xiao *et al.*, 1995), respectively.

PMMA macromonomer is another series of vinylic monomers with a long chain as substituent (Xie *et al.*, 1991). PMMA homopolymer with a grafted structure can be

realized by the copolymerization of MMA with PMMA macromonomer (Moad *et al.*, 1996). PMMA macromonomer had been copolymerized with MMA and 2-hydroethyl methacrylate (HEMA) to form the PHEMA-*co*-PMMA-*g*-PMMA graft copolymer (Fujioka *et al.*, 2003).

Telechelic poly(2-alkyl-2-oxazoline) can be ring-opening polymerized into macromonomers with various end functionalities (Shimano *et al.*, 1995). These macromonomers had been copolymerized with styrene, vinyl acetate, to produce graft copolymers (Uyama *et al.*, 1993).

2.3 Incorporation of Grafted Chains onto Substrate Surfaces

Most substrate surfaces are hydrophobic and chemically inert, which may limit their utility. Surface modification by grafting polymer chains is a new technology to promote the surface properties, including adhesion, biocompatibility, hydrophilicity, antistatics, lubrication, antibiotics (Ikada, 1994; Uyama *et al.*, 1998; Kato *et al.*, 2003). The grafted polymer chains can be introduced onto the substrate surface *via* several approaches similar to those adopted for polymer chains, *viz*. surface grafting of "living" polymer chains (*grafting onto*) and surface-initiated polymerization (*grafting from*), as shown in Figure 2.11, respectively. Substrates involved included organic polymers and inorganic materials, such as silicon gel and gold.

2.3.1 Surface Coupling/Grafting of "Living" Polymer Chains

Similar to the coupling with the side-functional polymers, the surface coupling with "living" polymer chains can be realized *via* active intermediate coupling, chain transfer, organic reaction and chain transfer with polymer chains. However, the strategy is dependant on the chemical nature of the substrates.

2.3.1.1 Reactive Coating on Organic Polymer Substrates

Organic polymer substrates can undergo various organic reactions to immobilize the reactive polymer chains, including active coupling, chain transfer and group reaction.

Active coupling occurs between the active or living polymers and the substrates. Such active groups include carbene, nitrene and carbocation. For examples, azide groups ($-N_3$) can decompose to nitrene (-N:) under UV irradiation or thermal induction to insert into the C-H bond (van der Heiden, 1996), as shown in Figure 2.12. After pretreatment with azide-containing silane, the silica gel was grafted with PS under UV irradiation, leading to a silica gel with a thin layer of PS film (Yan, 2004). This strategy is also adopted to prepare the surface-grafted PET film via the active coupling of PET with carbene-, nitrene-, and carbocation-functionalizd polymer (Ziani-Cherif *et al.*, 1999).

Chain transfer of propagating radicals occurs not only on the polymer chains, but also polymer substrate surfaces, which allows the surface photo-polymerization. In the photo-polymerization, the photo-initiator, under UV irradiation, decomposes into free radicals, which propagate and chain-transfer to the polymer surface to produce

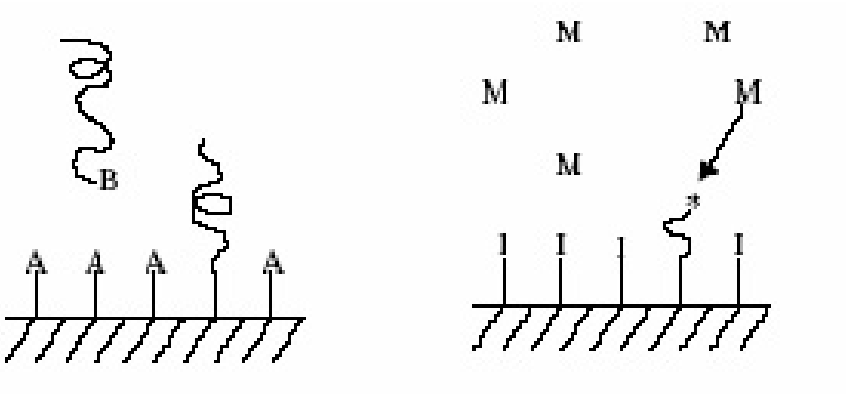

Figure 2.11: Schematic illustration of *grafting to* and *grafting from* approaches to surface with graft polymer chains.

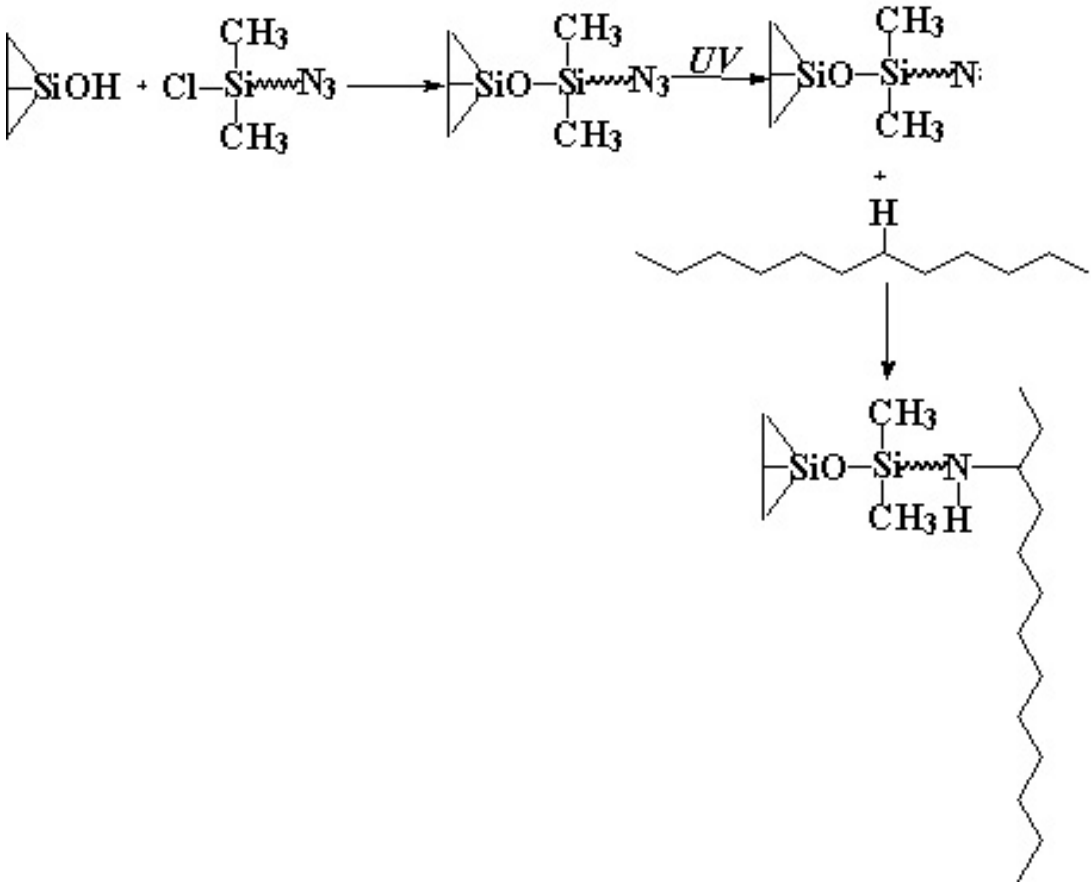

Figure 2.12: Active coupling of nitrene with polymer chains to produce surface-grafted polymer chains.

the grafted structures (Ranby, 1999). The substrates suitable for the photo-polymerization cover PAN (Jimbo *et al.*, 1998), PE (Matsumoto *et al.*, 2002), PVDF (Sergeyeva *et al.*, 2001), PP (Xu *et al.*, 2004), poly(vinylchloride) (PVC) (Decker, 1998).

Other organic reaction, such as esterification and amidization could also be utilized to form the graft structure on the organic substrate.

Esterification: for example, after the anionic ring-opening copolymerizatin, the carbon whisker had been coated with a layer of epoxy and cyclic anhydride copolymer. The esterification occurs among the surface polymer layer and the end functionalities of polyester, leading to a polyester layer grafting onto the carbon whisker surface (Tsubokawa, 1993a)

Amidization: for example, PEI had been immobilized onto the carboxylic acid-containing PET film, *via* the amidization reaction, to obtain a PET-*g*-PEI film surface (Kingshott *et al.*, 2003). The NH_2-terminated poly(tert-butyl acrylate) (PtBA) can be grafted onto the carboxylic acid-functionalized gold, aluminum, silicon, and polyethylene surfaces, to produce the surface-attached PtBA graft chains (Tao *et al.*, 2001).

2.3.1.2 Reactive Coating on Inorganic Substrates

In comparison to organic polymer, less organic reactions can undergo on such inorganic substrates as silicone materials, carbons, metal oxides and gold. Fortunately,

there are some special bondings between the inorganic substrate and other functional groups, which could be utilized for the polymer grafting.

For silicone materials, such as silica, glass and Si/SiO_2 wafer, they contain the surface precursor, silanol functional group, which could undergo sol-gel process with silane to immobilize the telechelic polymer onto the substrate surface. As shown in Figure 2.14, the polymer with end functionalities of trichlorosilane group (Tran, 2001), monochlorosilane (Reiter *et al.*, 1996), silanol (Auroy *et al.*, 1991) and trialkoxylsilane (Sakai K., 2003) had been immobilized onto the silicone materials surface through Langmuir-Blodgett (LB) Film or self-assembly monolayer technique. Both linear and dendritic polymer could be immobilized to design and improve the surface properties. Silicone materials could also be pretreated to introduce some functional groups, and thus, the end-functional polymer can be immobilized by the typical organic reaction. Cationic living polymer can couple with amine-terminated silica surface to produce surface grafted poly(isobutyl vinyl ether) (PIBVE) and poly(2-methyl-2-oxazoline) (PMOX) chains on silica surface (Tsubokawa, 1995).

Au can form stable covalent bond with sulfur species, which had been well adopted to immobilize the thiol- or disulfine-functionalized polymer onto Au particles (Heinz *et al.*, 2000; Thomas, 2003; Zhu *et al.*, 2004). The RAFT process, using the dithioester as the chain transfer agent, can produce the dithioester-terminated polymer, which could be reduced to thiol (Lowe *et al.*, 2002; Zhu *et al.*, 2004), as shown in Figure 2.15.

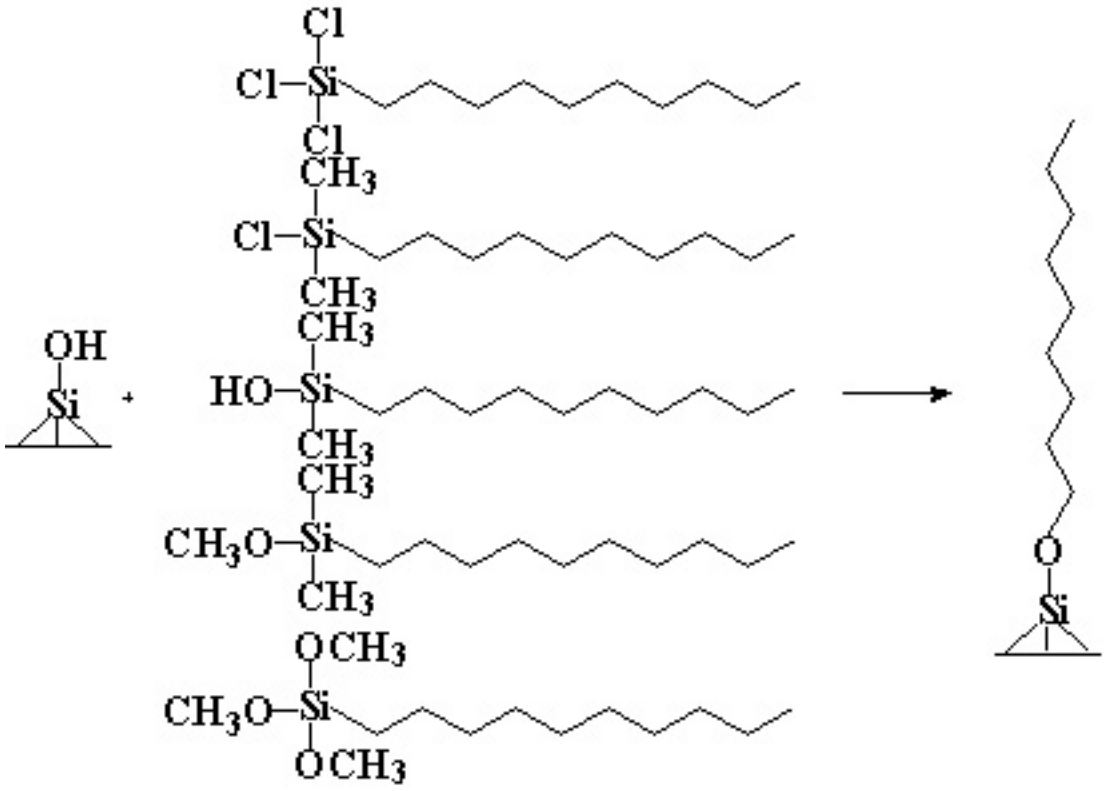

Figure 2.13: Reactive coupling of silicone-based substrates with silane-terminated polymers to produce surface-grafted polymer chains.

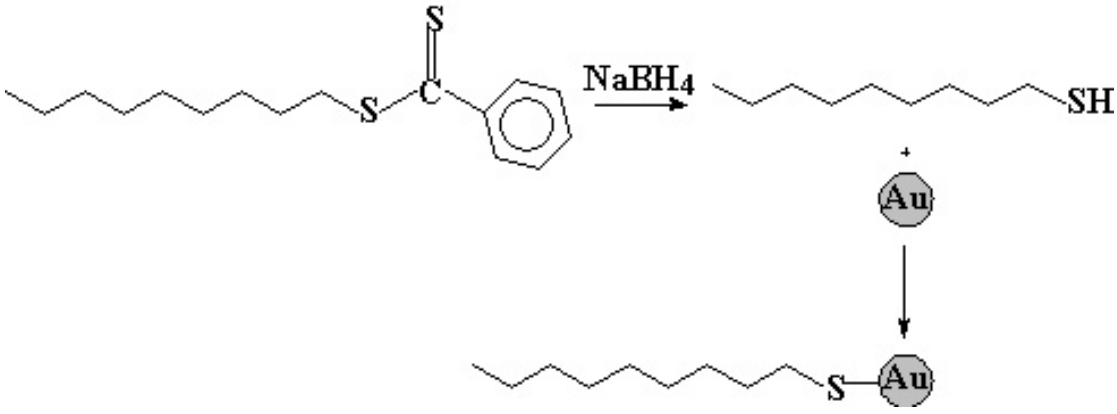

Figure 2.14: Reduction of RAFT-prepared polymer into a thiol-terminated chain to produce Au-immobilized polymer chains.

The strategy for metal oxide particle, such as Fe_2O_3, TiO_2, Al_2O_3, to intoruduc the graft chains is quite similar as that of silica gel. The metal oxide surfaces contain the hydroxyl groups, which could be utilized for the immobilization of the end-functional polymer. The end functionality involved may include trialkoxylsilyl (Takafuji *et al.*, 2004) and carboxylate acid (Tannenbaum *et al.*, 2004).

2.3.2 Surface-Initiated Polymerization (*Grafting from*)

Surface-initiated polymerization (SIP) of functional monomers can be implemented on those surfaces with initiator moiety. They are only a few substrates which contains initiator moieties originally. Most substrates have to be pretreated to introduce initiator, prior to the surface-initiated polymerization. So the emphasis of this part is on the strategy of immobilizing or introducing the initiator onto the surface. Because of the difference in their chemical nature, the strategies on polymer substrates and inorganic substrates are presented individually.

2.3.2.1 Surface-Initiated Polymerization on Organic Polymer Substrates

Generally, most of polymer substrates have inert surfaces, while some of them contain surface reactive groups. For the surface-inert polymer substrates, *surface pretreatment* is necessary to create the active sites for the SIP.

Surface pretreatment is suitable to introduce the active sites onto the chemically inert flat substrates by ozone pretreatment (Karlsson J. O., 1999), electron beam bombardment (Zouahri, 1996), ion beam (Lau, 1997), ion irradiation (Bhattacharya,

2000), plasma discharge (Kato *et al.*, 2003), γ-rays treatment (Chauhan *et al.*, 2000), and laser treatment (Saito *et al.*, 1997), as shown in Figure 2.16(a). After these surface pretreatments and subsequent exposures to atmosphere, the thermally labile peroxide and hydroperoxide groups are formed on the surfaces, which could undergo thermal decomposition to initiate free radical polymerization to introduce the polymer graft chains onto the substrate surface. These substrates may include fluoropolymer (Kang, 2000; Forsythe, 2000; Dargaville *et al.*, 2003), polyester (Saito *et al.*, 1997), PP (Singh, 1992), PE (Bergbreiter, 1994), polythiophene (PTH) (Kang et al., 1992), polycarbonate (PC) (Chen et al., 1998), PI (Inagaki *et al.*, 1996) and poly(aramide) (Mori *et al.*, 1994).

Unsaturated polymer substrate surfaces may deteriorate the thermal and chemical stability. However, they can also be functionalized to introduce the initiator moieties, as shown in Figure 2.16(b). For example, unsaturations on the PE, PVC and PP film surfaces can be hydroborated to create C-B bond, where oxygen can insert into to generate peroxide functionalities. The subsequent polymerization of vinyl monomers can produce surface graft structure (Bergbreiter *et al.*, 1994). This strategy had also been applied on the molecular graft copolymerization of PBD and PiP.

For the amine- or hydroxyl-functionalized substrates, azo or C-X moiety can be immobilized *via* amidization or esterification to initiate conventional free radical polymerization (Sugawara, 1994) or ATRP, respectively.

For hydroxyl-containing carbohydrate polymers, such as cellulose (McDowall *et al.*, 1984), polysaccharides (Berlin, 1992), dextrin (Chauvierre *et al.*, 2003) and PVA

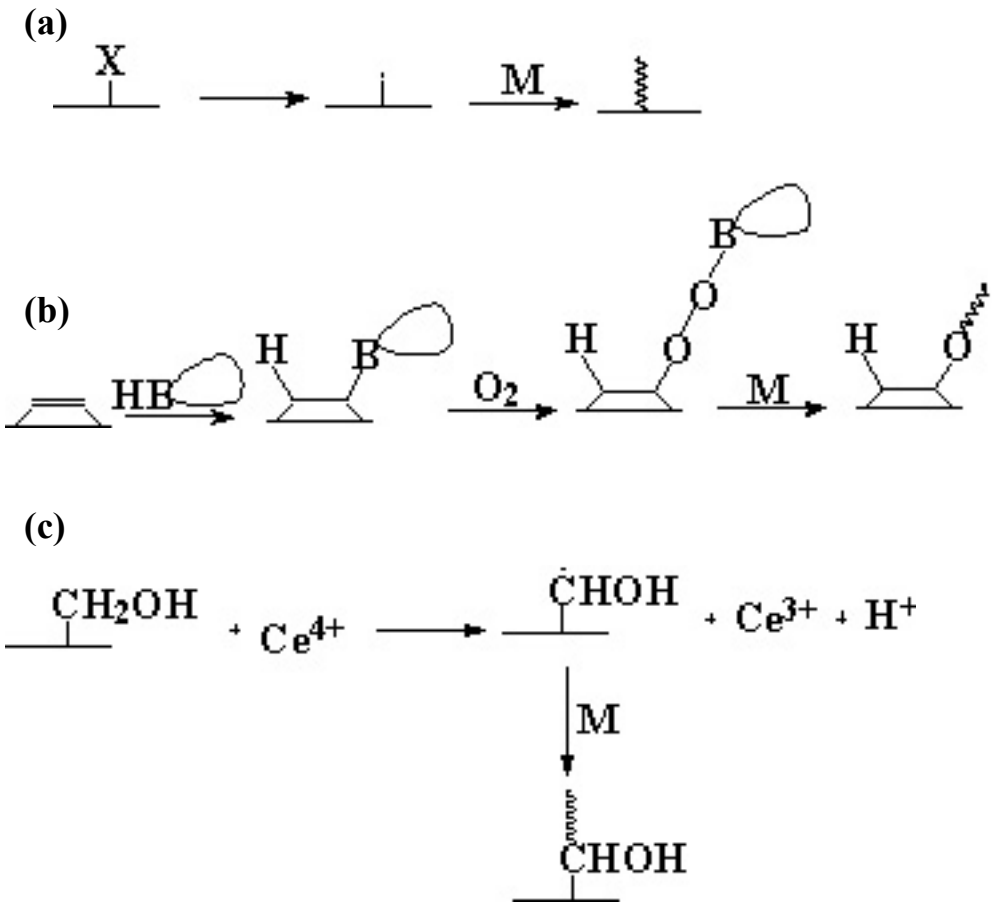

Figure 2.15: Three widely adopted strategies to prepared surface grafted with polymer chains.

film (Matsuda *et al.*, 1996), Ceric(IV) ion can be used to oxidize the hydroxyl groups into free radicals to initiate the polymerization and produce the surface-grafted polymer chains, as shown in Figure 2.16 (c). On the other hand, hydroxyl groups on the chitin can also be tosylated to introduce the thiol groups, which could initiate the polymerization of styrene to produce the surface-grafted PS chains (Kurita *et al.*, 1996).

The photolysis of polyesters, such as poly(ethylene terephthalate) (PET) and poly(butylene terephthalate) (PBT) had been well studied, as the ester groups could be involved in photolytic reaction to generate free radicals (Yagci, 1990). On the other hand, such photolysis reaction can be utilized to surface-initiate the free radical polymerization of hydrophilic monomers MAAc (Uchida *et al.*, 2000), PEGMA (Uchida *et al.*, 1994), AAc and DMAEMA (Zhang *et al.*, 1995) in the absence of a photoinitiator.

Although most surface-initiated polymerizations were conducted in a radical fashion, there are still some reports on the surface-initiated ionic polymerization. For instances, poly(glycolic acid) (PGLA) powders contains the carboxylic acid groups on the surface, which were found to initiate the cationic polymerization to produce surface-attached chains (Tsubokawa *et al.*, 1993b).

For some other substrates, they could be photo-oxidized or photo-reduced to incorporate the peroxide groups onto the surface under the UV–irradiation. The functionalized substrate surface could initiate the thermally-induced free radical

polymerization. These substrates include PCL (Zhu et al., 2002), poly(L-lactic acid) (PLLA) (Ma et al., 2003), and PTFE (Noh, 1997).

2.3.2.2 Surface-Initiated Polymerization on Inorganic Substrates.

The inorganic substrates involve silica, silicone wafer, glass bead, carbon, gold and metal oxide etc. The initiators can be introduced onto the inorganic substrate surface via surface pretreatment, organic reaction, and self-assembled monolayer techniques. The surface-initiated polymerization of the functional monomers on the inorganic substrate will produce the organic/inorganic composite or hybrid (Pyun, 2001).

Surface pretreatment, especially plasma pretreatment, can also be used on silicon wafer, followed by the conventional radical polymerization (Zhang *et al.*, 1999), in a similar approach to that of organic polymer substrates.

Some inorganic substrates, such as *silicon wafer*, *silica particle* and *glass*, contain surface silanol functionalities (*Si-OH*). Although there are reports on the in situ formation of azo initiator on the silica surface to form surface graft structure (Prucker, 1998), it is more convenient to immobilize the initiator monolayer through self-assembly technique.

Silanol functionality can directly be involved in the immobilization of initiator SAM, which could initiate the subsequent SIP (Ejaz, 2001). Therefore, it is the functionality in the coupling agent that determines the SIP strategy. Silanol can

undergo the sol-gel process with silane to immobilize the initiator SAM. For example, the isocyanate group was introduced onto the silica and glass surface, followed by the imidization of carboxylic acid-terminated azo initiator, which initiates conventional free radical polymerization (Tsubokawa *et al.*, 1994; Fujiki *et al.*, 1999). Hydroxyl-terminated silane coupling agent was immobilized to form a hydroxyl-terminated surfaces, initiating the ring-opening polymerization of L-lactide to produce a Si-g-PLLC substrate (Choi, 2001). Silica particle was functionalized with NH_2-containing silane, followed by the immobilization of azo initiator SAM through the amidization reaction. The azo SAM can initiate the free radical graft polymerization of styrene and *N*-vinylimidazole from the silica surface (Chen *et al.*, 1991). After coupling with 2-bromoisobutyryl-containing silane, the surface-initiated ATRP occurs readily on silica (Granville *et al.*, 2004). After coupling with an iniferter-functionalized trimethoxylsilane, the silicon wafer can initiate the the "living" photo-polymerization to produce Si-g-PMMA and Si-g-PS (de Boer *et al.*, 2000). After coating with a trichlorosilane containing an organometallic head group, the ring-opening metathesis polymerization (ROMP) could occur on the silicon wafer surface to produce a Si-g-polynorborene surface (Harada *et al.*, 2003). After coating with nitroxide-functionalized silane, the silica (Bartholome *et al.*, 2003) and silicon wafer (Husseman M., 1999) can inititiate the stable free radical polymerization to produce the surface attached PS polymer chains.

In addition to the silanol, other precursor can be formed on the silicon substrate surface, such as Si-H (Buriak, J. M., 2002). Si-H bond can couple with the C=C double bond to undergo the hydrosilylation reaction, resulting in the formation of the initiator SAM for the subsequent SIP (Yu, 2003).

The silicates or clay particles contain net positive charges, and thus the initiator with the ionic head groups can be immobilized onto the surface via the electrostatic attraction. This strategy had been adopted to immobilize 1,1-diphenylethylene (DPE) functionality for anionic living polymerization (Fan *et al.*, 2002) and bromoisobutyryl for ATRP (Zhao, 2003).

Complexation between Au and thiol had been extensively used to immobilize the initiator SAM on Au substrates (Ulman, 2001; Shenhar, 2003). Similar to that of silica, the functionality of the coupling agents determines the SIP strategy. For example, Au surface had been coated with thiol containing benzylic amine for initiating the oxidative polymerization of aniline (Sawall *et al.*, 2004) and with hydroxyl and primary C-Br for cationic ring-openign polymerization (Choi, 2001; Rusa *et al.*, 2004) The controlled or living polymerization are also carried out on Au particle surface. For example, Au particle had been coated with thiol containing a tertiary C-Br moiety for ATRP (Ma *et al.*, 2004; Brantley, 2004), containing a dithioester functionality for the RAFT process (Raula *et al.*, 2003) and with a diphenylethylene (DPE) (Advincula *et al.*, 2002) or bromobenzene (Jordan *et al.*, 1999) for anionic living polymerization. In addition, the thiol containing azo moiety could be coated onto the Au surface for conventional photopolymerization (Paul *et al.*, 2002) and thermal polymerization (Huang *et al.*, 2001), respectively.

Similar to the *"grafting from"* approach of metal oxide substrates, the initiator SAM was immobilized onto the metal oxide substrates for the subsequent SIP through the reaction of trichlorosilane (Marutani *et al.*, 2004), phosphoric acid (Matsuno *et al.*,

2004), trimethoxylsilyl (Huang *et al.*, 2001), carboxylic acid (Li *et al.*, 2004; Vestal, 2002). The typical SIP strategy on metal oxide substrates includes ATRP (Marutani *et al.*, 2004; Vestal, 2002; Li *et al.*, 2004), nitroxide-mediated polymerization (Matsuno *et al.*., 2004) and conventional thermal polymerization (Huang *et al.*, 2001).

The SIP on CdSn nanoparticle surface had also been studied. CdSn surfaces can be activated by phosphorine oxide. After coating of phosphorine oxide with nitroxide and metallocene functionalities, CdSn can undergo the nitroxide-mediated polymerization of styrene (Sill, 2004) and the metallocene-catalyzed ROMP of cyclic olefins (Skaff *et al.*, 2002).

Chapter 3:

pH-Sensitive Microfiltration Membrane from Poly(Vinylidene Fluoride) With Grafted 4-Vinylpyridine Polymer Side Chains

3.1 Poly(vinylidene fluoride) with Grafted 4-Vinylpyridine Polymer Side Chains for pH-sensitive Microfiltration Membranes

3.1.1 Experimental

3.1.1.1 Materials and Reagents

Poly(vinylidene fluoride) (PVDF, Kynar K-761) powders (MW=441,000) were obtained from Elf Atochem of North America Inc. The solvent, *N*-methyl-2-pyrrolidone (NMP, reagent grade) was obtained from Merck Chemical Co. They were used as received. The monomer, 4-vinylpyridine (4VP) of 95% in purity and purchased from Aldrich Chemical Company of Milwaukee, WI, USA, was distilled under reduced pressure before use.

3.1.1.2 Ozone Preactivation of PVDF and Thermally-Induced Graft Copolymerization of 4VP with the PVDF (the PVDF-*g*-P4VP Copolymer)

PVDF powders were dissolved in NMP to form a 7 wt% solution. A continuous O_3/O_2 mixture stream was bubbled through 30 ml of the PVDF/NMP solution at room temperature (~25^{o}C) for about 15 min. The O_3/O_2 mixture stream was generated from an Azcozon RMU16-40EM ozone generator. The flow rate was adjusted to 300 L/h to result in an ozone concentration of about 0.27 g/L in the gaseous mixture. After the ozone preactivation, the polymer solution was cooled in an ice bath. An argon stream was introduced for about 30 min to degas the ozone and oxygen dissolved in the solution.

The 4VP monomer and NMP solvent were then added to achieve a specific [4VP]/[-CH_2CF_2-] molar feed ratio and to adjust the total solution to 40 ml. After an additional 15 min of argon purging, the temperature of the water bath was raised to 60^{o}C to induce the decomposition of peroxide groups on the PVDF chains and to initiate the graft copolymerization of 4VP. During the 4-h of thermal graft polymerization, a constant flow of argon was maintained. After the reaction, the

reaction mixture was cooled in an ice bath and the resultant PVDF-*g*-P4VP copolymer was precipitated in an excess amount of absolute ethanol (a good solvent for 4VP and its homopolymer). After filtering, the copolymer was washed in an excess volume of ethanol for 48 h. The solvent was changed every 8 h. The copolymer sample was recovered and dried by pump under reduced pressure for subsequent characterization. The processes of ozone preactivation and thermally induced graft copolymerization are shown schematically in Figure 3.1.

3.1.1.3 Fabrication of the Microfiltration (MF) Membranes

The MF membranes were prepared by the phase inversion technique. The PVDF-*g*-P4VPcopolymer powders were dissolved in NMP to a concentration of 12 wt% at room temperature. The copolymer solution was cast on a glass plate and the glass plate was subsequently immersed in the doubly distilled water. After the membrane had detached from the glass plates, it was extracted in a second bath of doubly distilled water at 70^{o}C for 30 min. This procedure was to stabilize the pore structure and to refine the pore size distribution. The purified MF membrane was dried by pump under reduced pressure for the subsequent characterization. The structure of the MF membranes is also shown schematically in Figure 3.1.

3.1.1.4 Copolymer and Membrane Characterization

The chemical structure of the copolymer was characterized by FTIR. After dispersion in KBr, the FTIR spectra of the homopolymer and copolymer powders were measured on a Bio-Rad FTS 135 FT-IR spectrophotometer. Each spectrum was collected by cumulating 16 scans at a resolution of 8 wavenumbers.

The chemical composition of the copolymer was measured by the elemental

Scheme 1: Ozone Preactivation in NMP

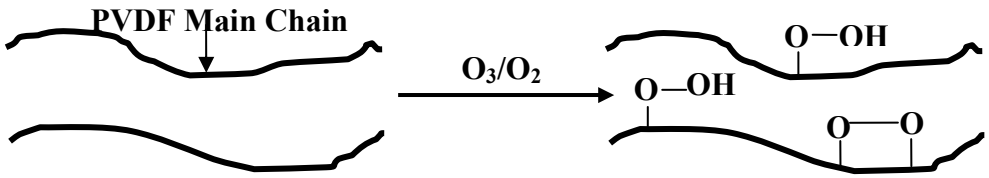

Scheme 2: Thermal Graft Copolymerization (in NMP under argon)

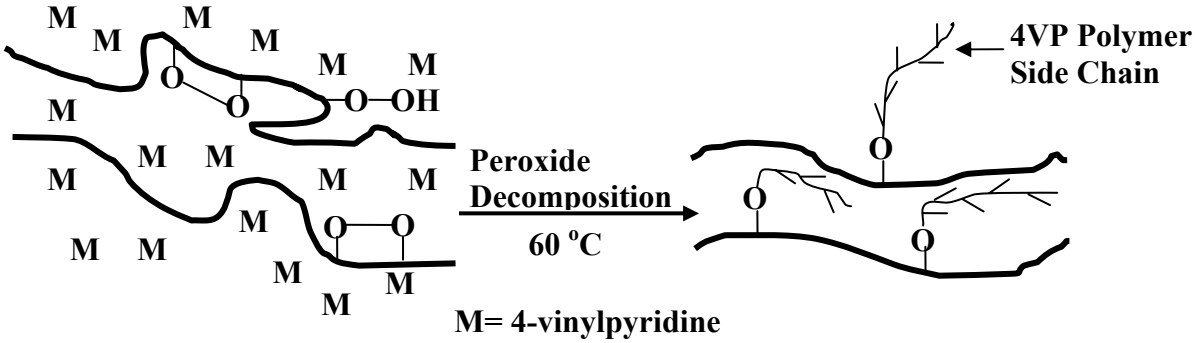

Scheme 3: Membrane Fabrication

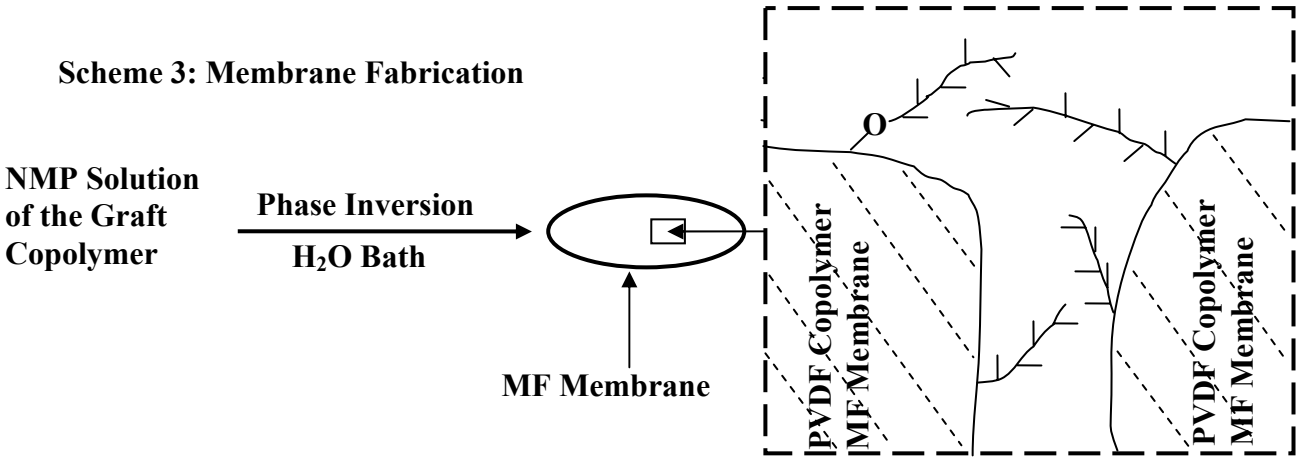

Figure 3.1: Schematic illustration of the processes of thermally-induced graft copolymerization of 4VP on the ozone-preactivated PVDF backbones in solution and the preparation of the PVDF-*g*-P4VP MF membranes by phase inversion.

analysis. The carbon, nitrogen and hydrogen elemental contents were determined using a Perkin-Elmer 2400 element analyzer. Taking into account the stoichiometries of the graft and the fluoropolymer chains, the bulk graft concentration, defined as the number of 4VP repeat units per repeat unit of PVDF, or the $([\text{-4VP-}]/[\text{-CH}_2\text{CF}_2\text{-}])_{bulk}$ ratio, can be calculated from Equation (3.1):

$$([\text{-4VP-}]/[\text{-CH}_2\text{CF}_2\text{-}])_{bulk} = 2[N]/([C]-7[N]) \times 100\% \quad \ldots (3.1)$$

where the factors 2 and 7 are introduced to account for the fact that there are 2 and 7 carbon atoms per repeat unit of PVDF and 4VP polymer, respectively.

The thermal stability of the PVDF-*g*-P4VP copolymers was studied by thermogravimetric analysis (TGA). The samples were heated from room temperature to about 700^{o}C at a rate of 10^{o}C/min under a dry nitrogen atmosphere in a Du Pont Thermal Analyst 2100 system, equipped with a TGA 2050 thermogravimetric thermal analyzer.

The surface morphology of the MF membranes was studied by the scanning electron microscopy (SEM), using a JEOL 6320 scanning electron microscope. The membranes were mounted on the sample studs by means of double-sided adhesive tapes. A thin layer of palladium was sputtered onto the membrane surface prior to the SEM measurement. The measurements were performed at an accelerating voltage of 8 kV.

The pore sizes and the pore size distributions of the PVDF-*g*-P4VP membranes were measured using a Coulter Porometer II apparatus, manufactured by Coulter Electronics Ltd., Buckinghamshire, UK. The commercial product, Porofil®, for the Coulter Porometer instrument was used as the wetting agent.

The surface chemical composition of the membranes was measured by XPS. XPS measurement was made on a Kratos AXIS HSi spectrometer with a monochromatized

Al Kα X-ray source (1486.6 eV photons) at a constant dwelling time of 100 ms and a pass energy of 40 eV. The anode current was 15 mA. The pressure during the analysis was maintained at below 5×10^{-8} Torr. The polymer membranes were mounted on the sample studs by means of double-sided adhesive tapes. The core-level signals were obtained at the photoelectron take-off angle (α, with respect to the sample surface) of 90^{o}. All binding energies (BE's) were referenced to the C 1s hydrocarbon peak at 284.6 eV or the $\underline{C}F_2$ peak of PVDF at 290.5 eV. In peak synthesis, the full width at half maximum (FWHM) of the Gaussian peaks was maintained constant for all components in a particular spectrum. Surface elemental stoichiometries were determined from peak-area ratios, after correcting with the experimentally determined sensitivity factors, and were reliable to $\pm$5%. The elemental sensitivity factors were determined using stable binary compounds of well-established stoichiometries.

For the flux measurement through the PVDF-*g*-P4VP MF Membranes, the PVDF-*g*-P4VP MF membrane was immersed in an aqueous HCl solution of a prescribed pH value for several minutes. It was then mounted on the microfilteration cell (Toyo Roshi UHP-25, Tokyo, Japan). An aqueous HCl solution of the same pH value was added to the cell. Sodium chloride was added to adjust the ionic strength of the aqueous solution to 0.1 mol/L. The flux was calculated from the weight of solution permeated per unit time and per unit area of the membrane surface under a nitrogen atmosphere of 0.03 kg/cm^2.

3.1.2 Results and Discussion

3.1.2.1 Ozone Pre-activation of PVDF and Graft Copolymerization of 4VP with the PVDF (the PVDF-*g*-P4VP Copolymer)

Ozone treatment has been widely adopted to generate the peroxide and hydroperoxide species on polymer chains and surfaces (Ying, 2003; Robin, 2004).

These functional groups can be used to initiate the free radical polymerization of vinyl monomers to produce the graft copolymers. For this and other chain polymerization reactions, in general, the initiator decomposition is the rate-limiting step. The activation energy and Arrhenius coefficient (ln A) for the decomposition reaction of the initiators on the ozone-preactivated PVDF chains are reported to be about 39 kJ/mol and 5.8, respectively (Boutevin *et al.*, 1992). Thus, the value of A is about $330s^{-1}$. Based on these data, the half-life of the peroxide groups at $60^{o}C$ is calculated to be about 45 min. Thus, it is probably sufficient to fix the reaction time at 4 h for the thermally induced initiator decomposition and graft copolymerization in this work. The processes of ozone preactivation, graft copolymerization, and MF membrane fabrication are illustrated schematically in Figure 3.1.

Composition Analyses of the PVDF-g-P4VP Copolymers

In general, the amount of peroxide groups created on the PVDF chains by the ozone pretreatment, or the initiator concentration, depends on the treatment temperature, ozone concentration and treatment time (Fargere *et al.*, 1994). Previous studies had shown that an ozone pretreatment time of 15 min under the present experimental conditions could result in a peroxide content of about 10^{-4} mol per gram of PVDF, as determined by the 2,2-diphenyl-1-picrylhydrazyl (DPPH) assay (Ying, 2003). Excessive ozone pretreatment will lead to the over-oxidation and degradation (scission) of the polymer chains, especially when the treatment time is above 15 min. Thus, the ozone pretreatment time is fixed at 15 min in the present work.

For the graft copolymerization of 4VP with PVDF, the 4VP monomer feed ratio is an important parameter that can be used to regulate the graft concentration. Elemental

analysis suggests that the bulk graft concentration, defined either as the ([-4VP-]/[-CH_2CF_2-])$_{bulk}$ ratio or simply as the ([N]/[C])$_{bulk}$ ratio, increases with the increase in the [4VP]/[-CH_2CF_2-] molar feed ratio used for the graft copolymerization. The bulk [N]/[C] ratio, obtained from the elemental analysis, and the corresponding bulk graft concentration, calculated from Equation (3.1), as a function of the monomer feed ratio ([4VP]/[-CH_2CF_2-] ratio) is shown in Figure 3.2. Comparison of the bulk graft concentration, or the ([-4VP-]/[-CH_2CF_2-])$_{bulk}$ ratio, with the molar feed ratio in Figure 3.2 indicates that the grafting efficiency, defined as the ratio of the amount of 4VP grafted onto the PVDF chains to that used for the graft copolymerization, decreases from about 6% to about 2% with the increase in the [4VP]/[-CH_2CF_2-] feed ratio from 0.61 to 3.66. This result suggests that the graft copolymerization reaction is limited by the peroxide initiator concentration, and not by monomer diffusion. Furthermore, at a low bulk graft concentration, a finite amount of PVDF homopolymer probably coexists in the grafted fraction. The removal of the PVDF homopolymer from the graft copolymers by solvent extraction will be difficult.

FTIR Spectra of the PVDF-g-P4VP Copolymers

The FTIR spectra of the PVDF-*g*-P4VP copolymers, obtained from different monomer feed ratios were also studied. Compared to that of the pristine PVDF and that of the 4VP homopolymer, the spectra of the PVDF-*g*-P4VP copolymers contain the characteristic absorption band for the pyridine groups (ν=1602 cm^{-1}), associated with the grafted 4VP chains (Shriner *et al.*, 1998). Since the concentration of a functional group is directly proportional to the absorption peak area in the FTIR spectrum, the ratio of the absorption peak area at 1602 cm^{-1} to that at 1120~1280 cm^{-1}

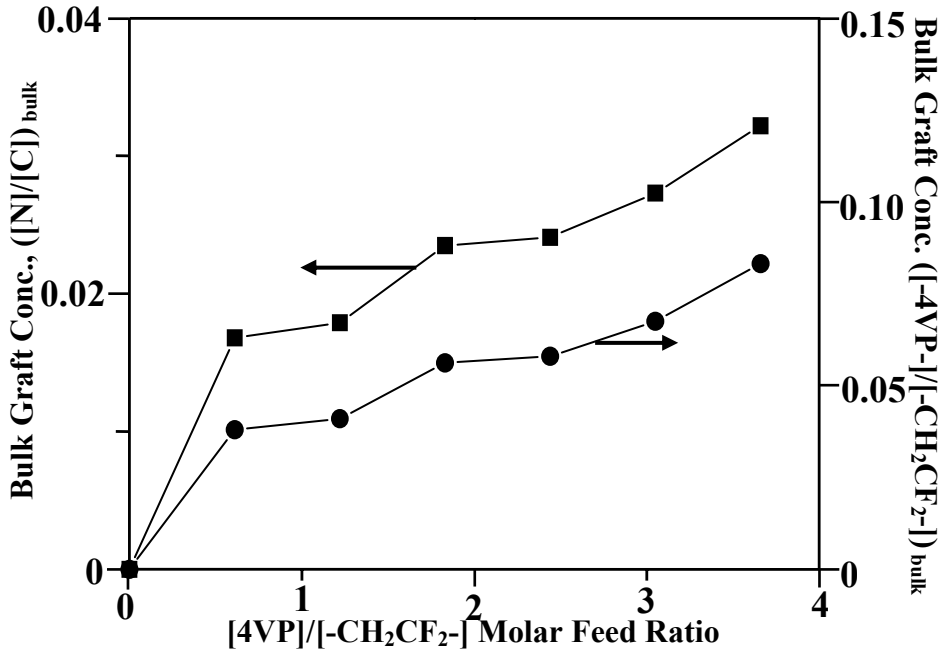

Figure 3.2: Effect of [4VP]/[-CH_2CF_2-] molar feed ratio on the bulk [N]/[C] ratio and bulk graft concentration ([-4VP-]/[-CH_2CF_2-]$_{bulk}$ ratio) of the PVDF-*g*-P4VP copolymer.

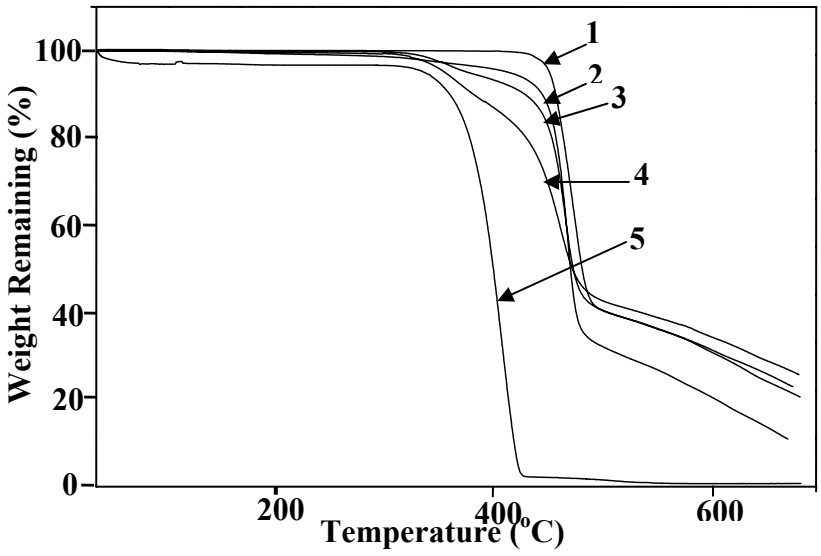

Figure 3.3: Thermogravimetric analysis curves of (1) the pristine PVDF; the PVDF-g-P4VP copolymers of bulk graft concentrations ([-4VP-]/[-CH_2CF_2-]$_{bulk}$ ratios) of (2) 0.038, (3) 0.068, (4) 0.083; (5) the 4VP homopolymer.

(the absorption band associated with the CF_2 groups of PVDF) is directly related to the bulk graft concentration of the 4VP side chains in the respective PVDF-*g*-P4VP copolymer. The FTIR spectroscopic results indicate that the bulk graft concentration increases with the increase in the respective [4VP]/[-CH_2CF_2-] molar feed ratio used for graft copolymerization. This result is in a good agreement with that obtained from the element analysis.

Thermogravimetric Analysis of the PVDF-*g*-P4VPCopolymers

One of the unique properties of the pristine PVDF is its outstanding thermal stability. The thermal stability of the PVDF-*g*-P4VPcopolymers was studied by thermogravimetric analysis (TGA). Figure 3.3 shows the respective TGA curves of three PVDF-*g*-P4VP copolymers of different bulk graft concentrations, the pristine PVDF and the 4VP homopolymer. In comparison with the pristine PVDF and 4VP homopolymer, the PVDF-*g*-P4VPcopolymers show an intermediate weight loss behavior. Differing from the two homopolymers, the PVDF-*g*-P4VP copolymers undergo a distinct two-step thermal decomposition process. The onset of the first major weight loss occurs at about 300^{o}C, corresponding to the decomposition of the 4VP side chains of the copolymer. The second major weight loss commences at about 450^{o}C, which coincides with the thermal decomposition temperature of the PVDF main chains. The TGA curves also indicate that the extent of weight loss of the PVDF-*g*-P4VP copolymer during the first step of thermal decomposition is approximately equal to the content of the 4VP segments in the respective graft copolymer.

3.1.2.2 Microfiltration (MF) Membranes Fabricated from the PVDF-*g*-P4VP Copolymers

After the PVDF-*g*-P4VP MF membranes were fabricated by the phase inversion technique in water and at room temperature from the 12 wt% NMP solutions of the respective copolymers, the surface composition and morphology of the membranes were investigated by XPS and SEM, respectively.

XPS Analysis of the PVDF-*g*-P4VP MF Membranes

The C 1s core-level spectra of the membranes cast from 12 wt% NMP solutions of the pristine PVDF, the ozone-preactivated PVDF, and the PVDF-*g*-P4VP copolymers from different molar feed ratios ([4VP]/[-CH_2CF_2-]=0.61, 2.44, and 3.66, respectively) are shown in Figure 3.4. For the pristine PVDF MF membrane, the C 1s core-level spectrum can be curve-fitted with two peak components at the binding energies (BE's) of about 285.8 eV and 290.5 eV, attributable to the $\underline{C}H_2$ and $\underline{C}F_2$ species, respectively (Ying, 2003). The ratio of the two species, determined from their spectral peak area ratio after curve-fitting, is about 1.06. The ratio is in a good agreement with the theoretical ratio of 1.0 dictated by the chemical structure of PVDF. The C 1s core-level spectrum of the PVDF membrane cast from the NMP solution after 15 min of ozone pretreatment can be curve-fitted with three peak components at the BE of about 285.8 eV, 286.2 eV and 290.5 eV, attributable to the $\underline{C}H_2$ species, the $\underline{C}O$ species created on the PVDF main chains during the ozone preactivation in the NMP solution, and the $\underline{C}F_2$ species, respectively. The C 1s core-level spectrum of the PVDF-*g*-P4VP MF membranes can be curve-fitted with five peak components using the following approach. The peak components of about equal intensities at about 285.8 eV and 290.5 eV are assigned to the $\underline{C}H_2$ and $\underline{C}F_2$ species, respectively, of the PVDF main chains of the copolymer. The peak components at about 284.6 eV and 285.5 eV are assigned to the $\underline{C}H$ and $\underline{C}N$ species of the grafted 4VP polymer side chains in the

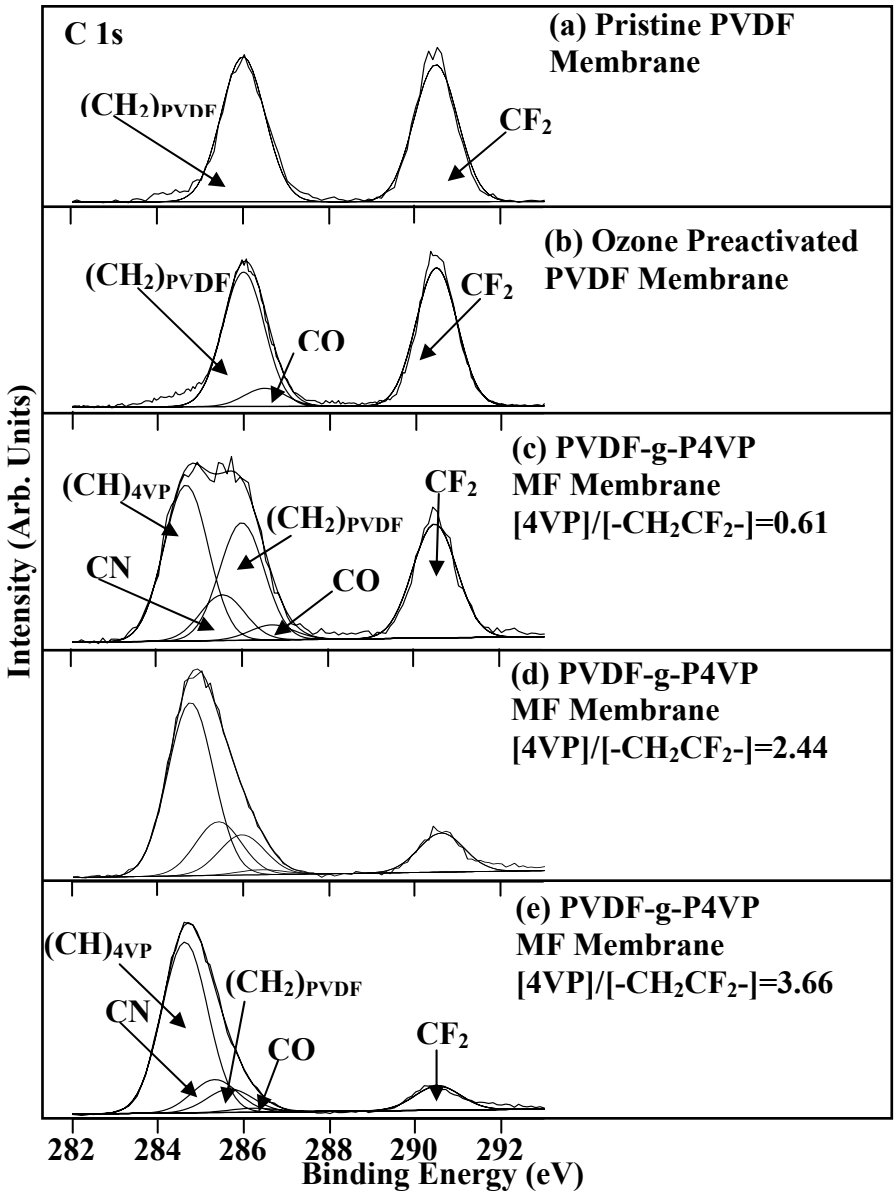

Figure 3.4: XPS C 1s core-level spectra of the MF membranes cast by phase inversion from 12 wt% NMP solutions of (a) the pristine PVDF homopolymer, (b) the PVDF after 15 min of ozone pretreatment, and the PVDF-*g*-P4VP copolymers prepared from the [4VP]/[-CH_2CF_2-] molar feed ratios of (c) 0.61, (d) 2.44 and (e) 3.66.

copolymers. The peak component at about 286.2 eV is assigned to the CO species (Ying, 2003).

The C 1s core-level spectra in Figure 3.4 show that after the ozone preactivation and graft copolymerization, the peak intensities of the $(\underline{C}H_2)_{PVDF}$ and $\underline{C}F_2$ species are reduced, especially when the [4VP]/[-CH_2CF_2-] molar feed ratios are greater than 2. The proportion of the CF_2 species, determined from the $\underline{C}F_2$ peak component spectral area, decreases from about 48% to about 10% when the [4VP]/[-CH_2CF_2-] feed ratio used for graft copolymerization increases from 0 (the pristine PVDF MF membrane) to 3.66. In addition to the actual graft copolymerization, surface enrichment of the grafted hydrophilic 4VP side chains has to be taken into account and will be discussed in details later. The spectra also indicate that the spectral area ratio of the $(\underline{C}H)_{4VP}$ component at 284.6 eV to that of the $\underline{C}F_2$ component at 290.5 eV increases with the increase in the [4VP]/[-CH_2CF_2-] feed ratio used for graft copolymerization, consistent with the increase in the graft concentration. The surface [N]/[C] ratio for the PVDF-*g*-P4VP MF membrane is determined from the respective N 1s to C 1s core-level spectral area ratio. The surface graft concentration of the 4VP polymer on the MF membranes, or $([\text{-4VP-}]/[\text{-}CH_2CF_2\text{-}])_{surface}$ ratio, is determined from the respective [N]/[C] ratio by taking into account the elemental stoichiometries of the graft and the fluoropolymer chains, as in the case of the bulk graft concentration. Figure 3.5 shows that the surface graft concentration of the 4VP polymer on the PVDF-g-P4VP MF membranes increases with the [4VP]/[-CH_2CF_2-] feed ratio used for graft copolymerization.

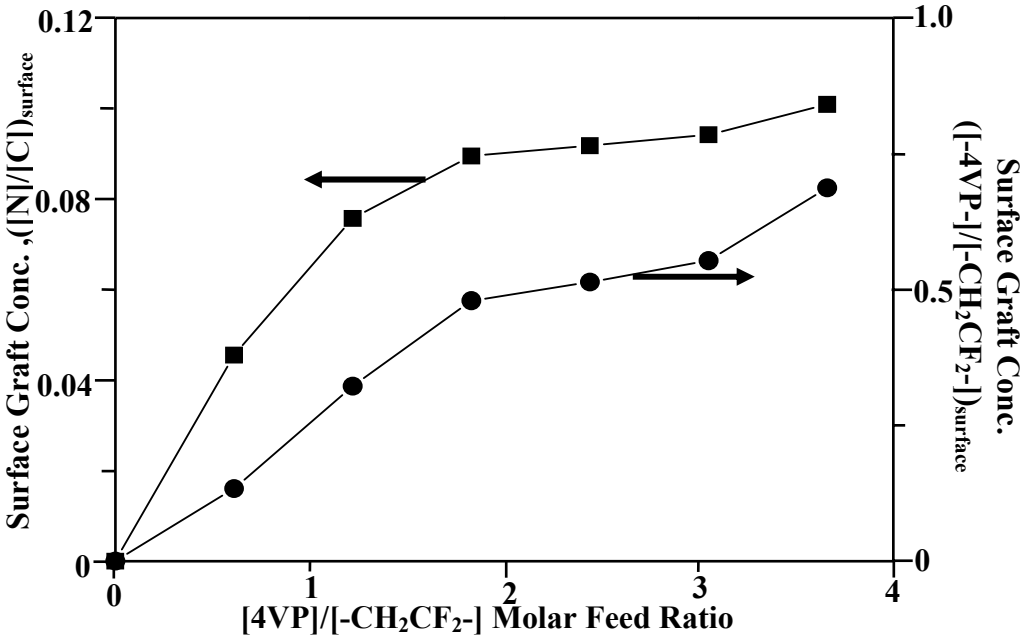

Figure 3.5: Effect of [4VP]/[-CH_2CF_2-] molar feed ratio on the surface [N]/[C] ratio and the surface graft concentration ([-4VP-]/[-CH_2CF_2-]$_{surface}$ ratio) of the PVDF-g-P4VP MF membranes.

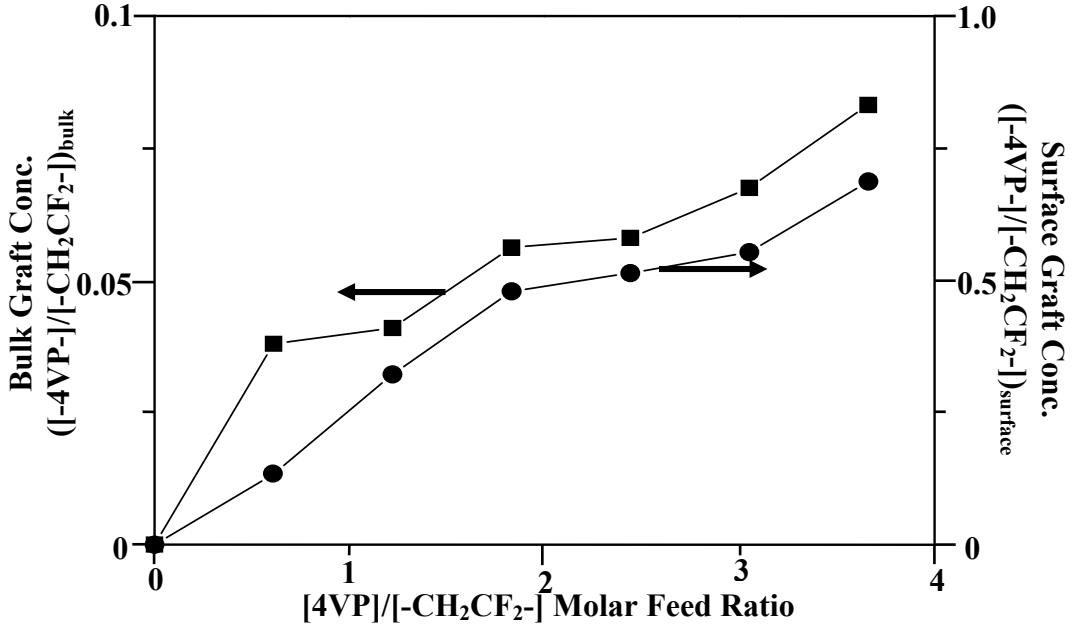

Figure 3.6: Comparison between the bulk graft concentration and the surface graft concentration of the PVDF-*g*-P4VP MF membrane cast by phase inversion from the 12 wt% NMP solution of the respective PVDF-*g*-P4VP copolymer.

The bulk graft concentration of the copolymers (determined by element analyses) and the surface graft concentration of the corresponding MF membranes fabricated by the phase inversion process (determined by XPS analyses) are compared in Figure 3.6. It is unambiguous that the surface graft concentration is always higher than the corresponding bulk graft concentration. Due to the immiscibility of the more hydrophilic 4VP polymer side chains with the hydrophobic PVDF main chains, surface enrichment of the hydrophilic component occurs in the copolymer membranes during the phase inversion process in water.

Surface Morphology of the PVDF-*g*-P4VP MF Membranes

The dependence of the surface morphology of PVDF-*g*-P4VP MF membranes on the graft concentration was investigated by SEM. The SEM images, obtained at a magnification of 5000×, for the MF membranes cast by the phase inversion technique at 25^{o}C from the 12 wt% NMP solutions of the pristine PVDF powders and three PVDF-*g*-P4VP copolymers (bulk graft concentration or $[\text{-4VP-}]/[\text{-}CH_2CF_2\text{-}]_{bulk}$ =0.038, 0.068 and 0.083, respectively) are shown in Figure 3.7. The SEM results indicate that the membranes cast from the NMP solutions of the PVDF-*g*-P4VP copolymer samples have a higher porosity than that cast from the NMP solution of the pristine PVDF and the pore size appears to increase with the bulk graft concentration of 4VP polymer in the copolymers. In the presence of the more hydrophilic 4VP polymer side chains, surface enrichment of the 4VP polymers takes place during phase inversion in water to maximize the interfacial interaction between the pore surface and water, resulting in an increase in the pore size. For the PVDF-*g*-P4VP MF membrane with a high graft concentration, mass migration and accumulation of the 4VP chains at the water-PVDF interface during phase inversion readily give rise to a

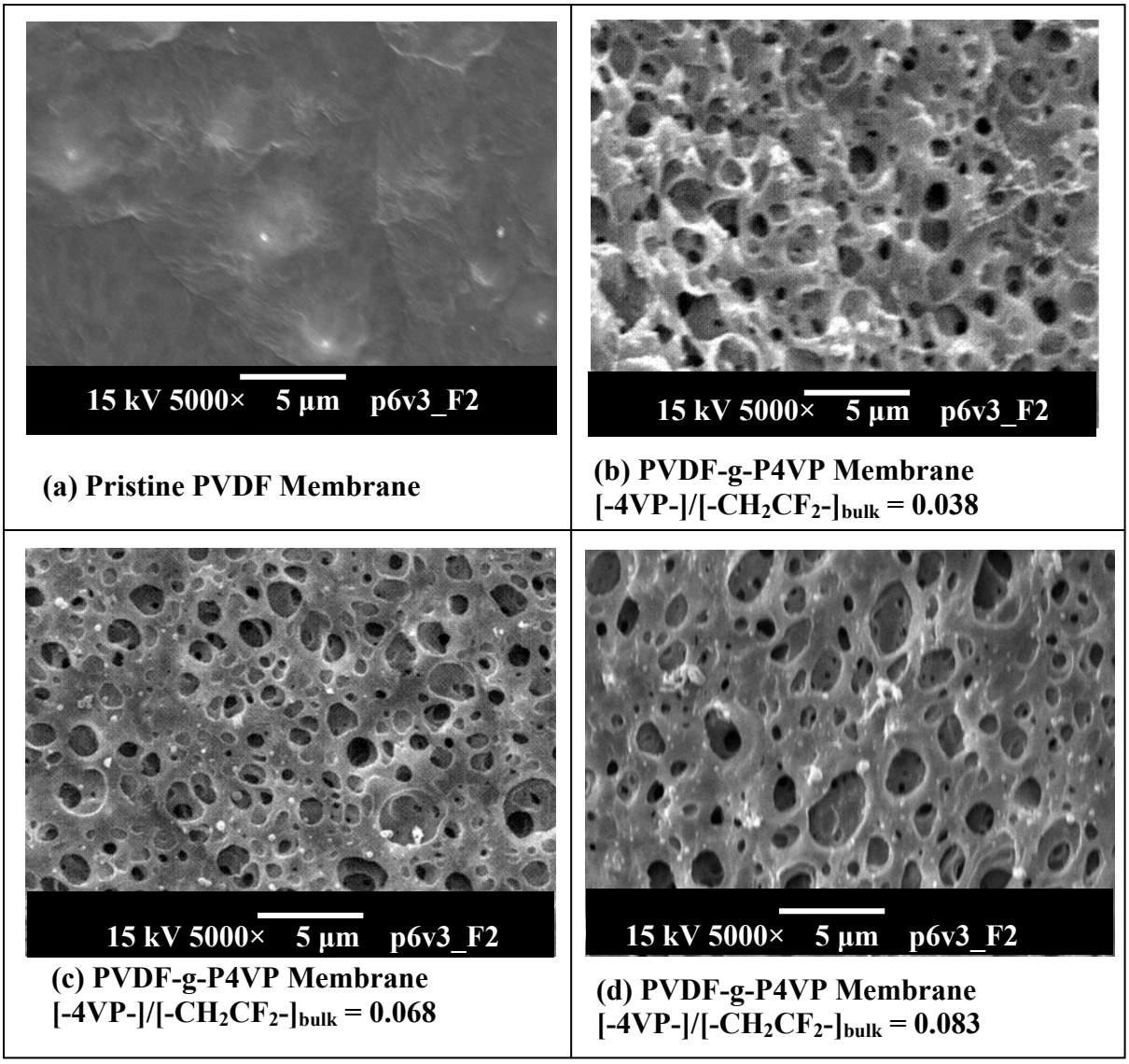

Figure 3.7: SEM micrographs of the MF membranes cast by phase inversion from the 12 wt% NMP solution of (a) the pristine PVDF, and the PVDF-*g*-P4VP copolymers of bulk graft concentrations ([-4VP-]/[-CH_2CF_2-]$_{bulk}$ ratios) of (b) 0.038, (c) 0.068 and (d) 0.083.

large pore size.

3.1.2.3 Pore-Size Measurements and pH-Sensitive Flux Behavior through the PVDF-*g*-P4VP MF Membranes

Pore-Size Measurements of the PVDF-*g*-P4VPMF Membranes

The pore sizes of the various PVDF-g-P4VP MF membranes were measured on a Coulter Porometer II apparatus using the commercial fluid Porofil® as the wetting agent. The Porofil®-wetted membrane samples were subjected to an increasing pressure from 0.1 to 8.6 kg/cm^2 exerted by nitrogen. As the imposed pressure increases, it will reach a point at which it can overcome the surface tension of the liquid in the largest pores and will push the liquid out. The pressure is termed the minimum bubble point and corresponds to the measurement of maximum pore size. Increasing the pressure will further allow the gas to flow through smaller pores until all the pores have been emptied.

The result is governed by the Washburn equation (Ying, 2003):

$$P\,r = 2\,\gamma\cos\theta = 32\ \text{mN/m} \qquad \ldots(3.2)$$

where P is the pressure, r is the average pore radius of the measured membrane sample, and $\gamma\cos\theta$ is the Wilhelmy surface tension. The average pore sizes of the various MF membranes cast from the PVDF-*g*-P4VP graft copolymers of different graft concentrations are shown in Table 3.1. It indicates that the average pore size of the PVDF-*g*-P4VP MF membrane increases with the graft concentration of the 4VP side chains in the copolymer.

The pore size decreases drastically with the increase in concentration of the PVDF-*g*-P4VP copolymer in the casting solution. At a low copolymer solution concentration, the extraction of the solvent from the bulk and the polymer-solvent

Table 3.1: Pore Size Distribution of the PVDF-*g*-P4VP MF Membranes[@]

Molar Feed Ratio [4VP]/[-CH_2CF_2-]	Bulk Graft Conc. [-4VP-]/[-CH_2CF_2-]	pH Value of Casting Bath	Conc. of Casting Solution	Min Pore Size (μm)	Max Pore Size (μm)	Mean Pore Size (μm)
(a) Effect of Bulk Graft Conc. on the Pore-Size Distribution						
0.61	0.038	6	12 wt%	0.23	2.l4	0.95
1.22	0.041	6	12 wt%	0.33	2.84	1.03
1.83	0.056	6	12 wt%	0.26	2.94	1.08
2.44	0.058	6	12 wt%	0.37	2.14	1.23
3.05	0.068	6	12 wt%	0.39	2.28	1.31
3.66	0.083	6	12 wt%	0.48	3.62	1.38
(b) Effect of Solution Conc. on the Pore-Size Distribution						
2.44	0.058	6	10 wt%	0.23	2.52	1.83
2.44	0.058	6	12 wt%	0.37	2.14	1.23
2.44	0.058	6	15 wt%	0.16	0.72	0.22

(a) Cast in doubly distilled water

(b) Cast in doubly distilled water

[@] For the commercial PVDF membranes with standard pore diameters *d*=0.45 and 0.65 μm:

PVDF (*d*=0.45μm): Max pore size=1.86μm; Min pore size=1.17μm; Mean pore size=1.41μm

PVDF (*d*=0.65μm): Max pore size=2.40μm; Min pore size=1.42μm; Mean pore size=1.96μm

phase is facilitated. As a result, larger pore sizes are obtained for the PVDF-*g*-P4VP MF membranes cast from the copolymer solution of lower concentration. The commercial PVDF membranes with d=0.45 μm and d=0.65 μm were selected as the pristine PVDF MF membranes for the comparative flux studies in the present work.

The effect of the pH of the aqueous casting bath on the mean pore size and the surface composition of the PVDF-*g*-P4VP MF membrane is shown in Figure 3.8. The pore size of the MF membranes increases gradually with the increase in proton concentration (decrease in pH value) of the casting bath. On the contrary, the surface graft concentration of the P4VP segments on the respective MF membranes, as determined by XPS analysis, decreases when the pH value of the casting bath is decreased from 6 to 1. Figure 3.9 shows the changes in the C 1s core-level lineshape of the PVDF-*g*-P4VP MF membranes with the pH of the aqueous casting bath. The pyridine groups interact with protons *via* hydrogen bonding and protonation (see also below) when the membrane is cast in an aqueous acid solution, leading to the formation of the positively charged pyridine groups on the MF membrane surfaces. Because of the electrostatic repulsion among the positively charged pyridine groups on the membrane surface, including the pore surfaces, at the low pH value of the casting bath, the pore size is enhanced while the surface concentration of the 4VP segments is reduced substantially. Thus, the higher extent of electrostatic repulsion has effectively limited the migration of P4VP segments from the bulk of polymer matrix to the membrane surfaces during the phase inversion process. On the other hand, hydration of positively charged ions may decrease the surface energy and as a result, enhance the surface concentration of 4VP.

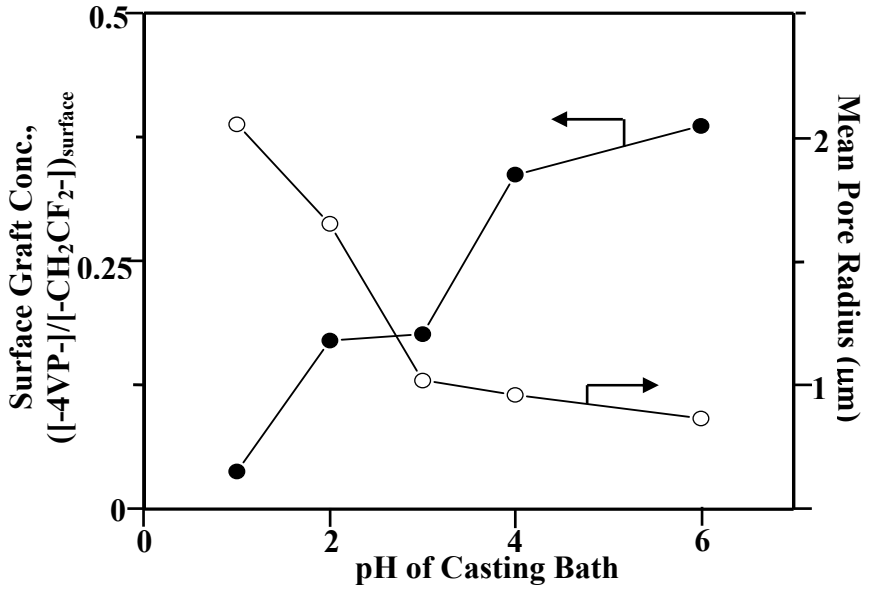

Figure 3.8: Effect of pH of the casting bath on the surface graft concentration (([-4VP-]/[-CH_2CF_2-]$_{surface}$ ratio) and the mean pore radius of PVDF-*g*-P4VP (([-4VP-]/[-CH_2CF_2-]$_{bulk}$=0.056) MF membranes cast from 12 wt% NMP solution in aqueous HCl solution with specific pH value. Sodium chloride was added to fix the ionic strength of the casting bath at 0.1 mol/L.

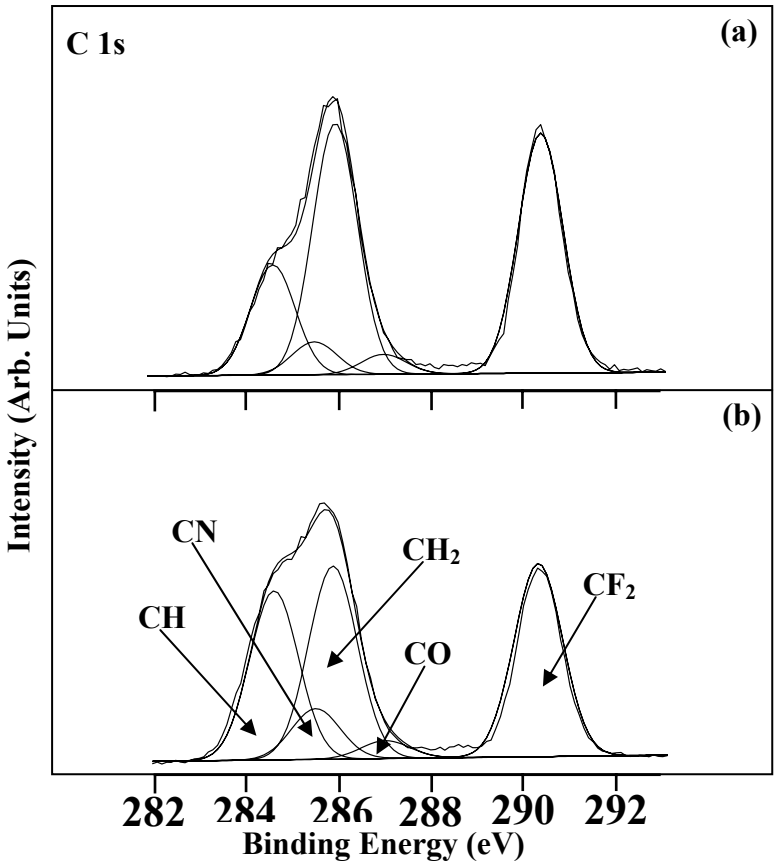

Figure 3.9: Effect of pH of the casting bath on the C 1s core-level lineshape of the PVDF-*g*-P4VP MF membranes; (a) cast in pH=1 and (b) cast in pH=6.

pH-Dependant Flux Behavior of Aqueous Solutions through the PVDF-*g*-P4VP MF Membranes

The pH-dependant flux behavior of aqueous solutions through the PVDF-*g*-P4VP MF membranes is shown in Figure 3.10. The permeability of aqueous solutions through the pristine PVDF MF membranes is pH-independant (Curves 3 and 4). On the other hand, the flux of the aqueous solution through the PVDF-g-P4VP MF membranes exhibits a pH-dependant behavior. The permeation rate increases with the increase in solution pH value from 1 to 6 (Curves 4 and 5). The pH-dependant flux behavior is opposite to that of the MF membranes prepared from PVDF with poly(acrylic acid) grafted side chains (Curve 1) (Ying, 2003). Furthermore, the sensitivity of the pH-dependant change in flux of the aqueous solution through the PVDF-*g*-P4VP MF membrane is enhanced by the increase in the 4VP polymer graft concentration.

The change in permeability or flux in response to the change in solution pH can be attributed to the change in conformations of the graft chains on the membrane surface, especially on the pore surfaces. Due to the non-ionizablity of the polymer chains in the pristine PVDF MF membranes, the polymer chain conformation and the membrane pore dimension will remain constant at all pH values. On the other hand, as a weak base, the pyridine groups of the grafted 4VP side chains are protonated and become complexed in an acid solution. The resulting ionic character and the electrostatic repulsion among the positively charged pyridinium nitrogen atoms overcome the hydrophobic interactions among the alkyl segments of the chains. The uncoiling of the polymer side chains and their interactions with the aqueous solution lead to an extended conformation in the pores (Tonge, 2001). As a result, the effective pore dimension, and thus the permeability of the aqueous solution through the MF

membrane, is reduced. The present pH-dependant flux results for the aqueous solution differ from the pH-dependant flux behavior of the aqueous solution through the MF membrane prepared from PVDF with grafted acid polymer side chains, in particular, the PVDF with grafted poly(acrylic acid) side chains (PVDF-*g*-PAAc copolymers) (Ying, 2003).

As a weak acid (pK_a=4.3), the carboxylic groups of the PVDF-g-PAAc copolymer can be ionized, or deprotonated, readily to become negatively charged. With increasing pH values (pH>3) of the solution, most of the carboxylic groups are transformed into carboxylic ions. Strong electrostatic repulsion among the carboxylic ions, together with their strong interaction with the aqueous solution, forces the AAc polymer side chains to adopt a highly extended conformation. The extension of the AAc polymer side chains into the pores reduces the effective pore dimension, and results in the reduced permeability of the aqueous solution of a high pH value through the PVDF-*g*-PAAc MF membrane. Thus, the present PVDF-*g*-P4VP MF membranes, prepared from PVDF with grafted basic polymer (4VP polymer) side chains, complement the PVDF-*g*-PAAc MF membranes in regulating the flux of the aqueous solutions in the pH range of 1 to 7.

3.1.2.4 Interaction of the 4VP Polymer with Protonic Acids

For the nitrogen-containing species, such as pyridine and imidazole, hydrogen bonding with the proton-donating species, such as phenols, carboxylic acids, inorganic acids and water, occurs readily (Xiang, *et al.*，1997；Houben *et al.*, 1996; Schlucker *et al.*, 2002; Goh *et al.*, 1996; Jiao et al.; 2002). Thus, the pyridine groups

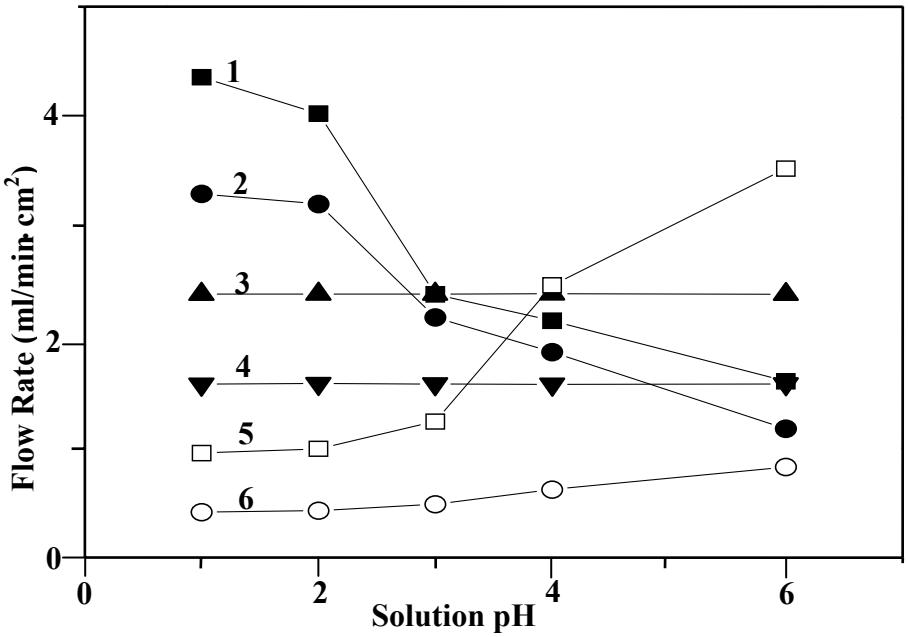

Figure 3.10: pH-dependant water permeability through the pristine PVDF, PVDF-*g*-PAAc and PVDF-*g*-P4VP MF membranes. Curves 1 and 2 are obtained from two PVDF-*g*-PAAc MF membranes with graft concentrations ([-AAc-]/[-CH_2CF_2-]$_{surface}$ ratios) of 0.97 and 0.13, respectively; Curves 3 and 4 are from fluxes through the commercial PVDF membranes (standard pore diameters: d=0.65 and 0.45 μm, respectively); Curves 5 and 6 are obtained from two PVDF-*g*-P4VP MF membranes with graft concentrations ([-4VP-]/[-CH_2CF_2-]$_{surface}$ ratios) of 0.55 and 0.13, respectively. (The mean pore sizes for all the membranes are given in Table 1)

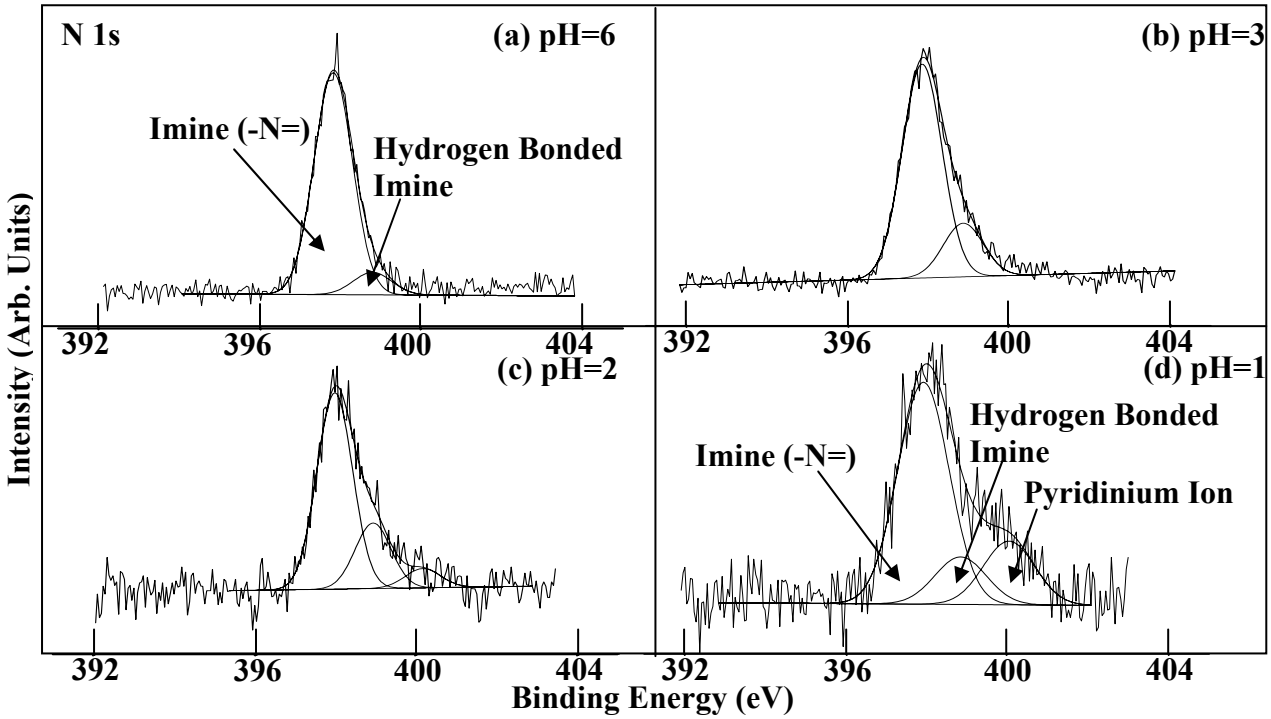

Figure 3.11: XPS N 1s core-level spectra of four MF membranes cast by phase inversion from a 12 wt% NMP solution of the PVDF-*g*-P4VP copolymer ([-4VP-]/[-CH_2CF_2-]$_{surface}$= 0.55) and after being immersed for 5 min in aqueous solutions of different pH value: (a) pH=6, (b) pH=3, (c) pH=2 and (d) pH=1

of the grafted P4VP side chains can become involved in two types of interaction in acidic solutions, *viz*., hydrogen bonding and pyridine protonation, that lead to the observed pH-dependant flux of the aqueous solutions through the PVDF-*g*-P4VP MF membrane. In order to investigate the interaction of the 4VP side chains in the acid solutions, XPS was employed to study the variation in the chemical state of the elemental nitrogen of the pyridine group after the PVDF-*g*-P4VP MF membrane has been exposed to acidic solutions of different pH values for 5 min and dried by pumping under reduced pressure overnite. The N 1s core-level spectra of the resulting membranes are shown in Figure 3.11. The XPS spectra can be curve-fitted with three components using the following approaches. The main peak component at about 398.5 eV is assigned to the imine (-N=) moiety of the pyridine rings, the peak component at about 399.5 eV is assigned to the hydrogen-bonded imine, and the peak component at about 400.8 eV is assigned to the protonated pyridinium ions (Tan *et al.*, 1990; Liu *et al.*, 1999; Li *et al.*, 1998). The latter species has been reported to undergo a positive BE shift of 2.1~2.5 eV from the neutral pyridine nitrogen (Tan *et al.*, 1990; Li *et al.*, 1998). The N 1s spectra in Figure 3.11 clearly indicate that, when the proton concentration is low, or when the pH value is higher than 2, the main form of interaction is hydrogen bonding. The percentage of N atoms involved in the hydrogen bonding increases from 9% to 21% when the pH value of the solution decreases from 6 to 3. When the pH value of the solution is decreased to 2, protonation of pyridine becomes significant. The percentages of imine groups involved in hydrogen bonding and protonation are about 21% and 7%, respectively. When the solution pH is further decreased to 1, the main form of interaction switches from hydrogen bonding to protonation or the formation of the pyridinium ions. The proportion of protonated

imine groups increases to 19%, while that of imine groups involved in hydrogen bonding is reduced to 14%.

3.1.3 Conclusion

A new graft copolymer, PVDF-*g*-P4VP, was successfully synthesized through the molecular graft copolymerization of 4VP with the ozone-preactivated PVDF backbone in NMP solution. The MF membranes prepared from the PVDF-*g*-P4VP copolymers of different graft concentrations by the phase inversion technique in water showed enrichment of the hydrophilic 4VP polymer on the surface. The mean pore size of the PVDF-*g*-P4VP MF membranes increased with the increasing 4VP polymer graft concentration, the decreasing pH value of the casting bath, and the decreasing concentration of the casting solution. The flux of the aqueous solution through the PVDF-*g*-P4VP MF membranes exhibited a strong dependence on solution pH in the pH range of 1 to 6, arising from the interaction of the grafted 4VP polymer on the pore surface with the aqueous solution through the hydrogen bonding and protonation. The present study has shown that molecular functionalization by graft copolymerization prior to membrane fabrication is a relatively simple and effective approach to the preparation of membranes with well-controlled pore size, uniform surface composition (including the composition of pore surface), and pH-sensitive flux properties.

3.2 pH- and Temperature-Sensitive Microfiltration Membranes from Blends of Poly(vinylidene fluoride)-*graft*-Poly(4-vinylpyridine) and Poly(*N*-isopropylacrylamide)

3.2.1 Experimental

3.2.1.1 Materials and Reagents

PVDF, 4VP and NMP were same as in Section 3.1. Poly(*N*-isopropylacrylamide) (PNIPAm) (MW=20,000~30,000) was purchased from Aldrich Chemical Company of Milwaukee, WI, USA. It was used as received.

3.2.1.2 Fabrication of the Microfiltration (MF) Membranes

The MF membranes were prepared by phase inversion. The PVDF-*g*-P4VP copolymer was synthesized as in the Section 3.1. The monomer feed ratio, defined as the [4VP]/[-CH_2CF_2-] molar ratio, used for the graft copolymerization, was 2.55 and the reaction time was fixed at 3 h. The bulk [N]/[C] ratio of the copolymer so-obtained was determined to be 0.025 from elemental analysis. The bulk graft concentration, defined as the number of 4VP repeat units per repeat unit of PVDF, or the $([\text{-4VP-}]/[\text{-}CH_2CF_2\text{-}])_{bulk}$ ratio, was calculated to be 0.06. After filtration and purification, the PVDF-*g*-P4VP copolymer powders were re-dissolved in NMP. PNIPAm was added to achieve the desirable blend ratio, defined as the number of NIPAM repeat units per repeat unit of PVDF, or the $([\text{-NIPAM-}]/([\text{-}CH_2CF_2\text{-}])_{solution}$ molar ratio. The polymer concentration of the casting solution, on the other hand, was based on the total weight of polymer blend in the solution. The polymer solution was cast onto a glass plate. The glass plate was subsequently immersed in doubly distilled water. After the membrane had detached from the glass plates, it was extracted in a second bath of doubly distilled water at 70^{o}C for several minutes. The purified MF

membrane was dried by pump under reduced pressure for the subsequent characterization.

3.2.1.3 Composition Analyses

The carbon, nitrogen and hydrogen elemental contents were determined in the similar approach in Section 3.1. The bulk graft concentration of the PVDF-*g*-P4VP copolymer used in this studied, or the $([\text{-4VP-}]/[\text{-CH}_2\text{CF}_2\text{-}])_{bulk}$ ratio, is determined to be about 0.06.

For the PVDF-*g*-P4VP/PNIPAM MF membrane, its $([N]/[C])_{bulk}$ ratio was also determined directly from elemental analyses. The bulk concentration, or the $([\text{-NIPAm-}]/[\text{-CH}_2\text{CF}_2\text{-}])_{bulk}$ ratio, is determined from the $([N]/[C])_{bulk}$ ratio according to Equation (3.2):

$$([\text{-NIPAm-}]/[\text{-CH}_2\text{CF}_2\text{-}])_{bulk}=(2([N]/[C]_{bulk})+7\times0.06\times([N]/[C])_{bulk}-0.06)/(1-6\times([N]/[C])_{bulk}) \quad \ldots(2)$$

where the factors 2, 7 and 6 are introduced to account for the fact that there are 2, 7 and 6 carbon atoms per repeat unit of PVDF, 4VP polymer and PNIPAm, respectively, while 0.06 stands for the bulk graft concentration of the PVDF-*g*-P4VP copolymer used in this study.

3.2.1.4 Membrane Characterizations

The morphology, pore-size distribution and surface composition of the MF membranes were studied by scanning electron microscopy, liquid-displacement porosimetry and X-ray photoelectron spectroscopy, respectively, as in the Section 3.1.

For the measurements of the temperature- and pH-dependant flux through the blend membranes, the blend membrane was immersed in an aqueous solution of

prescribed pH and temperature, before being mounted on the micro-filtration cell (Toyo Roshi UHP-25, Tokyo, Japan). An aqueous solution of the same prescribed pH and temperature, and at a fixed ionic strength of 0.1 mol/L, was added to the cell. The flux was calculated from the volume of permeate as a function of time. The micro-filtration cell containing the permeate was kept in a thermostated water bath for at least 20 min before the flow was initiated. The permeate temperature was checked by a thermometer installed at the outlet of the filtration cell.

3.2.2 Results and Discussion

3.2.2.1 Blending of the PVDF-*g*-P4VP Copolymer with PNIPAm and Fabrication of the PVDF-*g*-P4VP/PNIPAm MF Membrane

Details on the synthesis and characterization of the PVDF-*g*-P4VPcopolymer have been reported earlier. In this work, elemental analysis was employed to determine the composition of the PVDF-*g*-P4VP copolymer used for blending with PNIPAm, as well as that of the resulting PVDF-*g*-P4VP/PNIPAm MF membranes. The $([N]/[C])_{bulk}$ ratio of the pristine PVDF-*g*-P4VPmembrane and the PVDF-*g*-P4VP/PNIPAm MF membranes cast from different solution blend ratio, or the $([\text{-NIPAm-}]/[\text{-}CH_2CF_2\text{-}])_{solution}$ ratio, are compared to $([N]/[C])_{bulk}$ ratio pre-determined when preparing the blend in the casting solution. Figure 3.12 indicates that the $([N]/[C])_{bulk}$ ratio and the bulk blend concentration, or the $([\text{-NIPAm-}]/[\text{-}CH_2CF_2\text{-}])_{bulk}$ ratio of PVDF-*g*-P4VP/PNIPAm MF membrane, increases with the increase in the blend ratio used for membrane fabrication, or the $([\text{-NIPAM-}]/([\text{-}CH_2CF_2\text{-}])_{solution}$ ratio. Figure 3.12 also suggests that the $([N]/[C])_{bulk}$ ratio determined from elemental analysis is smaller than the theoretical $([N]/[C])_{bulk}$ ratio calculated from the solution blend ratio, so it can be concluded that part of PNIPAm in the blend solution was extracted into the coagulation bath during the phase inversion process.

3.2.2.2 Surface Characteristics of PVDF-*g*-P4VP/PNIPAm MF Membranes

After the PVDF-*g*-P4VP/PNIPAm blend membranes were fabricated, XPS and SEM were used to investigate the variation in chemical composition and surface morphology, respectively, of the MF membranes.

Surface Morphology of PVDF-g-P4VP/PNIPAm MF Membranes

The dependence of the morphology of the MF membrane on the amount of PNIPAM entrapped in the PVDF-*g*-P4VP matrix was investigated by SEM. The SEM images, obtained at a magnification of 5000×, for the MF membranes cast by phase inversion at 25^{o}C from the 12 wt% NMP solutions of PVDF-*g*-P4VP and PNIPAM at solution blend ratios of 0.014, 0.029 and 0.061, respectively, are shown in Figure 3.13 The SEM micrographs in Figure 3.13 indicate that the incorporation of PNIPAM into the PVDF-*g*-P4VP matrix gives rise to a decrease in pore size. This phenomenon is probably associated with the fact that a small pore size can lead to a large specific surface area, arising from the increased interaction of the hydrophilic 4VP and PNIPAM segments at the membrane surface with the aqueous medium during phase inversion. Figure 3.13 also shows that when the blend ratio is no more than 0.029, the PVDF-*g*-P4VP/PNIPAM MF membranes become corrugated at the surface. At the higher PNIPAM content, PVDF-*g*-P4VP/PNIPAM MF membrane adopts to a smooth morphology.

As a thermoresponsive polymer, PNIPAM is water-soluble at room temperature, but becomes micellized and forms aggregate when the aqueous medium is heated to above its LCST (Lowe, 2000). The effect of the temperature of the casting bath on the

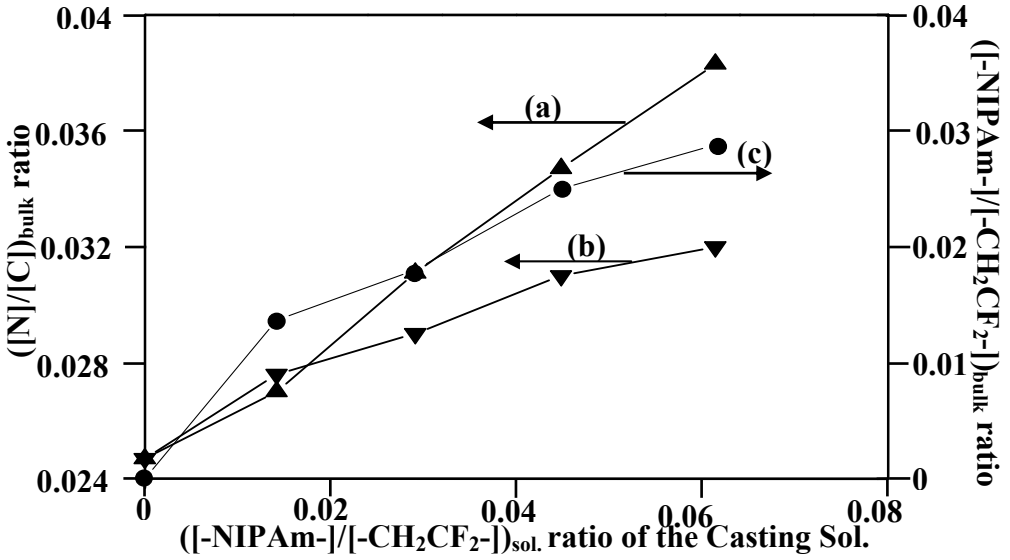

Figure 3.12: Dependence of the $([N]/[C])_{bulk}$ ratio and the $([\text{-NIPAm-}]/[\text{-}CH_2CF_2\text{-}])_{bulk}$ ratio of the PVDF-g-P4VP/PNIPAm blend membranes on the solution blend ratio: (a) the calculated $([N]/[C])_{bulk}$ ratio, (b) determined $([N]/[C])_{bulk}$ ratio and (c) the $([\text{-NIPAm-}]/[\text{-}CH_2CF_2\text{-}])_{bulk}$ ratio.

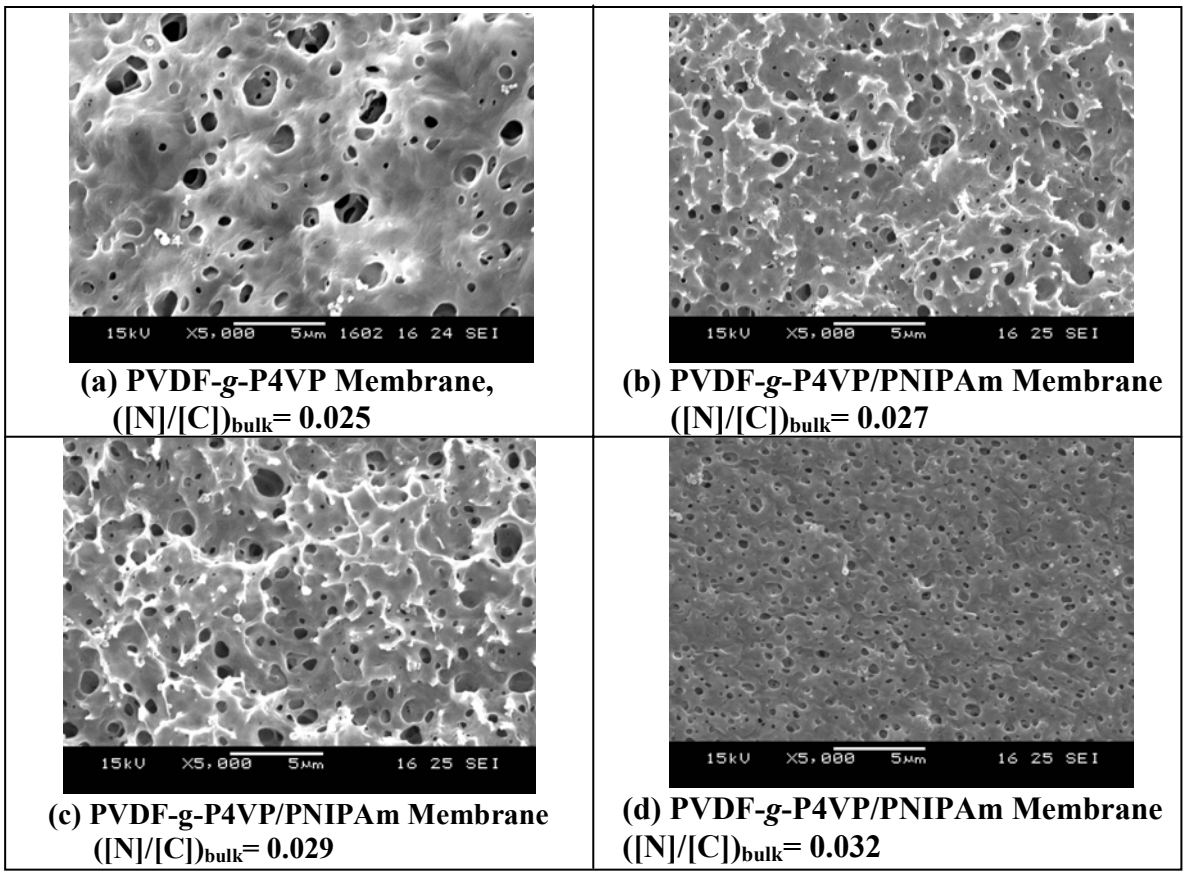

(a) PVDF-*g*-P4VP Membrane, $([N]/[C])_{bulk}$= 0.025

(b) PVDF-*g*-P4VP/PNIPAm Membrane $([N]/[C])_{bulk}$= 0.027

(c) PVDF-g-P4VP/PNIPAm Membrane $([N]/[C])_{bulk}$= 0.029

(d) PVDF-*g*-P4VP/PNIPAm Membrane $([N]/[C])_{bulk}$= 0.032

Figure 3.13: SEM micrographs of the PVDF-*g*-P4VP/PNIPAm MF membranes cast by phase inversion in water (pH=6) at room temperature from the 12 wt% NMP solution of different blend ratios of (a) 0, (b) 0.014, (c) 0.029 and (d) 0.061, respectively.

SEM. Figure 3.14 shows the SEM images, obtained at a magnification of 2000×, of the PVDF-*g*-P4VP/PNIPAM MF membranes (blend ratio=0.029) cast by phase inversion in a coagulation bath at temperatures of 0°C, 25°C, 45°C and 70°C, respectively. The SEM images in Figure 3.14 clearly suggest that the membranes cast at temperatures below the LCST of PNIPAM have a much smaller pore dimension than those cast at temperatures above 32°C.

The dependence of the surface morphology of the PVDF-g-P4VP/PNIPAM MF membranes on pH value of the coagulation bath was also investigated by SEM. Figure 3.15 shows the SEM images, obtained at a magnification of 2000×, of the PVDF-g-P4VP/PNIPAM MF membrane (blend ratio = 0.061) cast in aqueous media of different pH values (pH=6 and 2, respectively) by phase inversion at room temperature. Sodium chloride was added into the bath to fix the ionic strength at 0.1mol/L. The SEM images in Figure 3.15 suggest that the MF membrane cast at a lower pH value has a larger pore size than that cast at higher pH values. When cast in aqueous solution of different pH values, pyridine rings are involved in various degrees of interaction with the aqueous media. They become positively charged at low pH values. The electrostatic repulsion among the positively charged pyridine groups on the membrane surface enhances the pore sizes of the MF membrane when cast at the low pH values (high proton concentration).

XPS Analysis of the PVDF-*g*-P4VP/PNIPAm MF Membranes

The C 1s core-level spectra of the PVDF-*g*-P4VP/PNIPAm MF membranes cast from 12 wt% NMP solutions of the polymer blends are shown in Figure 3.16. For the PVDF-*g*-P4VP MF membrane (part (a)), the C 1s core-level spectrum can be curve-fitted with four peak components using the following strategy. The peak components

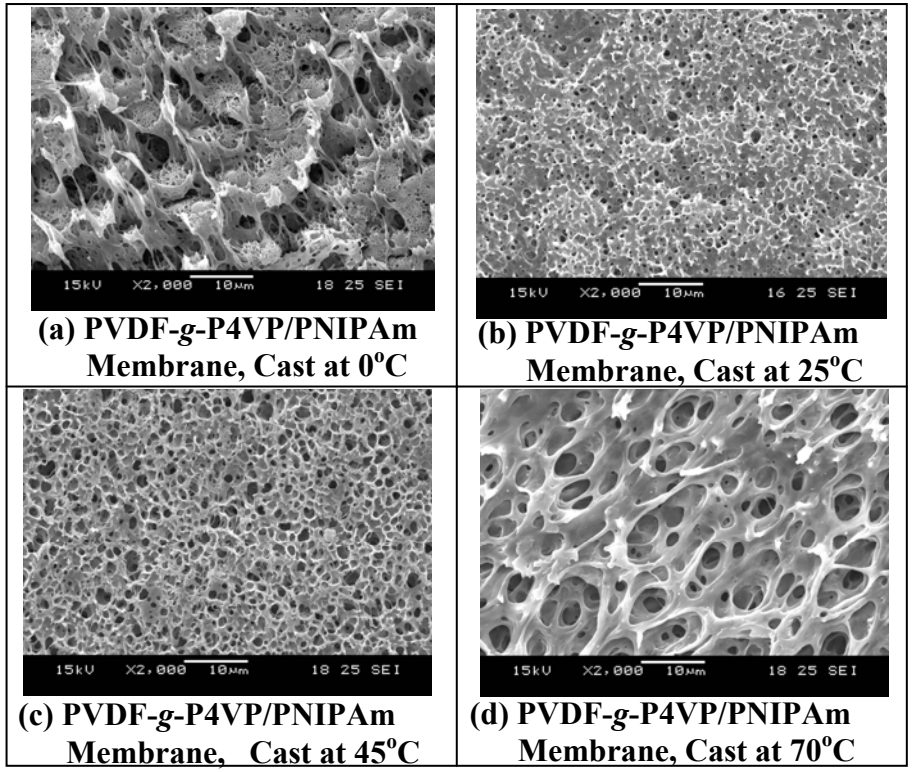

(a) PVDF-*g*-P4VP/PNIPAm Membrane, Cast at 0°C

(b) PVDF-*g*-P4VP/PNIPAm Membrane, Cast at 25°C

(c) PVDF-*g*-P4VP/PNIPAm Membrane, Cast at 45°C

(d) PVDF-*g*-P4VP/PNIPAm Membrane, Cast at 70°C

Figure 3.14: SEM micrographs of the PVDF-*g*-P4VP/PNIPAm MF membranes cast by phase inversion from the 12 wt% NMP solution of PNIPAm content of 0.029 in water (pH=6) at different temperatures of (1) 0°C, (2) 25°C, (3) 45°C and (4) 70°C, respectively.

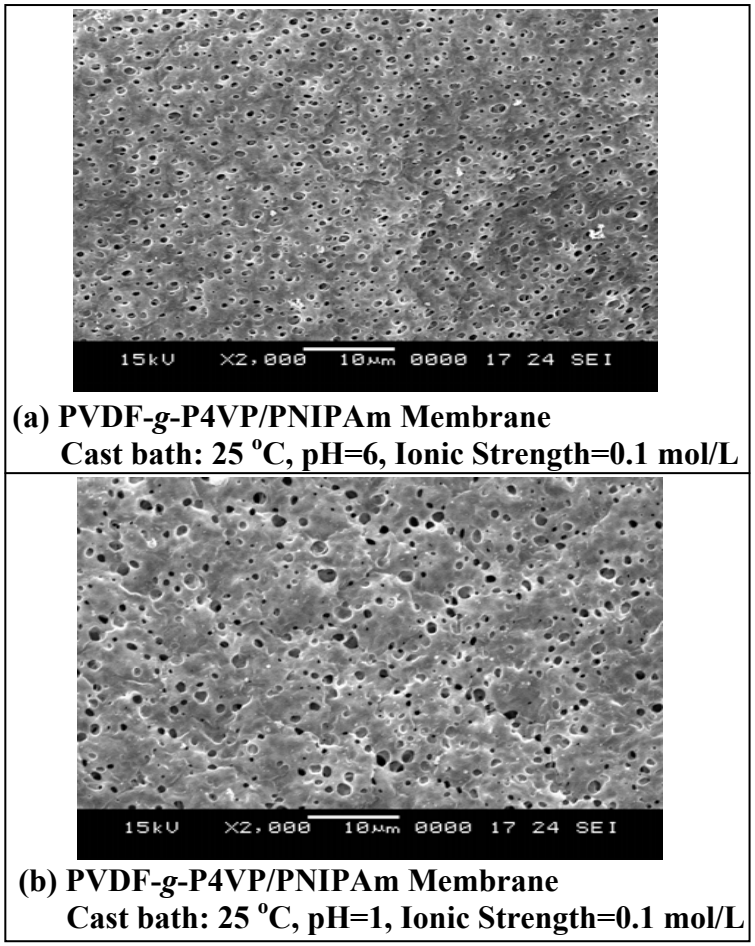

(a) PVDF-*g*-P4VP/PNIPAm Membrane Cast bath: 25 °C, pH=6, Ionic Strength=0.1 mol/L

(b) PVDF-*g*-P4VP/PNIPAm Membrane Cast bath: 25 °C, pH=1, Ionic Strength=0.1 mol/L

Figure 3.15: SEM micrographs of the PVDF-*g*-P4VP/PNIPAm MF membranes cast by phase inversion from the 12 wt% NMP solution (([-NIPAm-]/[-CH_2CF_2-])=0.061) in water at room temperature (the ionic strength is fixed at 0.1 mol/L) of different pH (1) 6 and (2) 1, respectively.

of about equal intensities at the BE's of about 285.8 eV and 290.5 eV are assigned, respectively, to the $\underline{C}H_2$ and $\underline{C}F_2$ species of the PVDF main chains of the copolymer. The peak components at the BE's of about 284.6 eV and 285.8 eV are assigned to the $\underline{C}H$ and $\underline{C}N$ species of the grafted 4VP polymer side chains in the copolymers (Ying, 2003). For the PVDF-*g*-P4VP/PNIPAm MF membranes, the C 1s core-level spectra can be curve-fitted using the following approach. Besides the peak components associated with the PVDF-*g*-P4VP, the carbon species at the PNIPAm backbone and the $\underline{C}N$ species of PNIPAm occurs at the BE's of about 284.6 and 285.8 eV, respectively, similar to those of the 4VP polymer side chains. In addition to the four peaks mentioned above, the peak component at the BE's of about 287.4 eV is assigned to the $HN\underline{C}=O$ species of the PNIPAm (Ying 2003).

The C 1s core-level spectra in Figure 3.16 show that due to the presence of PNIPAm on the membrane surface, the peak intensity of the $\underline{C}F_2$ species decreases with the increase in PNIPAm content. The proportion of the $\underline{C}F_2$ species, determined from the $\underline{C}F_2$ peak component spectral area, decreases from 27% to 9%, when the blend ratio increases from 0 (PVDF-*g*-P4VP MF membrane) to 0.061. On the other hand, Figure 3.14 also showed that the percentage of the $HN\underline{C}=O$ species of the PNIPAm segments, determined in a similar manner to that of the $\underline{C}F_2$ species, increases gradually from 0 to 7.5% with the blend ratio increases from 0 (PVDF-*g*-P4VP MF membrane) to 0.061.

The surface blend concentration of the PNIPAm on the PVDF-*g*-P4VP/PNIPAm blend membranes, or the ([-NIPAm-]/[-CH_2CF_2-])surface ratio, is directly determined

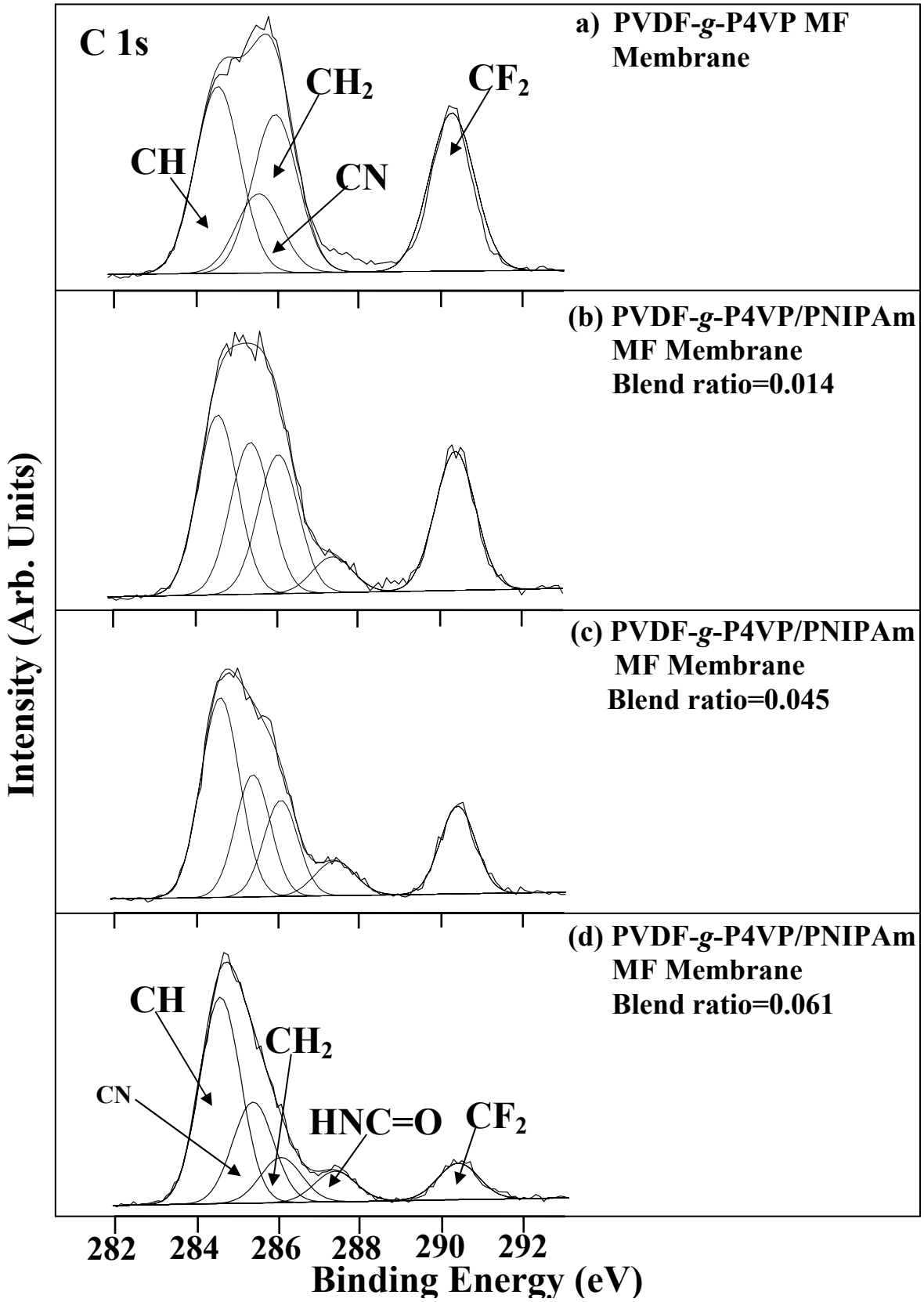

Figure 3.16: XPS C 1s core-level spectra of the PVDF-*g*-P4VP/PNIAPm MF membranes cast by phase inversion in water at room temperature from 12 wt% NMP solutions of different blend ratio (a) 0, (b) 0.014, (c) 0.045, and (d) 0.061

from the XPS spectral area ratios of the HN<u>C</u>=O species of the PNIPAM segments and <u>C</u>F_2 species of the PVDF backbones. Figure 3.17 shows the comparison between the bulk and surface blend concentration of the P4VP-*g*-PVDF/PNIPAm membranes cast from solution of different blend ratio. It is unambiguous that although both the bulk blend concentration and the bulk concentration increases with the increase in the solution blend ratio, the surface concentration is tens times higher than the bulk concentration. Although such a surface enrichment of PNIPAm chains had been observed in the MF membranes, it occurs much more significantly in the PVDF-g-P4VP/PNIPAm blend membrane than in the MF membrane prepared from the PVDF with PNIPAm side chains (the PVDF-*g*-PNIPAm copolymer) (Ying, 2003). It probably results from the fact that, in comparison to the grafted PNIPAm side chains, the hydrophilic PNIPAm homopolymers were much less hindered during the migration from the polymer matrix to the membrane surface to maximize the interfacial interaction with the aqueous media during the phase inversion process.

3.2.3 Pore Size of the PVDF-g-P4VP/PNIPAm MF Membranes

The pore sizes of the PVDF-g-P4VP/PNIPAm MF membranes cast under various conditions, such as polymer solution concentration, pH value, temperature and ionic strength of the coagulation bath, were measured on a Coulter Porometer II apparatus using the commercial liquid Porofil® as the wetting agent, as reported before.

The average pore sizes of the various PVDF-*g*-P4VP/PNIPAm MF membranes cast from the polymer solution in NMP (blend ratio =0.029) in the casting bath of different pH value are shown in Table 1. Besides the polydispersity in the pore-size distribution, the mean pore size of the MF membrane increases with the increase in proton concentration (decrease in pH value) of the casting bath. The pyridine rings

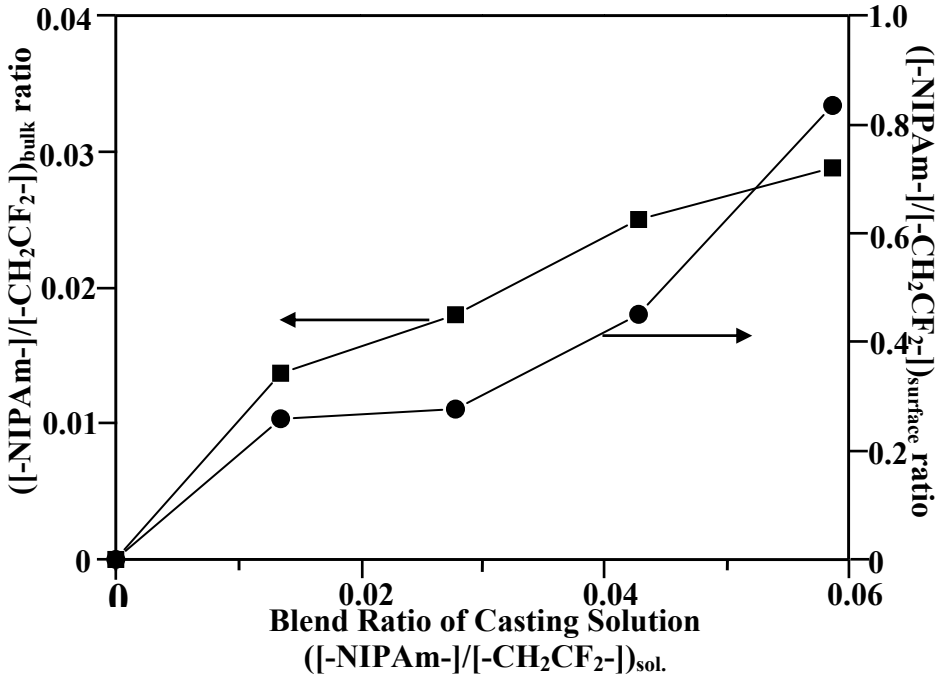

Figure 3.17: Dependence of the surface and bulk [-NIPAm-]/[-CH_2CF_2-] molar ratio of the P4VP-g-PVDF/PNIPAm blend membranes on the blend (mole) ratio for membrane casting solution ([-NIPAm-]/[-CH_2CF_2-]$_{solution}$)

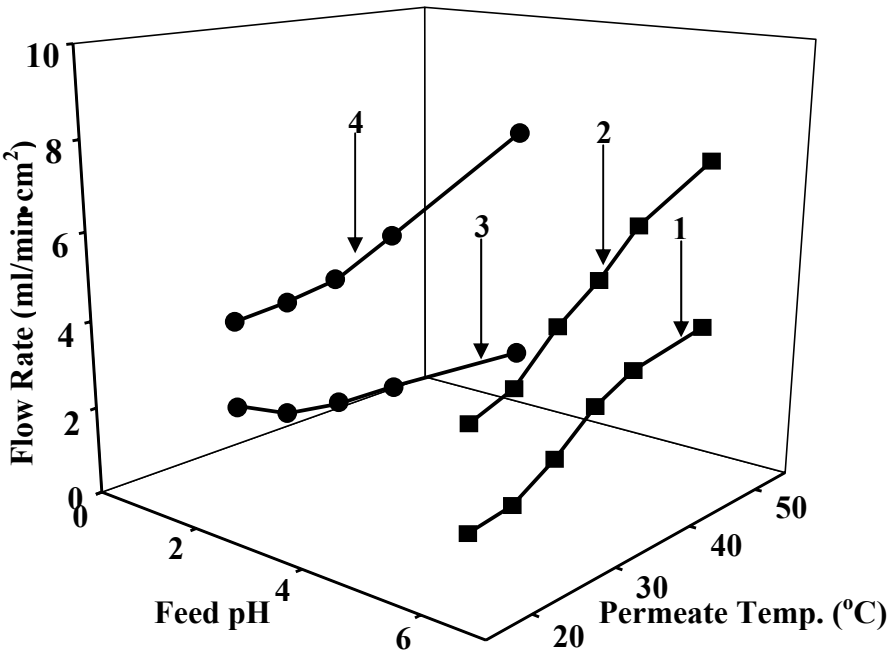

Figure 3.18: pH- and temperature-dependant flux behavior of aqueous solution through the PVDF-*g*-P4VP/PNIPAm blend membranes. Curves 1 and 2 are obtained from PVDF-g-P4VP/PNIPAm blend membranes (([-NIPAm-]/[-CH_2CF_2-]$_{bulk}$)=0.061, and 0.029, respectively). Curves 3 and 4 are obtained from blend membranes membranes (([-NIPAm-]/[-CH_2CF_2-]$_{bulk}$)=0.061, and 0.029, respectively). Curves 3 and 4 are from the fluxes through the PVDF-*g*-P4VP/PNIAPm MF membrane (([-NIPAm-]/[-CH_2CF_2-])=0.045, and 0.014, respectively).

interact with protons *via* hydrogen bonding and protonation when the membrane is cast in an aqueous acid solution, leading to the formation of the positively charged pyridine groups on the MF membrane surfaces. Because of the electrostatic repulsion among the positively charged pyridine groups on the membrane surface at low pH values of the casting bath, the pore size is enhanced.

The effect of the temperature of the casting bath on the pore-size distribution of the MF membrane (blend ratio = 0.029) was also studied. The results are also shown in Table 3.2. Due to the presence of thermoresponsive PNIPAm, the hydrophilic nature of the MF membrane surface decreases with the increase in the temperature of the casting bath during phase inversion, especially when the temperature of the casting bath is above 32^{o}C. As a result, PVDF-*g*-P4VP/PNIPAm MF membrane tends to form a larger specific surface area (smaller pore size) when cast in a bath at lower temperature than that at higher temperature.

The dependence of the pore-size distribution of PVDF-*g*-P4VP/PNIPAm MF membranes (blend ratio = 0.029) on the ionic strength of the casting bath is shown in Table 3.2. The mean pore size of the MF membrane decreases with the increase in the ionic strength of the casting bath with a presence of high proton concentration (pH=1). Our previous studies have shown that most pyridine rings can be protonated to form pyridinium cations when they interact with the aqueous solution of pH 1. The neutral 4VP polymer side chains are transformed into the positively charged polyelectrolyte side chains to some extent (Kee, 2002). At casting bath of low ionic strength (0.1 mol/L), the electrostatic repulsion among the positively charged pyridine rings maximizes the pore dimension to reduce the repulsion. When cast in the bath of

Table 3.2: Pore Size Distribution of the PVDF-*g*-P4VP/PNIPAm MF Membranes[@]

Blend Ratio	pH Value of Casting Bath	Temperature of Casting Bath	Ionic Strength of Casting Bath (mol/L)	Conc. of Casting Solution	Min Pore Size (μm)	Max Pore Size (μm)	Mean Pore Size (μm)
(a) Effect of pH Value of the Casting Bath on the Pore-Size Distribution							
0.029	6	25	**0.1**	12 wt%	0.20	2.33	1.15
0.029	4	25	**0.1**	12 wt%	0.23	3.62	1.23
0.029	3	25	**0.1**	12 wt%	0.23	3.18	1.45
0.029	2	25	**0.1**	12 wt%	0.84	2.89	1.51
0.029	1	25	**0.1**	12 wt%	0.50	3.18	1.67
(b) Effect of Temperature of the Casting Bath on the Pore-Size Distribution							
0.029	**6**	**0**	**0**	12 wt%	0.73	2.56	1.21
0.029	**6**	**25**	**0**	12 wt%	0.35	2.85	1.35
0.029	**6**	**45**	**0**	12 wt%	0.29	3.18	1.90
0.029	**6**	**70**	**0**	12 wt%	1.48	5.00	2.36
(c) Effect of Ionic strength of the Casting Bath on the Pore-Size Distribution							
0.029	**1**	**25**	**0.1**	**12 wt%**	0.50	3.18	1.67
0.029	**1**	**25**	**0.3**	**12 wt%**	0.20	1.84	0.96
0.029	**1**	**25**	**0.5**	**12 wt%**	0.66	1.84	0.92
0.029	**1**	**25**	**0.7**	**12 wt%**	0.20	1.52	0.71
0.029	**1**	**25**	**1**	**12 wt%**	0.25	1.72	0.67
(d) Effect of Polymer Concentration on the Pore-Size Distribution							
0.061	**6**	**25**	**0**	10%	0.23	5.00	1.94
0.061	**6**	**25**	**0**	12%	0.25	1.84	0.69
0.061	**6**	**25**	**0**	15%	0.12	0.61	0.18

(a) and (c) Hydrochloride and sodium chloride are added into the casting bath to achieve the desirable pH and ionic strength, Respectively; (b) and (d) Cast in doubly distilled water.

high ionic strength, such electrostatic repulsion is shielded by the cations (hydrogen ions and sodium ions) and anions (chloride ions) dissolved in the casting bath, (the so-called *polyelectrolyte effect*). As a result, the mean pore size is reduced due to the decrease in the electrostatic repulsion.

The pore size of the PVDF-*g*-P4VP/PNIPAm MF membranes is also dependant on the copolymer concentration of the casting solution, as shown in Table 3.2. The pore size decreases drastically with the increase in polymer concentration of the casting solution. At a low polymer concentration, the extraction of the solvent from the bulk matrix, and thus the polymer-solvent phase separation, are facilitated. As a result, larger pore sizes are obtained for the MF membranes cast from the copolymer solution of lower concentration. The pore-size measurement results of the PVDF-*g*-P4VP MF membranes also indicates that the pore-size distribution of the PVDF-*g*-P4VP/PNIPAM MF membranes is between those of the commercially-available hydrophilic PVDF MF membranes with standard pore size of 0.45μm and 0.65μm, respectively. Thus, these two commercial PVDF MF membranes are used for the comparative study of the flux behaviour of aqueous solution through the PVDF-*g*-P4VP/PNIPAM MF membranes in the later part of this work.

3.2.2.3 Stimuli-Responsive Permeability of Aqueous Solution through the PVDF-*g*-P4VP/PNIPAm MF Membranes

The simultaneous pH and temperature-dependant flow rates of aqueous solution through the PVDF-*g*-P4VP/PNIPAm blend membranes are shown in Figure 3.18. The imposed pressure to achieve such flow rates are 0.03 kg/cm^2 for Curve 1, 0.06kg/cm^2 for Curve 2 and 0.03kg/cm^2 for Curve 3 and 0.20 kg/cm2 for Curve 4, respectively. The PVDF-*g*-P4VP/PNIPAm blend membranes exhibit an increase in permeation rate

in response to the increase in the permeate temperature. The temperature-dependant permeation rate probably has resulted from the change in conformation of the PNIPAm polymer on the surface (including the pore surfaces) and sub-surface of the blend membrane. At a permeate temperature below the LCST of the PNIPAm polymer, the PNIPAm polymer are hydrophilic. Thus, the PNIPAm chains assume an extended conformation on the surface and in the near-surface regions of the pores, reducing the permeation rate of the aqueous solution. On the other hand, at permeate temperatures above the LCST, the PNIPAm polymer chains associate hydrophobically on the membrane pore surface and near-surface regions, resulting in the opening of the pores of the membrane, and hence the observed increase in the permeation rate.

The changes in permeation rate of the blend membranes in response to the changes in permeate pH may be attributed to the change in conformation of the grafted 4VP side chains of the PVDF-*g*-P4VP/PNIPAAM blend membrane. Diametrically opposite to AAc, pyridine group can become protonated (positively charged) at low pH, leading to electrostatic repulsion among the charged pyridine groups. The 4VP side chains are forced to switch from the coiled conformation to an extended one, resulting in a decrease in the effective pore dimension and, thus, the permeability to aqueous media of low pH.

3.2.2.4 pH-Induced Transition in the Chemical States on Pyridine Nitrogen

In order to elucidate the process and mechanism underlying stimuli-responsive permeability of the PVDF-*g*-P4VP/PNIPAm MF membranes to permeate pH, XPS is employed to investigate the variation in chemical states. After the MF membranes were flown through by aqueous solution of different pH value for 10 min and dried

under reduced vacuum, the N 1s XPS core-level spectra of the resulting PVDF-*g*-P4VP and PVDF-*g*-P4VP/PNIPAm MF membranes are shown in Figure 3.19. Non-volatile perchloric acid ($HClO_4$) and sodium chloride were added to the aqueous solution to achieve the desirable pH value and to fix the ionic strength at 0.1M, respectively. Previous studies have suggested that pyridine ring can be involved in two kinds of interaction, *viz.* protonation and hydrogen bonding, with water, acid and amide species in aqueous media. The XPS spectra can be curve-fitted with three components using the following approaches. The main peak component at about 398.5 eV is assigned to the neutral nitrogen (amine of the pyridine rings and amide of PNIPAM) (Moulder, 1992). The peak component at about 399.5 eV is assigned to the hydrogen-bonded nitrogen species, and the peak component at about 400.8 eV is assigned to the protonated pyridinium ions.

The N 1s core-level spectra in Figure 3.19 clearly indicates, when the proton concentration is low, or when the pH value is higher than 2, the main form of interaction is hydrogen bonding. For PVDF-*g*-P4VP and PVDF-*g*-P4VP/PNIPAm MF membrane, protonation becomes significant only when the pH value is decreased to 2 and 1, respectively. On the other hand, in comparison to the PVDF-*g*-P4VP MF membrane, the PVDF-*g*-P4VP/PNIPAm exhibits a less strong interaction with the aqueous acid solution of same pH value. Different from that of PVDF-*g*-P4VP MF membrane, the nitrogen species of the PVDF-*g*-P4VP/PNIPAm MF membrane surface is composed of the tertiary amine of the pyridine rings and the primary amide of the PNIPAm. Due to its extremely weak acidic nature, the nitrogen of the amide can not be protonated in aqueous acid solution. Hydrogen bonding is only interaction with the aqueous solution, leading to a reduced interaction, and thus a reduced

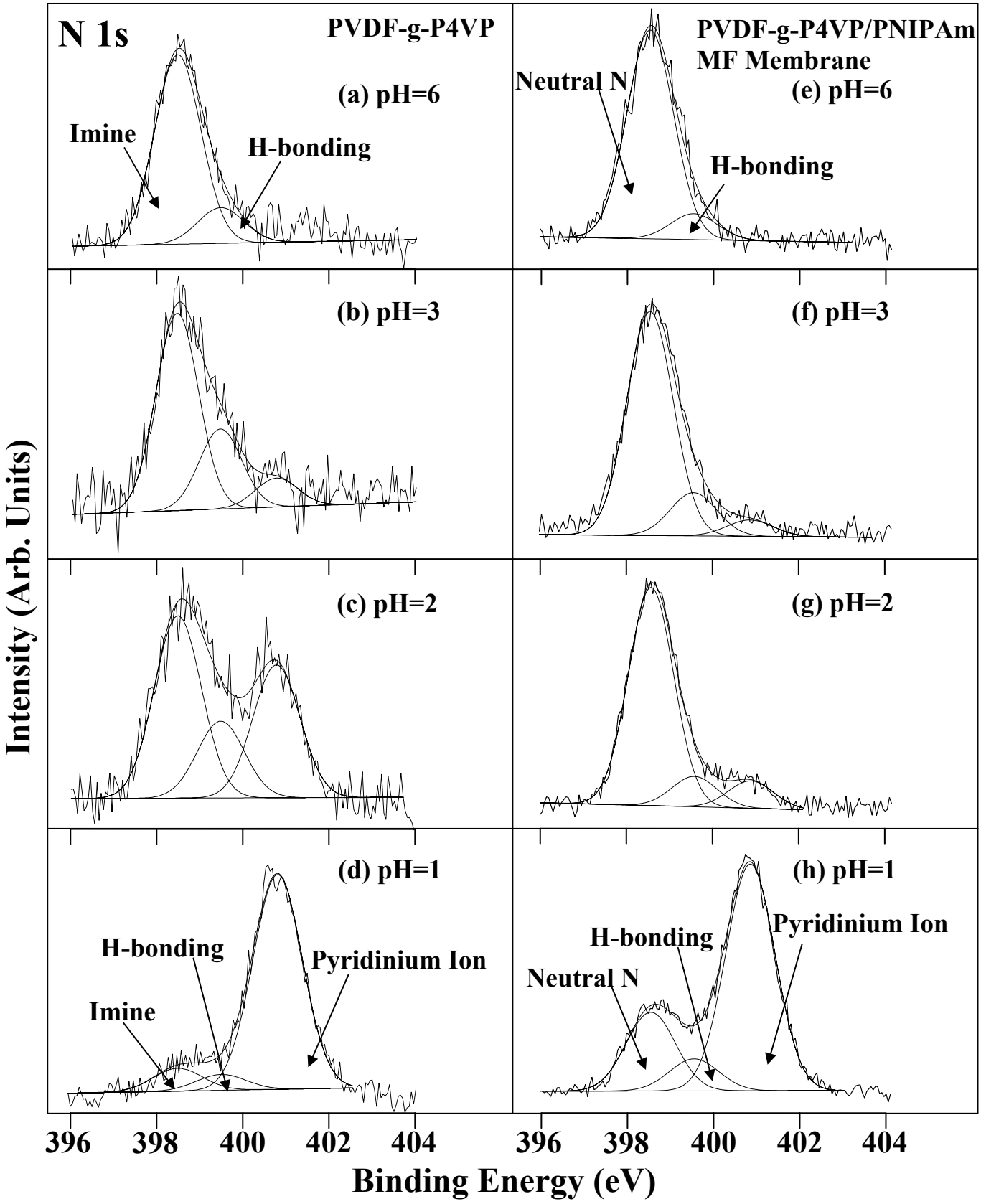

Figure 3.19: XPS N 1s core-level spectra of the PVDF-*g*-P4VP MF membrane and PVDF-*g*-P4VP/PNIPAm MF membrane (([-NIPAm-]/[-CH_2CF_2-])=0.029) after being immersed for 10 min in aqueous solutions of different pH values.

magnitude pH-sensitivity in the flux behaviour of aqueous solution through the PVDF-*g*-P4VP/PNIPAm MF membrane.

3.2.3 Conclusions

By blending the PVDF-*g*-P4VP copolymer and PNIPAM homopolymer in NMP, PVDF-*g*-P4VP/PNIPAM MF membrane was fabricated by phase inversion in aqueous media. Elemental analyses and XPS suggested the bulk and surface PNIPAM content increases with the increase in the blend ratio of PNIPAM. SEM and pore size measurements show that the pore size can be increased with an increased in temperature, and pH value of casting bath, and the decrease in PNIPAM content, ionic strength of the casting bath and polymer concentration of the cast solution. The permeation rate of PVDF-*g*-P4VP/PNIPAM MF membranes increase with the increase in the pH value and temperature of the aqueous solution, and the magnitude of the pH-sensitivity of PVDF-*g*-P4VP MF membrane was compromised with the temperature-sensitivity by PNIPAM entrapment. XPS revealed that the pH-sensitivity of the MF membrane was reduced due to the weakened interaction of the membranes surface with the aqueous acidic media. Such strategy proposed a convenient approach for fabricating multifunctional and multi-stimuli-responsive MF membranes.

Chapter 4:

Poly(Vinylidene Fluoride) with Grafted Zwitterionic Polymer Side Chains for Electrolyte-Responsive Microfiltration Membranes

4.1 Experimental

4.1.1 Materials and Reagents

PVDF and NMP are same as reported in earlier part.. The monomer, *N*,*N*′-dimethyl(methacryloyl ethyl) ammonium propane sulfonate (DMAPS) was prepared according to the methods reported earlier (Chen *et al.*, 2000). The chemical structure of DMAPS is shown below:

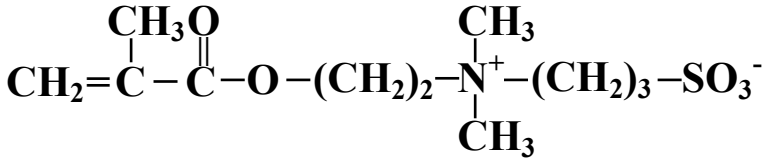

The solvent for the DMAPS powders, dimethylsulphoxide (DMSO), was obtained from Lab-Scan Asia Ltd., Bangkok, Thailand. It was used as received.

4.1.2 Preparation of the PVDF-*g*-PDMAPS Copolymer and PDMAPS Homopolymer

PVDF NMP solution was ozone-pretreated and graft-copolymerized with DMAPS to produce the PVDF-*g*-PDMAPS copolymer. 30 ml of PVDF NMP solution was ozone-pretreated as stated in Section 3.1. A pre-determined quantity of the DMAPS monomer was dissolved in 20 ml of DMSO. The monomer solution was added to the degassed solution of ozone-preactivated PVDF to achieve the desirable [DMAPS]/[-CH_2CF_2-] molar ratio. After an additional 15 min of argon purging, the temperature of the water bath was raised to 60ºC to induce the decomposition of peroxide groups on the PVDF chains and to initiate the graft copolymerization of DMAPS. A constant flow of argon was maintained during the 3 h of thermal graft polymerization. After the reaction, the reaction mixture was cooled in an ice bath and the resultant PVDF-*g*-PDMAPS copolymer was precipitated in an excess amount of doubly distilled water. After recovery by filtration, the copolymer was washed

repeatedly in ethanol and water for 48 h. The solvent was changed every 8 h. The copolymer sample was recovered and dried by pump under reduced pressure for subsequent characterization. The PVDF-*g*-PDMAPS membrane was prepared from 12 wt% DMSO solution of the copolymer by phase inversion technique, as reported earlier.

PDMAPS was prepared from the free radical homopolymerization of DMAPS. Fifty ml of doubly distilled water, 10 g of DMAPS and 0.05 g of ammonium peroxydisulfate ($(NH_4)_2S_2O_8$) were introduced into a flask. The temperature of the reaction mixture was raised to 60ºC to induce the polymerization reaction. After 24 h of reaction, the flask was cooled in an ice bath, and the reaction mixture was precipitated in excess NMP. The DMAPS homopolymer (PDMAPS) sample was recovered by filtration and dried in a vacuum oven.

4.1.3 Characterization of Polymers and Membranes

For the UV-Vis absorbance spectroscopy of PDMAPS aqueous solution, kown amounts of PDMAPS were added into aqueous media of different ionic strength. After the homopolymer had been dissolved completely at 70ºC, the absorbance of the solution at 500 nm was measured on a UV-Vis-NIR spectrophotometer (Shimadzu UV-3101PC scanning spectrophotometer, Kyoto, Japan) under the time course mode.

The chemical composition of the PVDF-g-PDMAPS copolymer was measured by elemental analysis. The carbon, nitrogen and hydrogen elemental contents were determined under the similar protocol described before,. Taking into account the elemental stoichiometries of both the graft and the fluoropolymer chains, the $([\text{-DMAPS-}]/[\text{-}C_2CF_2\text{-}])_{bulk}$ ratio can be calculated from Equation (4.1) below:

$$([\text{-DMAPS-}]/[\text{-}CH_2CF_2\text{-}])_{bulk} = 2[N]/([C]\text{-}11[N]) \quad \ldots (4.1)$$

where the factors 2 and 11 are introduced to account for the fact that there are 2 and 11 carbon atoms per repeat unit of PVDF and DMAPS polymer, respectively. The process of the TGA, XPS, SEM and pore-size measurement is the same as in Section 3.1.

For the measurement of the electrolyte-sensitive flux through the MF membranes, the PVDF-*g*-PDMAPS MF membrane was immersed in the doubly distilled water for several minutes. It was then mounted on the microfiltration cell (Toyo Roshi UHP-25, Tokyo, Japan). An aqueous NaCl solution of a specific concentration was added to the cell. The flux was calculated from the volume of solution permeated per unit time under a specific fixed pressure.

4.2 Results and Discussion

4.2.1 Ozone Pre-activation of PVDF and Graft Copolymerization of DMAPS with the PVDF (the PVDF-*g*-PDMAPS Copolymers)

Composition Analysis of the PVDF-*g*-PDMAPS Copolymers

Elemental analysis was used to determine the carbon and nitrogen contents in the copolymer powders. The bulk graft concentration, or the $([\text{-DMAPS-}]/[\text{-}CH_2CF_2\text{-}])_{bulk}$ ratio, is calculated from the $([N]/[C])_{bulk}$ ratio and Equation 4.1 (see Experimental Section). The $([N]/[C])_{bulk}$ ratio and the corresponding bulk graft concentration, or the $([\text{-DMAPS-}]/[\text{-}CH_2CF_2\text{-}])_{bulk}$ ratio, as a function of the monomer to PVDF feed ratio ([DMAPS]/[-CH_2CF_2-] ratio) is shown in Figure 4.1. The results indicate that the graft concentration increases with the increase in monomer to polymer feed ratio, or the DMAPS monomer concentration used for graft copolymerization.

Thermogravimetric Analysis (TGA) of the PVDF-*g*-PDMAPS Copolymers

One of the unique properties of PVDF is its excellent thermal stability. The thermal stability of the PVDF-*g*-PDMAPS copolymer is studied by TGA. Compared to the PVDF and DMAPS homopolymer, a distinct two-step degradation process was observed for the graft copolymers. The onset of the first major weight loss at about 330ºC corresponds to the decomposition of the DMAPS side chains of the copolymers. The second major weight loss commences at about 400ºC, corresponding to the decomposition of the PVDF main chain. TGA results also indicate that the extent of the first major weight loss of each graft copolymer coincides approximately with the DMAPS polymer content in the copolymer, as determined from elemental analysis.

4.2.2 Thermoresponsive Behavior of the DMAPS Homopolymer

After synthesis and purification, the DMPAS homopolymer (PDMAPS) was dissolved in an aqueous medium at 70ºC to achieve a specific polymer concentration. UV-visible absorption spectroscopy was used to measure the absorbance of the PDMAPS aqueous solution at the wavelength of 500 nm under different temperatures (Chen *et al.*, 2000).

Effect of Polymer Concentration on the Upper Critical Solution Temperature (UCST) of PDMAPS

Figure 4.3(a) shows the absorbance of the aqueous solutions of PDMAPS of different concentrations as a function of temperature. All PDMAPS aqueous solutions exhibit an abrupt increase in absorbance with the decrease in solution temperature

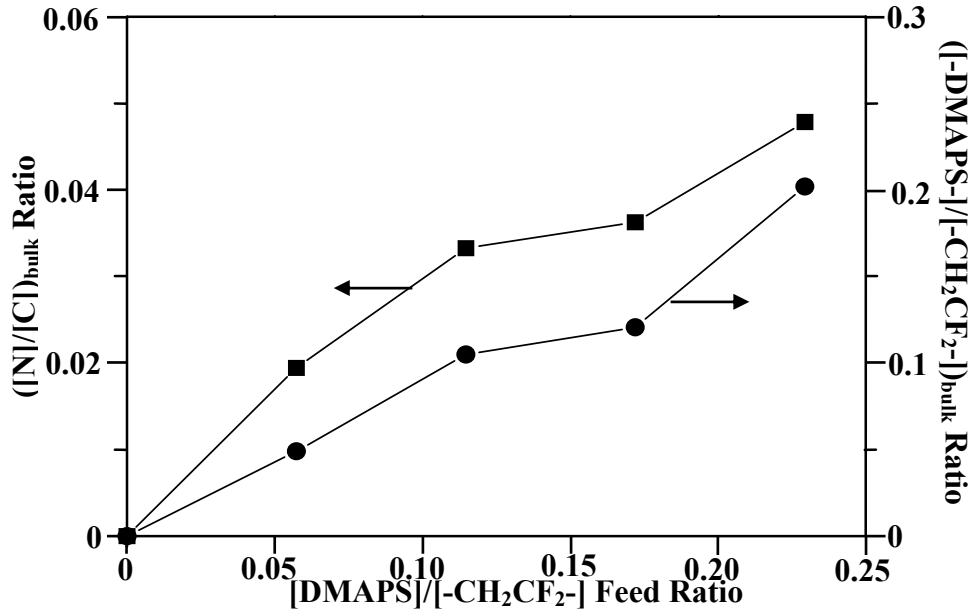

Figure 4.1: Effect of the [DMAPS]/[-CH_2CF_2-] molar feed ratio on the $([N]/[C])_{bulk}$ ratio and the bulk graft concentration ($([\text{-DMAPS-}]/[\text{-}CH_2CF_2\text{-}])_{bulk}$ ratio) of the PVDF-g-PDMAPS MF membrane.

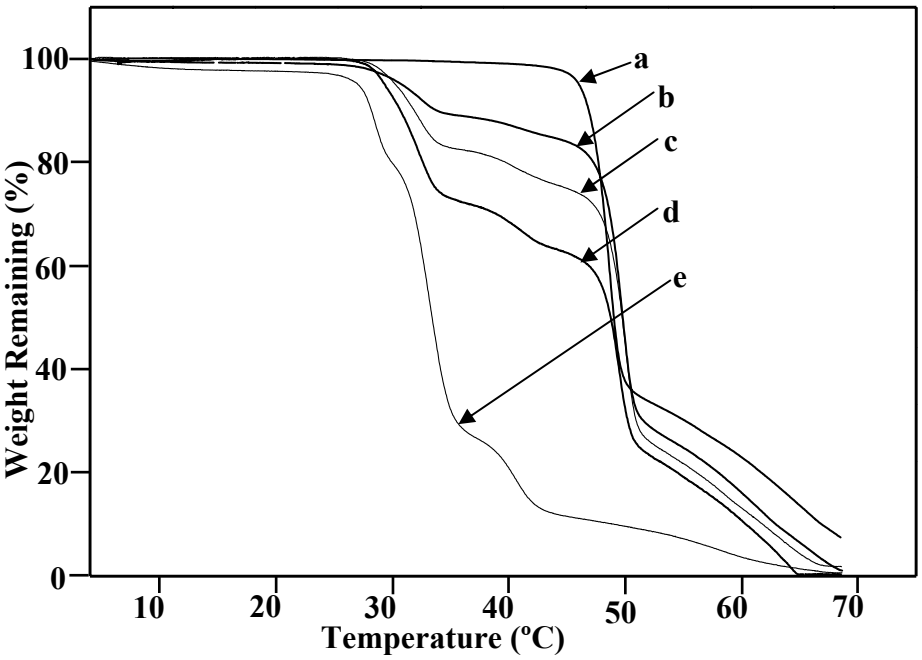

Figure 4.2: Thermogravimetric analysis curves of (a) the pristine PVDF, the PVDF-g-PDMAPS copolymers of bulk graft concentrations ($([\text{-DMAPS-}]/[\text{-}CH_2CF_2\text{-}])_{bulks}$ ratios) of (b) 0.05, (c) 0.12 and (d) 0.20, and (e) the PDMAPS homopolymer.

from 70ºC. This phenomenon corresponds to the transparent-opaque transition of the solution during the temperature declines. Such a transition is attributed to the phase separation of PDMAPS and water. At a high temperature, DMAPS polymer chains adopt an extended conformation and dissolve completely in the aqueous medium. With the temperature decreasing to the point on the phase boundary line, the intra- and inter-chain interactions of the DMAPS polymer lead to the formation of a well-defined micelle (dissolution-micellization transition). The polymer chain itself undergoes a hydrophilic-hydrophobic transformation. Figure 4.3(a) also indicates that the phase transition point on the phase boundary line of a binary system (polymer and solvent) of the PDMAPS solution exhibits a distinct dependence on the polymer solution concentration. When the concentration is very low (1~2 wt%, Curves 1 and 2), the UCST decreases very gradually to about 60ºC. It decreases rapidly to about 50ºC when the polymer concentration increases to 5 wt% (Curve 3). On the other hand, when the polymer concentration increases to over 10 wt% (Curves 4 and 5), the UCST remains almost constant at about 45ºC. Thus, a high concentration of the polymer chains retards the phase separation of the PDMAPS solution. The stabilization of the PDMAPS solution at a high polymer concentration probably has resulted from the increased spatial and intermolecular interactions among the chains in solution.

Effect of Electrolyte Concentration on the UCST of PDMAPS

The dependence of the UCST of the PDMAPS aqueous solution on the electrolyte concentration (ionic strength) is also analyzed, as shown in Figure 4.3(b). The absorbance data in Figure 4.3(b) suggest that the addition of a low molecular weight

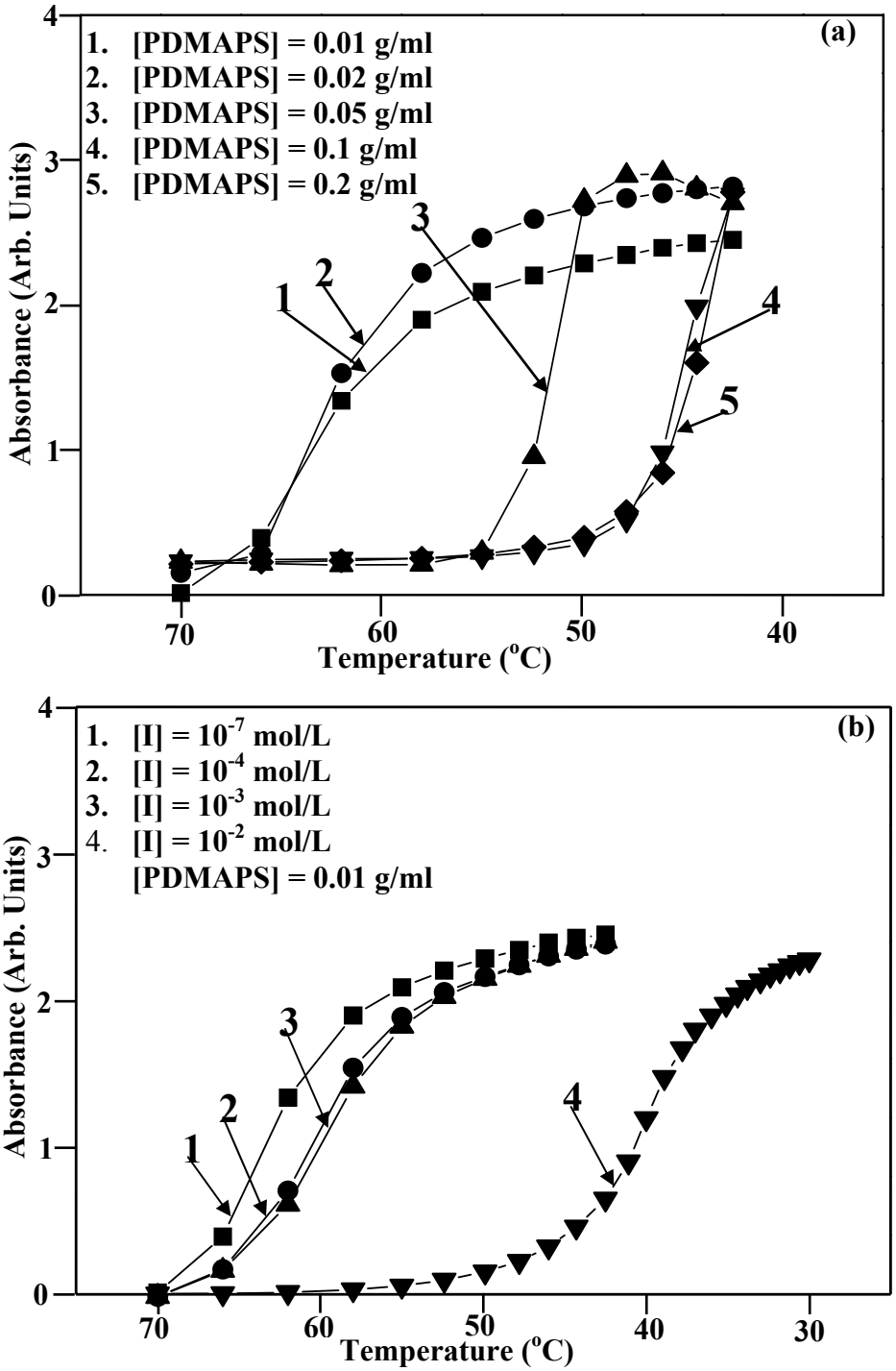

Figure 4.3: (a) UV-visible absorbance of aqueous solutions of PDMAPS of different concentrations as a function of temperature. (b) UV-visible absorbance of aqueous solutions of PDMAPS of different electrolyte concentration as a function of temperature.

salt (sodium chloride in this study) can greatly decrease the UCST of the PDMAPS aqueous solution. Thus, the phase separation is retarded, especially when the electrolyte concentration of the aqueous medium is over 0.01 M. The UCST of the PDMAPS solution decrease from over 65ºC to less than 40ºC, when the electrolyte concentration of the aqueous medium increases from about 10^{-7} to 10^{-2} mol/L. For the PDMAPS solutions with electrolyte concentration above 10^{-1} mol/L, no phase separation was observed even when the solution was cooled down to the ice bath temperature. The data in Figure 4.3(b) suggest that addition of electrolytes helps to stabilize the zwitterionic polymer solution and to prevent the phase separation.

The stabilization of the PDMAPS aqueous solution in the presence of an electrolyte can be attributed to the *anti-polyelectrolyte effect*. For PDAMPS solution of low ionic strength, the electrostatic attraction of the oppositely charged ions on DMAPS polymer chains is predominant, and the polymer chains tend to adopt a coiled conformation, leading to micellization in the solution when the temperature is decreased. In the solution of high electrolyte concentration, the electrostatic attraction in the polymer chains is shielded. As a result, the polymer chains adopt a more extended conformation *via* the Debye-Huckel shielding effect. It should be noted that the data in Figure 4.3 are influenced by both thermodynamic and kinetic effects, and should only be considered as rough estimates of the UCST's. They only provide semi-quantitative information with respect to the impact of solution conditions, such as graft and electrolyte concentration and temperature, on the membrane structure and on the membrane permeability.

4.2.3 Fabrication of MF Membranes from the PVDF-*g*-PDMAPS Copolymers

After the PVDF-*g*-PDMAPS MF membranes were cast by phase inversion in aqueous media of different ionic strength and temperature from the 12 wt% DMSO solution of the respective copolymers, the surface composition and morphology of the membrane were analyzed by XPS and SEM, respectively.

XPS Analysis of the MF Membranes

The surface composition of the PVDF-*g*-PDMAPS MF membranes was studied by XPS. Taking into consideration of the thermoresponsive nature of the DMAPS polymer side chain, XPS analysis of the surface composition of the copolymer membranes cast in coagulating bath heated to different temperature was first carried out. However, the XPS C 1s core-level lineshape of the copolymer membrane was found to undergo obvious changes only when the temperature of the coagulating bath was increased to about 100ºC. The changes in the C 1s core-level spectra of the pristine PVDF membrane and three PVDF-*g*-PDMAPS MF membranes of different graft concentrations cast at room temperature and at about 100ºC are compared in Figure 4.4.

For the pristine PVDF membrane cast at room temperature, the C 1s core-level spectrum can be curve-fitted with two peak components, having binding energies (BE's) at about 285.8 eV for the $\underline{C}H_2$ species and 290.5 eV for the $\underline{C}F_2$ species, respectively. The ratio for the two species, determined from the spectral peak component area, is about 1.04, which is in good agreement with the structure of PVDF. On the other hand, the C 1s core-level spectrum of PVDF membrane cast at 100ºC can be curve-fitted with three peak components. In addition to the two main components mentioned above, the minor peak component at the BE of about 284.6 eV

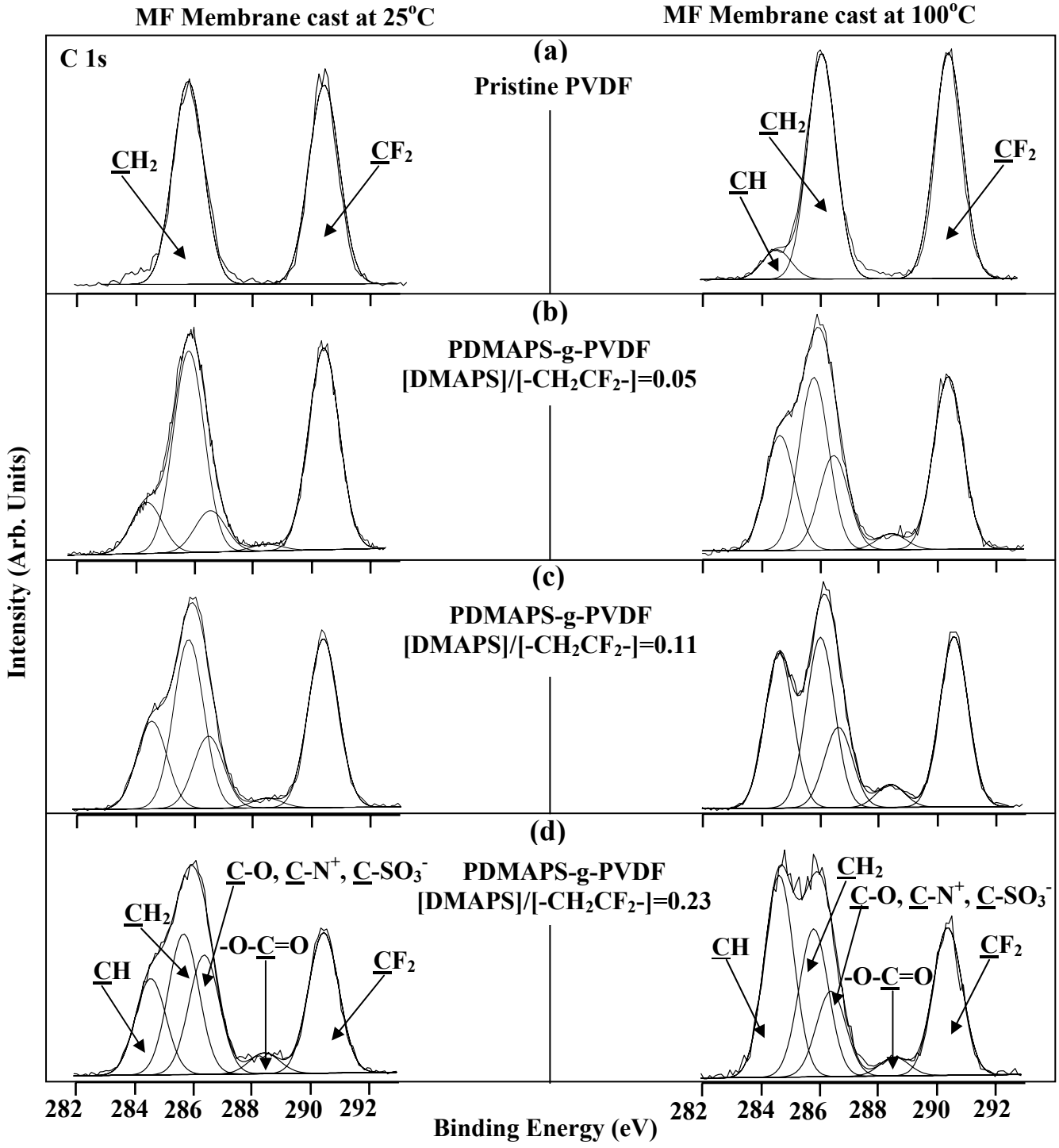

Figure 4.4: XPS C 1s core-level spectra of the membranes cast by phase inversion at 25ºC and at about 100ºC from 12 wt% DMSO solutions of (a) the pristine PVDF homopolymer, the PVDF-g-PDMAPS copolymers prepared from the [DMAPS]/[-CH_2CF_2-] molar feed ratios of (b) 0.05, (c) 0.11 and (d) 0.23.

is attributed the neutral hydrocarbon, arising from the branching sites and end groups of the PVDF chains (Russo, 1996). The C 1s core-level spectra of the PVDF-*g*-PDMAPS MF membranes are curve-fitted with five peak components using the following approach. The two peak components of about equal intensities at the BE's of about 285.8 eV and 290.5 eV are assigned to the $\underline{C}H_2$ and $\underline{C}F_2$ species of PVDF, respectively. The component at the BE of about 288.5 eV is assigned to the -O-$\underline{C}$=O species of the grafted DMAPS polymer chains (Moulder *et al.*, 1992; Fraser *et al.*, 2002). The component with the BE at 284.6 eV, on the other hand, is attributed to the hydrocarbon backbone of the grafted DMAPS polymer chain, or the $\underline{C}$H species. The peak component at the BE of about 287 eV arises from the combined contribution of the $\underline{C}$-O species (Ying 2003), $\underline{C}$-N^+ species (Li *et al.*, 1997) and $\underline{C}$-SO_3^- species (Ruangchuay *et al.*, 2002) of the DMAPS polymer side chains.

The C 1s core-level spectra in Figure 4.4 show that after ozone pre-activation, graft copolymerization and phase inversion in water at room temperature, the spectral area ratio of the $\underline{C}$H component at 284.6 eV to that of the $\underline{C}F_2$ component at 290.5 eV increases from 0 (pristine PVDF membrane) to over 65% when the feed ratio used for graft copolymerization increasing from 0 to 0.23. The XPS spectra in Figure 4.4 also show that both the pristine PVDF membrane and the PVDF-*g*-PDMAPS MF membranes cast at 100ºC always have a higher [$\underline{C}$H]/[$\underline{C}F_2$] ratio than that of the corresponding MF membrane cast at room temperature. The enhancement in surface graft concentration of the PVDF-*g*-PDMAPS MF membranes is attributable to the thermoresponsive nature of the DMAPS polymer side chains. At a high temperature, the DMAPS polymer becomes more hydrophilic than at a low temperature. When the

polymer solution undergoes phase inversion in an aqueous bath, the migration of the DMAPS polymer side chains from the bulk matrix to the surface occurs.

For the PVDF-*g*-PDMAPS MF membranes cast at the two temperature extremes, their surface graft concentration, or the $([\text{-DMAPS-}]/[\text{-}CH_2CF_2\text{-}])_{surface}$ ratio, can be determined from the $([N]/[C])_{surface}$ ratio and Equation 4.1, in a similar manner as that used to determine the bulk graft concentration. Figure 4.5 shows that the surface graft concentration of the MF membranes cast at different temperatures increases gradually with the increase in ([DMAPS]/[-CH_2CF_2-]) molar feed ratio used for graft copolymerization.

The surface graft concentration of the MF membrane determined by XPS and the bulk graft concentration determined by elemental analysis are compared (compared Figure 4.1 and Figure 4.5). It is unambiguous that the bulk graft concentration of the copolymer is always higher than the surface graft concentration of the corresponding MF membrane, despite the fact that a higher temperature of the casting bath can increase the surface graft concentration of the MF membrane. For other MF membranes involving PVDF with grafted hydrophilic side chains and cast in an aqueous medium, the surface graft concentration is always much higher than the corresponding bulk graft concentration, as a result of surface enrichment of the side chains (Ying, 2003; Wang *et al.*, 2001). Thus, the surface migration or re-arrangement of the zwitterionic graft chains in the PVDF-*g*-PDMAPS MF membranes is entirely different from that of the MF membranes prepared from PVDF with grafted acrylic acid (AAc), 4-vinylpyridine (4VP), poly(ethylene glycol) methacrylate and *N*-isopropylacrylamide (NIPAm) side chains. Arising from reduced hydrodynamic

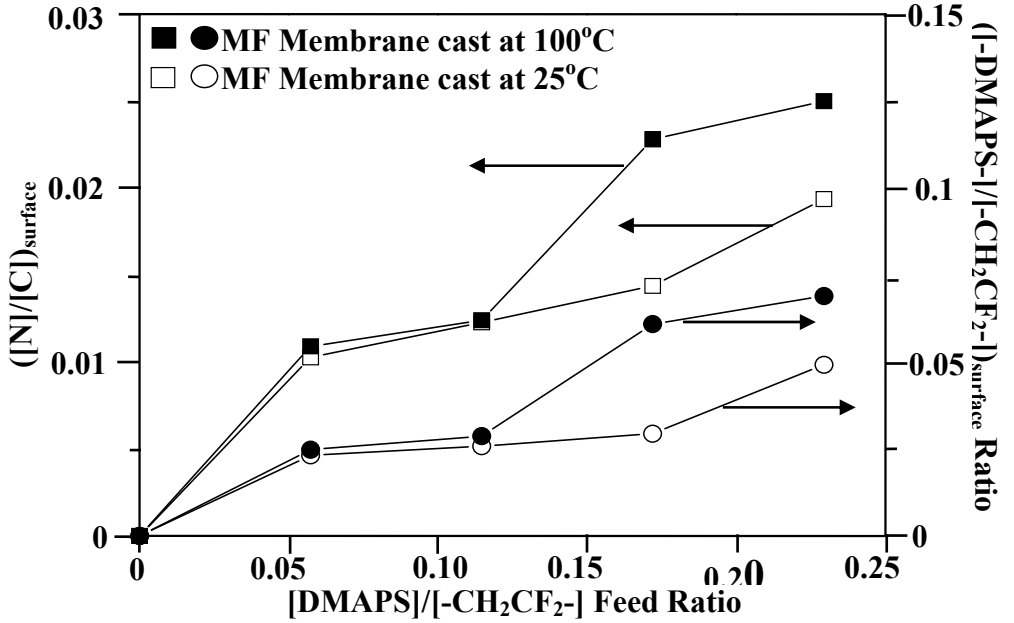

Figure 4.5: Effect of [DMAPS]/[-CH_2CF_2-] molar feed ratio on the $([N]/[C])_{surface}$ ratio and the surface graft concentration $([\text{-DMAPS-}]/[\text{-}CH_2CF_2\text{-}])_{surface}$ ratio) of the PVDF-*g*-PDMAPS MF membrane cast at room temperature and at 100ºC, respectively.

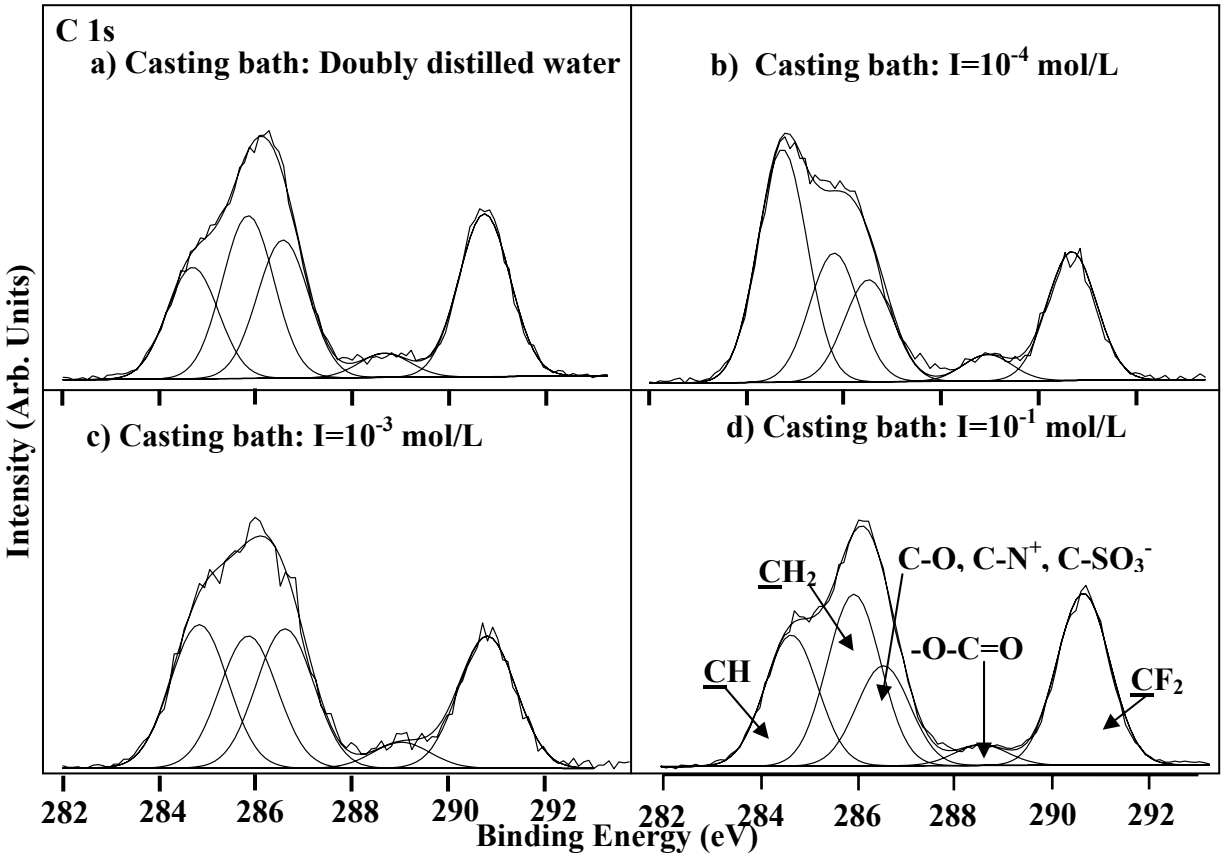

Figure 4.6: XPS C 1s core-level spectra of PVDF-g-PDMAPS MF membrane ($([\text{-DMAPS-}]/[\text{-}CH_2CF_2\text{-}])_{bulk}$=0.20) cast from 12 wt% DMSO solution at room temperature by phase inversion in aqueous media of different electrolyte strength: (a) doubly distilled water, (b) 10^{-4}, (c) 10^{-3} and (d) 10^{-1} mol/L of the electrolyte.

interactions, especially for membranes cast below the UCST of DMAPS polymer in aqueous (non-electrolyte) media, the micellization of the zwitterionic polymer in the surface and near-surface regions, as a result of the phase inversion process, probably has reduced substantially the effective surface concentration of the DMAPS polymer probed by XPS. The low degree of surface aggregation of the DMAPS side chains can also be attributed to their relatively short chain length. The average degree of polymerization of DMAPS, defined as the average number of repeat units of DMAPS per initiation site, is estimated to be in the range of 4 to 16 when the monomer to polymer feed ratio used for graft copolymerization is increased from 0.05 to 0.23.

The XPS C 1s core-level spectra of the MF membranes cast from 12 wt% DMSO solution of the PVDF-g-PDMAPS copolymer (($[\text{-DMAPS-}]/[\text{-CH}_2\text{CF}_2\text{-}]$)$_{bulk}$=0.20) in aqueous medium of different electrolyte concentrations (I's) at room temperature are shown in Figure 4.6. The spectral area ratio of the ($\underline{C}$H)$_{DMAPS}$ component to the ($\underline{C}$F$_2$)$_{PVDF}$ component increases initially with the electrolyte concentration of the casting bath up to about 10^{-4} mol/L. The ratio, however, undergoes a gradual decrease when the electrolyte concentration of the casting bath is increased further. Low molecular weight electrolyte has a complicated effect on the behavior of DMAPS polymer chains in an aqueous medium (Chen *et al.*, 2002). When the ionic strength of the aqueous solution becomes large, the electrostatic attraction of the polymer chains is gradually shielded by the ions in the aqueous medium, and the distribution of DMAPS polymer side chains on the membrane surface, partially driven by the electrostatic attraction, is reduced. As a result, the spectral area ratio of the ($\underline{C}$H)$_{DMAPS}$ species to the ($\underline{C}$F$_2$)$_{PVDF}$ species decreases at a high electrolyte concentration of the casting bath.

Surface Morphology of the MF Membranes

The surface morphologies of the PVDF-*g*-PDMAPS MF membranes and pristine PVDF membrane were revealed by SEM. Figure 4.7 shows the SEM images obtained at a magnification of ×5000 for the MF membranes cast from 12 wt% DMSO solution by phase inversion in doubly distilled water at room temperature. SEM images reveal that the incorporation of the DMAPS side chains increases the porosity of the PVDF-*g*-PDMAPS MF membranes, while the mean pore size decreases with the increase in bulk graft concentration. The formation of the microporous membrane structure probably can be attributed to the interactions of the grafted DMAPS chains with the aqueous medium during the phase inversion process. The hydrodynamic interactions arise from the dissolution-micellization effect of the DMAPS graft chains, as well as the increase in hydrophilicity of PVDF after graft copolymerization with DMAPS. The water contact angle of the PVDF-*g*-PDMAPS copolymers decreases from about 110^{o} to about 90^{o} when the graft concentration (([-DMAPS-]/[-CH_2CF_2-])$_{bulk}$ ratio) increases from 0.05 to 0.2.

The morphology of the PVDF-*g*-PDMAPS MF membrane (([-DMAPS-]/[-CH_2CF_2-])$_{bulk}$=0.20) cast from 12 wt% DMSO solution in aqueous media of different electrolyte concentrations (I's) at room temperature was studied by SEM. The SEM results reveal that the pore dimension of the PVDF-*g*-PDMAPS MF membrane increases gradually with the ionic strength of the casting bath. When coagulated in the bath of low electrolyte concentration, electrostatic attraction will result in a reduction in pore dimension. On the other hand, when cast in the aqueous bath of high

electrolyte concentration, the interaction of the zwitterionic graft chains with the aqueous electrolyte during the phase inversion process shields the electrostatic attraction among the graft chains (the *anti-polyelectrolyte effect*). The anti-polyelectrolyte effect forces the DMAPS chains in the surface and near-surface regions to assume the fully extended conformation. The subsequent dissolution-micellization transition during the phase inversion process gives rise to the increased pore dimension in the "dried" membrane.

3.2.4 Pore-Size Measurements of the MF Membranes

The pore sizes and pore-size distribution of the PVDF-*g*-PDMAPS membranes cast from copolymer solutions of different graft concentrations in aqueous media of different electrolyte concentrations are measured on the Coulter Porometer II, according to the procedures reported earlier.

The pore size and pore-size distribution of the MF membranes cast from 12 wt% DMSO solution of the respective copolymers in doubly distilled water are summarized in Table 4.1. The data suggest that the mean pore size decreases gradually with the increase in bulk graft concentration of the PVDF-*g*-PDMAPS copolymer. The dependence of the pore size and pore-size distribution of the PVDF-*g*-PDMAPS MF membrane on the electrolyte strength of the casting bath is also shown in Table 4.1. Thus, the mean pore size of the PVDF-*g*-PDMAPS MF membrane increases with the electrolyte concentration of the casting bath. This phenomenon is attributed to the *anti-polyelectrolyte effect* as mentioned above. The pore-size measurement also indicates that the PVDF-*g*-PDMAPS MF membranes

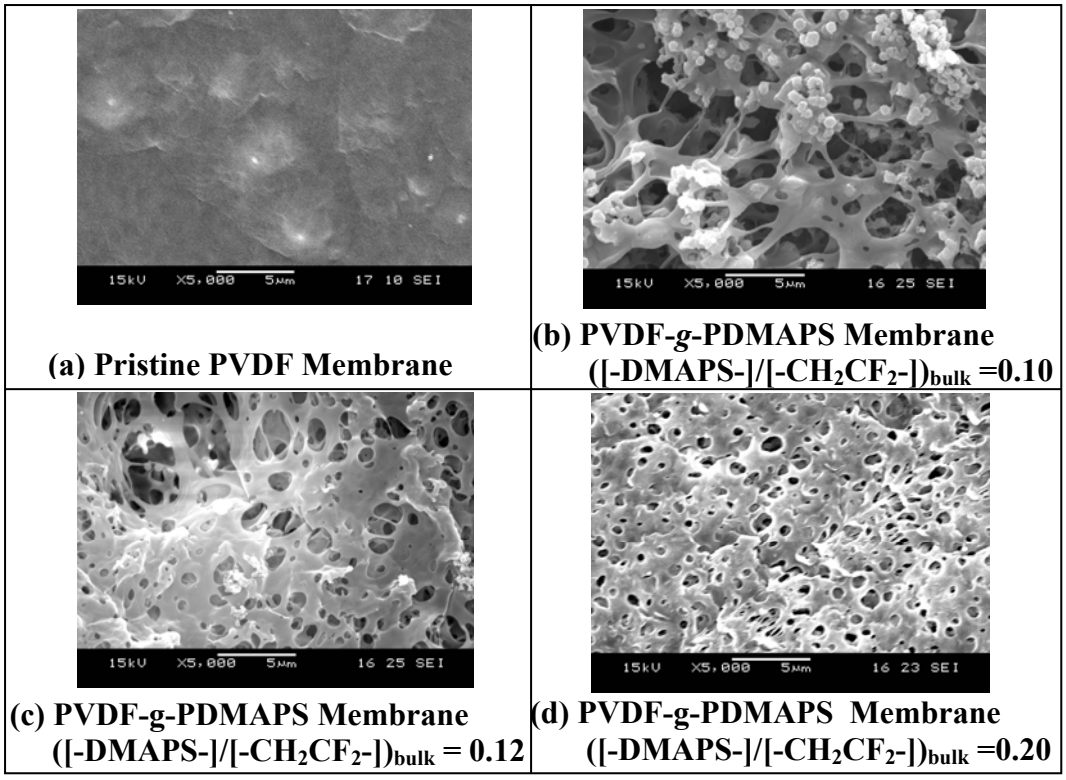

Figure 4.7: SEM micrographs of the MF membranes cast by phase inversion from the 12 wt% DMSO solutions of (a) the pristine PVDF, and the PVDF-g-PDMAPS copolymers of different bulk graft concentrations of (b) 0.10, (c) 0.12 and (d) 0.20.

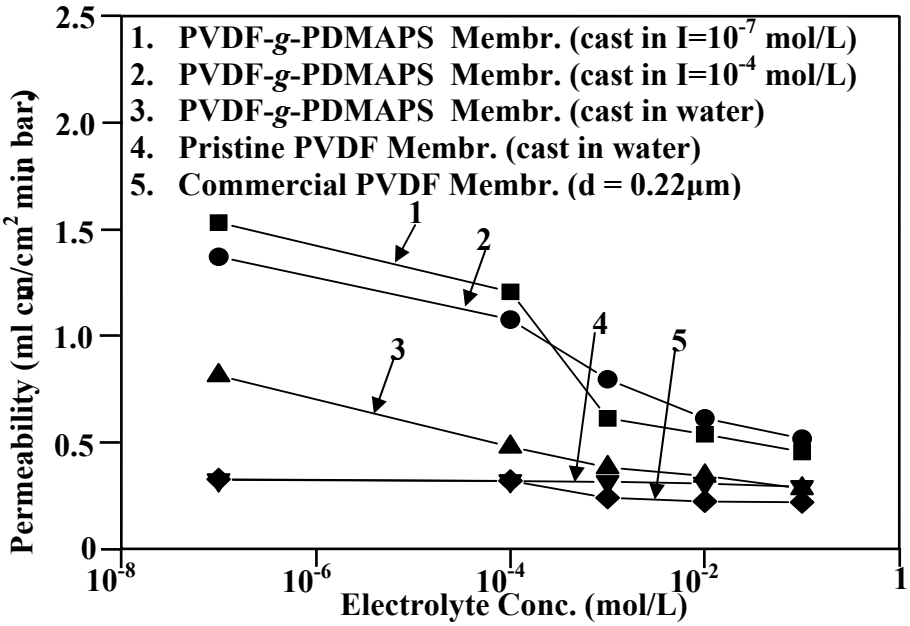

Figure 4.8: Electrolyte-dependant permeability of aqueous solution through the PVDF-*g*-PDMAPS MF membranes. Curves 1 and 2 are the permeability through the MF membranes cast from PVDF-*g*-PDMAPS copolymer (([-DMAPS-]/[-CH_2CF_2-])$_{bulk}$=0.10) in the coagulation bath with an electrolyte strength of 10^{-7} and 10^{-4} mol/L, respectively, at room temperature. Curve 3 is through the PVDF-*g*-PDMAPS (([-DMAPS-]/[-CH_2CF_2-])$_{bulk}$=0.20) cast in doubly distilled water. Curve 4 is through the membrane cast from the PVDF homopolymer. Curve 5 is through the commercial PVDF membrane with a standard pore diameter of d=0.22 μm.

have a comparable effective mean pore size as the commercial hydrophilic PVDF MF membrane with a standard pore diameter of 0.22 μm. Thus, the latter was used for the comparative study of the electrolyte-dependant flux behavior with the present PVDF-*g*-PDMAPS MF membranes.

4.2.5 Flux Behavior through the PVDF-*g*-PDMAPS MF Membranes

The electrolyte-dependant permeability of aqueous solutions through the PVDF-*g*-PDMAPS MF membranes is defined as the ratio of flux to pressure drop across the ionic strength of the solution. The flux of the aqueous solution through the pristine PVDF membrane cast from the 12 wt% DMSO solution by phase inversion exhibits an electrolyte-independant behavior (Curve 4). However, the flux of the aqueous media through the commercial hydrophilic PVDF MF membrane of comparable effective pore size (obtained from Millipore Corporation, Bedford, MA) shows a weak dependence on the electrolyte concentration of the medium, especially in the high electrolyte concentration range (Curve 5). On the other hand, the flux of the aqueous solution through the PVDF-g-PDMAPS MF membranes decreases with the increase in electrolyte concentration from 10^{-7} to 10^{-1} mol/L, with the most drastic change in flux being observed at electrolyte concentrations between 10^{-7} and 10^{-3} mol/L (Curves 1 to 3).

The dependence of permeation rate through the PVDF-*g*-PDMAPS MF membrane on the electrolyte concentration is attributable to the conformational change of the DMAPS polymer side chains on the membrane surface and sub-surface, especially on the pore surface and sub-surface regions. When the electrolyte concentration is very low, the electrostatic attraction among the ammonium cations and sulfate anions

Table 4.1: Pore Size Distribution of the PVDF-*g*-PDMAPS MF Membranes[a)]

Molar Feed Ratio [DMAPS]/[-CH_2CF_2-]	Bulk Graft Conc. [-DMAPS-]/[-CH_2CF_2-]	Temperature of Casting Solution (°C)	Electrolyte Strength of Casting Bath (mol/L)	Min Pore Size (μm)	Max Pore Size (μm)	Mean Pore Size (μm)
(a) Effect of Bulk Graft Concentration on the Pore-Size Distribution[b)]						
0.06	0.05	25	0	0.29	1.30	0.64
0.11	0.10	25	0	0.35	1.12	0.52
0.17	0.12	25	0	0.33	0.89	0.48
0.23	0.20	25	0	0.23	0.82	0.31
(b) Effect of Ionic Strength of the Casting Bath on the Pore-Size Distribution[c)]						
0.23	0.20	25	1.0E-07	0.23	0.82	0.31
0.23	0.20	25	1.0E-04	0.22	0.88	0.32
0.23	0.20	25	1.0E-02	0.24	0.96	0.35
0.23	0.20	25	1	0.23	1.14	0.44

[a)] The commercial PVDF MF membrane (obtained from Millipore Corporation, Bedford, MA) has a standard pore diameter designation of d=0.22 μm. The actual pore characteristics are:
max pore size=0.72 μm; min pore size=0.52 μm; mean pore size=0.57 μm
[b)] Cast in doubly distilled water
[c)] Cast in aqueous NaCl solution of different concentrations

forces the DMAPS side chains to adopt a coiled conformation. On the other hand, due to the electrostatic screening effect, a high electrolyte concentration will shield the electrostatic attraction among the ammonium cations and sulfate anions. The DMAPS graft chains in the surface and sub-surface regions adopt a more expanded conformation as a result of the *anti-polyelectrolyte effect*. The effective pore dimension is reduced, resulting in a reduced flux through the MF membrane. The conformational change of the DMAPS chains in the sub-surface regions will result in a marked contraction or expansion of the micron-size pores. This mechanism is particularly important to the "valve effect" of the present membrane having relatively short graft chains and transmembrane pore sizes in the micron region. Although the swelling of the graft chains on the surface as a function of electrolyte concentration has a maximum at an electrolyte concentration around 10^{-4} mol/L, the permeability of the electrolyte continues to decrease at higher electrolyte concentrations. The phenomenon can probably be attributed to the fact that the *anti-polyelectrolyte effect* of the DMAPS chains in the sub-surface regions of the pores continues to increase at electrolyte concentration well above 10^{-4} mol/L. As a result, the effective pore size, and thus the permeability, continues to decrease gradually at electrolyte concentration approaching 1 mol/L. Since there are no ionic functional groups on the surface of the pristine PVDF membrane, the conformation of the PVDF chains remains unchanged when exposed to aqueous media of different electrolyte concentrations. The weakly electrolyte-dependant flux through the commercial hydrophilic PVDF MF membrane may have resulted from the functional groups tethered on the membrane surface after surface modification.

Although the surface graft concentration of the DMAPS-g-PVDF MF membrane cast in an aqueous medium at 100^{o}C has been enhanced to some extent (Figure 4.4), the membrane exhibits an electrolyte-independant and much larger flow rate in comparison to other MF membranes prepared in this study. This phenomenon can be explained from the morphological point of view. For the membrane cast in boiling water, SEM image reveals the presence of both the microporous and macroporous structures. The conformational change of the DMAPS side chains exerts only minimal effect on the effective pore dimension. As a result, the membrane exhibits an electrolyte-independant and a much larger flow rate. Finally, it is conceivable that the present microporous membrane is not the best membrane morphology to be used for studying the stimuli-sensitive behavior. Enhanced stimuli-responsiveness can be expected from membranes having ultrafiltration (UF) characteristics. Attempts are currently being made to prepare UF membranes from the graft copolymers.

4.3 Conclusions

A new graft copolymer, PVDF-*g*-PDMAPS, was successfully synthesized through the molecular graft copolymerization of the zwitterionic DMAPS with the ozone-preactivated PVDF backbone. Elemental and thermogravimetric analyses reveals that the bulk graft concentration of the copolymer increases with the monomer to polymer feed ratio used for graft copolymerization. The MF membranes were cast by phase inversion in aqueous media of different electrolyte concentration and temperature. Arising from the interaction of the zwitterionic DMAPS graft chains with the aqueous electrolyte during phase inversion, the mean pore size of the PVDF-*g*-PDMAPS MF membranes decreased with the increase in the graft concentration and increased with the increase in electrolyte strength of the casting bath. The flux of the aqueous solution through the PVDF-*g*-PDMAPS MF membranes exhibited a strong

dependence on the electrolyte concentration of the solution, as a result of the interaction of the DMAPS polymer chains on the pore surface and sub-surface region with the electrolyte solution (the *anti-polyelectrolyte effect*). However, the temperature-dependant perameability of the aqueous solution through the PVDF-g-PDMAPS MF membranes was not observed. The present study has shown that molecular functionalization by graft copolymerization prior to membrane fabrication is a relatively simple and effective approach to the preparation of membranes with well-controlled pore size, uniform surface composition (including the composition of pore surface), and electrolyte-sensitive permeability.

Chapter 5:

Inimer Graft-Copolymerized Poly(Vinylidene Fluoride) for the Preparation of Arborescent Copolymers and "Surface-Active" Copolymer Membranes

5.1 Experimental

5.1.1 Materials

PVDF, DMSO, and NMP are the same as earlier. 2-hydroxyethyl acrylate (HEA) was obtained from Fluka Chemie of Neu-Ulm, Germany. The water content in HEA was removed by molecular sieve (20 nm). Triethylamine and 2-bromoisobutyryl bromide were purchased from Aldrich Chemical Company, of Milwaukee, WI, and were used as received. Poly(ethylene glycol) methacryate (PEGMA) (MW=360) was also obtained from Aldrich Chemical Company. The inhibitor in PEGMA was removed by column chromatography. The anionic monomer, sodium 4-styrenesulfonate (NaSS), the catalysts, copper (I) chloride (CuCl) and copper (II) chloride ($CuCl_2$), and the ligand for the ATRP, bipyridine (bPy), were also purchased from Aldrich Chemical Company. They were used as received.

5.1.2 Synthesis of the Inimer, 2-(2-bromoisobutyryloxy)ethyl acrylate (BIEA)

The inimer, 2-(2-bromoisobutyryloxy)ethyl acrylate (BIEA), with the structure shown below, was synthesized according to the procedures reported in the literature (Matyjaszewski *et al.*, 1997).

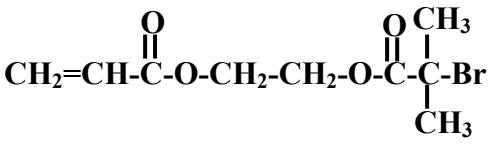

About 200 ml of dry THF, 20 ml of HEA (0.17 mol) and 25 ml of triethylamine (0.17 mol) were added into a 500 ml flask, equipped with a magnetic follower and kept in an ice bath. 28 ml of 2-bromoisobutyl bromide (0.23 mol) was added into the flask drop-wise through a funnel. After the addition, the flask was sealed and the mixture was left to react at room temperature for 14 h. After the reaction, the mixture was washed with 3×200 ml of water to remove the THF, HEA residue, 2-

bromoisobutyl carboxylic acid and triethylammonium bromide. After drying over anhydrous $MgSO_4$, the remaining yellow liquid was distilled under vacuum at 75^{o}C for about 30 min. About 30 g of a yellow viscous liquid was obtained. The detailed polymerization of the inimer had been reported (Matyjaszewski *et al.*, 1998; Matyjaszewski, 1997).

5.1.3 Preparation of Copolymers and Membrane *via* ATRP

The preparation of PVDF-*g*-PBIEA copolymer was carried out in a similar approach as reported earlier for the graft copolymerization of vinyl monomer with the ozone-pretreated PVDF. After the ozone-pretreatment, 30 ml of PVDF/NMP solution, with a concentration of 7 wt%, was degassed by argon stream that was introduced for about 30 min to remove the ozone and oxygen dissolved in the solution. Two grams of BIEA monomer and 12 ml of NMP were then added into the reaction mixture. After an additional 15 min of argon purging, the temperature of the water bath was raised to 60^{o}C to induce the decomposition of peroxide groups on the PVDF chains and to initiate the graft copolymerization of BIEA. After 6 h of reaction, the reaction mixture was cooled in an ice bath and the resultant PVDF-*g*-PBIEA copolymer was precipitated in an excess amount of absolute ethanol. After filtering, the copolymer was re-dissolved in NMP and re-precipitated in ethanol. The copolymer was washed in an excess volume of ethanol for 48 h. The solvent was changed every 8 h. The copolymer sample was recovered and dried by pump under reduced pressure for subsequent characterization. The processes of ozone preactivation of PVDF and thermally induced graft copolymerization of BIEA are shown schematically in Figure 5.1.

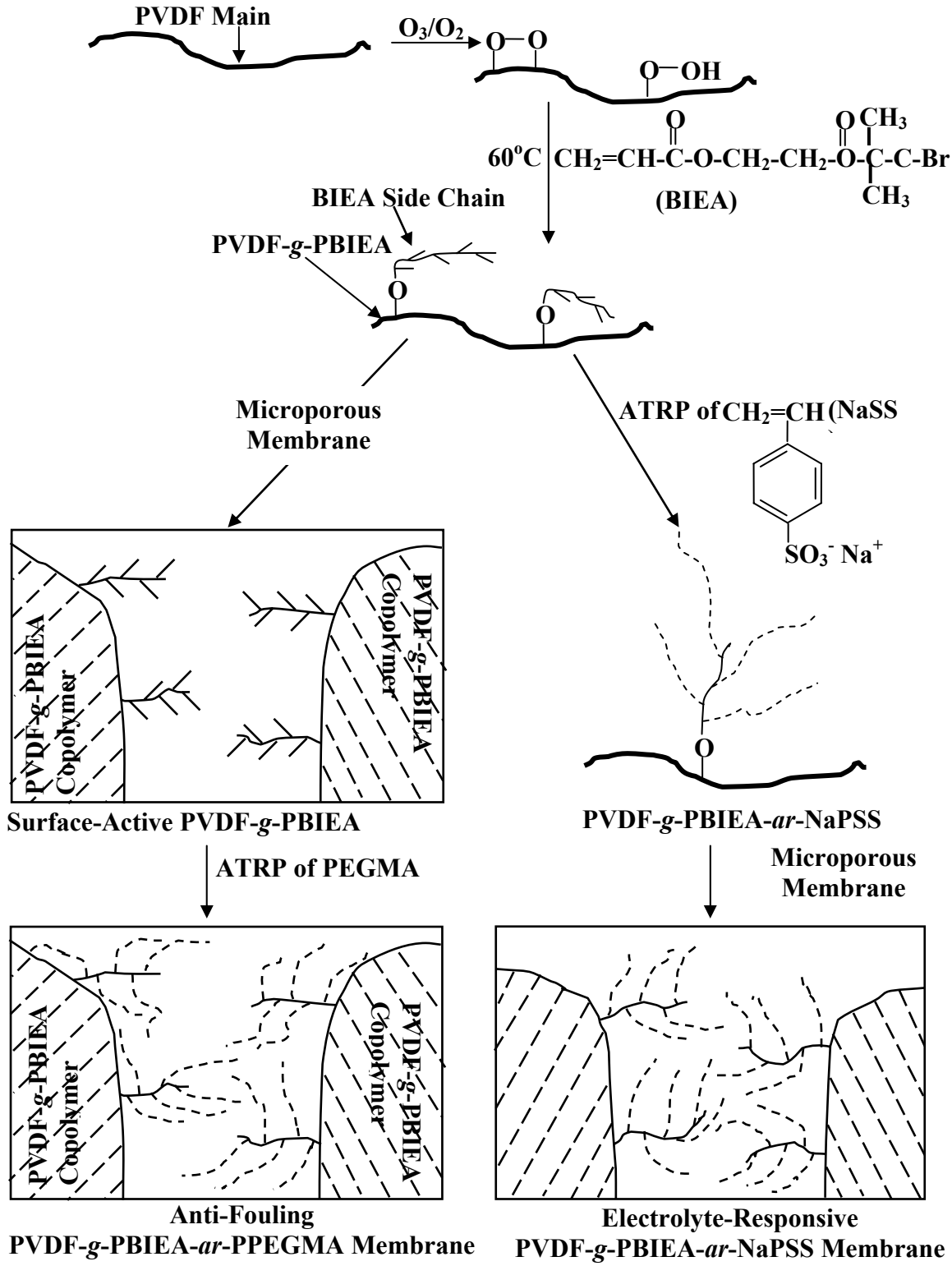

Figure 5.1: Schematic illustration of the process of ozone-pretreatment and graft copolymerization of PVDF with inimer BIEA, preparation of "surface-active" PVDF-*g*-PBIEA membrane by phase inversion, the molecular functionalization of the PVDF-*g*-PBIEA graft copolymer *via* ATRP of NaSS, preparation of the electrolyte-responsive membrane from PVDF-*g*-PBIEA-*ar*-NaPSS copolymer by phase inversion, and surface-initiated ATRP of PEGMA on the PVDF-*g*-PBIEA membrane.

For the preparation of arborescent copolymer, PVDF-*g*-PBIEA-*ar*-NaPSS, 0.5 g of PVDF-*g*-PBIEA copolymer powder was introduced into 15 ml of DMSO. The temperature of the thermostated bath was increased to 50^{o}C to facilitate the dissolution, which took about 2 h. After the complete dissolution, the water bath was cooled to room temperature. An argon stream was introduced to degas the DMSO solution for 30 min. 2 g of sodium 4-styrenesulfonate (NaSS), 158 mg of 2,2'-bipyridine, 13.5 mg of $CuCl_2$ and 40 mg of CuCl were added to the solution. After the addition and dissolution, the solution became a brown liquid. The mixture was sealed and allowed to react at 40^{o}C for 6 h. At the end of the reaction, the reaction mixture was cooled down in an ice bath, and the copolymer was precipitated in excessive ethanol. After recovery by filtration, the copolymer was washed in an excess volume of ethanol for 48 h. The solvent was changed every 8 h. The resulting arborescent copolymer (PVDF-*g*-PBIEA-*ar*-NaPSS) was recovered and dried by pump under reduced pressure for subsequent characterization. The preparation of the arborescent PVDF-*g*-PBIEA-*ar*-NaPSS copolymer is also shown schematically in Figure 5.1.

After the membrane fabrication by phase inversion in the similar approach as specified in Section 3.1, PVDF-g-PBIEA membrane was cast from the copolymer solution in NMP. The surface-initiated ATRP of PEGMA was conducted on the PVDF-g-PBIEA to create the PVDF-g-PBIEA-ar-PPEGMA membrane. For the surface-initiated ATRP of the macromonomer, PEGMA, on the PVDF-*g*-PBIEA MF membrane, 15 ml of doubly distilled water, 2 ml of PEGMA and 1 piece of the PVDF-g-PBIEA MF membrane of about 1cm × 1 cm in area were added into a 25 ml single-necked round-bottom flask. A purified argon stream was introduced to degas the mixture for about 15 min. 158 mg of 2,2'-bipyridine, 13.5 mg of $CuCl_2$ and 40 mg

of CuCl were added to the solution. The polymerization reaction was allowed to proceed for 1 h with stirring. After the reaction, the membrane was washed with copious amount of doubly distilled water over a period of about 2 h, followed by drying under reduced pressure. The process of the surface-initiated ATRP of PEGMA on the PVDF-*g*-PBIEA membrane is also shown schematically in Figure 5.1.

5.1.4 Copolymer and Membrane Characterization

FTIR, TGA, SEM and XPS was same as in Section 3.1. The chemical structure of PVDF-g-PBIEA was also investigated by proton nuclear magnetic resonance (^{1}H NMR) spectroscopy measured on a Bruker ARX 300 instrument at room temperature with deuterated DMSO as the solvent.

The chemical composition of the copolymers was determined by the elemental analysis. The carbon and bromide elemental contents were determined by the Microanalysis Laboratory, National University of Singapore. Taking into account the stoichiometries of the graft and the fluoropolymer chains, the bulk graft concentration of the PVDF-*g*-PBIEA copolymer, defined as the number of BIEA repeat units per repeat unit of PVDF, or the $([\text{-BIEA-}]/[\text{-CH}_2\text{CF}_2\text{-}])_{bulk}$ ratio, can be calculated from Equation (5.1):

$$([\text{-BIEA-}]/[\text{-CH}_2\text{CF}_2\text{-}])_{bulk} = 2[\text{Br}]/([\text{C}]-9[\text{Br}]) \quad \ldots(5.1)$$

where the factors 2 and 9 are introduced to account for the fact that there are 2 and 9 carbon atoms per repeat unit of PVDF and BIEA polymer, respectively. The graft concentration of NaSS in the PVDF-*g*-PBIEA-*ar*-NaPSS arborescent copolymer, or the $([\text{-NaSS-}]/[\text{-CH}_2\text{CF}_2\text{-}])_{bulk}$ ratio, is estimated from Equation (5.2):

$$([\text{-NaSS-}]/[\text{-CH}_2\text{CF}_2\text{-}])_{bulk} = 2[\text{S}]/([\text{F}]) \quad \ldots (5.2)$$

where the factor 2 accounts for the fact that there are two fluorine atom per repeat unit of the PVDF polymer and one sulfur atom per repeat unit of the NaPSS polymer, respectively.

In order to assess the effect of surface-initiated ATRP of PEGMA from the PVDF-*g*-PBIEA membrane on the resistance of the latter to protein fouling, protein adsorption assays were performed on both the PVDF-*g*-PBIEA membrane and the PVDF-*g*-PBIEA-*ar*-PPEGMA membrane (time of polymerization = 1 h). The membranes (about 1 cm ×1 cm) were hydrated in methanol for 30 min initially, followed by washing 3 times with the phosphate-buffer saline (0.01 M PBS, pH=7.4). The membranes were subsequently equilibrated in PBS solution for 1 h prior to the protein adsorption experiment. For the protein adsorption, the membranes were immersed in the PBS containing 2 mg/ml of γ-globulin for 24 h at room temperature. After the protein adsorption, the membranes were washed with copious amount of PBS and doubly distilled water. The membranes were dried by pumping under reduced pressure at room temperature. The surface composition of the membranes after protein adsorption was analyzed by XPS, using the N 1s signal as a marker for the adsorbed protein.

5.2 Results and Discussion

5.2.1 Preparation of the PVDF-*g*-PBIEA Graft Copolymer

Preparation of the Inimer, 2-(2-bromoisobutyryloxy)ethyl acrylate (BIEA)

The initiator-monomer or the AB*-type "inimer" (A: polymerizable group and B*: initiator moiety) is designed for the synthesis of hyperbranched polymers, because the AB* inimer can become involved in polymerization and initiation simultaneously

(Frechet *et al.*, 1995; Morri, 2003). For the addition polymerization, "*A*" typically represents the C=C double bond, while a variety of initiator moieties can be introduced as "*B**". Examples of "B*" include an alkoxy or chloroalkyl group for living cationic polymerization (Frechet *et al.*, 1995; Paulo, 2001), an organolithium group for anionic living polymerization (Baskaran, 2003), a nitroxide group for stable free radical polymerization (Hawker *et al.*, 1995), an alkyl halide group for transition metal-catalyzed atom transfer radical polymerization (ATRP) (Matyjaszewski, 1997; Matyjaszewski et al., 1997; Matyjaszewski *et al.*, 1998a), a dithioester group for photo-initiated addition-fragmentation chain transfer process (Ishizu *et al.*, 2002), and a trimethylsiloxyl group for group transfer polymerization (GTP) (Simon, 2001).

As a controlled radical polymerization technique, ATRP is versatile to a variety of monomers containing appropriate functional groups. In this study, the ATRP inimer, BIEA, was prepared *via* the esterification of HEA with 2-bromoisobutyryl bromide in dry THF and in the presence of triethylamine to neutralize the hydrogen bromide produced. The Fourier transform infrared (FTIR) spectra of HEA and BIEA were compared. After the esterification reaction, the absorption band at the wavenumber of about 3600 cm^{-1} (Shriner *et al.*, 1998), associated with the hydroxyl group of HEA, has disappeared almost completely, and the absorption band at the wavenumber of about 1740 cm^{-1}, associated with the ester carbonyl group (Shriner *et al.*, 1998), has been enhanced. The results indicate that esterification reaction has occurred between HEA and 2-bromoisobutyryl bromide to form the AB* inimer, BIEA. The broad absorption band in the wavenumber region of 1100~1400 cm^{-1} is attributable to the dimethyl group of the initiator moiety (Shriner *et al.*, 1998).

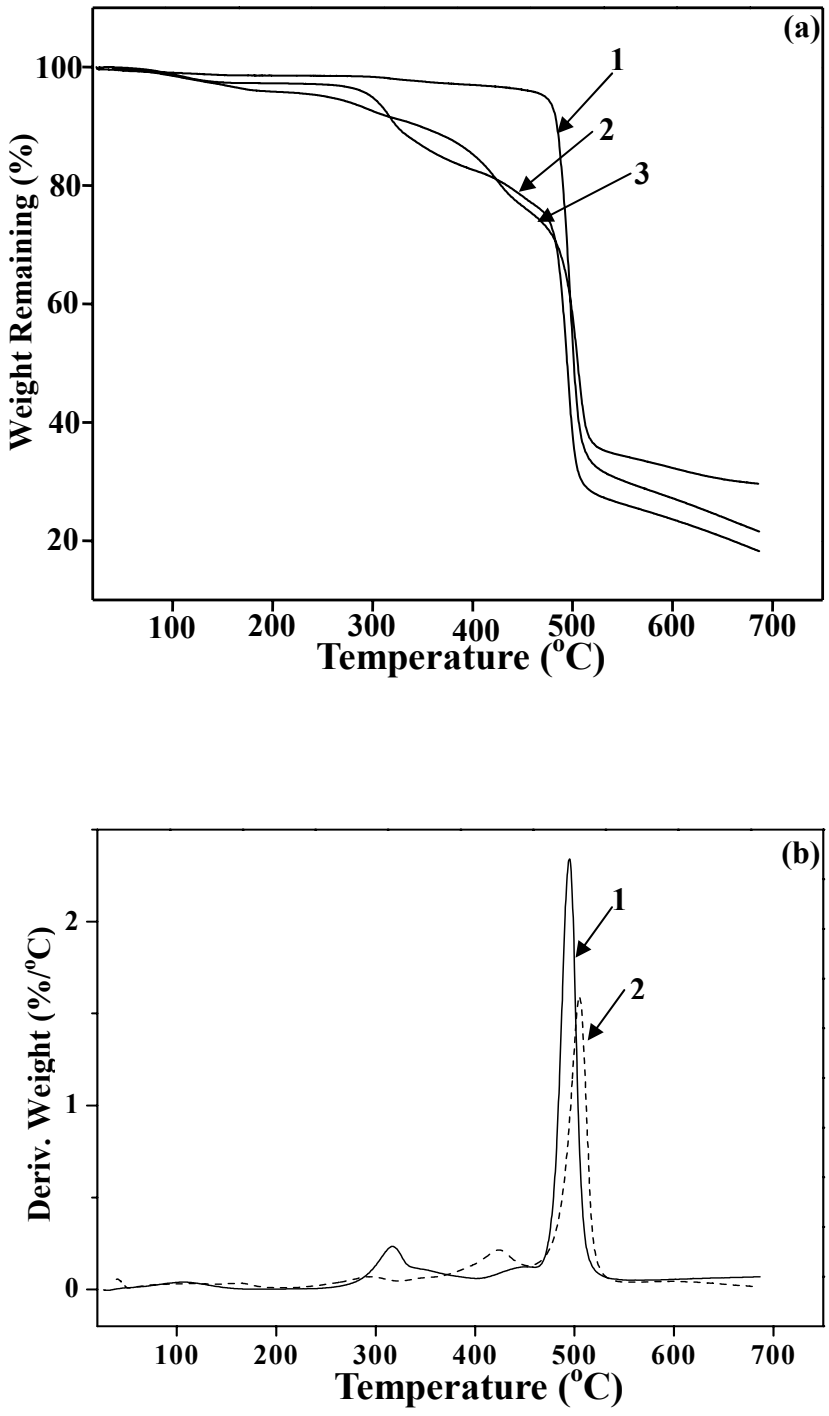

Figure 5.2: (a) TGA weight loss curves of (1) PVDF homopolymer, (2) PVDF-*g*-PBIEA copolymer ([-BIEA-]/[-CH_2CF_2-]$_{bulk}$=0.05) and (3) PVDF-*g*-PBIEA-*ar*-NaPSS copolymer ([-NaSS-]/[-CH_2CF_2-]$_{bulk}$= 0.22). (b): TGA derivative curves of (1) the PVDF-*g*-PBIEA copolymer and (2) the PVDF-*g*-PBIEA-*ar*-NaPSS copolymer.

Ozone Pretreatment and Thermally-Induced Graft Copolymerization of PVDF with BIEA: the PVDF-*g*-PBIEA Copolymer

Ozone pretreatment of the PVDF solution was adopted to generate peroxide groups along the polymer main chain. The peroxide groups decomposed into radicals under thermal induction to initiate the chain polymerization of the vinyl monomer to produce the graft copolymer (Boutevin *et al.*, 1992; Karlsson, 1999). Based on the activation energy and Arrhenius coefficient reported in the literature, the half-life of this kind of peroxide groups is estimated to be about 45 min at 60^{o}C. Thus, in this study, the time of polymerization was set at 6 h, both to increase the graft concentration of the BIEA side chains and to consume the peroxide residues completely.

Elemental analysis results indicate that the $([Br]/[C])_{bulk}$ ratio of the copolymer is about 0.02. The bulk graft concentration of the BIEA polymer (PBIEA) in PVDF-*g*-PBIEA, defined as the number of BIEA repeat units per repeat unit of PVDF, or the $([\text{-BIEA-}]/[\text{-}CH_2CF_2\text{-}])_{bulk}$ ratio, is estimated by Equation (5.1) (Experimental Section) to be about 0.05. The chemical structure of the PVDF-*g*-PBIEA copolymer was analyzed by FTIR and compared to that of PVDF homopolymer. For the pristine PVDF homopolymer, the characteristic absorption band in the wavenumber region of 1120~1350 cm^{-1} is associated with the $-CF_2-$ group of the PVDF main chains (Shriner *et al.*, 1998). A new absorption band at the wavenumber of about 1740 cm^{-1}, attributable to the ester carbonyl group (Shriner *et al.*, 1998), has appeared after graft copolymerization with BIEA. Thus, the FTIR spectroscopic results confirm the presence of the BIEA side chains, in agreement with the results of the elemental analysis.

Figure 5.2 shows the thermal gravimetric analysis (TGA) curves of the PVDF homopolymer and the PVDF-*g*-PBIEA copolymer. The PVDF homopolymer exhibits only one thermal decomposition step, commencing at about 470^{o}C. On the other hand, the PVDF-*g*-PBIEA copolymer exhibited a two-step thermal decomposition process. The first main weight loss occurs at about 300^{o}C, attributable to degradation of the PBIEA side chains, while the second weight loss commences at about 470^{o}C, attributable to the decomposition of the PVDF main chains. The TGA curve also shows that the weight loss during the first decomposition step is about 14 wt%, which translates into a $([\text{-BIEA-}]/[\text{-}CH_2CF_2\text{-}])_{bulk}$ ratio of about 0.06. This ratio is comparable to that obtained from the elemental analysis. Both the FTIR spectra and the TGA results confirm that the BIEA have been graft-copolymerized with the ozone-pretreated PVDF main chains.

The chemical structure of the PVDF-*g*-PBIEA copolymer is shown in Figure 5.3 and verified by 1H NMR spectroscopy. The chemical shifts at 2.9 and 2.2 ppm are attributable to the CH_2 species of PVDF, arising from the head-to-tail (ht) and head-to-head (hh) stereo regularities. On the other hand, the chemical shifts at 4.2-4.3 ppm and 1.9-2.0 ppm are assigned to the –CH_2CH_2- species and the isobutyryl species of the PBIEA side chains, respectively (Mori, 2004). The ^{1}H NMR and the TGA results of the PVDF-g-PBIEA copolymer also indicate that transfer to the brominated monomer during graft copolymerization probably had not occurred to a significant extent, as the process can lead to crosslinking. The PVDF-*g*-PBIEA copolymer remains soluble and can be readily cast into porous membranes (see below).

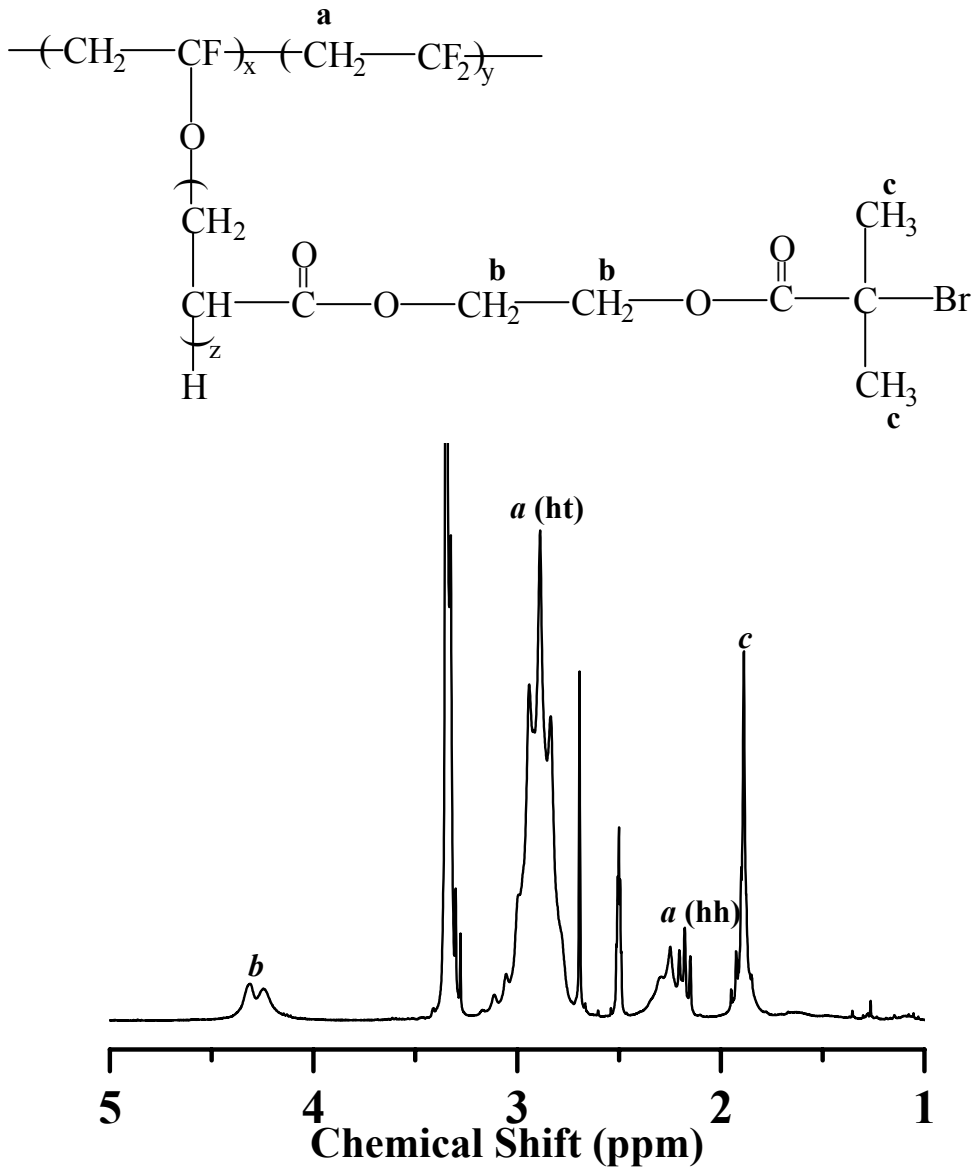

Figure 5.3: ^{1}H NMR spectrum of the PVDF-*g*-PBIEA copolymer.

5.2.2 PVDF-*g*-PBIEA Membranes Cast by Phase Inversion

The PVDF-*g*-PBIEA microporous membranes were fabricated by phase inversion in doubly distilled water at room temperature from 12 wt% NMP solutions of the PVDF-*g*-PBIEA copolymer. The morphology and surface chemical composition of the membrane were analyzed by SEM and XPS, respectively. Figures 5.4(a) and 5.4(b) show the respective SEM images, obtained at a magnification of ×2000, for the air and glass substrate sides of the PVDF-*g*-PBIEA membranes. Thus, the PVDF-*g*-PBIEA copolymer can be cast into a microporous membrane by the phase inversion technique. Cross-sectional SEM images also indicate that the membrane is asymmetric, although the porosity and pore size distribution for the two surfaces can differ substantially.

Figures 5.5(a) to 5.5(c) show, respectively, the XPS wide-scan, Br 3d and C 1s core-level spectra of the PVDF-*g*-PBIEA membrane. Carbon, bromine, fluorine and oxygen signals are detected in the wide-scan spectrum of the PVDF-*g*-PBIEA membrane. The Br 3d core-level spectrum was resolved into Br $3d_{3/2}$ and Br $3d_{5/2}$ peak components with an energy separation of 1.05 eV. The Br $3d_{5/2}$ peak component with a binding energy at about 70.5 eV is characteristic of that of covalently bonded bromine (Touihri et al., 2002). The surface graft concentration of the PVDF-*g*-PBIEA membrane, or the $([\text{-BIEA-}]/[\text{-}CH_2CF_2\text{-}])_{surface}$ ratio, is determined to be about 0.07 from Equation 5.(1), based on the XPS-derived $([Br]/[C])_{surface}$ ratio of about 0.03. The $([\text{-BIEA-}]/[\text{-}CH_2CF_2\text{-}])_{surface}$ ratio is slightly higher than the bulk graft concentration of the PVDF-*g*-PBIEA copolymer, indicating that surface enrichment of the BIEA side chains occurs to some extent during the phase inversion process of the PVDF-*g*-PBIEA/NMP copolymer solution in water.

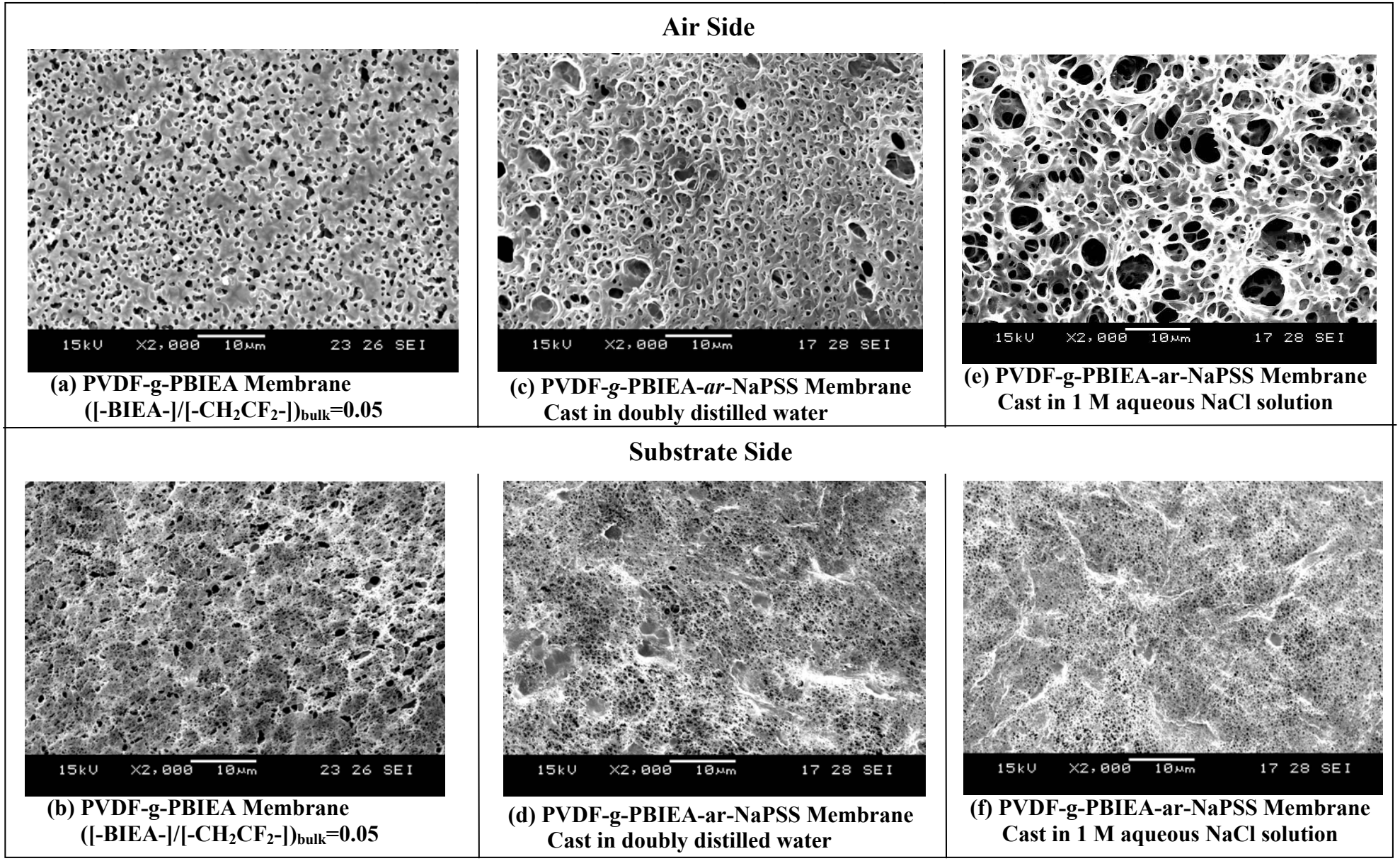

Figure 5.4: SEM micrographs of the membranes cast from the 12 wt% NMP solution of corresponding copolymer by phase inversion: (a) air side and (b) substrate (glass plate) side of PVDF-*g*-PBIEA membrane cast in water; (c) air and (d) substrate side of PVDF-*g*-PBIEA-*ar*-NaPSS membrane cast in water; (e) air and (f) substrate side of PVDF-*g*-PBIEA-*ar*-NaPSS membrane cast in 1 M aqueous NaCl solution.

The C 1s core-level spectrum of the PVDF membrane was curve-fitted with peak components for the –$\underline{C}H_2$- and -$\underline{C}F_2$- species, at the BE of about 286.0 eV and 290.5 eV, respectively (Figure 5.5(d)). The molar ratio of the two species, determined from the spectral area ratio of the two peak components, is about 1.06, in good agreement with the theoretical value of 1:1. The C 1s core-level spectrum of the PVDF-*g*-PBIEA membrane (Figure 5.5(b)) was curved-fitted with five species, adopting the following strategy. The peak components of approximately equal intensity with BE's at 286.0 eV and 290.5 eV are attributed to the -$\underline{C}H_2$- and -$\underline{C}F_2$- species, respectively, of the PVDF main chains. The peak components with BE's at about 284.6 eV and 288.8 eV are associated, respectively, with the neutral -$\underline{C}H_2$- and the O=$\underline{C}$-O species of the BIEA side chains. The peak component with the BE at about 286.5 eV arises from combined contributions of the $\underline{C}$-O species and the $\underline{C}$-Br terminus of the BIEA side chains. For the comparison of the C 1s core-level spectra of the PVDF and PVDF-*g*-PBIEA membranes, it is clear that the peak intensity of the –$\underline{C}F_2$- species of the PVDF main chains has decreased substantially, after grafting of the BIEA side chains. The molar ratio of the –$\underline{C}F_2$- species to the total carbon species in the PVDF-*g*-PBIEA membrane is determined to be about 0.28, significantly lower than about 0.48 for the membrane prepared from the PVDF homopolymer.

5.2.3 The PVDF-*g*-PBIEA-*ar*-NaPSS Arborescent Copolymer *via* ATRP

The BIEA side chains of the PVDF-*g*-PBIEA copolymer and on the PVDF-*g*-PBIEA membrane surface can function as the ATRP macro-initiators, because the tertiary C-Br moiety of each BIEA repeat unit will be able to initiate the ATRP of functional monomers (Matyjaszewski, 2001). The ATRP of substituted styrenic monomers had been well investigated using the Cu/bPy catalyst system (Qiu, 1997).

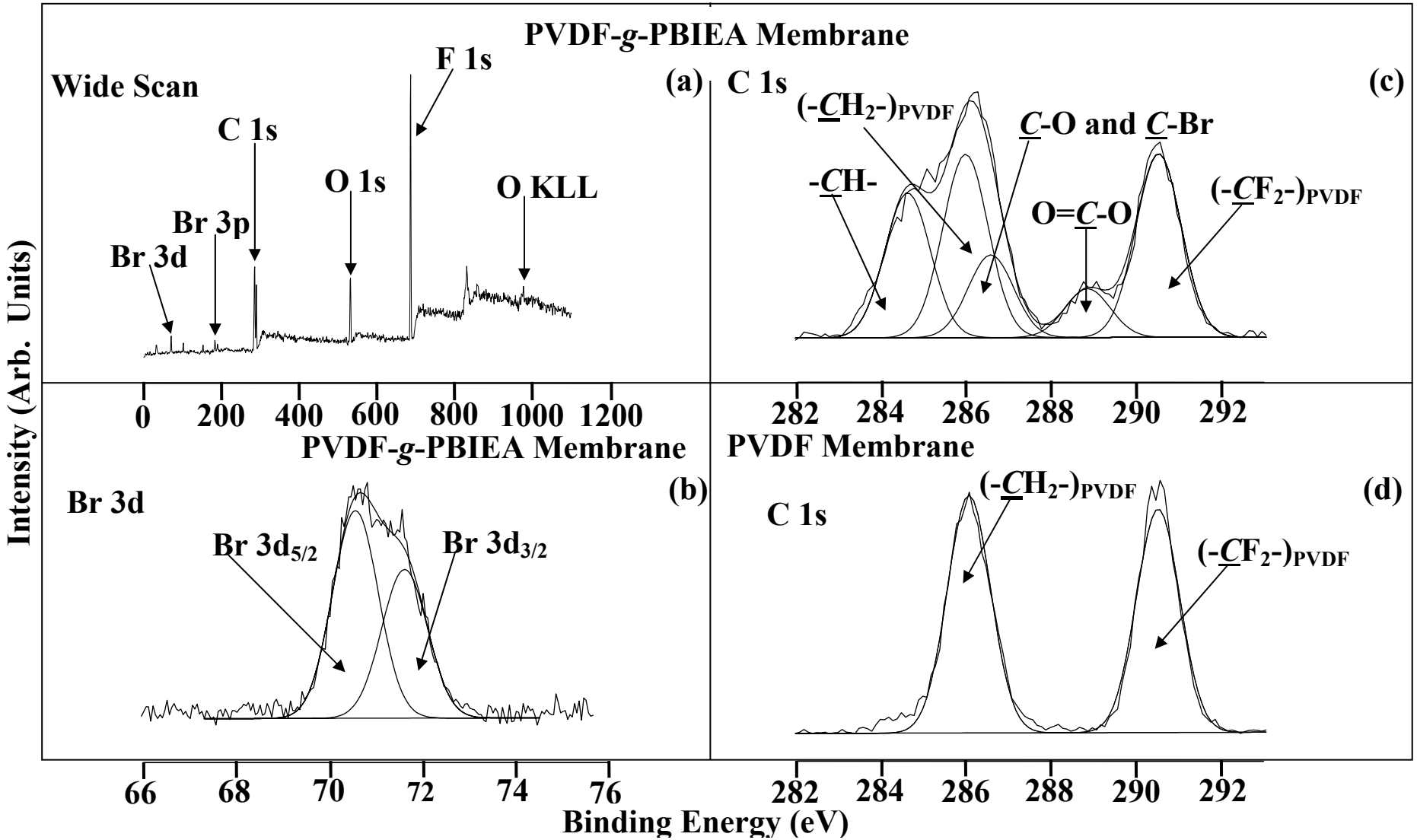

Figure 5.5: XPS wide-scan, Br 3d and C 1s core-level spectra of the PVDF-*g*-PBIEA membrane and C 1s core-level spectrum of the PVDF membrane. Both membranes are cast from their corresponding 12 wt% NMP solution in doubly distilled water by the phase inversion technique.

In specific, the ATRP of sodium 4-styrenesulfonate (NaSS) has been carried out in the presence of the Cu(I)/bPy catalyst system in a water/methanol mixed medium to produce polyelectrolytes dissolved in solution or grafted on the silica particle surface (Chen et al., 2003; Iddon et al., 2004). As an amphiphilic polyelectrolyte, the NaSS polymer (NaPSS) can switch its conformation from an extended to a coiled state in an aqueous medium upon the addition of a low molecular weight electrolyte, because the latter can shield the electrostatic repulsion among the sulfonate anions alongside the NaPSS chains. Thus, NaPSS exhibits an electrolyte-responsive behavior (*the polyelectrolyte effect*) (Lowe, 2000; McCormick, 1996).

The arborescent copolymer with the NaPSS side chains, or the PVDF-*g*-PBIEA-*ar*-NaPSS copolymer, was prepared *via* solution polymerization of NaSS, initiated by the BIEA repeat units of the PVDF-*g*-PBIEA copolymer and catalyzed by the $CuCl/CuCl_2$/bPy system in DMSO. The sulfur, fluorine and carbon contents of the PVDF-*g*-PBIEA-*ar*-NaPSS copolymer were determined by elemental analysis. The $([S]/[F])_{bulk}$ ratio of the copolymer was determined to be about 0.11. Thus, the bulk graft concentration, defined as the number of NaSS repeat units per PVDF repeat unit, or the $([\text{-NaSS-}]/[\text{-}CH_2CF_2\text{-}])_{bulk}$ ratio, is determine to be about 0.22 (Equation (5.2), Experimental Section). After copolymerization with NaSS, a new absorption band in the wavenumber region of 1050 cm^{-1}, associated with the sulfonate groups of the NaPSS side chains (Moulder *et al.*, 1998), appears in the FTIR spectrum of the PVDF-*g*-PBIEA-*ar*-NaPSS copolymer. On the other hand, the absorption band in the wavebumber region of 1100~1300 cm^{-1}, corresponding to the aromatic C-H in-plane bending mode (Moulder *et al.*, 1998), also serves to indicate that the NaPSS side chains have been incorporated into the copolymer.

The TGA curve of the PVDF-*g*-PBIEA-*ar*-NaPSS copolymer was compared to that of PVDF-*g*-PBIEA polymer in Figure 5.2. Figure 5.2(a) shows the weigh loss curves of the PVDF homopolymer, the PVDF-*g*-PBIEA copolymer and the PVDF-*g*-PBIEA-*ar*-NaPSS copolymer. In comparison with the PVDF-*g*-PBIEA copolymer, the PVDF-*g*-PBIEA-*ar*-NaPSS copolymer exhibits a large weight loss in the temperature range of 300^{o}C~480^{o}C, attributable to the decomposition of the PBIEA and NaPSS graft chains. Figure 5.2(b) shows the derivative of the weight curves as a function of the temperature for the PVDF-*g*-PBIEA and PVDF-*g*-PBIEA-*ar*-NaPSS copolymers. For the PVDF-*g*-PBIEA copolymer, the derivative curve contains two major peaks at temperatures of 310^{o}C and 490^{o}C, attributable to the PBIEA side chains and PVDF main chains, respectively. However, for the PVDF-*g*-PBIEA-*ar*-NaPSS copolymer, these two peaks diminish and a new decomposition peak emerges at the temperature of about 425^{o}C, attributable to the NaPSS side chains. The NaPSS content of the copolymer cannot be determined unambiguously from the weight loss curve of the copolymer. Attempts were made to improve the bulk graft concentration of NaPSS in the PVDF-*g*-PBIEA-*ar*-NaPSS copolymer by increasing the NaSS monomer concentration in the reaction mixture or extending the time of polymerization from 6 h to 12 h. It was found that the solubility of the PVDF-*g*-PBIEA-*ar*-NaPSS copolymer in NMP was compromised by the high content of NaPSS. Therefore, the ATRP of NaSS initiated from PVDF-*g*-PBIEA was not carried out at a higher monomer feed ratio or for a longer polymerization time.

5.2.4 Electrolyte-Responsive Membrane cast from the PVDF-*g*-PBIEA-*ar*-NaPSS Copolymer

The morphology, surface composition and the electrolyte-responsive nature of the PVDF-*g*-PBIEA-*ar*-NaPSS membranes were investigated. Figure 5.6 shows the respective XPS wide-scan, C 1s, S 2p and Na 1s core-level spectra of the PVDF-*g*-PBIEA-*ar*-NaPSS membranes cast from a 12 wt% NMP solution of the PVDF-*g*-PBIEA-*ar*-NaPSS copolymer by phase inversion in doubly distilled water and in 1 M aqueous NaCl solution. In the wide-scan spectra of the two membranes, not only are the C 1s, F 1s, and O 1s signals detected, the Na 1s and S 2p signals are also discernible. For both membranes, the intensity of the Br 3d signal for the PVDF-*g*-PBIEA-*ar*-NaPSS membrane has been reduced considerably, in comparison with that of the Br 3d signal for the PVDF-*g*-PBIEA membrane. The membrane cast in 1 M aqueous NaCl solution exhibits a higher Na 1s and S 2p signal intensities, compared to those of the membrane cast in water. The XPS-derived surface elemental composition, or the $([C]:[Na]:[S]:[Br])_{surface}$ ratio, determined from the respective spectral peak areas, shifted from 100:1.3:2.0:0.3 to 100:4.0:4.6:0.8 when the ionic strength of the casting bath was increased from about 0 (for doubly distilled water) to 1 M (for the 1 M aqueous NaCl solution). Thus, the surface composition data indicate a significant surface enrichment of the PBIEA-*g*-NaPSS side chains for the membrane cast in 1 M aqueous NaCl solution.

The C 1s core-level spectra of the PVDF-*g*-PBIEA-*ar*-NaPSS membranes cast in doubly distilled water and in 1 M aqueous NaCl solution were curve-fitted using the approach similar to that used for the PVDF-*g*-PBIEA membrane, except that the peak component with BE at about 286.5 eV is deemed to have resulted from a combined contribution from the <u>*C*</u>-O, <u>*C*</u>-Br and <u>*C*</u>-SO_3 species (Ruangchuay *et al.*, 2002). From the C 1s spectra, it is clear that the intensity of the -<u>*C*</u>H- species, associated with the

PBIEA-*g*-NaPSS side chain, increases while that of the $(-\underline{C}F_2-)_{PVDF}$ species decreases when the ionic strength of the casting bath is increased to 1 M. The XPS-derived $([-\underline{C}F_2-]_{PVDF}/[-\underline{C}H-])_{surface}$ ratio, determined from the corresponding C 1s peak component spectral area ratio, decreases from 1.1 to 0.86, suggesting that more PBIEA-*g*-NaPSS side chains have migrated from the bulk to the surface during the phase inversion process in 1 M aqueous NaCl solution. The S 2p core-level spectrum of the PVDF-*g*-PBIEA-*ar*-NaPSS membrane, cast in doubly distilled water, was curve-fitted with S $2p_{1/2}$ and S $2p_{3/2}$ peak components with an energy separation of 1.2 eV, as shown in Figure 5.6.

The microporous morphology of the PVDF-*g*-PBIEA-*ar*-NaPSS membranes is also dependant on the electrolyte concentration. Figures 5.4(c) to 5.4(f) show the respective SEM micrographs, obtained at a magnification of ×2000, for the air side and substrate side of the PVDF-*g*-PBIEA-*ar*-NaPSS membranes cast in doubly distilled water and in 1 M aqueous NaCl solution. With the increase in ionic strength of the casting bath, the morphology and pore structure do not change significantly on the substrate side. However, significant differences in the surface morphology and pore structure are observed on the air side of the PVDF-*g*-PBIEA-*ar*-NaPSS membrane. The membrane cast in 1 M aqueous NaCl solution exhibits a much larger pore size and a less uniform pore-size distribution, in comparison to those of the membrane cast in doubly distilled water. When cast in the aqueous NaCl medium, the membrane surfaces is enriched by the NaPSS chains. Pores of larger size are formed to minimize the interfacial interaction between the membrane surface and the aqueous electrolyte medium, as larger pores correspond to smaller specific surface area. The cross sectional SEM images of the PVDF-*g*-PBIEA-*ar*-NaPSS membranes revealed a

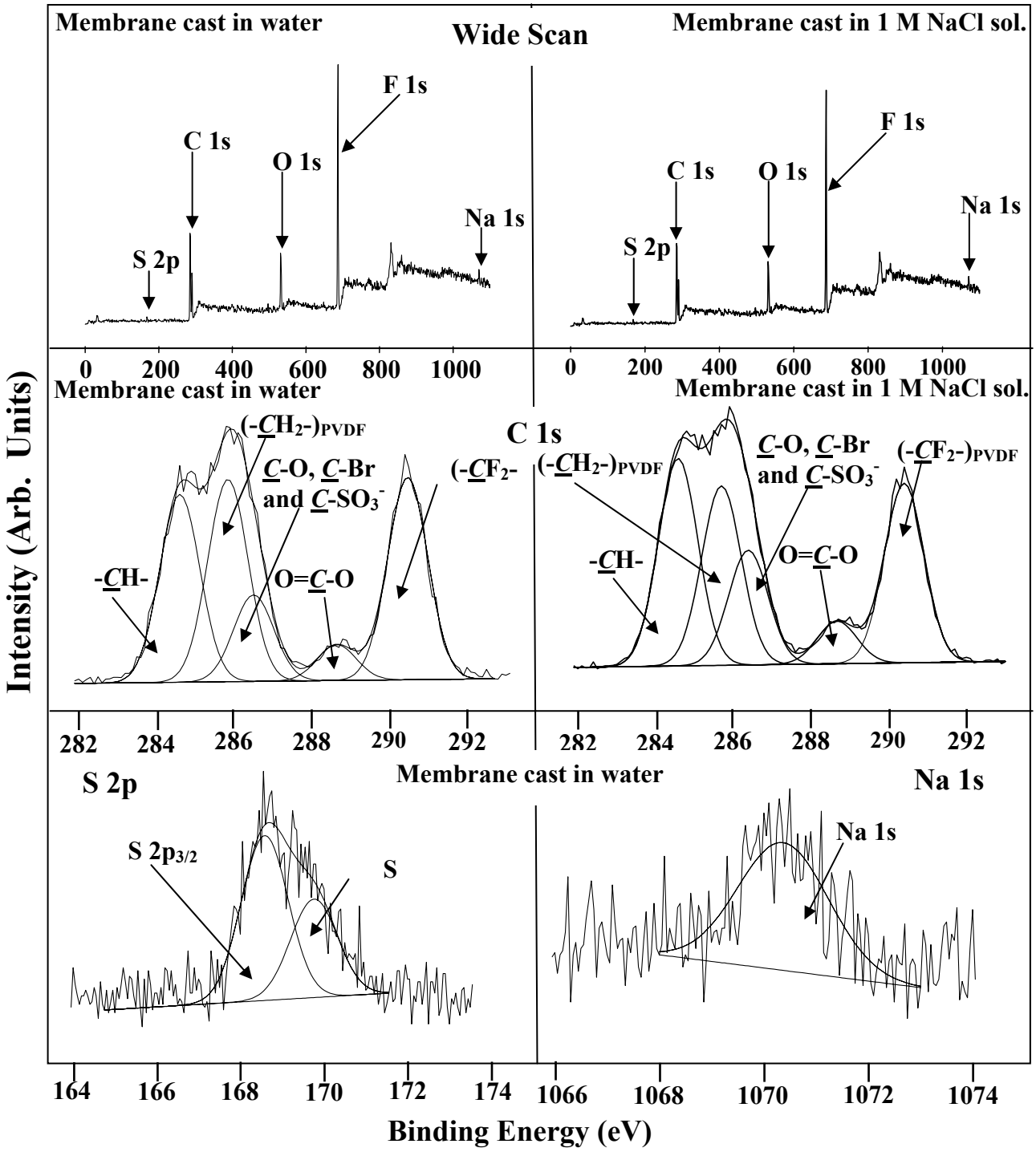

Figure 5.6: XPS wide-scan, C 1s, S 2p and Na 1s core-level spectra of the PVDF-*g*-PBIEA-*ar*-NaPSS membranes cast from the 12 wt% NMP solution by phase inversion in doubly distilled water and in 1 M aqueous NaCl solution.

"through pore" structure of the membrane, although the pore size differs on both sides of the membrane.

The nature of the NaPSS side chain as a polyelectrolyte accounts for the electrolyte-responsive characteristics of the surface chemical composition and morphology of the PVDF-*g*-PBIEA-*ar*-NaPSS copolymer membrane. When the PVDF-*g*-PBIEA-*ar*-NaPSS polymer solution was cast into doubly distilled water, the strong electrostatic repulsion among the sulfonate anions alongside the NaPSS chains on the newly formed membrane surface prohibited extensive migration of the NaSS side chains from the bulk of the polymer solution to the outer layer of the membranes. On the other hand, when cast into 1 M aqueous NaCl solution, the electrostatic repulsion was mostly shielded by the electrolyte ions in the casting bath (*polyelectrolyte effect*), allowing more extensive migration of the NaPSS side chains to the membrane surface, including the surface of the pores.

5.2.5 Functionalization of the PVDF-*g*-PBIEA Membrane *via* Surface-Initiated ATRP of the Poly(ethylene glycol) methacrylate (PEGMA): the Anti-fouling PVDF-*g*-PBIEA-*ar*-PPEGMA Membrane

For the porous membrane cast from the PVDF-*g*-PBIEA copolymer, each repeat unit of the PBIEA side chains on the membrane and pore surfaces can initiate the ATRP of a functional monomer to endow specific surface functionalities to the as-cast PVDF-*g*-PBIEA membranes. Poly(ethyl glycol) (PEG) and poly(ethylene oxide) (PEO) have attracted considerable attention because they can impart anti-fouling, non-adhesive and biocompatible characteristics to the materials (Feldman *et al.*, 1999; Dalsin *et al.*, 2003). ATRP of the PEGMA macromonomer has been extensively studied during the last few years, because the process allows the preparation of well-

defined PEGMA polymer (PPEGMA) (Ali, 2003; Robinson *et al.*, 2001; Neugebauer *et al.*, 2003). The Cu/bPy catalyst system can also result in a controlled fashion in the ATRP of methacrylate monomer (Neugebauer *et al.*, 2003; Wang *et al.*, 1997a), therefore, in this study, PEGMA was graft copolymerized directly onto the PVDF-*g*-PBIEA membrane surface, *via* ATRP in an aqueous medium and catalyzed by the $CuCl/CuCl_2/bPy$ system, with the intention of improving the anti-fouling properties of the PVDF-*g*-PBIEA membrane.

Figure 5.7(a) shows the XPS wide-scan and C 1s core-level spectra of the PVDF-*g*-PBIEA-*ar*-PPEGMA membrane after 1 h of surface-initiated ATRP of PEGMA. Compared to those of the PVDF-*g*-PBIEA membrane (see Figure 5.5), significant changes in the XPS wide-scan and C 1s core-level spectra of the PVDF-*g*-PBIEA-*ar*-PPEGMA membrane are observed. The F 1s signals associated with the underlying PVDF main chains are no longer discernible in the wide-scan spectrum, indicating that the thickness of the PEGMA polymer film on the PVDF-*g*-PBIEA membrane surface, after a 1 h of polymerization, has exceeded the sampling depth of the XPS technique (~7.5 nm for organic matrix (Tan *et al.*, 1993)). The same result is also deduced from the changes in the C 1s core-level lineshape of the PVDF-*g*-PBIEA-*ar*-PPEGMA membrane. The C 1s core-level spectrum of the PVDF-*g*-PBIEA-*ar*-PPEGMA membrane was curve-fitted using the similar approach as that for the PVDF-*g*-PBIEA membrane. However, the two species associated with the PVDF main chains, $(-\underline{C}H_2-)_{PVDF}$ and $(-\underline{C}F_2-)_{PVDF}$ with BE's at 285.8 eV and 290.5 eV, respectively, have disappeared completely. On the other hand, the peak component with a BE of about 286.2 eV, attributed to the $\underline{C}$-O species of the PBIEA and PPEGMA side chains, has been greatly enhanced. Similar to that of the PVDF-*g*-

PBIEA-*ar*-NaPSS membrane cast from the PVDF-*g*-PBIEA-*ar*-NaPSS copolymer, the intensity of the Br 3d component has been greatly reduced after the surface-initiated ATRP of PEGMA with the PVDF-*g*-PBIEA membrane. The $([Br]/[C])_{surface}$ ratio has decreased from 0.03 to about 0.02, arising probably from the irreversible termination and halogen exchange of the propagating radicals during the surface-initiated ATRP process (Davis, 2001; Matyjaszewski *et al.*, 1998b; Matyjaszewski *et al.*, 1998c).

Protein adsorption study on both the PVDF-*g*-PBIEA membrane and the PVDF-*g*-PBIEA-*ar*-PPEGMA membrane was carried out to evaluate the anti-fouling properties of the membrane surface after the surface-initiated ATRP of PEGMA. The amount of surface-adsorbed protein (γ-globulin) was quantified by XPS, because the N 1s signal associated with γ-globulin can be used as a convenient marker for the protein. Figures 7(b) and 7(c) show the respective XPS wide-scan and N 1s core-level spectra of the PVDF-*g*-PBIEA and PVDF-*g*-PBIEA-*ar*-PPEGMA membranes after 24 h of exposure to 2 mg/ml γ-globulin solution. For the PVDF-*g*-PBIEA membrane, in addition to the Br 3d, C 1s, O 1s and F 1s signals of the PVDF-*g*-PBIEA membrane substrates, a strong N 1s signal at the BE of about 399.3 eV was also detected in the wide-scan spectrum. After the surface-initiated ATRP of PEGMA on the PVDF-*g*-PBIEA membrane, the membrane exhibited significant resistance to protein adsorption. For the PVDF-*g*-PBIEA-*ar*-PPEGMA membrane, the wide-scan spectrum is dominated by the C 1s and O 1s signals while the N 1s signal is barely discernible. The N 1s core-level spectra of the two membranes are also compared in Figure 5.7. The $([N]/[C])_{surface}$ ratios, determined from the respective peak component area ratios, were about 0.02 and 0.16 for the PVDF-*g*-PBIEA-*g*-PPEGMA membrane and

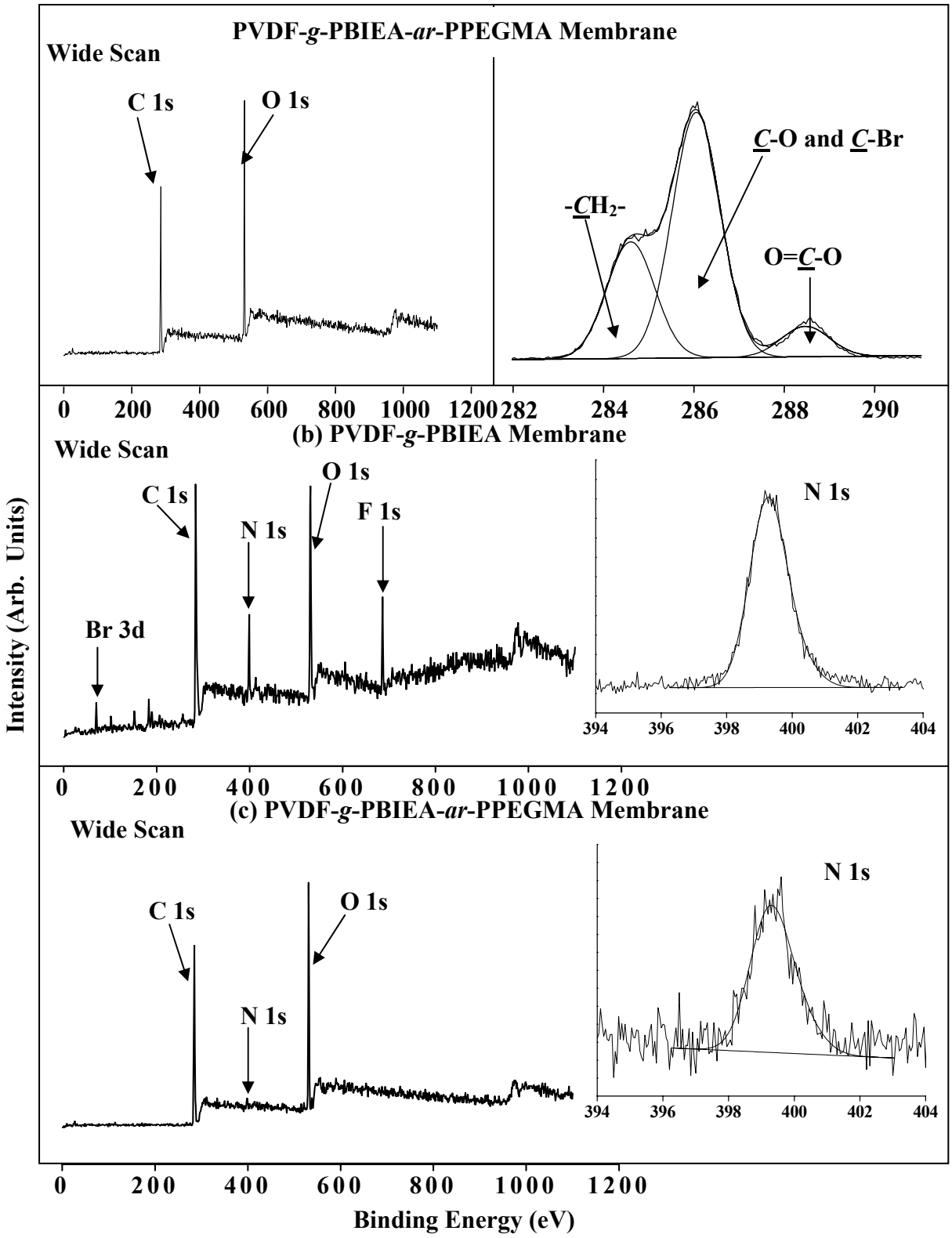

Figure 5.7: (a) XPS wide-scan and C 1s core-level spectra of the PVDF-*g*-PBIEA-*ar*-PPEGMA membrane (time of polymerization = 1 h); XPS wide-scan and N 1s core-level spectra of (b) the PVDF-*g*-PBIEA membrane and (c) PVDF-*g*-PBIEA-*ar*-PPEGMA membrane after a 24 h of γ-globulin adsorption.

PVDF-*g*-PBIEA membrane, respectively. These results indicate that the anti-fouling property of the PVDF-*g*-PBIEA membrane has been improved substantially by the surface-initiated ATRP of PEGMA.

5.3 Conclusions

PVDF with grafted ATRP-inimer, BIEA, side chains allowed the preparation of arborescent copolymer. Both the PVDF-*g*-PBIEA and its arborescent copolymer of a polyelectrolyte, NaPSS, could be readily cast into microporous membranes with surface-enriched graft chains *via* phase inversion in an aqueous medium. The surface composition and morphology of the PVDF-*g*-PBIEA-*ar*-NaPSS membranes exhibited electrolyte-responsive behavior. The BIEA units on the PVDF-*g*-PBIEA membranes could serve as the macro-initiators for the surface-initiated ATRP to further functionalize the membrane. The inimer graft copolymerization technique provided an alternative approach to the functionalization of membranes both at the molecular level (prior to the casting of membrane) and at the membrane surface level. Because of the end functionality associated with the ATRP technique, such membrane surface exhibited a 'living' character, allowing for additional surface-initiated reactions to introduce well-defined functional polymers and moieties. The porous membrane with active or 'living' surfaces thus provides exciting opportunities for the direct molecular design and engineering of the membrane and pore surfaces.

Chapter 6:

Functionalization of Hydrogen-Terminated Silicon with Polybetaine Brushes *via* Surface-Initiated Reversible Addition-Fragmentation Chain Transfer (RAFT) Polymerization

6.1 Experimental

6.1.1 Materials

(100)-oriented single crystal silicon wafers, or Si(100) wafers, with a thickness of about 0.7 mm and a diameter of 150 mm, were obtained from Unisil Co. of Santa Clara, CA. It was sliced into rectangular strips of about 1 cm × 3 cm in size. They were washed in "piranha" solution, a mixture of 98 wt% sulfuric acid (70 vol%) and hydrogen peroxide solution (30 vol%) to remove the surface organic residues. After rinsing with copious amounts of doubly distilled water and dried with a stream of purified argon, the Si(100) strips were immersed in 10 vol% hydrofluoric acid solution in individual Teflon® vials for about 5 min to remove the native oxide layer and to form the hydrogen-terminated Si(100) surface (Si-H surface).

NaSS and DMAPS were the same as stated in earlier part. The initiator, 4,4'-azo-bis(4-cyanopentanoic acid) (ACPA) was purchased from Aldrich Chemical Company of Milwaukee, WI. The intermediate compound, bis(dithiobenzoyl) disulfide, was synthesized and purified as reported (Vosloo et al., 2002), from which the target chain transfer agent (CTA), 4-cyanopentanioc acid dithiobenzoate, was obtained, after conversion, separation and purification (Thang *et al.*, 1999; Mitsukami *et al.*, 2001; Donovan *et al.*, 2002).

6.1.2 Surface Functionalization of the Si-H Substrate

The surface functionalization of the Si-H surface was performed to give rise to a hydroxyl-terminated silicon (Si-CH_2OH) surface (Yu, 2003). A small amount of 10-undecylenic acid methyl ester was introduced onto the freshly prepared Si-H surface. The substrate was sandwiched between two quartz plates. Thus, the Si-H surface was covered by a thin liquid film of 10-undecylenic acid methyl ester. The set-up was

placed in a Pyrex® tube and subjected to UV irradiation in a Riko rotary photochemical reactor (model RH400-10W, manufactured by Riko Denki Kogyo of Chiba, Tokyo) at 25°C for 1 h. The reactor was equipped with a 1000 W Hg lamp. After the UV irradiation, the ester-modified silicon (Si-$COOCH_3$) substrate was washed thoroughly with copious amount of acetone and ethanol to remove the residual ω-unsaturated ester. The Si-$COOCH_3$ surface was dried by pumping under reduced pressure. For the reduction of the Si-$COOCH_3$ surface by $LiAlH_4$ to generate the hydroxyl-terminated surface, 100 ml of dry ether and five pieces of Si-$COOCH_3$ substrates were added into a dry flask. About five grams of $LiAlH_4$ were introduced slowly into the flask under the stirring. The mixture was sealed and was left to react at room temperature for 2 h. After the reaction, the so-prepared silicon substrate (Si-CH_2OH substrate) was washed with copious amounts of ethanol and water, and dried by pumping under reduced pressure.

For the immobilization of the azo initiator, 30 ml of dry dichloromethane and 10 g of 4,4'-azo-bis(4-cyanopentanoic acid) were added into a 100 ml three-necked round bottom flask kept in an ice bath. After 4 ml of thionyl chloride ($SOCl_2$) was added dropwise into the reaction mixture, the flask was sealed and the reaction was allowed to proceed at room temperature. The hydrogen chloride gas generated was absorbed into the aqueous sodium hydroxide solution. After 10-h of reaction at room temperature, the dichloromethane and thionyl chloride residue in the reaction mixture were distilled off under reduced pressure at room temperature. A greenish powder, 4,4'-azo-bis(4-cyanopentanoic acid chloride), remained inside the flask. Fifty ml of dry dichloromethane, 2 ml of pyridine and 5 pieces of the Si-CH_2OH wafers were introduced into the flask. The reaction mixture was sealed and left to react at room

temperature for another 10 h. After the reaction, the silicon substrates with the surface immobilized azo initiator (Si-Azo surfaces) were recovered from the reaction mixture and washed with acetone, ethanol and water repeatedly. The functionalization of the Si-H surface and the immobilization of the azo initiator are illustrated schematically in Figure 6.1.

6.1.3 Synthesis of the Polybetaine Brushes on the Silicon Wafer Surface

For the synthesis of the polybetaine brushes on the Si-Azo surface, 50 ml of doubly distilled water and 5 g of DMAPS monomer were introduced into a round-bottom flask. CTA (0.125g) was added and solublized at room temperature. A purified argon stream was introduced to degas the solution for 60 min. The temperature of the reaction mixture was raised to 70^{o}C to facilitate the dissolution of the CTA. One piece of the Si-Azo wafer and 0.025 g ACPA were added into the solution to initiate the graft polymerization of DMAPS on the Si-Azo surface. After the reaction was allowed to proceed for a pre-determined length of time, the flask was cooled in an ice bath, and the reaction mixture was precipitated in excess acetone (a very good solvent for the CTA). The silicon substrate surface with grafted DMAPS polymer (the Si-*g*-PDMAPS surface) was washed with copious amounts of acetone and water to remove the physically adsorbed polymer on the surface. The silicon substrate was dried by pumping under reduced pressure. The synthesis of the polybetaine brushes on the Si-H surface is also illustrated schematically in Figure 6.1.

As shown in Figure 6.1, the synthesis of the diblock copolymer brushed was carried out on the Si-*g*-PDMAPS surface. The procedures are similar to those used for

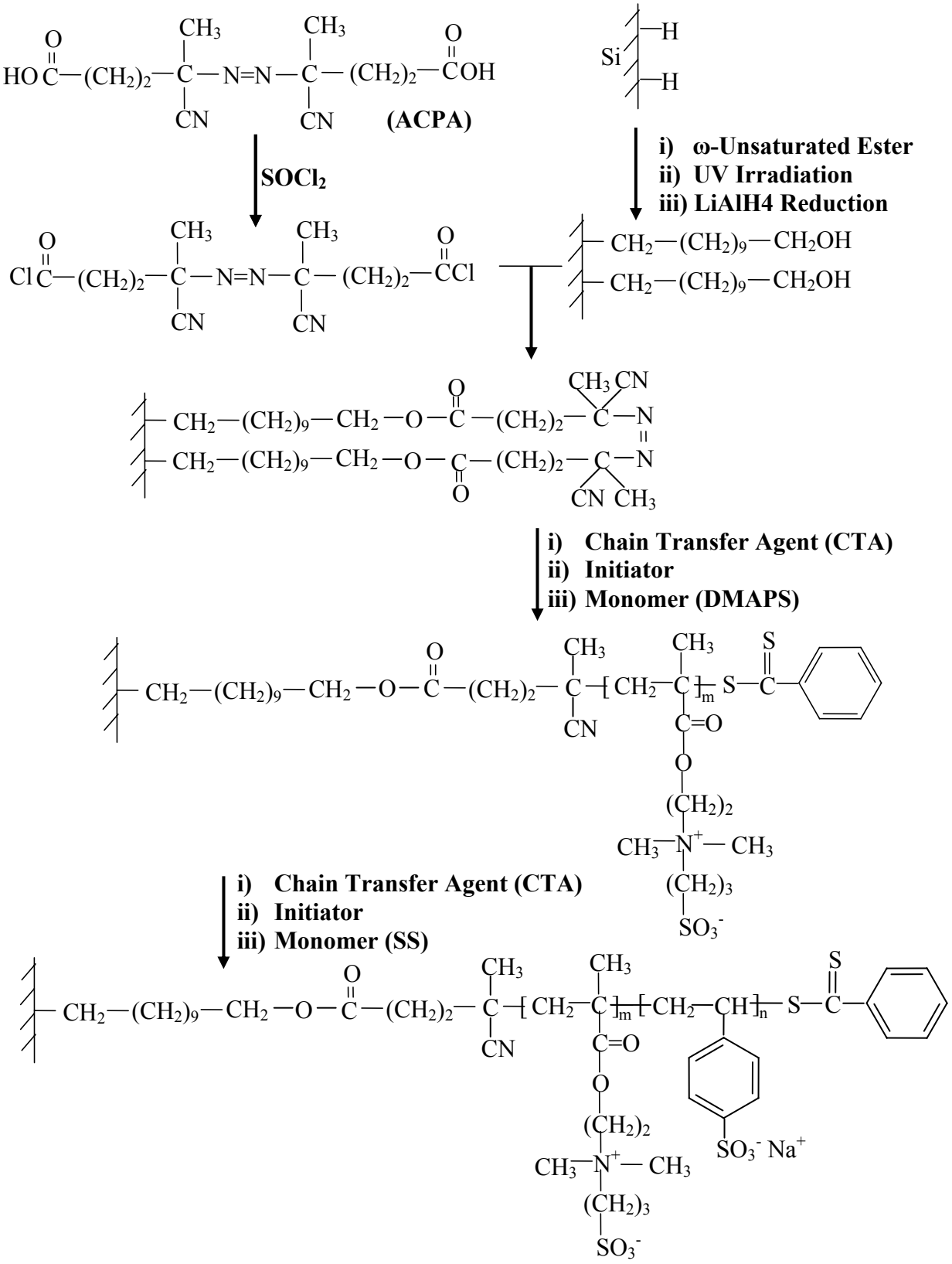

Figure 6.1: Schematic illustration of surface functionalization of the silicon substrate, immobilization of the azo initiator, and the RAFT-mediated synthesis of the polymer brushes.

the synthesis of the Si-*g*-PDMAPS brushes, except that 5 g of the anionic monomer, sodium 4-styrene sulfonate (SS) and a piece of freshly prepared Si-*g*-PDMAPS wafer were used to give rise to a Si-*g*-PDMAPS-*b*-PSS surface. The synthesis of the diblock polymer brush is also illustrated in Figure 6.1.

6.1.4 Characterization

The surface composition of the silicon wafer was characterized by XPS, the same as in Section 3.1. The topography of the modified silicon surfaces was probed by atomic force microscopy (AFM), using a Nanoscope IIIa AFM from the Digital Instrument Inc. A 5 μm × 5 μm surface area was scanned using the tapping mode. The drive frequency was 330±15 kHz, and the voltage was between 3.0-4.0 V. The drive amplitude was about 300 mV and the scan rate was 0.5-1.0 Hz.

The thickness of the polymer films grafted on the silicon wafer was measured by ellipsometry, using a variable angle spectroscopic ellipsometer (model VASE®, J. A. Woollam Inc. Lincoln, NE) at incident angles of 65°, 70° and 75° and in the wavelength range of 200 to 1000 nm. All measurements were conducted in dry air at room temperature. The refractive index of the dried polymer films was determined to be 1.5. For each sample, the thickness measurements were performed on three different surface locations. Thickness data reported were average values based on film thickness measurements that did vary by more than ±1 nm. Data were recorded and processed using the VASE® software package.

Static water contact angles of the silicon surface were measured at room temperature and 60% relative humidity by the sessile drop method, using a 3-μl water droplet in a telescopic goniometer (Rame-Hart, Model 100-00-(230)), manufactured by the Rame-Hart, Inc. (Mountain Lakes, NJ)). The telescope with a magnification

power of 23× was equipped with a protractor of 1° graduation. For each sample, the measurements were conducted on at least three different surface locations and the results were averaged. Each contact angle reported was reliable to +3°.

6.2 Results and Discussion

6.2.1 Functionalization of the Hydrogen-Terminated Silicon Surface and Immobilization of the Azo Initiator

The hydrogen-terminated silicon (Si-H) surface is first transformed into the hydroxyl-terminated surface, because the labile hydroxyl group can be utilized to immobilize the azo initiator or to introduce other functional groups. The Si-H surface was functionalized *via* a two-step process. A self-assembled monolayer (SAM) of 10-undecylenic methyl ester (CH_2=CH-$(CH_2)_8$-$COOCH_3$) was covalently coupled to the Si-H surface under UV irradiation to give rise to an ester-terminated silicon (Si-$COOCH_3$) surface, followed by reduction of the ester groups into the hydroxyl groups by $LiAlH_4$, leading to the hydroxyl-terminated silicon (Si-CH_2OH) surface. The presence of a slightly higher proportion of the <u>*C*</u>-O species than the O-<u>*C*</u>=O species on the Si-$COOCH_3$ surface probably has resulted from oxidation of the coupled ester monolayer by the UV irradiation (Yu, 2003).

Figures 6.2(a) and 6.2(b) show the respective C 1s core-level spectra of the Si-$COOCH_3$ surface and Si-CH_2OH surface. The C 1s spectrum of the Si-$COOCH_3$ surface was curve-fitted with four peak components using the following protocols. The peak components at the binding energies (BE's) of about 283.9 eV and 284.6 eV are assigned to the Si-<u>*C*</u> species and <u>*C*</u>H_2 species, respectively. The peak components at the BE's of about 286.2 eV and 288.8 eV are attributed to the <u>*C*</u>-O and O-<u>*C*</u>=O

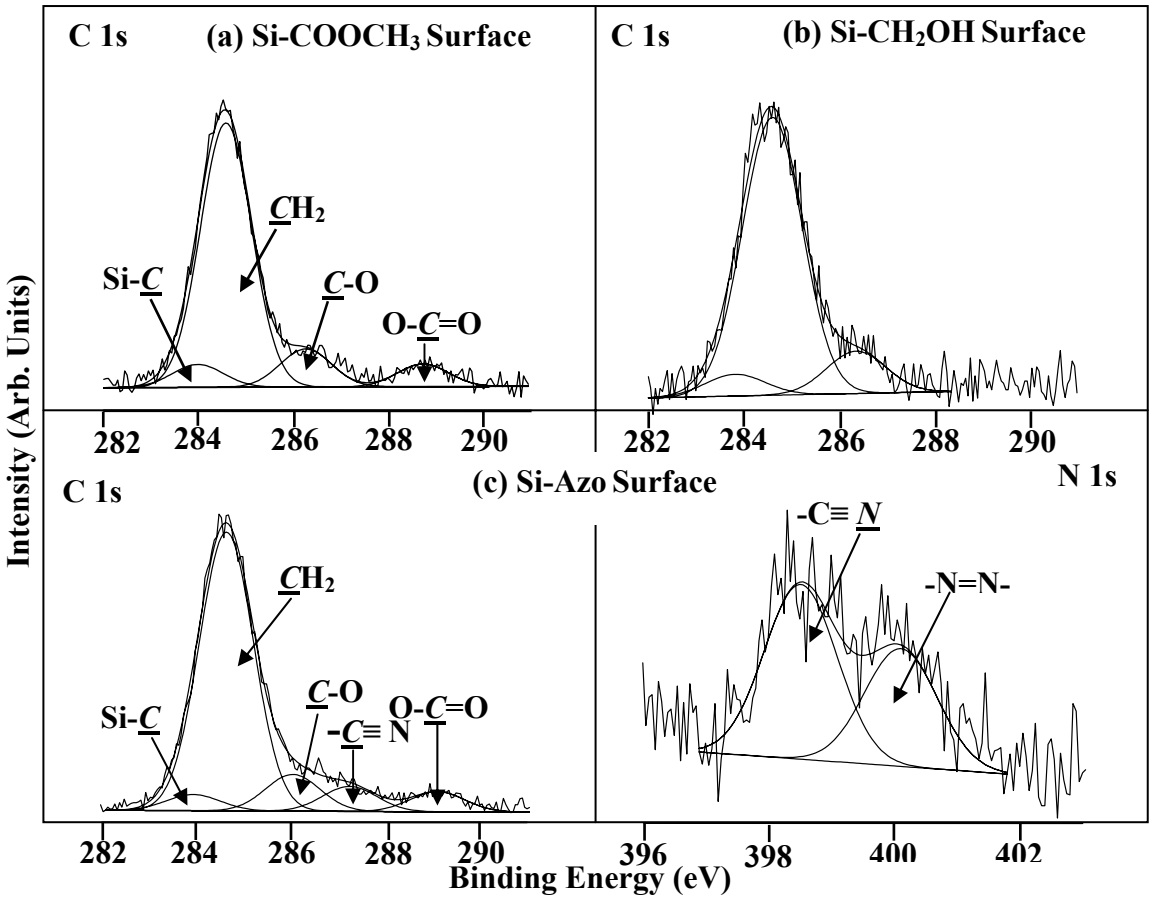

Figure 6.2: XPS C 1s core-level spectra of (a) the Si-$COOCH_3$ and (b) the Si-CH_2OH; (c) XPS C 1s and N 1s core-level spectra of the Si-Azo surface.

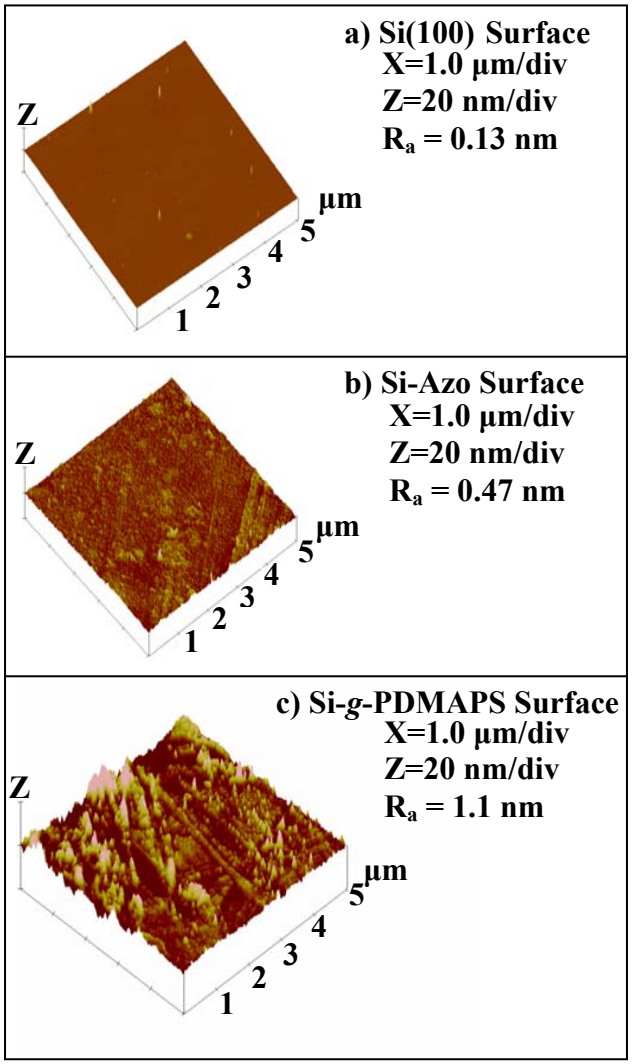

Figure 6.3: AFM micrographs of the silicon surface: (a) the pristine Si(100) surface; (b) the Si-Azo surface and (c) the Si-*g*-PDMAPS surface (polymerization time =12 h, PDMAPS thickness ≈ 9 nm).

species, respectively. For the Si-$COOCH_3$ surface, the molar ratio of the $\underline{C}$-O species to O-$\underline{C}$=O species, as determined from the spectral peak component areas, is about 1.6:1, which deviated somewhat from the theoretical ratio of 1:1. This deviation is probably due to photolysis of the ester group under the UV irradiation. On the other hand, the molar ratio of the $\underline{C}H_2$ species and the Si-$\underline{C}$ species is about 11.5, in good agreement with the theoretical value of 11 for the 10-undecylenic methyl ester. For the Si-CH_2OH surface, the C 1s peak component associated with the O-$\underline{C}$=O species has disappeared, while the other three peak components remain. The change in C 1s line shape indicates that the ester groups on the silicon surface have been completely transformed into the hydroxyl groups after reduction by $LiAlH_4$. Since the hydroxyl group is much more hydrophilic than the ester group, the static water contact angle of the resulting Si-CH_2OH surface decreases from about 60^o to only about 25^o. Efficient esterification of hydroxyl groups with carboxyl acid occurs only in the presence of certain catalysts (Ishihara *et al.*, 2000; Wakasugi *et al.*, 2000; Otera, 2001; Xiang *et al.*, 2001). In the present study, the carboxylic acid group of ACPA was first transformed into acid chloride by reaction with thionyl chloride, because the latter is more reactive toward esterification of the hydroxyl group, especially at room temperature (von Werne *et al.*, 2003; Sugiyama *et al.*, 1992).

Figure 6.2(c) shows the C 1s and N 1s core-level spectra of the silicon surface after immobilization of the azo initiator (Si-Azo surface). The C 1s core-level spectrum is curved-fitted with five peak components. Besides the four peak components found for the Si-$COOCH_3$ surface, the peak component at the BE of about 287.2 eV is attributable to the –$\underline{C}$≡N species of the azo moiety. Upon immobilization of the azo compound on the Si-CH_2OH surface, the O-$\underline{C}$=O species

has re-appeared, indicating that the esterification reaction has occurred on the silicon surface. The appearance of the C≡N peak component confirms that the azo initiator has been immobilized on the silicon surface. The N 1s core-level spectrum of the Si-Azo surface is curve-fitted with two peak components at the BE's of about 398.5 eV and 400.2 eV, attributable to the C≡N and –N=N- species of the azo initiators, respectively. The molar ratio of the two species, as determined from their corresponding spectral area ratio, is about 0.70. This ratio deviated somewhat from the theoretical value of 1:1 for the azo initiator ACPA. The deviation probably has resulted from the decomposition of some of the azo moieties during the preparation and storage of the Si-Azo substrate. The persistence of the C-O species in Figure 6.2(c), as well as the fact that the [N]/[C] ratio of the Si-Azo surface is only about 0.09 (as determined from the N 1s and C 1s core-level spectral area ratio) instead of about 0.12 for the idealized structure shown in Figure 6.1, suggest that not all the azo-containing moieties attach to the hydroxyl-terminated Si-CH_2OH surface *via* both ends. After the esterification of the hydroxyl groups and immobilization of the azo initiator, the static water contact angle of the silicon wafer increases from about 25^o to about 40^o. The "surface density" of the initiators can probably be defined as the extent of esterification of the Si-CH_2OH surface by the azo chloride moieties. Thus, the surface density of the initiators can be determined from the XPS-derived O-C=O to C-O ratio.

6.2.2 Surface-Initiated RAFT Polymerization of DMAPS on the Functionalized Si-H Substrate

The RAFT-mediated polymerization of the zwitterionic monomer, DMAPS, in aqueous media had been reported. A conversion of about 97% was achieved in 3 h,

when the monomer concentration was about 0.71 mol/L (Donovan *et al.*, 2002). A lower monomer concentration of about 0.35 mol/L was used in the present study to reduce the polymerization rate. After the immobilization of the azo initiator, the polymerization of DMAPS was initiated from the surface-bounded initiator to give rise to the surface-grafted DMAPS polymer (PDMAPS). The surface is referred to as the Si-*g*-PDMAPS surface. The topography, chemical state and polymer film thickness of the Si-*g*-PDMAPS surface are probed by AFM, XPS, and ellipsometry, respectively. Due to the small thickness (~10 nm) of the grafted PDMAPS on the silicon substrate, attempts to study the chemical structure of the graft PDMAPS directly by attenuated total reflectance Fourier transform infrared (ATR-FTIR) fail to produce additional structural information.

Figures 6.3(a) to 6.3(c) show the topography of the pristine Si(100) surface, the Si-Azo surface and the Si-*g*-PDMAPS surface (polymerization time=12 h), respectively. The pristine Si(100) substrate exhibits an atomically flat surface, with a root-mean-square surface roughness (R_a) of about 0.13 nm. After surface functionalization and immobilization of the azo initiator, the R_a value of the Si-Azo surface has increased slightly to about 0.47 nm. After the surface-initiated RAFT polymerization of DMAPS for 12 h in an aqueous medium, the Si-*g*-PDMAPS surface exhibits an R_a value of about 1.1 nm. The AFM image of the Si-g-PDMAPS surface reveals the presence of a distinctive overlayer.

Figure 6.4 shows the respective C 1s and N 1s core-level spectra of the Si-*g*-PDMAPS surface (surface film thickness ≈ 11 nm) and the PDMAPS homopolymer. The N 1s core-level spectrum of the PDMAPS homopolymer was curve-fitted with

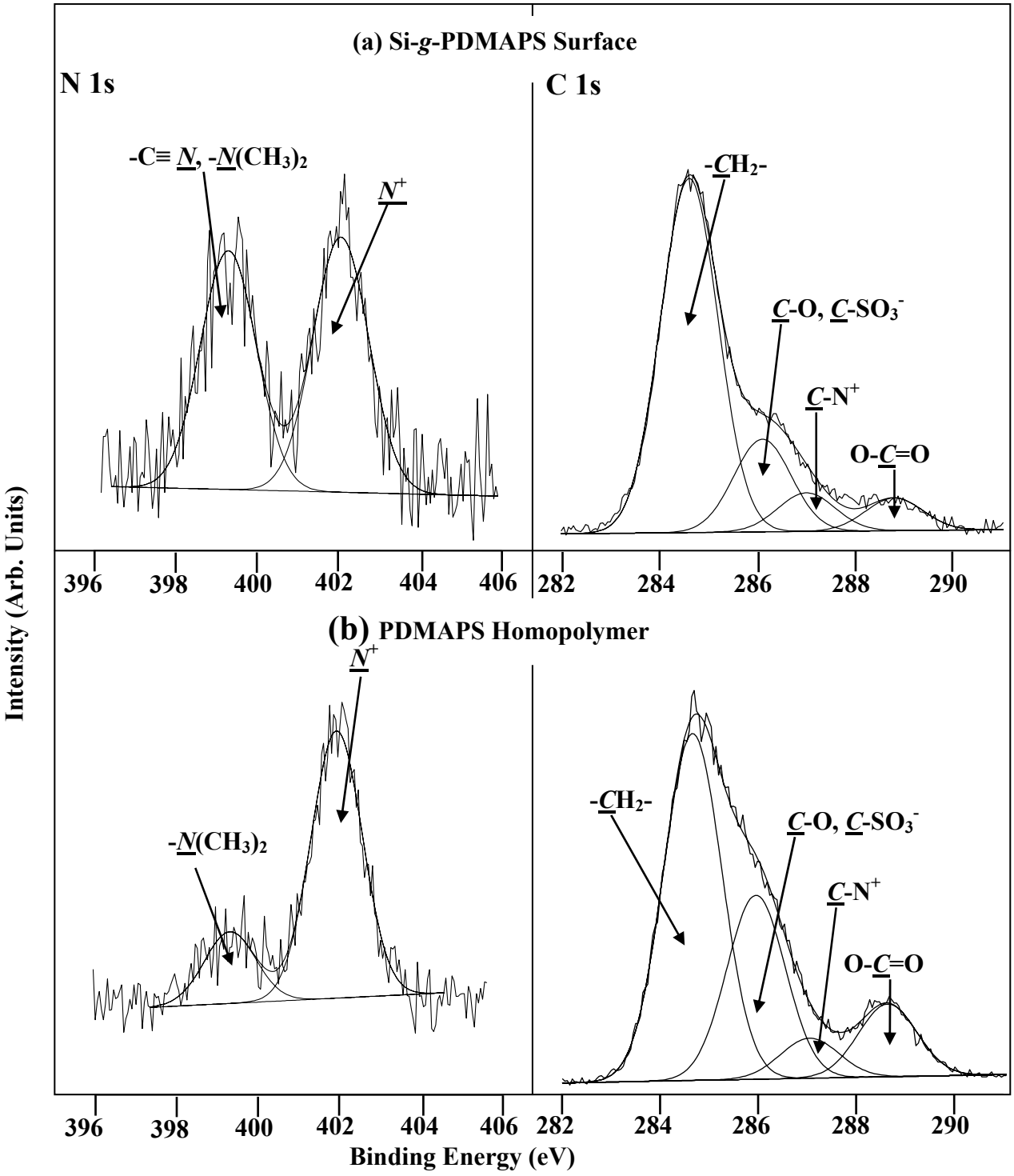

Figure 6.4: XPS N 1s and C 1s core-level spectra of (a) the Si-*g*-PDMAPS surface (polymerization time=18 h) and (b) the PDMAPS homopolymer.

two peak components. The major peak component at the BE of about 402 eV is assigned to the quaternary ammonium cations of the sulfobetaine, or the C-$\underline{N}^+$ species, while the minor peak component at the BE of about 399.5 eV is attributable to the tertiary amine, or the C-$\underline{N}(CH_3)_2$ species, arising probably from decomposition or hydrolysis of the quaternary ammonium cation of DMAPS.[31,32] The molar ratio of the two species, or the $([C\text{-}\underline{N}^+]/[C\text{-}\underline{N}(CH_3)_2])_{surface}$ ratio, determined from their peak component area ratio, is about 3.7. The N 1s core-level spectrum of the Si-*g*-PDMAPS surface can also be curve-fitted with two peak components. The peak intensity of the tertiary amine species at the BE of 399.5 eV has been enhanced. The $([C\text{-}\underline{N}^+]/[C\text{-}\underline{N}(CH_3)_2])_{surface}$ ratio of the Si-*g*-PDMAPS surface has decreased to about 1.1, consistent with the further decomposition and hydrolysis of the DMAPS chains to form the C-$\underline{N}(CH_3)_2$ species during the surface-initiated RAFT polymerization.

The C 1s core-level spectra of the Si-*g*-PDMAPS surface and the PDMAPS homopolymer were curve-fitted with four peak components using the following approach. The peak components at the BE's of 284.6 eV and 288.8 eV are attributed to the -$\underline{C}H_2$- and O-$\underline{C}$=O species, respectively, as mentioned before. The peak component at the BE of about 287.0 eV is assigned to the $\underline{C}$-N^+ species of the DMAPS polymer film.[40] The peak component at the BE of about 286 eV is attributed to the combined contribution of the $\underline{C}$-O and $\underline{C}$-SO_3^- species. The C 1s core-level line shape of the Si-*g*-PDMAPS surface differs considerably from that of the Si-Azo surface. Due to the presence of surface-grafted PDMAPS, the peak component associated with the Si-$\underline{C}$ species has been obscured. The enhanced proportion of the $\underline{C}$-O and $\underline{C}$-SO_3^- species, associated with the DMAPS repeat units, in the C 1s core-

level spectrum of the Si-g-PDMAPS surface over that of the C-O species in the C 1s spectrum of the Si-Azo surface confirms the presence of surface-grafted PDMAPS.

The thickness of the grafted DMAPS polymer film on the silicon substrate was determined by ellipsometry. Figure 6.5 shows the dependence of the thickness of the PDMAPS film of the Si-*g*-PDMAPS surface on the polymerization time. Figure 6.5 shows that the thickness of the PDMAPS film increases almost linearly with the polymerization time. Previous study has shown that the "living" or controlled polymerization of DMAPS could be achieved *via* the RAFT-mediated process using 4-cyanopentanioc acid dithiobenzoate (sodium salt) as the CTA (Donovan *et al.*, 2002). The molecular weight exhibited a linear increase with the increase in conversion. A polydispersity index of less than 1.4 was achieved in the PDMAPS polymer from the RAFT-mediated process (Donovan *et al.*, 2002). Although the thickness of the grafted PDMAPS polymer film, initiated by the azo species bound on the Si-H surface increases linearly with the increase in polymerization time, the surface-initiated "living" polymerization may differ substantially from the bulk "living" polymerization. In the former process, additional constraints, such as the excluded volume effect of neighboring chains, are imposed on the growing chains to give rise to a different set of polymerization kinetics. The steric hindrance from the neighboring chains at the surface can result in irreversible termination or chain transfer reaction of the propagating radicals, giving rise to gradual or partial deactivation of the polymer chains. The latter phenomenon, in turn, will increase the polydispersity of the surface-initiated DMAPS chains.

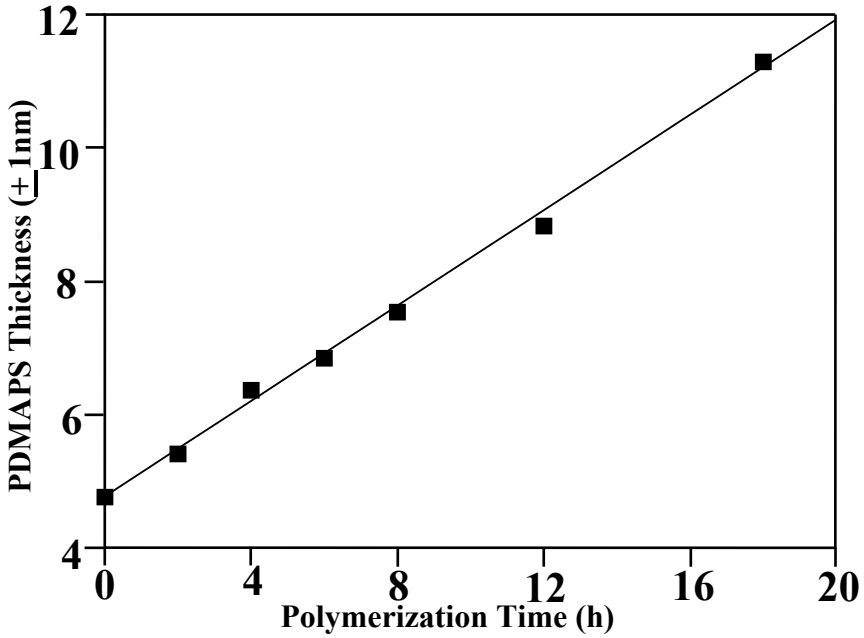

Figure 6.5: Dependence of the PDMAPS film thickness of the Si-*g*-PDMAPS surface on the polymerization time.

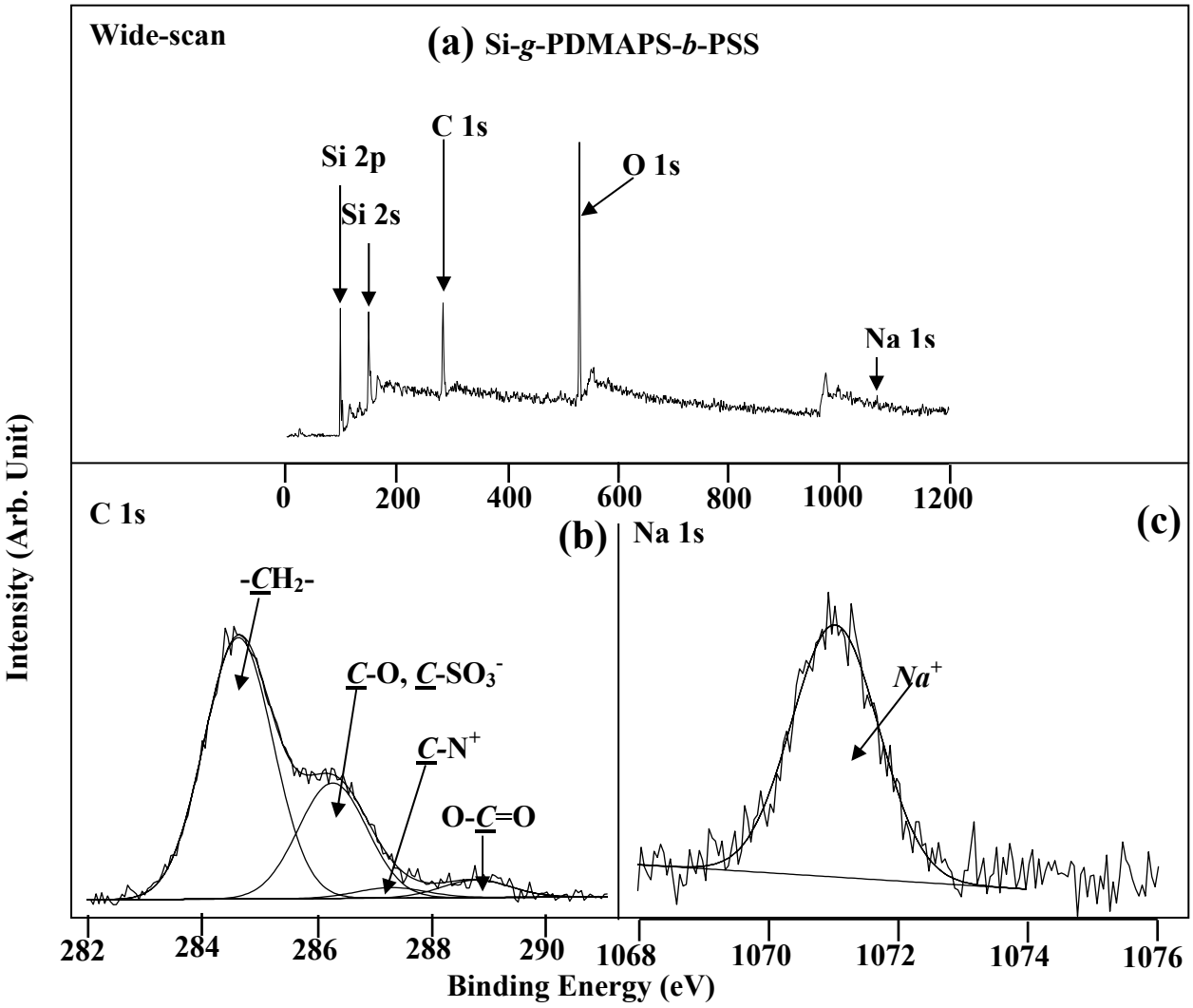

Figure 6.6: XPS wide scan, C 1s and Na 1s core-level spectra of the Si-*g*-PDMAPS-*b*-PSS surface.

For all the controlled radical polymerizations, it is essential to avoid the propagating radicals from the irreversible termination or chain transfer reactions. During the RAFT polymerization of DMAPS in an aqueous medium in the presence of the CTA, the primary free radicals are produced from the thermal decomposition of the azo initiator and form the propagating radicals of PDMAPS. The propagating radicals chain-transfer to the added CTA, a dithioester, and form the dormant PDMAPS polymer chains with a dithiobenzoate end group, or macro-CTAs. Equilibrium is eventually established between the macro-CTAs and the propagating radicals. The PDMAPS polymer can fragment from the macro-CTA to undergo further propagation. PDMAPS with a narrow molecular weight distribution is thus produced through the RAFT-mediated process (Mitsukami *et al.*, 2001; Donovan *et al.*, 2002; Chiefari *et al.*, 1998; Chong *et al.*, 1999).

6.2.3 Synthesis of the Diblock Brushes on the Si-*g*-PDMAPS Surface

As mentioned above, the polymer prepared *via* the RAFT-mediated process has an end functionality of the dithiobenzoate group. Thus, the so-prepared graft chains on the silicon substrate can serve as macro-CTAs for the subsequent block polymerization or further functionalization (Thang *et al.*, 1999; Chiefari *et al.*, 1998; Chong *et al.*, 1999; Lowe *et al.*, 2002). In order to ascertain the RAFT-mediated nature of the Si-*g*-PDMAPS surface, and the "living" character of the dithiobenzoate end functionality of the PDMAPS brushes, efforts were made to incorporate another polymer block to form the diblock polymer brushes on the silicon surface. The anionic monomer, sodium 4-styrene sulfonate (NaSS) was chosen for the block copolymerization because there had been reports on the RAFT-mediated polymerization of SS using the same thio compound as the CTA (Mitsukami *et al.*,

2001). In addition, the NaSS repeat unit contains the sodium salt, which can serve as a marker in the XPS analysis (Santos et al., 2001).

After graft copolymerization for 8 h in an aqueous medium of NaSS to produce the diblock polymer brushes (Si-*g*-PDMAPS-*b*-NaPSS surface) from a freshly prepared Si-*g*-PDMAPS surface (initial film thickness ≈ 11 nm), its surface chemical composition and chemical states were determined by XPS. Figures 6.6(a) to 6.6(c) show the XPS wide scan, C 1s and Na 1s core-level spectra, respectively, of the Si-*g*-PDMAPS-*b*-NaPSS surface. The C 1s spectrum can be curve-fitted with four peak components by the same strategy as that employed for the Si-*g*-PDMAPS surface. Compared to that of the Si-*g*-PDMAPS surface, the molar ratio of the O-$\underline{C}$=O species from DMAPS to the sum of the $\underline{C}$-O and $\underline{C}$-SO_3^- species for the Si-*g*-PDMAPS-*b*-PSS surface decreases from 0.25 to about 0.15, indicating that the O-$\underline{C}$=O (or $\underline{C}$-N^+) species associated with the PDMAPS block has been partially obscured by the PSS polymer film and the $\underline{C}$-SO_3^- (or $\underline{C}$-N^+) species have been enhanced after the introduction of the PSS blocks. In addition to changes in the C 1s lineshape, the Na 1s signal is also detected in the XPS wide scan spectrum of the Si-*g*-PDMAPS-*b*-NaPSS surface, as shown in Figure 6.6(a). Figure 6.6(c) shows the Na 1s core-level spectrum of the Si-*g*-PDMAPS-*b*-NaPSS surface. The $([Na]/[C])_{surface}$ molar ratio of the Si-*g*-PDMAPS-*b*-NaPSS surface, determined from the Na 1s and C 1s core-level spectral area ratio, is about 0.03. On the other hand, the $([S]/[C])_{surface}$ molar ratio has increased from about 0.05 to about 0.1, consistent with the incorporation of the SS polymer. Ellipsometry analysis result indicates that after 8 h of block copolymerization, although the uniformity of the surface was reduced, the thickness of the polymer film on the silicon substrate has increased by about 3 nm. These results

confirm that NaSS has been successfully block copolymerized by the dithiobenzoate end group of the Si-*g*-PDMAPS brushes.

6.3 Conclusions

Surface-initiated reversible addition-fragmentation chain transfer (RAFT) polymerization of a zwitterionic monomer, *N,N'*-dimethyl(methylmethacryloyl ethyl) ammonium propane sulfonate (DMAPS), was successfully carried out on the hydrogen-terminated silicon (Si-H) surface to produce the Si-*g*-PDMAPS surface. AFM images revealed that the roughness of the Si-H substrate was increased after surface functionalization and the surface-initiated RAFT polymerization of DMAPS. XPS results inferred significant changes in the chemical states of carbon and nitrogen of the silicon substrate, indicating the fact that the DMAPS polymer has been grafted on the substrate. Because of the "living" character of the surface-initiated RAFT process, ellipsometric results have shown that the thickness of the PDMAPS film on the Si-*g*-PDMAPS surface increases linearly with the polymerization time of the polymer brush. Since the so-obtained polymer brush contains a dithioester end group from RAFT polymerization, diblock polymer brushes were prepared *via* the block polymerization of sodium styrene sulfonate (NaSS) on the Si-*g*-PDMAPS surface to result in the Si-*g*-PDMAPS-*b*-PSS surface. The presence of the NaPSS block was confirmed by XPS analysis and the increase in surface film thickness.

Chapter 7：

Conclusions

PVDF graft copolymer with functional side chains was successfully prepared via the ozone-pretreatment of PVDF in solution and graft copolymerization with specific monomers, such as weak base 4VP and zwitterionic DMAPS (PVDF-*g*-P4VP and PVDF-*g*-PDMAPS copolymers). The microfiltration membranes were fabricated from the respective copolymer solutions by phase inversion.

Due to the weak base nature of the P4VP side chains, both the surface morphology, pore-size distribution and surface composition is dependent on the pH value of the casting bath. With the increasing pH of the casting bath, the pore size decreases while the surface enrichment of the graft chains occurs. The flux of aqueous solution through the PVDF-*g*-P4VP membrane exhibits a pH-sensitive behavior. The flow rate increases with the increase in the solution pH. XPS results revealed that the hydrogen bonding and protonation of the pyridine groups accounts for such a phenomenon.

The pH- and temperature- sensitive membranes were prepared from the blend of P4VP-*g*-P4VP and PNIPAm in solution by phase inversion. It was revealed that both the surface morphology and the pore-size distribution of the PVDF-*g*-P4VP/PNIPAm blend membrane were dependent on the pH value, temperature and ionic strength of the casting bath, as the low temperature and high pH of the casting bath enhance the surface concentration of the graft chains and the hydrophilicity of the membrane surface. The flow rate of the aqueous media through the blend increases with the increases in both the pH value and the temperature of the aqueous media.

The aqueous solution of DMAPS homopolymer (PDMAPS) exhibits a typical polyzwitterion behavior, depending on both the temperature and the ionic strength of the aqueous solution. Accordingly, the surface morphology and the surface composition of the PVDF-g-PDMAPS membrane were also responsive to the ionic strength and temperature of the casting bath. The flow rate of aqueous media through the membrane decreases with the increase in the ionic strength, resulting from the globular-to-coiled conformational transition of the PDMAPS side chains in response to the increase in the electrolyte concentration, or *anti-polyelectrolyte effect*.

The molecularly and surface-initiated ATRP were also carried out to prepare PVDF graft copolymer. The ATRP-type AB* inimer was graft-copolymerized with the ozone-pretreated PVDF to produce PVDF-*g*-PBIEA copolymers. The ATRP of NaSS was initiated by the PBIEA side chains to produce the PVDF-*g*-PBIEA-*ar*-NaPSS copolymer. Due to the presence of NaPSS side chains, the morphology and surface composition of the PVDF-g-PBIEA-g-NaPSS membrane are responsive to the ionic strength of the casting bath. The migration of the NaPSS from the bulk to the surface was promoted in a high ionic strength casting bath, as the electrostatic repulsion was shielded by the mobile ions (*polyelectrolyte effect*). The surface-initiated ATRP of PEGMA was carried out on the PVDF-*g*-PBIEA membrane surface to produce the PVDF-*g*-PBIEA-*ar*-PPEGMA membrane. The biocompatible PEGMA polymer had enhanced significantly the anti-fouling properties of the membranes.

The surface-initiated RAFT process was also extended to the silicon substrate to produce the well-defined polymer brushes. After the immobilization of azo initiator onto the silicon substrate, the RAFT-mediated process of DMAPS was initiated from

the surface-bound azo moiety to produce Si-*g*-PDMAPS brushes. The thickness of the polymer layer increased linearly with the increase in polymerization time. In order to verify the presence of end-functionality, NaSS was copolymerized to produce the Si-*g*-PDMAPS-*b*-NaPSS brushes.

Chapter 8:

Recommendations for Futher Work

Based on the research work I performed during these 3 years, there are severa recommendations for future work from my point of view.

1 Stimuli-responsive Polymers

One of most interesting apsectes of polymers is that multiple properties or characters can be integreated into a whole by copolymerization, and structures of the copolymers, including sequencing, architechture, molecular weight etc, can be custom-designed and tailer-made with the aid of precision polymerization, especially the controlled radical polymerization. The stilimuli-responsive polymers constitute a special family of functional polymers of great academic and application potentials. The synthesis of multicomponent copolymer with precisely defined architectures have lead to a more interesting stimuli-responsive behavior, which could integrate the sensitive physicochemical properties in reponse to pH, temperature and ionic strength. Beyond the membrane formation, there is a huge space for the study of stimuli-responsive polymers, especially the controlled self-assembly in the solution or at the interface.

Even limited in membrane formation of stimuli-responsive copolymer, there are still more spaces to explore. For instance, the PVDF used in this study has a rather wide molecular weight distribution (MWD), and the side chains introduced to the PVDF backbones has a degree of polymerization of great randomcy. Adopting some technique to controlled the MWD of PVDF backbones and side chains may produce more direct results and indications for this study.

2 Visualization of Stimuli-responsive Behaivor

When explaining the responsive behavior of the membranes, especially the flow rates, it was typically believed to result from the conformational changes of the side

chains distributed on the pore walls; however, these claims need to be justified and they are just tentatively based on the assumption and previous work on hydeogel by other research groups.For the membranes, the most direct proof is to visualize the change in the pore size or in the chain conformation. For the future work, it is suggested to visualize such a responsive change to justifiy these claims.

3 Surface-initiated Living Radical Polymerization

Although the controlled radical polymerization, such as atom transfer radical polymerization (ATRP) and reversible addition-fragmentation chain transfer process (RAFT), have been widely investigated in the formation of solution reaction, the hetereogeneous ATRP or RAFT are still in their premature state. One of the key advantages of ATRP and RAFT is to control the MW and MWD; however, for the surface-initiated ATRP or RAFT, due to different mobility and, thus, reactivity, the MW and MWD could be hardly maintained as ideal as those of homogenous reaction. For the surface-initated RAFT, what is more, since the polymerization rate is significantly retarded by the presence of CTA, the chain-transfer efficiency could not be sufficiently high, indicating that all the terminal groups of RAFT-prepared polymers could not necessarily be dithioester functionality. As a suggestion, the surface-initatied RAFT should be avoided in the synthesis of surface-bonded polymers, except that a high reaction rate could be achieved for the monomers to be studied .

4 Instrumental Analysis

For the students and research staffs of lab of Surface and Interface Engineering, the author used a spectrum of modern instruments to characterize the materials

obtained. However, since the materials studied in this work are basically organic in nature, the utility of some modern instrument could be improved, especially for nucluear-magentic resonance (NMR). NMR could provide a both qualative and quantitative description of the chemical structure. On the other hand, the usage of x-ray photoelectron spectroscopy (XPS) has been relied on excessively, although it was not very necessary on some occasions.

5 Mechanistic Understanding

The author generally adopted the mature techniques to prepare the copolymers and to characterization their structure and properties, implying that the author has made few exploration into the unknown field, especially in the copolymerization kinectics and so on. More efforts could be input during the Ph.D study.

Chapter 9:

References

Advincula R.; Q. G. Zhou; M. Park; S. G. Wang; J. Mays; G. Sakellariou; S. Pispas and N. Hadjichristidis Polymer brushes by living anionic surface initiated polymerization on flat silicon (SiOx) and gold surfaces: Homopolymers and block copolymers *Langmuir* 18, pp.8672-8684. 2002.

Ali M. M. and H. D. H. Stover Polymeric capsules prepared by in situ synthesis and cross-linking of amphiphilic copolymer by atom transfer radical polymerization, *Macromolecule*s, 36, pp1793-1801. 2003.

Annenkov V. V.; E. N. Danilovtseva; V. V. Saraev and A. I. Mikhaleva Complexation of copper(II) ions with imidazole-carboxylic polymeric systems *J. Polym. Sci.: Polym. Chem.* 41, pp.2256-2263. 15 2003.

Aoi K. and M. Okada Polymerization of Oxazolines *Prog. Polym. Sci.* 21, pp.151-208. 1996

Armentrout R. S.; E. E. Kathmann and C. L. McCormick Synthesis and Aqueous Solution Behavior of Novel Polyampholytes Containing Zwitterionic Monomers 3-[(2-Acrylamido-2-methyl propyl)dimenthylammonio]-1-propanesulfonate or 3-(N,N-Diallyl-N-methylammonio)-1-propanesulfonate in *Specialty monomers and polymers : synthesis, properties, and applications* / Kathleen O. Havelka, editor, Charles L. McCormick, ed. Washington, DC : American Chemical Society, 2000a.

Armentrout R. S. and McCormick C. L. Water soluble polymers. 76. Electrolyte responsive cyclocopolymers with sulfobetaine units exhibiting polyelectrolyte or polyampholyte behavior in aqueous media *Macromolecules* 33, pp.419-424, 2000b.

Arotcarena M.; B. Heise; S. Ishaya and A. Laschewsky Switching the inside and the outside of aggregates of water-soluble block copolymers with double thermoresponsivity *J. Am. Chem. Soc.*124, pp.3787-3793. 2002.

Auroy P.; L. Auvray and L. Leger Characterization of the Brush Regime for Grafted Polymer Layers at the Solid-Liquid Interface *Phys. Rev. Lett*. 66, pp.719-722.1991.

Barbucci R.; M. Casolaro; A. Ditommaso and A. Magnani Thermodynamic and Spectroscopic Studies on the Protonation of Optically-Active Polyampholyte *Macromolecules* 22, pp.3138-3143. 1989.

Bartholome C.; E. Beyou; E. Bourgeat-Lami; P. Chaumont and N. Zydowicz Nitroxide-mediated polymerizations from silica nanoparticle surfaces: "Graft from" polymerization of styrene using a triethoxysilyl-terminated alkoxyamine initiator *Macromolecules* 36, pp.7946-7952. 2003.

Baskaran D. Hyperbranched polymers from divinylbenzene and 1,3-diisopropenylbenzene through anionic self-condensing vinyl polymerization, *Polymer*, 44, pp.2213-2220. 2003.

Bergbreiter D. E. Polyethylene Surface-Chemistry *Prog. Polym. Sci.* 19, pp.529-560. 1994.

Bergbreiter D. E.; G. F. Xu and C. Zapata Heterogeneous Grafting Chemistry using Residual Unsaturation as a Graft Site Precursor *Macromolecules* 27, pp.1597-1602. 1994.

Berlin A. A. and V. N. Kislenko Kinetics and Mechanism of Radical Graft Polymerization of Monomers onto Polysaccharides *Prog. Polym. Sci.* 17, pp.765-825. 1992.

Bhattacharya A. Radiation and industrial polymers *Prog. Polym. Sci.* 25, pp.371-401. 2000.

Biesalski M.; D. Johannsmann and J Ruhe Electrolyte-induced collapse of a polyelectrolyte brush *J. Chem. Phys.* 120, pp.8807-8814. 2004.

Bokias G.; V. V. Vasilevskaya; I. Iliopoulos; D. Hourdet and A. R. Khokhlov Influence of migrating ionic groups on the solubility of polyelectrolytes: Phase behavior ionic poly(N-isopropylacrylamide) copolymers in water, *Macromolecules* 33. pp.9757-9763. 2000.

Boutevin B. From telomerization to living radical polymerization *J. Polym. Sci.: Polym. Chem.* 38, pp.3235-3243. 2000.

Boutevin B.; J. J. Robin and A. Serdani Synthesis and applications of Graft-Copolymers from Ozonized Poly(Vinylidene Fluoride) .2. *Euro. Polym. J.* 28, pp.1507-1511. 1992.

Bowden N. B.; M. Dankova; W. Wiyatno; C. J. Hawker and R. M. Waymouth Synthesis of polyethylene graft block copolymers from styrene, butyl acrylate, and butadiene *Macromolecules* 35, pp.9246-9248. 2002.

Brantley E. L. and G. K. Jennings Fluorinated polymer films from acylation of ATRP surface-initiated poly(hydroxyethyl methacrylate) *Macromolecules* 37, pp.1476-1483. 2004.

Buriak, J. M. Organometallic chemistry on silicon and germanium surfaces. *Chem. Rev.* 102, 1271, 2002,

Bywater S. Anionic Polymerization, *Prog. Polym. Sci.* 4, pp.27-69. 1975.

Capek I. Radical polymerization of polyoxyethylene macromonomers in disperse systems *Adv. Polym. Sci.* 145, pp.1-55. 1999

Cartier H. and G. H. Hu Styrene-assisted melt free radical grafting of glycidyl methacrylate onto polypropylene *J. Polym. Sci.: Polym. Chem.* 36, pp.1053-1063. 1998.

Chauhan G. S.; H. Lal; S. Mahajan and M. Bansal Synthesis and characterization of 4-vinyl pyridine-crafted Teflon-PFA film for water technologies *J. Polym. Sci.: Polym. Chem.* 38, 4506-4518. 2000.

Chauvierre C.; Labarre D; Couvreur P.; Vauthier C. Radical emulsion polymerization of alkylcyanoacrylates initiated by the redox system dextran-cerium(IV) under acidic aqueous conditions *Macromolecules* 36, pp.6018-6027. 2003.

Chen L.; Y., Honma; T. Mizutani; D. J., Liaw; J. P. Gong and Y. Osada Effects of polyelectrolyte complexation on the UCST of zwitterionic polymer *Polymer* 41, pp.141-147. 2000.

Chen W.; G. Boven and G. Challa Studies on Immobilized Polymer-Bound Imidazole-Copper(II) Complexes as Catalysts.3. Immobilization of Copper(II) Complexes of Poly(Styrene-co-*N*-Vinylimidazole) by Grafting on Silica and Their Catalysis of Oxidative Coupling of 2,6-Disubstituted Phenols *Macromolecules* 24, pp.3982-3987. 1991.

Chen W.; K. G. Neoh; E. T. Kang; K. L. Tan; D. J. Liaw and C. C. Huang Surface modification and adhesion characteristics of polycarbonate films after graft copolymerization, *J. Polym. Sci.: Polym. Chem.* 36, pp.357-366. 1998.

Chen X. Y.; D. P. Randall; C. Perruchot; J. F. Watts; T. E. Patten; T. von Werne and S. P. Armes Synthesis and aqueous solution properties of polyelectrolyte-grafted silica particles prepared by surface-initiated atom transfer radical polymerization, *J. Colloid Interf. Sci.* 257, pp.56-64. 2003.

Chiefari J.; Y. K. Chong; F. Ercole; J. Krstina; J. Jeffery; T. P. T. Le; R. T. A. Mayadunne; G. F. Meijs; C. L. Moad; G. Moad; E. Rizzardo and S. H. Thang Living free-radical polymerization by reversible addition-fragmentation chain transfer: The RAFT process. *Macromolecules* 1998, 31, 5559.

Choi I. S. and R. Langer Surface-initiated polymerization of L-lactide: Coating of solid substrates with a biodegradable polymer, *Macromolecules* 34, pp.5361-5363. 2001.

Chong B. Y. K.; T. P. T. Le; G. Moad; E. Rizzardo and S. H. A Thang more versatile route to block copolymers and other polymers of complex architecture by living radical polymerization: The RAFT process, *Macromolecules* 1999, 32, 2071.

Chung T. C.; Janvikul W.; Bernard R.; Jiang G. J. Synthesis of Ethylene-Propylene Rubber Graft-Copolymers by Borane Approach, *Macromolecules* 27, pp.26-31. 1994.

Chung T. C. Polyolefin copolymers containing p-methylstyrene units: Preparation by metallocene catalysts and application in the functionalization of polyolefins, *ACS Sym. Ser.* 749, pp.104-127. 2000.

Chung T. C. Synthesis of functional polyolefin copolymers with graft and block structures, *Prog. Polym. Sci.* 27, pp.39-85. 2002.

Dalsin J. L.; B. H. Hu; B. P. Lee and P. B. Messersmith Mussel adhesive protein mimetic polymers for the preparation of nonfouling surfaces, *J. Am. Chem. Soc.* 125, pp.4253-4258. 2003.

Dargaville T. R.; G. A. George; D. J. T. Hill and A. K. Whittaker High energy radiation grafting of fluoropolymers, *Prog. Polym. Sci.* 28, pp.1355-1376. 2003.

Davis K. A. and K. Matyjaszewski ABC triblock copolymers prepared using atom transfer radical polymerization techniques, *Macromolecules* 34, pp.2101-2107. 2001.

de Boer B.; H. K. Simon; M. P. L. Werts; E. W. van der Vegte and G. Hadziioannou "Living" free radical photopolymerization initiated from surface-grafted iniferter monolayers, *Macromolecules* 33, pp.349-356. 2000.

Decker C. and K. Zahouily Light-stabilization of polymeric materials by grafted UV-cured coatings, *J. Polym. Sci.: Polym. Chem.* 36, pp.2571-2580. 1998.

Dedecker K. and G. Groeninckx Interfacial graft copolymer formation during reactive melt blending of polyamide 6 and styrene-maleic anhydride copolymers, *Macromolecules* 32, pp.2472-2479. 1999.

Deffieux A.; and M. Schappacher Synthesis and characterization of star and comb polystyrenes using isometric poly(chloroethyl vinyl ether) oligomers as reactive backbone, *Macromolecules* 32, pp.1797-1802. 1999.

Dharmarajan N. and S. Datta Toughening Styrene Maleic-Anhydride Copolymers with Functionalized Ethylenen Propylene Rubbers, *Polymer* 33, pp.3848-3857. 1992.

Donovan M. S.; B. S. Sumerlin; A. B. Lowe and C. L. McCormick Controlled/"living" polymerization of sulfobetaine monomers directly in aqueous media via RAFT, *Macromolecules* 2002, 35, 8663.

Drifford M. and M. Delsanti Polyelectrolyte Solutions with Multivalent Added Salts: Stability, Structure, and Dynamics, in Physical chemistry of polyelectrolytes, Tsetska Radeva ed New York : Marcel Dekker, c2001, pp135-162.

Eckert A. R. and S. E. Webber Naphthalene-tagged copolymer micelles based on polystyrene-*alt*-maleic anhydride-graft-poly(ethylene oxide), *Macromolecules* 29, pp.560-567. 1996.

Ejaz M. Controlled Surface Grafting of Well-Defined Polymers by Living Radical Polymerization Techniques. Ph D. Dissertation 2001, Kyoto University, Japan

Fan X. W.; Q. Y. Zhou; C. J. Xia; W. Cristofoli; J. Mays and R. Advincula Living anionic surface-initiated polymerization (LASIP) of styrene from clay nanoparticles using surface bound 1,1-diphenylethylene (DPE) initiators, *Langmuir* 18, pp.4511-4518. 2002.

Fargere T.; Abdennadher M.; Delmas M.; Boutevin B. Synthesis of Graft Polymers from an Ozonized Ethylene-Vinyl Acetate Copolymer (EVA).1. Study of the Radical

Polymerization of Styrene Initiated by an Ozonized EVA, *J. Polym. Sci.: Polym. Chem.* 32, pp.1377-1384. 1994.

Feldman K.; G. Hahner; N. D. Spencer; P. Harder; and M. Grunze Probing resistance to protein adsorption of oligo(ethylene glycol)-terminated self-assembled monolayers by scanning force microscopy, *J. Am. Chem. Soc.* 121, pp.10134-10141, 1999.

Forsythe J. S. and D. J. T. Hill the radiation chemistry of fluoropolymers, *Prog. Polym. Sci.* 25, pp.101-136. 2000.

Fraser S.; R. D. Short; D. Barton and J. W. Bradley A multi-technique investigation of the pulsed plasma and plasma polymers of acrylic acid: Millisecond pulse regime *J. Phys. Chem. B.* 106, pp.5596-5603. 2002.

Frechet J. M. J.; M. Henmi; I. Gitsov; S. Aoshima; M. R. Leduc and R. B. Grubbs Self-Condensing Vinyl Polymerization- an Approach to Dendritic Materials, *Science* 269, pp.1080-1083. 1995.

Fujiki K.; M. Sakamoto; A. Yoshida and H. Maruyama Radical grafting from glass fiber surface: Graft polymerization of vinyl monomers initiated by azo groups introduced onto the surface, *J. Polym. Sci.: Polym. Chem.* 37, pp.2121-2128. 1999.

Fujioka M.; G. H. Ma; Y. Z. Du; K. Ogino; M. Nagai and S. Omi Synthesis of functional graft copolymers by solution copolymerization and their evaluation as dispersants in nonaqueous phase dispersion polymerization, *J. Polym. Sci.: Polym. Chem.* 41, pp.1788-1798. 2003.

Galia A.; A. Giaconia; V. Iaia and G. Filardo Synthesis of hydrophilic polymers in supercritical carbon dioxide in the presence of a siloxane-rased macromonomer surfactant: Heterogeneous polymerization of 1-vinyl-2 pyrrolidone, *J. Polym. Sci.: Polym. Chem.* 42. pp.173-185. 2004.

Galin J. C. in The Polymeric Materials Encyclopedia; Salamone J. C., Ed.; CRC Press: Boca Raton, Florida, 1996; Vol. 7, p 5462-5476.

Gauthier M. and M. Moller Uniform Highly Branched Polymers by Anionic Grafting – Arborescent Graft Polymers, *Macromolecules* 24, pp.4548-4553. 1991.

Gauthier M.; L. Tichagwa; J. S. Downey and S. Gao Arborescent graft copolymers: Highly branched macromolecules with a core-shell morphology, *Macromolecules* 29, pp.519-527. 1996.

Gauthier M.; J. M. Li and J. Dockendorff Arboreseent polystyrene-graft-poly(2-vinylpyridine) copolymers as unimolecular micelles. Synthesis from acetylated ubstrates, *Macromolecules* 36, pp.2642-2648. 2003.

Gnambodoe M.; T. Hamaide and A. Revillon Dilute solution behaviour of carboxylatobetaine end-capped polyisoprenes, *Polymer* 37, pp.603-613. 1996.

Goh S. H.; S. Y. Lee; J. Dai and K. L. Tan X-ray photoelectron spectroscopic studies of ionic interactions between sulfonated polystyrene and poly(styrene-co-4-vinylpyridine) *Polymer* 37, pp.5305-5308. 1996.

Goloub T.; de Keizer A. and M. A. C. Stuart Association Behavior of Ampholytic Copolymer, *Macromolecules* 32, pp.8441-8446, 1999

Granville A. M.; S. G. Boyes; B. Akgun; M. D. Foster and W. J. Brittain Synthesis and characterization of stimuli-responsive semifluorinated polymer brushes prepared by atom transfer radical polymerization, *Macromolecules* 37, pp.2790-2796. 2004.

Grasmuller M.; J. C. Rueda-Sanchez; B. I. Voit and O. Nuyken Polyfunctional polyisobutenes as building blocks for amphiphilic graft polymers *Macromol. Symp.* 127, pp.109-114. 1998.

Harada Y.; G. S. Girolami and R. G. Nuzzo Catalytic amplification of patterning via surface-confined ring-opening metathesis polymerization on mixed primer layers formed by contact printing, *Langmuir* 19, pp.5104-5114. 2003.

Hawker C. J.; J. M. J. Frechet; R. B. Grubbs and J. Dao Preparation of Hyperbranched and Star Polymers by a Living, Self-Condensing Free-Radical Polymerization, *J. Am. Chem. Soc.* 117, pp.10763-10764. 1995.

Hawker C. J.; A. W. Bosman and E. Harth New polymer synthesis by nitroxide mediated living radical polymerizations, *Chem. Rev.* 101, pp.3661-3688. 2001.

Heinz B. S.; A. Laschewsky; E. D. Rekai; E. Wischehoff and T. Zacher Grafting of Functionalized Water Soluble Polymers on Gold Surfaces: Stable Sitmuli-responsive Think Hydrogel Films exhibiting a LCST or a UCST. in Stimuli-Responsive Water Soluble Polymers, ACS Symposium Series 780, Ed. Charles L. McCormick, American Chemical Society: Washington D.C., (2000), pp. 162-180.

Hempenius M. A.; W. Michelberger and M. Moller Arborescent graft polybutadienes, *Macromolecules* 30, pp.5602-5605. 1997.

Houben L.; K. Schoone and G. Maes Analysis of the vibration correlation diagram of base center dot HCl(DCl) H-bonded complexes in Ar matrices: Type II and intermediate type I->II systems *Vib. Spectrosc.* 10, pp.147-159. 1996

Hu G. H. and M. Lambla Chemical-Reactions between Immiscible Polymers in the Melt- Transesterfication of Poly(Ethylene-co-Methyl Acrylate) with Mono-Hydroxylated Polystyrenes, *J. Polymer Sci.: Polym. Chem.* 33, pp.97-107. 1995.

Huang N. J. and D. C. Sundberg Fundamental-Studies of Grafting Reactions in Free-Radical Copolymerization. 2. Grafting of Styrene, Acrylate, and Methacrylate Monomers onto cis-Polybutadiene using AIBN Initiator in Solution Polymerization, *J. Polym. Sci.: Polym. Chem.* 33, pp.2551-2570. 1995

Huang W. X.; G. Skanth; G. L. Baker and M. L. Bruening Surface-initiated thermal radical polymerization on gold, *Langmuir* 17, pp.1731-1736. 2001.

Huglin M. B. and J. M. Rego Influence of a Salt on the Properties of Hydrogels of 2-Hydroxyethyl methacrylate with a sulfobetaine Comomer, *Macromolecules* 26, pp.3118-3126. 1993.

Husseman M.; E. E. Malmstrom; M. McNamara; M. Mate; D. Mecerreyes; D. G. Benoit; J. L. Hedrick; P. Mansky; E. Huang; T. P. Russell and C. J. Hawker Controlled synthesis of polymer brushes by "Living" free radical polymerization techniques, *Macromolecules* 32, pp.1424-1431. 1999.

Iddon P. D.; K. L. Robinson and S. P. Armes Polymerization of sodium 4-styrenesulfonate via atom transfer radical polymerization in protic media, *Polymer* 45, pp.759-768. 2004.

Ikada Y. Surface Modification of Polymers for Medical Applications, *Biomaterials* 15, pp.725-736. 1994.

Inagaki N.; S. Tasaka and M. Masumoto Improved adhesion between kapton film and copper metal by plasma graft polymerization of vinylimidazole, *Macromolecules* 29, pp.1642-1648. 1996.

Inoue Y.; T. Matsugi; N. Kashiwa and K. Matyjaszewski Graft copolymers from linear polyethylene via atom transfer radical polymerization, *Macromolecules* 37, pp.3651-3658. 2004.

Ionov L.; S. Minko; M. Stamm; J. F. Gohy; R. Jerome and A. Scholl Reversible chemical patterning on stimuli-responsive polymer film: Environment-responsive lithography, *J. Am. Chem. Soc.* 125, pp.8302-8306. 2003.

Ishihara, K.; S. Ohara and H. Yamamoto Direct condensation of carboxylic acids with alcohols catalyzed by hafnium(IV) salts, *Science* 2000, 290, 1140.

Ishizu K.; Y. Ohta; S. Kawauchi Kinetics of hyperbranched polystyrenes by free radical polymerization of photofunctional inimer, *Macromolecules* 35, pp.3781-3784. 2002.

Ito Y.; Y. S. Park and Y. Imanishi Visualization of critical pH-controlled gating of a porous membrane grafted with polyelectrolyte brushes, *J. Am. Chem. Soc.* 119, pp.2739-2740. 1997.

Ito K. Polymeric design by macromonomer technique, *Prog. Polym. Sci.* 23, pp.581-757. 1998.

Ito K. and S. Kawaguchi Poly(macromonomes): Homo- and Copolymerization, *Adv. Polym. Sci.* 142, pp.129-178. 1999.

Iwata H.; I. Hirata and Y. Ikada Atomic force microscopic analysis of a porous membrane with pH-sensitive molecular valves, *Macromolecules* 31, pp.3671-3678. 1998.

Jiao H.; Goh S. H.; Valiyaveettil S. Surfactant-induced mesomorphic structures in poly(1-vinylimidazole)-alkanoic acid complexes, *Langmuir* 18, pp.1368-1373. 2002.

Jimbo T.; A. Tanioka and N. Minoura Characterization of an amphoteric-charged layer grafted to the pore surface of a porous membrane, *Langmuir* 14, pp.7112-7118. 1998.

Jones C. D. and L. A. Lyon Synthesis and characterization of multiresponsive core-shell microgels, *Macromolecules* 33, pp.8301-8306. 2000.

Jordan R.; A. Ulman; J. F. Kang; M. H. Rafailovich and J. Sokolov Surface-initiated anionic polymerization of styrene by means of self-assembled monolayers, *J. Am. Chem. Soc.* 121, pp.1016-1022. 1999.

Kang E. T.; K. G. Neoh and K. L. Tan Surface Modifications of Poly(3-Alkylthiophene) Films by Graft-Copolymerization, *Macromolecules* 25, pp.6842-6848. 1992.

Kang E. T. and Y. Zhang Surface modification of fluoropolymers via molecular design, *Adv. Mater.* 12, pp.1481-1494. 2000.

Karlsson J. O.and P. Gatenholm Surface mobility of grafted hydrogels, *Macromolecules* 32, pp.7594-7598. 1999.

Kathmann E. E.; L. A. White; C. L. McCormick Water soluble polymers. 69. pH and electrolyte responsive copolymers of acrylamide and the zwitterionic monomer 4-(2-acrylamido-2-methyl propyldimethyl-ammonio) butanoate: Synthesis and solution behaviour, *Polymer* 38, pp.871-878.

Kato T.; M. Kawaguchi; A. Takahashi; T. Onabe and H. Tanaka Adsorption of sulfobetaine polyampholyte on silica surfaces from aqueous salt solutions, *Langmuir* 15, pp.4302-4305. 1999.

Kato K.; E. Uchida; E. T. Kang; Y. Uyama and Y. Ikada Polymer surface with graft chains, *Prog. Polym. Sci.* 28, pp.209-259. 2003.

Kawaguchi S.; M. A. Winnik and K. Ito Dispersion Copolymerization of *N*-Butyl Methacrylate With Poly(Ethylene Oxide) Macromonomers in Methanol-Water – Comparison of Experiment with Theory, *Macromolecules* 28, pp.1159-1166. 1995.

Kee R. A. and M. Gauthier Arborescent polystyrene-graft-polyisoprene copolymers, *Macromolecules* 32, pp.6478-6484. 1999.

Kee R. A. and M. Gauthier Arborescent polystyrene graft-poly(2-vinylpyridine) copolymers: Synthesis and enhanced polyelectrolyte effect in solution, *Macromolecules* 35, pp.6526-6532. 2002.

Kim B. and N. A. Peppas Analysis of molecular interactions in poly(methacrylic acid-g-ethylene glycol) hydrogels, *Polymer* 44, pp.3701-3707. 2003.

Kim H. Y.; U. Jeong and J. K. Kim Reaction kinetics and morphological changes of reactive polymer-polymer interface, *Macromolecules* 36, pp.1594-1602. 2003.

Kingshott P.; J. Wei; D. Bagge-Ravn; N. Gadegaard and L. Gram Covalent attachment of poly(ethylene glycol) to surfaces, critical for reducing bacterial adhesion, *Langmuir* 19, pp.6912-6921. 2003.

Kiriy A.; G. Gorodyska; S. Minko; W. Jaeger; P. Stepanek and M. Stamm Cascade of coil-globule conformational transitions of single flexible polyelectrolyte molecules in poor solvent, *J. Am. Chem. Soc.* 124, pp.13454-13462. 2002.

Kirwan L. J.; P. D. Fawell and W. van Bronswijk An in situ FTIR-ATR study of polyacrylate adsorbed onto hematite at high pH and high ionic strength, *Langmuir* 20, pp.4093-4100. 2004a.

Kirwan L. J.; G. Papastavrou; M. Borkovec and S. H. Behrens Imaging the coil-to-globule conformational transition of a weak polyelectrolyte by tuning the polyelectrolyte charge density, *Nano Letters* 4, pp.149-152. 2004b.

Ko Y. G.; Y. H. Kim; K. D. Park; H. J. Lee; W. K. Lee; H. D. Park; S. H. Kim; G. S. Lee and D. J. Ahn Immobilization of poly(ethylene glycol) or its sulfonate onto polymer surfaces by ozone oxidation, *Biomaterials* 22, pp.2115-2123. 2001.

Kudaibergenov S. E. Recent advances in the study of synthetic polyampholytes in solutions, *Adv. Polym. Sci*. 144, pp.115-197. 1999.

Kudaibergenov S. E. Polyampholytes: synthesis, characterization, and application, New York : Kluwer Academic/Plenum Publishers, 2002.

Kurita K.; S. Hashimoto; H. Yoshino; S. Ishii and S. I. Nishimura Preparation of chitin/polystyrene hybrid materials by efficient graft copolymerization based on mercaptochitin, *Macromolecules* 29, pp.1939-1942. 1996.

Kwak J.; P. Lacroix-Desmazes; J. J. Robin; B. Boutevin and N. Torres Synthesis of mono functional carboxylic acid poly(methyl methacrylate) in aqueous medium using sur-iniferter. Application to the synthesis of graft copolymers polyethylene-g-poly(methyl methacrylate) and the compatibilization of LDPE/PVDF blends, *Polymer* 44, pp.5119-5130. 2003.

Lau W. M. Ion beam techniques for functionalization of polymer surfaces, *Nucl. Inst. Meth. B* 131, pp.341-349. 1997.

Li G. F.; J. D. Fan; R. Jiang and Y. Gao Cross-linking the linear polymeric chains in the ATRP synthesis of iron oxide/polystyrene core/shell nanoparticles, *Chem. Mater.* 16, pp.1835-1837. 2004.

Li J. M. and M. Gauthier A novel synthetic path to arborescent graft polystyrenes, *Macromolecules* 34, pp.8918-8924. 2001.

Li J. M.; M. Gauthier; S. J. Teertstra, H. Xu and S. S. Sheiko Synthesis of arborescent polystyrene-graft-polyisoprene copolymers using acetylated substrates, *Macromolecules* 37, pp.795-802. 2004.

Li L.; C. M. Chan; L. T. Weng; M. L. Xiang; M. Jiang Specific interaction between poly(styrene-co-4-vinylphenol) and poly(styrene-co-4-vinylpyridine) studied by C-ray photoelectron spectroscopy and time-of-flight secondary ion mass spectrometry, *Macromolecules* 31, pp.7248-7255. 1998.

Li Z. F.; E. T., Kang; K. G., Neoh; K. L., Tan; C. C., Huang and D. J., Liaw Surface structures and adhesive-free adhesion characteristics of polyaniline films after modification by graft copolymerization, *Macromolecules* 30, pp.3354-3362. 1997.

Lin H. B.; Z. C. Zhao; C. Garciaecheverria; D. H. Rich and S. L. Cooper Synthesis of a Novel Polyurethane Copolymer Containing Covalently Attached RGD Peptide, *J. Biomat. Sci. Polym. E.* 3, pp.217-227. 1992.

Liu N. C.; H. Q. Xie and W. E. Baker Comparison of the Effectiveness of Different Basic Functional-Group for the Reactive Compatibilization of Polymer Blends, *Polymer* 34, pp.4680-4687. 1993.

Liu X. H.; Q. J. Wu; L. A. Berglund; J. Q. Fan and Z. N. Qi Polyamide 6-clay nanocompositles/polypropylene-grafted-maleic anhydride alloys, *Polymer* 42, pp.8235-8239. 2001.

Liu Y.; Goh S. H.; Lee S. Y.; Huan C. H. A. Miscibility and interactions in blends and complexes of poly(N-acryloyl-N '-methylpiperazine) with poly(p-vinylphenol), *Macromolecules* 32, pp.1967-1971, 1999.

Lohse D. J.; S. Datta; E. N. Kresge Graft Copolymer Compatibilizers for Blends of Polypropylene and Ethylene Propylene Copolymers, *Macromolecules* 24, pp.561-566. 1991

Lowe, A. B. and C. L. McCormick Stimuli-Responsive Water-Soluble and Amphiphilic Copolymers, in Stimuli-Responsive Water Soluble Polymers, ACS Sym. Ser 780, Ed. Charles L. McCormick, American Chemical Society: Washington D.C., (2000), pp. 12-24.

Lowe A. B. and C. L. McCormick Synthesis and solution properties of zwitterionic polymers *Chem. Rev.* 102, pp.4177-4189. 2002.

Lowe A. B.; B. S. Sumerlin; M. S. Donovan and C. L. McCormick Facile preparation of transition metal nanoparticles stabilized by well-defined (Co)polymers synthesized via aqueous reversible addition-fragmentation chain transfer polymerization, *J. Am. Chem. Soc.* 124, pp.11562-11563. 2002

Ma H. W.; J. H. Hyun; P. Stiller and A. Chilkoti "Non-fouling" oligo(ethylene glycol)-functionalized polymer brushes synthesized by surface-initiated atom transfer radical polymerization, *Adv. Mater.* 16, pp.338-341. 2004.

Ma Y. H.; Tang Y. Q.; Billingham N. C.; Armes S. P.; Lewis A. L.; Lloyd A. W.; Salvage J. P. Well-defined biocompatible block copolymers via atom transfer radical polymerization of 2-methacryloyloxyethyl phosphorylcholine in protic media *Macromolecules* 36, pp.3475-3484. 2003.

Ma Z. W.; C. Y. Gao; Y. H. Gong and J. C. Shen Chondrocyte behaviors on poly-L-lactic acid (PLLA) membranes containing hydroxyl, amide or carboxyl groups, *Biomaterials* 24, pp.3725-3730. 2003.

Mafe S.; J. A. Manzanares; A. E. English and T. Tanaka Multiple phases in ionic copolymer gels, *Phys. Rev. Lett.* 79, pp.3086-3089. 1997.

Mani R.; M. Bhattacharya and J. Tang Functionalization of polyesters with maleic anhydride by reactive extrusion, *J. Polym. Sci.: Polym. Chem.* 37, pp.1693-1702. 1999.

Marechal P.; R. Legras and J. M. Dekoninck Molecular-Weight Segregation Induced by Interfacial Melt Reactivity in Polyamide-6 Reactive-Rubber Blends, *J. Polym. Sci.: Polym. Phys.* 33, pp.1895-1906. 1995.

Marutani E.; S. Yamamoto; T. Ninjbadgar; Y. Tsujii; T. Fukuda and M. Takano Surface-initiated atom transfer radical polymerization of methyl methacrylate on magnetite nanoparticles, *Polymer* 45, pp.2231-2235. 2004.

Matsumoto H.; Y. Koyama and A. Tanioka Interaction of organic molecules with weak amphoteric charged membrane surfaces: Effect of interfacial charge structure, *Langmuir* 18, pp.3698-3703. 2002.

Matsuno R.; K. Yamamoto; H. Otsuka and A. Takahara Polystyrene- and poly(3-vinylpyridine)-grafted magnetite nanoparticles prepared through surface-initiated nitroxide-mediated radical polymerization, *Macromolecules* 37, pp.2203-2209. 2004.

Matsuda T.; N. Saito and T. Sugawara Ceric-ion-initiating surface graft polymerization with regional control and dimensional precision, *Macromolecules* 29, pp.7446-7451. 1996.

Matyjaszewski K.; S. G., Gaynor; A., Kulfan and M. Podwika Preparation of hyperbranched polyacrylates by atom transfer radical polymerization .1. Acrylic AB* monomers in "living" radical polymerizations, *Macromolecules* 30, pp.5192-5194, 1997.

Matyjaszewski K. and S. G. Gaynor Preparation of hyperbranched polyacrylates by atom transfer radical polymerization .3. Effect of reaction conditions on the self-condensing vinyl polymerization of 2-((2-bromopropionyl)oxy)ethyl acrylate, *Macromolecules* 30, pp.7042-7049. 1997.

Matyjaszewski K.; J. Pyun and S. G. Gaynor Preparation of hyperbranched polyacrylates by atom transfer radical polymerization, 4 - The use of zero-valent copper, *Macromol. Rapid Comm.* 19, pp.665-670. 1998a.

Matyjaszewski K.; J. L. Wang; T. Grimaud and D. A. Shipp. Controlled/"living" atom transfer radical polymerization of methyl methacrylate using various initiation systems, *Macromolecules* 31, pp.1527-1534. 1998b.

Matyjaszewski K.; D. A. Shipp; J. L. Wang; T. Grimaud; T. E. Patten Utilizing halide exchange to improve control of atom transfer radical polymerization, *Macromolecules* 31, pp.6836-6840. 1998c.

Matyjaszewski K. and J. H. Xia. Atom transfer radical polymerization, *Chem. Rev.* 101, pp.2921-2990. 2001.

McCormick C. L. and E. E. Kathmann in *The Polymeric Materials Encyclopedia*; Salamone J. C., Ed.; CRC Press: Boca Raton, Florida, 1996; Vol. 7, p 7189-7201.

McDowall D. J.; B. S. Gupta and V. T. Stannett Grafting of vinyl monomers to cellulose by ceric ion initiation, *Prog. Polym. Sci.* 10, pp.1-50. 1984

Minakata A.; K. Takayama; S. Yano; Y. Tanaka; T. Araki and T. Shimizu Polyelectrolytic Behavior of a novel fluorine-containing ionomer, PPFNA, *J. Phys. Chem. B* 107, pp.8146-8151. 2003.

Minko S.; A. Kiriy; G. Gorodyska and M. Stamm Single flexible hydrophobic polyelectrolyte molecules adsorbed on solid substrate: Transition between a stretched chain, necklace-like conformation and a globule, *J. Am. Chem. Soc.* 124, pp.3218-3219. 2002.

Mitsukami, Y.; M. S. Donovan; A. B. Lowe and C. L. McCormick Water-soluble polymers. 81. Direct synthesis of hydrophilic styrenic-based homopolymers and block copolymers in aqueous solution via RAFT, *Macromolecules* 2001, *34*, 2248.

Moad C. L.; G. Moad; E. Rizzardo and S. H. Thang Chain transfer activity of omega-unsaturated methyl methacrylate oligomers, *Macromolecules* 29, pp.7717-7726. 1996.

Moad G. the synthesis of polyolefin graft copolymers by reactive extrusion, *Prog. Polym. Sci.* 24, pp.81-142. 1999.

Moulder J. F.; W. F. Stickle; P. E. Sobol and K. Bomben The Handbook of X-ray Photoelectron Spectroscopy, Perkin-Elmer Corporation (Physical Electronics), 1992 (2nd edition)

Mori M.; Y. Uyama and Y. Ikada Surface Modification of Aramid Fiber by Graft-Polymerization, *Polymer* 35, pp.5336-5341. 1994.

Mori H. and A. H. E. Muller Hyperbranched (Meth)acrylates in Solution, Melt and Grafted From Surfaces, *Top Curr. Chem.* 228, pp.1-37. 2003.

Mori H.; A. Walther; X. Andre; M. G. Lanzendorfer and A. H. E. Muller Synthesis of highly branched cationic polyelectrolytes via self-condensing atom transfer radical copolymerization with 2-(diethylamino)ethyl methacrylate, *Macromolecules* 37, pp.2054-2066. 2004.

Muchtar Z.; M. Schappacher and A. Deffieux Hyperbranched nanomolecules: Regular polystyrene dendrigrafts, *Macromolecules* 34, pp.7595-7600. 2001.

Navarre S. and B. Maillard Efficiency of peroxyderivatives in the chemical modification of polyethylene, *J. Polym. Sci.: Polym. Chem.* 38, pp.2957-2963. 2000.

Neugebauer D.; Y. Zhang; T. Pakula; S. S. Sheiko and K. Matyjaszewski Densely-grafted and double-grafted PEO brushes via ATRP. A route to soft elastomers, *Macromolecules* 36, pp.6746-6755. 2003.

Noh I. and J. A. Hubbell Photograft polymerization of acrylate monomers and macromonomers on photochemically reduced PTFE films, *J. Polym. Sci.: Polym. Chem.* 35, pp.3467-3482. 1997.

Okaniwa M. and Y. Ohta Novel emulsion graft copolymerization onto the silylmethyl group of poly(dimethylsiloxane), *J. Polym. Sci.: Polym. Chem.* 35, pp.2607-2617. 1997.

Paul R.; R. Schmidt; J. X. Feng and D. J. Dyer Photoinitiated polymerization of styrene from self-assembled monolayers on gold. II. Grating rates and extraction, *J. Polym. Sci.: Polym. Chem.* 40, pp.3284-3291. 2002.

Paulo C. and J. E. Puskas. Synthesis of hyperbranched polyisobutylenes by inimer-type living polymerization. 1. Investigation of the effect of reaction conditions, *Macromolecules* 34, pp.734-739. 2001.

Poe G. D. and C. L. McCormick Synthesis, complex formation, and dilute-solution associative behavior of linear poly(methacrylic acid)-graft-poly(2-ethyl-2-oxazoline), *J. Polym. Sci.: Polym. Chem.* 42, pp.2520-2533. 2004.

Power-Billard K. N.; P. Wieland; M. Schafer; O. Nuyken and I. Manners Moderating the reactivity of living anionic poly(ferrocenyldimethylsilane) with a diphenylethylene chain end: Synthesis and characterization of polystyrene-polyferrocenylsilane graft copolymers, *Macromolecules* 37, pp.2090-2095. 2004.

Prucker O. and J. Ruhe Synthesis of poly(styrene) monolayers attached to high surface area silica gels through self-assembled monolayers of azo initiators, *Macromolecules* 31, pp.592-601. 1998.

Pyun J. and K. Matyjaszewski Synthesis of nanocomposite organic/inorganic hybrid materials using controlled/"living" radical polymerization, *Chem. Mater.* 13, pp.3436-3448. 2001.

Qiu J. and K. Matyjaszewski Polymerization of substituted styrenes by atom transfer radical polymerization, *Macromolecules* 30, pp.5643-5648. 1997.

Otera J. In search of practical esterification. *Angew Chem-Int. Edit.* 2001, 40, 2044.

Ranby B. Surface modification and lamination of polymers by photografting, *Intl J. Adhes. Adhes.* 19, pp.337-343. 1999.

Raula J.; J. Shan; M. Nuopponen; A. Niskanen; H. Jiang; E. I. Kauppinen and H. Tenhu Synthesis of gold nanoparticles grafted with a thermoresponsive polymer by surface-induced reversible-addition-fragmentation chain-transfer polymerization, *Langmuir* 19, pp.3499-3504. 2003.

Reiter G.; P. Auroy and L. Auvray Instabilities of thin polymer films on layers of chemically identical grafted molecules, *Macromolecules* 29, pp.2150-2157. 1996.

Robin J. J. the Use of Ozone in the Synthesis of New Polymers and the Modification of Polymers, *Adv. Polym. Sci.* 167, pp.35-79. 2004.

Robinson K. L.; M. V. de Paz-Banez; X. S. Wang and S. P. Armes. Synthesis of well-defined, semibranched, hydrophilic-hydrophobic block copolymers using atom transfer radical polymerization, *Macromolecules* 34, pp.5799-5805. 2001.

Ruangchuay L.; J. Schwank and A. Sirivat Surface degradation of alpha-naphthalene sulfonate-doped polypyrrole during XPS characterization, *Appl. Surf. Sci.* 199, pp.128-137, 2002.

Rusa M.; J. K. Whitesell and M. A. Fox Controlled fabrication of gold/polymer nanocomposites with a highly structured poly(N-acylethylenimine) shell, *Macromolecules* 37, pp.2766-2774. 2004.

Russell K. E. Free radical graft polymerization and copolymerization at higher temperatures, *Prog. Polym. Sci.* 27, pp.1007-1038. 2002.

Russo S.; M. Pianca and G. Moggi Poly(vinylidene fluoride) (Synthesis, Microstructure and Chain Conformations) In *The Polymeric Materials Encyclopedia*; Salamone J. C., Ed.; CRC Press: Boca Raton, Florida, 1996; Vol. 7, p 7123-7138.

Saito N.; S. Yamashita and T. Matsuda Laser-irradiation-induced surface graft polymerization method, *J. Polym. Sci.: Polym. Chem.* 35, pp.747-750. 1997.

Sakai K.; T. C. Teng; A. Katada; T. Harada; K. Yoshida; K. Yamanaka; Y. Asami; M. Sakata; C. Hirayama and M. Kunitake Designable size exclusion chromatography columns based on dendritic polymer-modified porous silica particles, *Chem. Mater.* 15, pp.4091-4097. 2003.

Santos J. P.; E. R. Welsh; B. P. Gaber and A. Singh Polyelectrolyte-assisted immobilization of active enzymes on glass beads, *Langmuir* 2001, 17, 5361.

Sawall D. D.; R. M. Villahermosa; R. A. Lipeles and A. R. Hopkins Interfacial Polymerization of Polyaniline Nanofibers Grafted to Au Surfaces, *Chem. Mater.* 16, pp.1606-1608. 2004.

Schappacher M. and A. Deffieux New polymer chain architecture: Synthesis and characterization of star polymers with comb polystyrene branches, *Macromolecules* 33, pp.7371-7377. 2000.

Schappacher M.; A. Deffieux; J. L. Putaux; P. Viville and R. Lazzaroni. Synthesis and characterization of water-soluble amphipatic polystyrene-based dendrigrafts, *Macromolecules* 36, pp.5776-5783. 2003.

Schlucker S.; M. Heid; R. K. Singh; B. P. Asthana; J. Popp and W. Kiefer Vibrational dynamics in hydrogen-bonded (pyridine plus water) complexes studied by spectrally resolved femtosecond CARS, *Z. Phys.Chem.* 216, pp.267-278. 2002.

Schmaljohann D.; J. Oswald; B. Jorgensen; M. Nitschke; D. Beyerlein and C. Werner Thermo-responsive PNiAAm-g-PEG films for controlled cell detachment, *Biomacromolecules* 4, pp.1733-1739. 2003.

Sergeyeva T. A.; H. Matuschewski; S. A. Piletsky; J. Bendig; U. Schedler and M. Ulbricht Molecularly imprinted polymer membranes for substance-selective solid-phase extraction from water by surface photo-grafting polymerization, *J. Chromatogr. A* 907, pp.89-99. 2001.

Sfika V. and C. Tsitsilianis Association phenomena of poly(acrylic acid)-b-poly(2-vinylpyridine)b-poly(acrylic acid) triblock polyampholyte in aqueous solutions: From transient network to compact micelles, *Macromolecules* 36, pp.4983-4988. 2003.

Schafer M.; P. C. Wieland and O. Nuyken Synthesis of new graft copolymers containing polyisobutylene by a combination of the 1,1-diphenylethylene technique and cationic polymerization, *J. Polym. Sci.: Polym. Chem.* 40, pp.3725-3733. 2002.

Shenhar R. and V. M. Rotello Nanoparticles: Scaffolds and building blocks, *Accounts Chem. Res.* 36, pp.549-561. 2003.

Shimano Y.; K. Sato and S. Kobayashi Synthesis of novel Macromonomers and Telechelics of Poly(2-Alkyl-2-Oxazoline)s, *J. Polym. Sci.: Polym. Chem.* 33, pp.2715-2723. 1995.

Shinoda H.; P. J. Miller and K. Matyjaszewski Improving the structural control of graft copolymers by combining ATRP with the macromonomer method, *Macromolecules* 34, pp.3186-3194. 2001.

Shriner R. L.; C. K. E. Hermann; T. C. Morrill; D. Y. Curtin and R. C. Fuson, *The Systematic Identification of Organic Compounds*, 7th ed.; Ed.; J. Wiley & Sons: New York, 1998.

Sill K. and T. Emrick Nitroxide-mediated radical polymerization from CdSe nanoparticles, *Chem. Mater.* 16, pp.1240-1243. 2004.

Simon P. F. W. and A. H. E. Muller Synthesis of hyperbranched and highly branched methacrylates by self-condensing group transfer copolymerization, *Macromolecules* 34, pp.6206-6213. 2001.

Singh R. P. Surface grafting onto Polypropylene – a Survey of Recent Development, *Prog. Polym Sci.* 12, pp.251-281. 1992.

Skaff H.; M. F. Ilker; E. B. Coughlin and T. Emrick Preparation of cadmium selenide-polyolefin composites from functional phosphine oxides and ruthenium-based metathesis, *J. Am. Chem. Soc.* 124, pp.5729-5733. 2002.

Sugawara T. and T. Matsuda Novel Surface Graft-Copolymerization Method with Micron-Order Regional Precision, *Macromolecules* 27, pp.7809-7814, 1994.

Sugiyama K.; K. Shiraishi and T. Matsumoto Assembly of amphiphilic poly[2-(methacryloyloxy)ethyl phosphorylcholine] with cholesteryl moieties as terminal groups, *J. Polym. Sci.: Polym. Chem.* 2003, 41, 1992.

Sui Z. J. and J. B. Schlenoff Controlling electroosmotic flow in microchannels with pH-responsive polyelectrolyte multilayers, *Langmuir* 19, pp.7829-7831. 2003.

Takafuji M.; S. Ide; H. Ihara and Z. H. Xu Preparation of poly(1-vinylimidazole)-grafted magnetic nanoparticles and their application for removal of metal ions, *Chem. Mater.* 16, pp.1977-1983. pp.2004

Takeda Y. and D. R. Paul Morphology of Nylon-6 Blends with Styrenic Polymers, *J. Polym. Sci.: Polym. Phys.* 30, pp.1273-1284. 1992.

Tan K. L.; B. T. G. Tan; E. T. Kang and K. G. Neoh X-Ray Photoelectron Spectroscopic Studies of some Polyvinylpyridine Acceptor Complexes *J. Mol. Electron.* 6, pp.5-13. 1990.

Tan K. L.; L. L. Woon; H. K. Wong; E. T. Kang and K. G. Neoh Surface Modification of Plasma-Pretreated Poly(tetrafluoroethylenen) Films by Graft-Copolymerization, *Macromolecules* 26, pp.2832-2836. 1993.

Tang Y.; J. R. Lu; A. L. Lewis; T. A. Vick and P. W. Stratford Swelling of zwitterionic polymer films characterized by spectroscopic ellipsometry, *Macromolecules* 34, pp.8768-8776. 2001.

Tannenbaum R.; S. King; J. Lecy; M. Tirrell and L. Potts Infrared study of the kinetics and mechanism of adsorption of acrylic polymers on alumina surfaces, *Langmuir* 20, pp.4507-4514. 2004.

Tao G. L.; A. J. Gong; J. J. Lu; H. J. Sue and D. E. Bergbreiter Surface functionalized polypropylene: Synthesis, characterization, and adhesion properties, *Macromolecules* 34, pp.7672-7679. 2001.

Teertstra S. J. and M. Gauthier Dendrigraft polymers: macromolecular engineering on a mesoscopic scale, *Prog. Polym. Sci*. 29, pp.277-327. 2004.

Thang, S. H.; Y. K. Chong; R. T. A. Mayadunne; G. Moad and E. Rizzardo A novel synthesis of functional dithioesters, dithiocarbamates, xanthates and trithiocarbonates. *Tetrahedron Lett.* 1999, 40, 2435.

Thomas K. G. and P. V. Kamat Chromophore-functionalized gold nanoparticles, *Acc. Chem. Res.* 36, pp.888-898. 2003.

Tomalia D. A.; D. M. Hedstrand and M. S. Ferritto Comb-Burst Dendrimer Topology- New Macromolucular Architecture Derived from Ddendritic Grafting, *Macromolecules* 24, pp.1435-1438. 1991.

Tong J. D.; F. E. Du Prez and E. J. Goethals Synthesis of PTHF-grafted PMMA based on the reaction of methyl esters with quaternary ammonium salts, *Macromolecules* 34, pp.761-767. 2001.

Tonge S. R. and B. J. Tighe Responsive hydrophobically associating polymers: a review of structure and properties, *Adv. Drug Deliver. Rev.* 53, pp.109-122. 2001.

Touihri S.; J. C. Bernede; P. Molinie and D. Legoff Modification of poly (N-vinyl-carbazole) thin films by bromine doping, *Polymer* 43, pp.3123-3129. 2002.

Tran Y. and P. Auroy Synthesis of poly(styrene sulfonate) brushes, *J. Am. Chem. Soc.* 123, pp.3644-3654. 2001.

Tsubokawa N.; M. Inagaki; H. Kubota and T. Endo Gamma-Poly(Glutamic Acid) as an Initiator of Cationic Polymerization of *N*-Vinylcarbazole and *N*-Vinyl-2-Pyrrolidone, *J. Polym. Sci.: Polym. Chem.* 31, pp.3193-3198. 1993a.

Tsubokawa N.; M. Inagaki; H. Kubota and T. Endo Gamma-Poly(Glutamic Acid) as an Initiator of Cationic Polymerization of *N*-Vinylcarbazole and *N*-Vinyl-2-Pyrrolidone, *J. Polym. Sci.: Polym. Chem.* 31, pp.3193-3198. 1993b.

Tsubokawa N.; Y. Shirai; H. Tsuchida and S. Handa Photografting of Vinyl-Polymers onto Ultrafine Inorganic Particles-Photopolymerization of Vinyl Monomers Initiated by Azo Groups Introduced onto these Surfaces, *J. Polym. Sci.: Polym. Chem.* 32, pp.2327-2332. 1994.

Tsubokawa N. and Yoshikawa S. Grafting of Polymers with Controlled Molecular-Weight onto Ultrafine Silica Surface, *J. Polym. Sci.: Polym. Chem.* 33, pp.581-586.1995.

Uchida E.; Y. Uyama and Ikada Y. Grafting of Water-Soluble Chains onto a Polymer Surface, *Langmuir* 10, pp.481-485. 1994.

Uchida M.; M. Kurosawa and Osada. Y. Swelling process and order-disorder transition of hydrogel containing hydrophobic ionizable groups, *Macromolecules* 28, pp.4583-4586, 1995.

Uchida E.; H. Iwata and Y. Ikada Surface structure of poly(ethylene terephthalate) film grafted with poly(methacrylic acid), *Polymer* 41, pp.3609-3614. 2000.

Ulman A. Self-assembled monolayers of 4-mercaptobiphenyls, *Acc. Chem. Res.* 34, pp.855-863. 2001.

Uyama H.; Y. Honda and S. Kobayashi Synthesis and Emulsion Copolymerization of Amphiphilic Poly(2-oxazoline) Macromonomer Possessing A Vinyl Ester Group, J. *Polym. Sci.: Polym. Chem.* 31, pp.123-128. 1993.

Uyama Y.; K. Kato and Y. Ikada Surface Modification of Polymers by Grafting, *Adv. Polym. Sci.* 137: 1-39 1998

van der Heiden A. P. and L. H. Koole Photochemical coupling of aryl azides to poly(ether urethane) surfaces: Studies with a fluorescent model compound, *Macromolecules* 29, pp.7012-7015. 1996.

van der Maarel J. R. C. and W. Groenewegen; S. U. Egelhaaf and A. Laap Salt-induced contraction of polyelectrolyte diblock copolymer micelles, *Langmuir* 16, pp.7510-7519. 2000.

Vasilevskaya V. V. Conformational Transition in Polyelectrolyte Molecules: Influence of Osmotic Pressure of Counterions in Physical chemistry of polyelectrolytes, Tsetska Radeva ed New York : Marcel Dekker, c2001, pp181-202.

Vedikhina L.; A. Kurmaeva; R. Tukhvatullin and W. Barabanov Ionization equilibrium in salt-containing aqueous solutions of synthetic polyampholytes, *J. Polym. Sci.: Polym. Phys.* 38, pp.1824-1831. 2000.

Vestal C. R. and Z. J. Zhang Atom transfer radical polymerization synthesis and magnetic characterization of MnFe2O4/polystyrene core/shell nanoparticles, *J. Am. Chem. Soc.* 124, pp.14312-14313. 2002.

Virtanen J. Self-Assembling of Thermally Responsive Block and Graft Copolymers in Aqueous Solutions, Ph D. Dissertation, University of Helsinki, Finland, 2002.

von Werne T. A.; D. S. Germack; E. C. Hagberg; V. V. Sheares; C. J. Hawker and K. R. Carter A versatile method for tuning the chemistry and size of nanoscopic features by living free radical polymerization, *J. Am. Chem. Soc.* 2003, 125, 3831.

Vosloo, J. J.; D. De Wet-Roos; M. P., Tonge and R. D. Sanderson Controlled free radical polymerization in water-borne dispersion using reversible addition-fragmentation chain transfer, *Macromolecules* 2002, 35, 4894.

Walter H.; P. Muller-Buschbaum; J. S. Gutmann; C. Lorenz-Haas; C. Harrats; R. Jerome and M. Stamm Lateral structures of thin films of ampholytic diblock copolymers adsorbed from dilute aqueous solution at the solid/liquid interface, *Langmuir* 15, pp.6984-6990. 1999.

Wakasugi K.; T. Misaki; K. Yamada and Y. Tanabe Diphenylammonium triflate (DPAT): efficient catalyst for esterification of carboxylic acids and for

transesterification of carboxylic esters with nearly equimolar amounts of alcohols. *Tetrahedron Lett.* 2000, 41, 5249.

Wang C. H. and G. H. Hsiue Synthesis and characterization of temperature- and pH-sensitive hydrogels based on poly(2-ethyl-2-oxazoline) and poly(D,L-lactide), *J. Polym. Sci.: Polym. Chem*. 40, pp.1112-1121. 2002.

Wang J. L.; T. Grimaud and K. Matyjaszewski Kinetic study of the homogeneous atom transfer radical polymerization of methyl methacrylate, *Macromolecules* 30, pp.6507-6512. 1997.

Wang J.; R. Nomura and T. Endo One-pot formation of a reactive polymer possessing anion sites along the polymer backbone and its application to graft polymerization of epsilon-caprolactone, *Macromolecules* 29, pp.2707-2708. 1996.

Wang J.; R. Nomura and T. Endo Samarium poly(oxamide) polyanions as novel polymeric initiators. One-pot syntheses of graft copolymers, *J. Polym. Sci.: Polym. Chem.* 35, pp.1381-1387. 1997.

Wang J. W.; Q. D. Shen; C. Z. Yang and Q. M. Zhang High dielectric constant composite of P(VDF-TrFE) with grafted copper phthalocyanine oligomer, *Macromolecules* 37, pp.2294-2298. 2004.

Wang P.; K. L., Tan; E. T., Kang and K. G. Neoh Synthesis, characterization and anti-fouling properties of poly(ethylene glycol) grafted poly(vinylidene fluoride) copolymer membranes, *J. Mater. Chem.* 11, pp.783-789, 2001.

Watanabe H.; T. Amemiya; T. Shimura and T. Kotaka Anionic Synthesis of Graft Block-Copolymers with Poly(2-Vinylpyridine) Trunks-Effects of Trunk and Branch Molecular-Weights, *Macromolecules* 27, pp.2336-2338. 1994.

Wu C. and S. Q. Zhou Thermodynamically Stable Globule State of A Single Poly(N-isopropylacrylamide) Chain in Water, *Macromolecules* 28, pp.5388-5390. 1995.

Xiang M. L.; Jiang M.; Zhang Y. B.; Wu C.; Feng L. X. Intermacromolecular complexation due to specific interactions .4. The hydrogen-bonding complex of vinylphenol-containing copolymer and vinylpyridine-containing copolymer, *Macromolecules* 30, pp.2313. 1997.

Xiang J. N.; S. Toyoshima; A. Orita and J. Otera A practical and green chemical process: Fluoroalkyldistannoxane-catalyzed biphasic transesterification, *Angew Chem-Int. Edit.* 2001, 40, 3670.

Xiao H. N.; R. Pelton and A. Hamielec The Association of Aqueous Phenolic Resin With Polyethylene Oxide and Poly(Acrylamide-co-ethylene Glycol), *J. Polym. Sci.: Polym. Chem.* 33, pp.2605-2612. 1995.

Xie H. Q.; J. G. Xu and S. B. Zhou Polymer Blends with 2 Kinds of Elastomeric Ionomers, *Polymer* 32, pp.95-102. 1991.

Xu Z. K.; Q. W. Dai; J. Wu; X. J. Huang and Q. Yang Covalent attachment of phospholipid analogous polymers to modify a polymeric membrane surface: A novel approach, *Langmuir* 20, pp.1481-1488. 2004.

Yagci Y. and W. Schnabel Light-Induced Synthesis of Block and Graft-Copolymers, *Prog. Polym. Sci.* 15, pp.551-601. 1990.

Yamamoto T.; K. Aoshima; H. Ohmura; Y. Moriya; N. Suzuki and Y. Oshibe New Manufacturing Processes for Block and Graft-Copolymers by Radical Reactions, *Polymer* 32, pp.19-28. 1991

Yan M. D. and J. Ren Covalent immobilization of ultrathin polymer films by thermal activation of perfluorophenyl azide, *Chem. Mater.* 16, pp.1627-1632. 2004.

Yang L. Q.; F. R. Zhang; T. Endo and T. Hirotsu Microstructure of maleic anhydride grafted polyethylene by high-resolution solution-state NMR and FTIR spectroscopy, *Macromolecules* 36, pp.4709-4718. 2003.

Yim H.; M. S. Kent; A. Matheson; M. J. Stevens; R. Ivkov; S. Satija; J. Majewski and G. S. Smith Adsorption of sodium poly(styrenesulfonate) to the air surface of water by neutron and X-ray reflectivity and surface tension measurements: Polymer concentration dependence, *Macromolecules* 35, pp.9737-9747. 2002.

Ying L. stimuli-responsive microfiltration membranes and surfaces from copolymers with grafted functional side chains, Ph D. dissertation, National University of Singapore, Singapore, 2003

Yu W. H. Surface Functionalization of Silicon Wafer via Graft Copolymerization, Ph D. Dissertation, National University of Singapore, Singapore. 2003.

Ziani-Cherif H.; K. Imachi and T. Matsuda Preparation of aryldiazonium-, aryldiazo-, and arylazido-derivatized copolymers and their surface photografting, *Macromolecules* 32, pp.3438-3447. 1999.

Zhang J. F.; E. Uchida; Y. Uyama and Y. Ikada Adhesive Interaction in Aqueous-Media between Polymer Surfaces Grafted with Anionic and Cationic Polymer-Chains, *Langmuir*, 11, pp.1688-1692. 1995.

Zhang J. F.; C. Q. Cui; T. B. Lim; E. T. Kang; K. G. Neoh; S. L. Lim; K. L. Tan Chemical modification of silicon (100) surface via UV-induced graft polymerization, *Chem. Mater*. 11, pp.1061-1068. 1999.

Zhao H. Y. and D. A. Shipp Preparation of poly(styrene-block-butyl acrylate) block copolymer-silicate nanocomposites, *Chem. Mater.* 15, pp.2693-2695. 2003.

Zhu M. D.; L. Q. Wang; G. J. Exarhos and A. D. Q. Li Thermosensitive gold nanoparticles, *J. Am. Chem. Soc.* 126, pp.2656-2657. 2004.

Zhu Y. B.; C. Y. Gao and J. C. Shen Surface modification of polycaprolactone with poly(methacrylic acid) and gelatin covalent immobilization for promoting its cytocompatibility, *Biomaterials* 23, pp.4889-4895. 2002.

Zouahri A. and A. Elmidaoui Synthesis of perfluorinated cation exchange membranes by preirradiation grafting of acrylic acid onto ethylene-tetrafluoroethylene films, *J. Polym. Sci.: Polym. Chem.* 34, pp.1793-1798. 1996.

Publications

My thesis was primarily based on the following papers. However, several of them were not integrated into the the thesis.

1. **Zhai G. Q.**; Ying L.; Kang E. T.; Neoh K. G. Poly(vinylidene fluoride) with grafted 4-vinylpyridine polymer side chains for pH-sensitive microfiltration membranes *J. Mater. Chem.* **2002**, *12*, 3508.
2. **Zhai G. Q.**; Ying L.; Kang E. T.; Neoh K. G. Synthesis and characterization of poly(vinylidene fluoride) with grafted acid/base polymer side chains *Macromolecules* **2002**, *35*, 9653.
3. **Zhai G. Q.**; Kang E. T.; Neoh K. G. Poly(2-vinylpyridine)- and poly(4-vinylpyridine)-*graft*-poly(vinylidene fluoride) copolymers and their pH-sensitive microfiltration membranes *J. Membr. Sci.* **2003**, *217*, 243.
4. **Zhai G. Q.**; Toh S. C.; Tan W. L.; Kang E. T.; Neoh K. G.; Huang C. C.; Liaw D. J. Poly(vinylidene fluoride) with grafted zwitterionic polymer side chains for electrolyte-responsive microfiltration membranes *Langmuir* **2003**, *19*, 7030.
5. Ying L.; **Zhai G. Q.**; Winata A. Y.; Kang E. T.; Neoh K. G. pH effect of coagulation bath on the characteristics of poly(acrylic acid)-grafted and poly(4-vinylpyridine)-grafted poly(vinylidene fluoride) microfiltration membranes *J. Colloid Interface Sci.* **2003**, *265*, 396.
6. **Zhai G. Q.**; Yu W. H.; Kang E. T.; Neoh K.G.; Huang C. C.; Liaw D. J. Functionalization of Hydrogen-Terminated Silicon with Polybetaine Brushes *via* Surface-Initiated Reversible Addition-Fragmentation Chain Transfer (RAFT) Polymerization *Ind. Eng. Chem. Res.* **2004**, *43*, 1673.

7. **Zhai G. Q.**; Ying L.; Kang E. T.; Neoh K.G. Surface and Interface Characterization of Smart Membranes *Surf. Interface. Anal.* **2004**,*36*, 1048
8. **Zhai G. Q.**; Kang E. T.; Neoh K. G. Inimer Graft-Copolymerized Poly(Vinylidene Fluoride) for the Preparation of Arborescent Copolymers and "Surface-Active" Copolymer Membranes, *Macromolecules* **2004**, *37*, 7240
9. **Zhai G. Q.**; Shi Z. L.; Kang E. T.; Neoh K. G. Surface-Initiated Atom Transfer Radical Polymerization on Poly(Vinylidene Fluoride) Membrane for Antibacterial Ability, *Macromolecular Bioscience, accepted*
10. **Zhai G. Q**.; Xu F. J.; Kang E. T.; Neoh K. G. Synthesis of Comb-Like Polymer Brushes on Hydrogen-Terminated Silicon Wafer *via* Atom Transfer Radical Polymerization of Hydroxyl-Functional Monomers, *submitted*